

Received Signal Power Measurements On Select Air Traffic Control Radars In Utah

Jeffery A. Wepman
Edward F. Drocella
April Lundy
Mike Chang
Linh P. Vu
Kenneth J. Brewster
Paul M. McKenna



report series

Received Signal Power Measurements On Select Air Traffic Control Radars In Utah

Jeffery A. Wepman
Edward F. Drocella
April Lundy
Mike Chang
Linh P. Vu
Kenneth J. Brewster
Paul M. McKenna



U.S. DEPARTMENT OF COMMERCE

October 2019

DISCLAIMER

Certain commercial equipment and materials are referenced in this report to specify adequately the technical aspects of the reported results. In no case does such reference imply recommendation or endorsement by the National Telecommunications and Information Administration, nor does it imply that the material or equipment referenced is the best available for this purpose.

CONTENTS

Figures.....	vi
Tables.....	xv
Acronyms/Abbreviations	xvii
Glossary	xix
1. Introduction.....	1
2. Measurement System	3
2.1 Measurement System Design.....	3
2.2 Measurement System Noise Floor Characterization	7
3. Measurement Location Selection.....	11
3.1 Previous Measurement Location Selection Methodology	11
3.2 New Measurement Location Selection Methodology	11
4. Measurement Procedure.....	17
5. Radar Measurements.....	18
6. Data Processing and Analysis.....	25
7. Summary.....	36
8. Acknowledgements.....	38
9. References.....	39
Appendix A : Received Power Histograms for ASR-9 Measurements	40
Appendix B : Received Power Histograms for CARSR Measurements	89

FIGURES

Figure 1. Block diagram of the measurement system.....	3
Figure 2. ITS PSCR Measurement Van (modified Chevrolet Express 3500 Passenger Van).....	4
Figure 3. Simplified block diagram of the preselector (Ethernet control is not shown).....	Error! Bookmark not defined.
Figure 4. Over-the-air system noise floor of the measurement system at 2860 MHz in a 3 MHz RBW using peak detection without the low-noise amplifier (AC power via measurement vehicle’s internal DC to AC power inverter).....	8
Figure 5. Over-the-air system noise floor of the measurement system at 2860 MHz in a 3 MHz RBW using peak detection with the low-noise amplifier (AC power via measurement vehicle’s internal DC to AC power inverter).....	8
Figure 6. Over-the-air system noise floor of the measurement system at 1327 MHz in a 300-kHz RBW using peak detection without the low-noise amplifier (AC power via measurement vehicle’s internal DC to AC power inverter).....	9
Figure 7. Over-the-air system noise floor of the measurement system at 1327 MHz in a 300-kHz RBW using peak detection with the low-noise amplifier (AC power via measurement vehicle’s internal DC to AC power inverter).....	9
Figure 8. Spectrum usage contour, radar transmitter, and actual measurement locations for the ASR-9 in Trout Creek, Utah. An expanded view of the map showing the area inside the rectangle is given in Figure 9.	13
Figure 9. Expanded view of the map showing actual measurement locations for the ASR-9 in Trout Creek, Utah.	14
Figure 10. Spectrum usage contour, radar transmitter, and actual measurement locations for the CARSR in Cedar City, Utah. An expanded view of the map showing the area inside the rectangle is given in Figure 11.	15
Figure 11. Expanded view of the map showing actual measurement locations for the CARSR in Cedar City, Utah.	16
Figure 12. Example of a relatively strong signal received at Location 1 in Zone C2 for the ASR-9.	20
Figure 13. Magnified view of the first peak of the signal received at Location 1 in Zone C2 for the ASR-9.	20
Figure 14. Example of a relatively strong signal received at Location 2 in Zone F4 for the CARSR.	21

Figure 15. Magnified view of the first peak in the signal received at Location 2 in Zone F4 for the CARSR.	21
Figure 16. Example of a relatively weak signal received at Location 5 in Zone D1 for the ASR-9.	22
Figure 17. Example of a relatively weak signal received at Location 5 in Zone D1 for the CARSR.	22
Figure 18. Example of a received radar transmission showing severe multipath at Location 1 in Zone C1 for the ASR-9.	23
Figure 19. Example of a received radar transmission showing severe multipath at Location 6 in Zone H1 for the CARSR.	24
Figure 20. Median peak received signal power vs. distance between the radar transmitter and the receiver for all measurement locations for the ASR-9.	27
Figure 21. Median peak received signal power vs. distance between the radar transmitter and the receiver for all measurement locations for the CARSR.	27
Figure A-1. Received radar signal power statistics at Location 1 in Zone A1 for the ASR-9.	40
Figure A-2. Received radar signal power statistics at Location 2 in Zone A1 for the ASR-9.	41
Figure A-3. Received radar signal power statistics at Location 3 in Zone A1 for the ASR-9.	42
Figure A-4. Received radar signal power statistics at Location 4 in Zone A1 for the ASR-9.	43
Figure A-5. Received radar signal power statistics at Location 5 in Zone A1 for the ASR-9.	44
Figure A-6. Received radar signal power statistics at Location 6 in Zone A1 for the ASR-9.	45
Figure A-7. Received radar signal power statistics at Location 1 in Zone A2 for the ASR-9.	46
Figure A-8. Received radar signal power statistics at Location 2 in Zone A2 for the ASR-9.	47
Figure A-9. Received radar signal power statistics at Location 3 in Zone A2 for the ASR-9.	48

Figure A-10. Received radar signal power statistics at Location 4 in Zone A2 for the ASR-9.....	49
Figure A-11. Received radar signal power statistics at Location 5 in Zone A2 for the ASR-9.....	50
Figure A-12. Received radar signal power statistics at Location 6 in Zone A2 for the ASR-9.....	51
Figure A-13. Received radar signal power statistics at Location 1 in Zone A3 for the ASR-9.....	52
Figure A-14. Received radar signal power statistics at Location 2 in Zone A3 for the ASR-9.....	53
Figure A-15. Received radar signal power statistics at Location 3 in Zone A3 for the ASR-9.....	54
Figure A-16. Received radar signal power statistics at Location 4 in Zone A3 for the ASR-9.....	55
Figure A-17. Received radar signal power statistics at Location 5 in Zone A3 for the ASR-9.....	56
Figure A-18. Received radar signal power statistics at Location 6 in Zone A3 for the ASR-9.....	57
Figure A-19. Received radar signal power statistics at Location 1 in Zone B1 for the ASR-9.....	58
Figure A-20. Received radar signal power statistics at Location 1 in Zone C1 for the ASR-9.....	59
Figure A-21. Received radar signal power statistics at Location 2 in Zone C1 for the ASR-9.....	60
Figure A-22. Received radar signal power statistics at Location 3 in Zone C1 for the ASR-9.....	61
Figure A-23. Received radar signal power statistics at Location 4 in Zone C1 for the ASR-9.....	62
Figure A-24. Received radar signal power statistics at Location 5 in Zone C1 for the ASR-9.....	63
Figure A-25. Received radar signal power statistics at Location 6 in Zone C1 for the ASR-9.....	64

Figure A-26. Received radar signal power statistics at Location 1 in Zone C2 for the ASR-9.....	65
Figure A-27. Received radar signal power statistics at Location 2 in Zone C2 for the ASR-9.....	66
Figure A-28. Received radar signal power statistics at Location 3 in Zone C2 for the ASR-9.....	67
Figure A-29. Received radar signal power statistics at Location 4 in Zone C2 for the ASR-9.....	68
Figure A-30. Received radar signal power statistics at Location 5 in Zone C2 for the ASR-9.....	69
Figure A-31. Received radar signal power statistics at Location 1 in Zone D1 for the ASR-9.....	70
Figure A-32. Received radar signal power statistics at Location 2 in Zone D1 for the ASR-9.....	71
Figure A-33. Received radar signal power statistics at Location 3 in Zone D1 for the ASR-9.....	72
Figure A-34. Received radar signal power statistics at Location 4 in Zone D1 for the ASR-9.....	73
Figure A-35. Received radar signal power statistics at Location 5 in Zone D1 for the ASR-9.....	74
Figure A-36. Received radar signal power statistics at Location 1 in Zone D2 for the ASR-9.....	75
Figure A-37. Received radar signal power statistics at Location 2 in Zone D2 for the ASR-9.....	76
Figure A-38. Received radar signal power statistics at Location 3 in Zone D2 for the ASR-9.....	77
Figure A-39. Received radar signal power statistics at Location 4 in Zone D2 for the ASR-9.....	78
Figure A-40. Received radar signal power statistics at Location 5 in Zone D2 for the ASR-9.....	79
Figure A-41. Received radar signal power statistics at Location 6 in Zone D2 for the ASR-9.....	80

Figure A-42. Received radar signal power statistics at Location 1 in Zone D3 for the ASR-9.....	81
Figure A-43. Received radar signal power statistics at Location 2 in Zone D3 for the ASR-9.....	82
Figure A-44. Received radar signal power statistics at Location 3 in Zone D3 for the ASR-9.....	83
Figure A-45. Received radar signal power statistics at Location 4 in Zone D3 for the ASR-9.....	84
Figure A-46. Received radar signal power statistics at Location 5 in Zone D3 for the ASR-9.....	85
Figure A-47. Received radar signal power statistics at Location 1 in Zone D4 for the ASR-9.....	86
Figure A-48. Received radar signal power statistics at Location 1 in Zone D5 for the ASR-9.....	87
Figure A-49. Received radar signal power statistics at Location 1 in Zone E1 for the ASR-9.....	88
Figure B-1. Received radar signal power statistics at Location 1 in Zone F1 for the CARSR.....	89
Figure B-2. Received radar signal power statistics at Location 2 in Zone F1 for the CARSR.....	90
Figure B-3. Received radar signal power statistics at Location 3 in Zone F1 for the CARSR.....	91
Figure B-4. Received radar signal power statistics at Location 4 in Zone F1 for the CARSR.....	92
Figure B-5. Received radar signal power statistics at Location 5 in Zone F1 for the CARSR.....	93
Figure B-6. Received radar signal power statistics at Location 1 in Zone F2 for the CARSR.....	94
Figure B-7. Received radar signal power statistics at Location 2 in Zone F2 for the CARSR.....	95
Figure B-8. Received radar signal power statistics at Location 3 in Zone F2 for the CARSR.....	96

Figure B-9. Received radar signal power statistics at Location 4 in Zone F2 for the CARSR.....	97
Figure B-10. Received radar signal power statistics at Location 5 in Zone F2 for the CARSR.....	98
Figure B-11. Received radar signal power statistics at Location 1 in Zone F3 for the CARSR.....	99
Figure B-12. Received radar signal power statistics at Location 2 in Zone F3 for the CARSR.....	100
Figure B-13. Received radar signal power statistics at Location 3 in Zone F3 for the CARSR.....	101
Figure B-14. Received radar signal power statistics at Location 4 in Zone F3 for the CARSR.....	102
Figure B-15. Received radar signal power statistics at Location 5 in Zone F3 for the CARSR.....	103
Figure B-16. Received radar signal power statistics at Location 1 in Zone F4 for the CARSR.....	104
Figure B-17. Received radar signal power statistics at Location 2 in Zone F4 for the CARSR.....	105
Figure B-18. Received radar signal power statistics at Location 3 in Zone F4 for the CARSR.....	106
Figure B-19. Received radar signal power statistics at Location 4 in Zone F4 for the CARSR.....	107
Figure B-20. Received radar signal power statistics at Location 5 in Zone F4 for the CARSR.....	108
Figure B-21. Received radar signal power statistics at Location 1 in Zone G1 for the CARSR.....	109
Figure B-22. Received radar signal power statistics at Location 2 in Zone G1 for the CARSR.....	110
Figure B-23. Received radar signal power statistics at Location 3 in Zone G1 for the CARSR.....	111
Figure B-24. Received radar signal power statistics at Location 4 in Zone G1 for the CARSR.....	112

Figure B-25. Received radar signal power statistics at Location 5 in Zone G1 for the CARSR.....	113
Figure B-26. Received radar signal power statistics at Location 1 in Zone G2 for the CARSR.....	114
Figure B-27. Received radar signal power statistics at Location 2 in Zone G2 for the CARSR.....	115
Figure B-28. Received radar signal power statistics at Location 3 in Zone G2 for the CARSR.....	116
Figure B-29. Received radar signal power statistics at Location 4 in Zone G2 for the CARSR.....	117
Figure B-30. Received radar signal power statistics at Location 5 in Zone G2 for the CARSR.....	118
Figure B-31. Received radar signal power statistics at Location 1 in Zone G3 for the CARSR.....	119
Figure B-32. Received radar signal power statistics at Location 2 in Zone G3 for the CARSR.....	120
Figure B-33. Received radar signal power statistics at Location 3 in Zone G3 for the CARSR.....	121
Figure B-34. Received radar signal power statistics at Location 4 in Zone G3 for the CARSR.....	122
Figure B-35. Received radar signal power statistics at Location 5 in Zone G3 for the CARSR.....	123
Figure B-36. Received radar signal power statistics at Location 6 in Zone G3 for the CARSR.....	124
Figure B-37. Received radar signal power statistics at Location 1 in Zone H1 for the CARSR.....	125
Figure B-38. Received radar signal power statistics at Location 2 in Zone H1 for the CARSR.....	126
Figure B-39. Received radar signal power statistics at Location 3 in Zone H1 for the CARSR.....	127
Figure B-40. Received radar signal power statistics at Location 4 in Zone H1 for the CARSR.....	128

Figure B-41. Received radar signal power statistics at Location 5 in Zone H1 for the CARSR.....	129
Figure B-42. Received radar signal power statistics at Location 6 in Zone H1 for the CARSR.....	130
Figure B-43. Received radar signal power statistics at Location 1 in Zone I1 for the CARSR.....	131
Figure B-44. Received radar signal power statistics at Location 2 in Zone I1 for the CARSR.....	132
Figure B-45. Received radar signal power statistics at Location 3 in Zone I1 for the CARSR.....	133
Figure B-46. Received radar signal power statistics at Location 4 in Zone I1 for the CARSR.....	134
Figure B-47. Received radar signal power statistics at Location 1 in Zone J1 for the CARSR.....	135
Figure B-48. Received radar signal power statistics at Location 2 in Zone J1 for the CARSR.....	136
Figure B-49. Received radar signal power statistics at Location 3 in Zone J1 for the CARSR.....	137
Figure B-50. Received radar signal power statistics at Location 4 in Zone J1 for the CARSR.....	138
Figure B-51. Received radar signal power statistics at Location 5 in Zone J1 for the CARSR.....	139
Figure B-52. Received radar signal power statistics at Location 1 in Zone J2 for the CARSR.....	140
Figure B-53. Received radar signal power statistics at Location 2 in Zone J2 for the CARSR.....	141
Figure B-54. Received radar signal power statistics at Location 3 in Zone J2 for the CARSR.....	142
Figure B-55. Received radar signal power statistics at Location 4 in Zone J2 for the CARSR.....	143
Figure B-56. Received radar signal power statistics at Location 5 in Zone J2 for the CARSR.....	144

Figure B-57. Received radar signal power statistics at Location 1 in Zone J3 for the CARSR.....	145
Figure B-58. Received radar signal power statistics at Location 2 in Zone J3 for the CARSR.....	146
Figure B-59. Received radar signal power statistics at Location 3 in Zone J3 for the CARSR.....	147
Figure B-60. Received radar signal power statistics at Location 4 in Zone J3 for the CARSR.....	148
Figure B-61. Received radar signal power statistics at Location 5 in Zone J3 for the CARSR.....	149
Figure B-62 Received radar signal power statistics at Location 1 in Zone D4 for the CARSR.....	150
Figure B-63 Received radar signal power statistics at Location 1 in Zone D5 for the CARSR.....	151

TABLES

Table 1. Median peak over-the-air system noise power for each preselector path.....	10
Table 2. Measured received power statistics at measurement locations for the ASR-9 radar in Trout Creek, Utah.....	29
Table 3. Measured received power statistics at measurement locations for the CARSR radar in Cedar City, Utah.....	31
Table 4. ASR-9 radar transmitter and receiver parameters for ITM predicted power.....	35
Table 5. CARSR radar transmitter and receiver parameters for ITM predicted power.....	35

ACRONYMS/ABBREVIATIONS

AC	alternating current
AGL	above ground level
Ant	antenna
ASR-9	Airport Surveillance Radar, Model 9
BPF	bandpass filter
CARSR	Common Air Route Surveillance Radar
CW	continuous wave
dB	decibel(s)
dB_i	decibel(s) referenced to isotropic
dB_m	decibel(s) referenced to 1 milliwatt
Freq	frequency
GHz	gigahertz
GPS	Global Positioning System
IF	intermediate frequency
ITM	Irregular Terrain Model
ITS	Institute for Telecommunication Sciences
kHz	kilohertz
km	kilometer(s)
Lat	latitude
LNA	low-noise amplifier
Lon	longitude
LPF	low-pass filter
m	meter(s)
Max	maximum

Min	minimum
MHz	megahertz
NC	normally closed
NTIA	National Telecommunications and Information Administration
Num	number
OSM	Office of Spectrum Management
ppr	pulse repetition rate
pps	pulses per second
Prop	propagation
PSCR	Public Safety Communications Research
Pwr	power
Quart	quartile
RBW	resolution bandwidth
RF	radio frequency
RSMS-5G	Radio Spectrum Measurement System Fifth Generation
Rx	receiver
SPDT	single-pole, double-throw
Tx	transmitter
W	watt(s)

GLOSSARY

60 dB/ 3 dB Shape Factor: A measure of the steepness of the rolloff of a filter; given as the ratio of the 60-dB bandwidth divided by the 3-dB bandwidth of the filter.

Frequency Assignment: An NTIA-issued frequency authorization allowing an agency to operate an RF system on a specific frequency or frequencies at a particular location or within a defined area with specified technical parameters.

Irregular Terrain Model (ITM): A radio propagation model, developed by ITS, that predicts the median attenuation of a radio signal as a function of distance and the variability of the signal in time and in space, for frequencies between 20 MHz and 20 GHz.

Median Peak Over-The-Air System Noise Power: Median of the peak-detected RF power of the measurement system with the antenna connected to the RF input of the preselector and no intentionally emitted signals observable.

Multipath: Multiple received copies of a transmitted signal (radar signal in this case) caused by the direct ray and reflected rays from the transmitter (radar) antenna main beam, sidelobes, and backlobe.

Noise Diode Calibration: A measurement procedure performed on an RF measurement system that provides the overall measurement system noise figure and preselector gain (if a preselector is present).

Noise Figure: A measure of the amount of noise a device or system produces above the thermal noise level; formally defined as the ratio of the input signal to noise ratio divided by the output signal to noise ratio of a device or system, expressed in decibels.

Over-The-Air System Noise Floor: The peak-detected power, measured by the measurement system with the antenna connected to the RF input of the preselector, as a function of frequency with no intentionally emitted signals observable.

Peak Detected Time Signature: The shape of the received signal power of the radar as the radar rotates and is captured with the spectrum analyzer sweep in zero-span mode.

Peak Detection: A spectrum analyzer detection mode where the value of each display point is the peak value of all digitized samples that were collected within the time duration used to generate the display point. For example, if the time duration used to generate an analyzer display point is 1 millisecond but 1,000 digitized samples were collected by the analyzer during that millisecond, then the peak-detected value for the display point is the highest-power of the 1,000 samples.

Potential Radar Signal: A signal identified by the automated data processing that appears to be a radar signal.

Preselector: A device used on the input of a radio receiver measurement system, after the receive antenna, that attenuates unwanted out-of-band signals, improves the sensitivity of the measurement system, and enables measurement system calibrations.

Propagation Mode: The classification of the type of radio propagation a signal experiences (line-of-sight, diffraction, tropospheric scatter) over a geographical path as predicted by ITM.

Quantitative Assessments of Spectrum Usage: Data from the frequency assignment for each RF system's individual transmitting and receiving stations used to develop an approximation of each RF system's actual use of the spectrum in terms of frequency, geography, and time.

Received Signal Power: The strength of a radio signal as measured at the receiver (RF input of the preselector in this measurement system), typically given in units of dBm in the receiver's resolution bandwidth (RBW).

Resolution Bandwidth (RBW): A measure of the width of the intermediate frequency (IF) filter (typically the 3 dB bandwidth) in a spectrum analyzer. It gives an indication of how closely spaced in frequency two continuous-wave (CW) signals can be and yet remain distinguishable.

Spectrum Analyzer Sweep: A set of signal power measurements collected and displayed on a spectrum analyzer at specified time intervals over a specified duration when the analyzer is in zero-span mode (or at specified frequency intervals over a specified frequency range when the analyzer is in its default mode). For example, a spectrum analyzer sweep might consist of 2,501 displayed points (each a separately measured power value) collected over the duration of 2.5 seconds. Each power value in the sweep represents the behavior of the analyzer's detector, in the analyzer's selected resolution bandwidth, for, in this example,

$$\frac{2500 \text{ milliseconds}}{(2501 \text{ points} - 1)} = 1 \text{ millisecond of time.}$$

Spectrum Usage Contour: The geographical region surrounding a transmitter outside of which the received signal power from the transmitter is predicted to be less than a pre-defined threshold relative to the thermal noise floor.

System Noise Floor: The peak-detected internal noise power, measured by the measurement system with a 50 Ω load on the RF input of the preselector, as a function of frequency.

Time-domain Measurements: Signal power measurements that are taken at specified intervals of time.

Valid Radar Signal: A potential radar signal that has all n data points ($n = 8$ for both the ASR-9 and CARSR) of its peak detected time signature above a threshold (6dB above the median peak over-the-air system noise power level).

Zero-span Mode: A spectrum analyzer operating mode where the local oscillator is held at a constant frequency (the local oscillator sweeps in frequency in the spectrum analyzer default mode), causing the data output to be signal power as a function of time.

RECEIVED SIGNAL POWER MEASUREMENTS ON SELECT AIR TRAFFIC CONTROL RADARS IN UTAH

Jeffery A. Wepman,¹ Edward F. Drocella,² April Lundy,² Mike Chang,¹
Linh P. Vu,¹ Kenneth J. Brewster,¹ and Paul M. McKenna¹

Received signal power measurements were performed on the Common Air Route Surveillance Radar (CARSR) operating in the 1300-1370 MHz band in Cedar City, Utah, and on the Airport Surveillance Radar (ASR-9) operating in the 2700-2900 MHz band in Trout Creek, Utah. The measurements were taken at sites relatively far from each radar transmitter. The measurement locations represent different predicted propagation modes (such as line-of-sight, diffracted, tropospheric scatter, etc.) and varying predicted received signal powers (from strong to weak). Distances from the transmitter to the measurement locations varied from roughly 56 km to 141 km for the ASR-9 and 17 km to 194 km for the CARSR. Multiple peak received signal power measurements were made at each location to provide statistically significant results. In another effort, these measurements will be used to validate spectrum usage contours and the methodology used to generate them as developed by the Office of Spectrum Management (OSM) of the National Telecommunications and Information Administration (NTIA).

Keywords: Received signal power measurements, peak received signal power, ASR-9, CARSR, radar measurements, spectrum usage contours

1. INTRODUCTION

The objective of this work was to conduct received signal power measurements on select air traffic control radars and provide measured data results that can be used (in a separate effort) to validate spectrum usage contours³ and the Quantitative Assessments of Spectrum Usage methodology used to generate them, as developed by the Office of Spectrum Management (OSM) of the National Telecommunications and Information Administration (NTIA) [1].

Initially, to address this objective, the Institute for Telecommunication Sciences (ITS) performed received signal power measurements in May 2017 on the Common Air Route Surveillance Radar

¹ The authors are with the National Telecommunications and Information Administration (NTIA), Institute for Telecommunication Sciences (ITS), U.S. Dept. of Commerce, 325 Broadway St., Boulder, Colorado 80305.

² The authors are with the NTIA Office of Spectrum Management (OSM), U.S. Dept. of Commerce, 1401 Constitution Ave. NW, Washington, DC 20021.

³ A spectrum usage contour represents the geographical region surrounding a transmitter outside of which the received signal power from the transmitter is predicted to be less than a pre-defined threshold relative to the thermal noise floor.

(CARSR) operating in the 1300–1370 MHz band in Parker, Colorado and the Airport Surveillance Radar (ASR-9) operating in the 2700–2900 MHz band in Platteville, Colorado. Those measurements are described in detail in [2].

Continuing to address this objective, this report describes received signal power measurements performed by ITS on two new radars during April and May 2018: the CARSR operating in the 1300–1370 MHz band in Cedar City, Utah and the ASR-9 operating in the 2700–2900 MHz band in Trout Creek, Utah. Received signal power measurements were taken at a received antenna height of 2.2 m above ground level (AGL) at a set of fixed locations along accessible roads at varying distances from the transmitter locations. Multiple received signal power measurements at each fixed location were made to provide statistically significant results.

Hereafter in this report, the initial ITS measurements on the CARSR and ASR-9 in Colorado taken in May 2017, will be referred to as the Colorado measurements.

2. MEASUREMENT SYSTEM

2.1 Measurement System Design

A block diagram of the measurement system used during the data collection is shown in Figure 1. The system consists of an antenna, a preselector, a spectrum analyzer, a GPS antenna and receiver, and a measurement controller. For these measurements, the measurement system was installed in the ITS Public Safety Communications Research (PSCR) measurement van, a modified Chevrolet Express 3500 Passenger Van. This vehicle is shown in Figure 2. The use of this vehicle represents several improvements over the ITS modified Chevrolet Express 3500 Extended Cargo Van used for the Colorado measurements. The primary advantages of using the PSCR measurement van instead of the Cargo Van are the smaller size, a diesel engine, built-in DC to AC power inverter (which exhibits significantly less radiated noise at 1300 MHz than the built-in gasoline generator in the Cargo Van), more secure seating for additional measurement personnel (when more than two people are required for the measurements), and four-wheel drive.

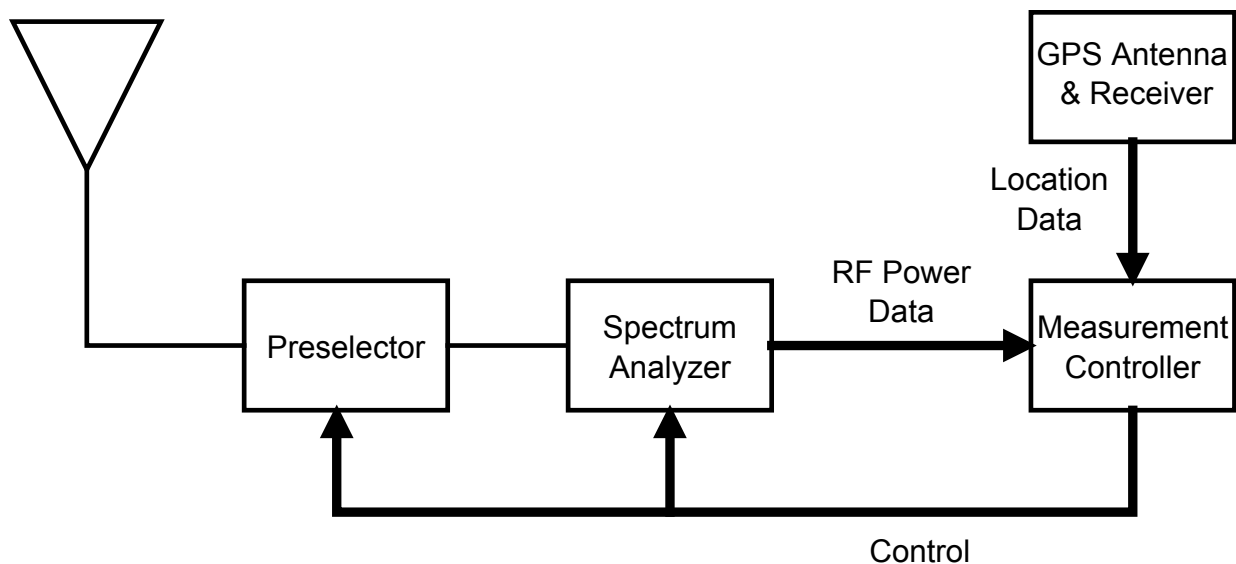


Figure 1. Block diagram of the measurement system.



Figure 2. ITS PSCR Measurement Van (modified Chevrolet Express 3500 Passenger Van).

Frequency assignment records list the polarizations of the antennas for both the ASR-9 and the CARSR as right and left-hand circular. The measurement system uses a slant-polarized, omnidirectional, biconical antenna (Watkins-Johnson WJ-48955). The slant-polarized antenna has the distinct advantage of being able to receive vertically, horizontally, and both left- and right-hand circularly-polarized signals with the same gain, albeit 3 dB lower than for slant-polarized signals. Hence it is an appropriate antenna to use for these measurements.

Antenna gain and azimuthal pattern measurements were made with the slant-polarized omnidirectional antenna mounted on the measurement vehicle (as shown in Figure 2) using the antenna turntable at the ITS Table Mountain Field Site and Radio Quiet Zone in 1 MHz steps at frequencies 1305–1390 MHz and 2700–2900 MHz. The antenna measurements were made using the three-antenna method for determining antenna gain [3]. This method uses three different antennas (antennas A, B, and C) to determine the gain of all three antennas. Three separate antenna gain and pattern measurements were made using antennas A for receive and B for transmit, antennas A for receive and C for transmit, and antennas B for receive and C for transmit. In this case, antenna A was the slant-polarized omnidirectional antenna used in the received signal power radar measurements. Antennas B and C were general purpose, wideband, vertically-polarized omnidirectional antennas. The transmission loss between each of the three antenna combinations as a function of azimuthal angle was measured. From this, the median antenna gain (median of dBi values) of the slant-polarized omnidirectional antenna over all azimuthal angles was determined to be -2.8 dBi for the CARSR (1318 MHz) and -2.2 dBi for the ASR-9 (2860 MHz). Since the slant-polarized antenna will receive left or right-hand circularly-polarized signals with the same gain as a vertically-polarized signal, these gain values are valid for the circularly-polarized transmissions of the ASR-9 and CARSR radars.

A simplified block diagram of the preselector is shown in Figure 3. The preselector is custom-built by ITS and performs several crucial functions for the measurement system. It attenuates unwanted out-of-band signals via RF filtering, improves the sensitivity of the system with a low-noise amplifier, and enables measurement system calibrations via a built-in noise diode. Measurement system calibrations provide assurance that the measurement system is operating properly. They also provide measurements of the preselector gain and system noise figure. Preselector gain is particularly important to be able to determine absolute received power at the input to the preselector.

The preselector provides the capability to automatically switch between two filter paths under software control. Each filter path consists of a manually-tunable bandpass filter with a 5% 3 dB bandwidth whose center frequency is set to the center frequency of the radar to be measured. One tunable bandpass filter covers the 1000–2000 MHz range with a 60 dB/3 dB shape factor of 3.2 while the other covers the 2000–4000 MHz range with a 60 dB/3 dB shape factor of 3.7. A low-noise amplifier can be invoked under software control after each of these filter paths to improve the sensitivity of the measurement system. This enables measurement of the low-level transmissions expected at distances far from the radar transmitter. The preselector also contains a noise diode that is utilized under software control to perform measurement system calibrations.

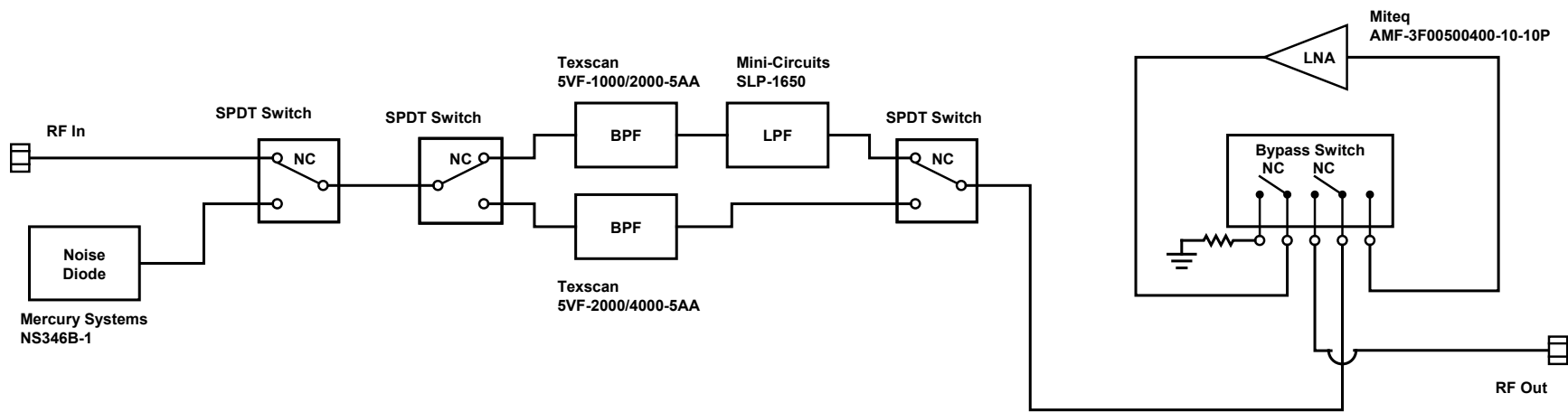


Figure 3. Simplified block diagram of the preselector (Ethernet control is not shown).

The spectrum analyzer (Keysight N9030B⁴) is the core of the overall measurement system. It takes the RF signals received by the antenna and conditioned by the preselector, and provides peak power measurements of the received radar transmissions in a user-selected resolution bandwidth (RBW). Automated control of the preselector and spectrum analyzer is provided by the measurement controller. The measurement controller is also custom-built by ITS and consists of a custom-built computer, Ethernet switch, and power supply for the preselector.

The spectrum analyzer, GPS antenna and receiver (GlobalSat Technology Corporation BU-353S4), and measurement controller combination collects the received signal RF peak power measurement data tagged with location information, formats the data, and saves the data to a local hard drive on the measurement controller.

2.2 Measurement System Noise Floor Characterization

To obtain an understanding of the received power levels that can be detected with the measurement system, a set of over-the-air noise measurements was performed to characterize the over-the-air system noise floor. These measurements were performed with the measurement system installed in the measurement vehicle with AC power supplied by the vehicle's DC to AC power inverter with the engine running. For these measurements, the vehicle was parked in the parking area of Building A4 at the U.S. Department of Commerce ITS Table Mountain Field Site and Radio Quiet Zone near Boulder, Colorado. For these noise measurements, the system was tuned to center frequencies as close as possible to the Trout Creek ASR-9 and the Cedar City CARSR radar center frequencies but where no signals were detected at our Table Mountain location. A frequency of 2860 MHz was used to represent the ASR-9 and 1327 MHz was used to represent the CARSR since no signals were seen at these frequencies at the Table Mountain location.

Figures 4 and 5 show the over-the-air system noise floor of the measurement system (referenced to the RF input of the preselector) at 2860 MHz (right at the center frequency of the Trout Creek ASR-9) both without and with the low-noise amplifier, respectively. Note that the RBW and detection mode were the same as used in the radar measurements, namely a 3 MHz RBW and peak detection. Comparison of these measurements with system noise floor measurements taken with a 50 Ω load on the RF input to the preselector show negligible difference, indicating that any external noise is below the system noise floor. The median peak over-the-air system noise power (referenced to the RF input of the preselector) for the ASR-9 is -61.2 dBm without the low-noise amplifier and -92.8 dBm with the low-noise amplifier.

⁴ Using the Keysight N9030B spectrum analyzer in place of the Agilent E4440A spectrum analyzer that was used during the Colorado measurements improved the reliability of the measurement system.

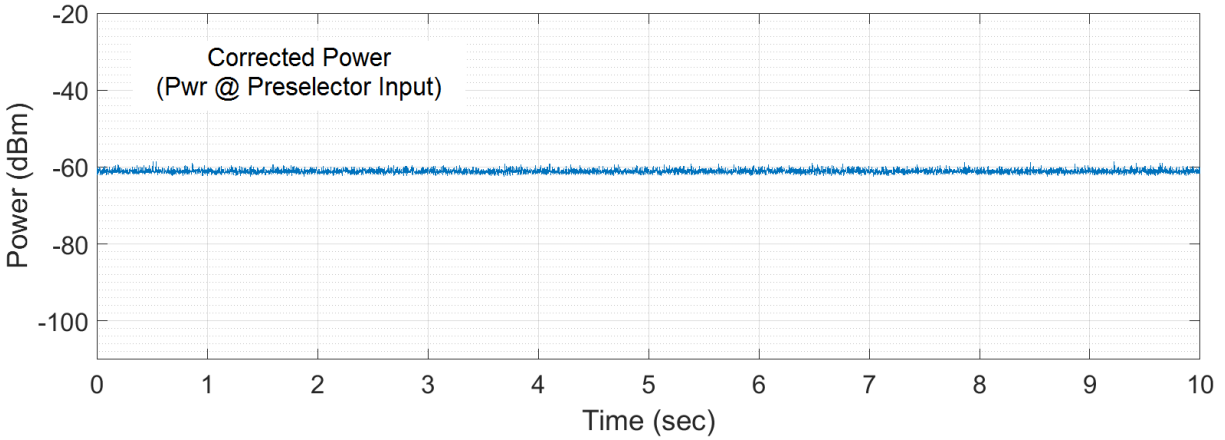


Figure 4. Over-the-air system noise floor of the measurement system at 2860 MHz in a 3 MHz RBW using peak detection without the low-noise amplifier (AC power via measurement vehicle’s internal DC to AC power inverter).

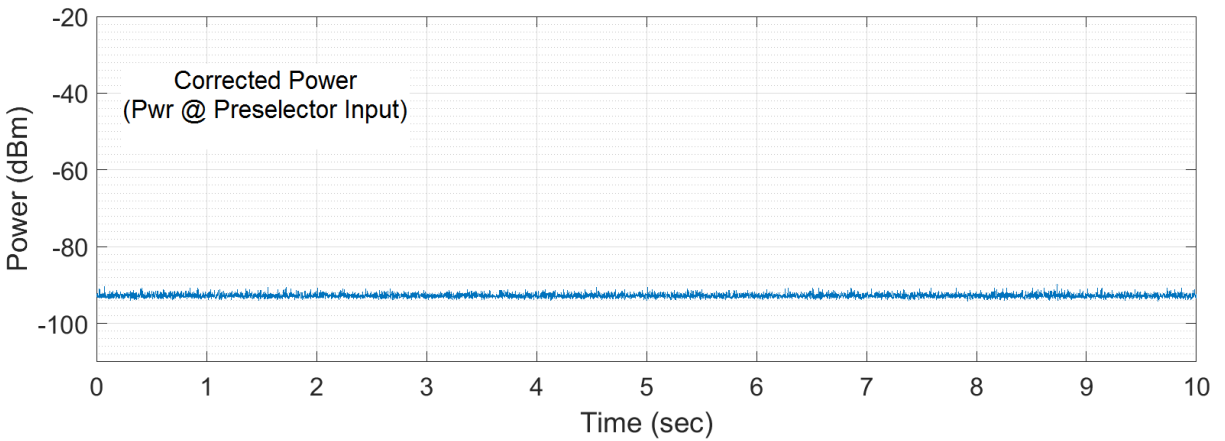


Figure 5. Over-the-air system noise floor of the measurement system at 2860 MHz in a 3 MHz RBW using peak detection with the low-noise amplifier (AC power via measurement vehicle’s internal DC to AC power inverter).

Figures 6 and 7 show the over-the-air system noise floor of the measurement system (referenced to the RF input of the preselector) at 1327 MHz (near the center frequency of the Cedar City CARSR) both without and with the low-noise amplifier, respectively. Note that the RBW and detection mode were also the same as used in the radar measurements, namely a 300 kHz RBW and peak detection. Comparison of these measurements with noise floor measurements taken with a 50 Ω load on the RF input to the preselector show negligible difference, indicating that any external noise is also below the system noise floor. The median peak over-the-air system noise power (referenced to the RF input of the preselector) for the CARSR is -77.6 dBm without the low-noise amplifier and -106.9 dBm with the low-noise amplifier.

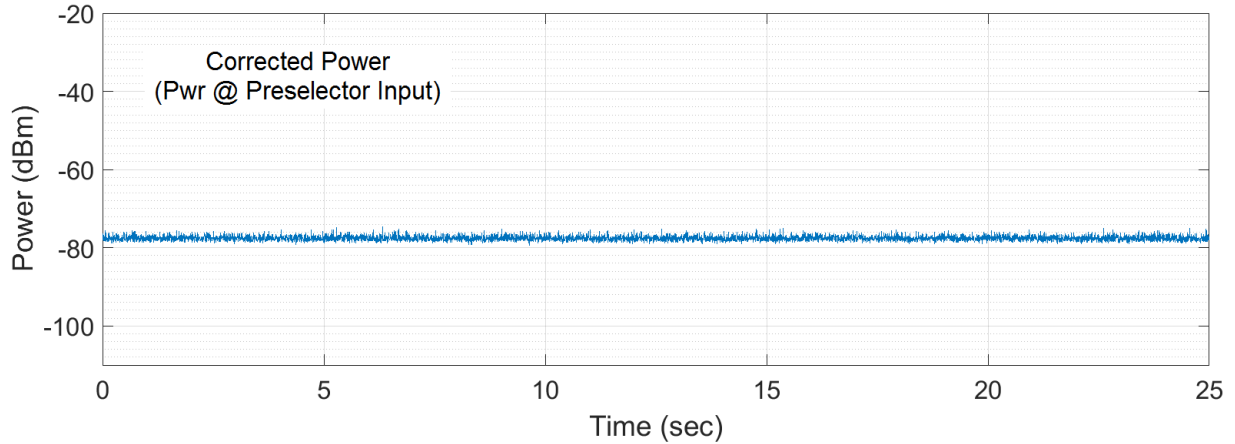


Figure 6. Over-the-air system noise floor of the measurement system at 1327 MHz in a 300-kHz RBW using peak detection without the low-noise amplifier (AC power via measurement vehicle’s internal DC to AC power inverter).

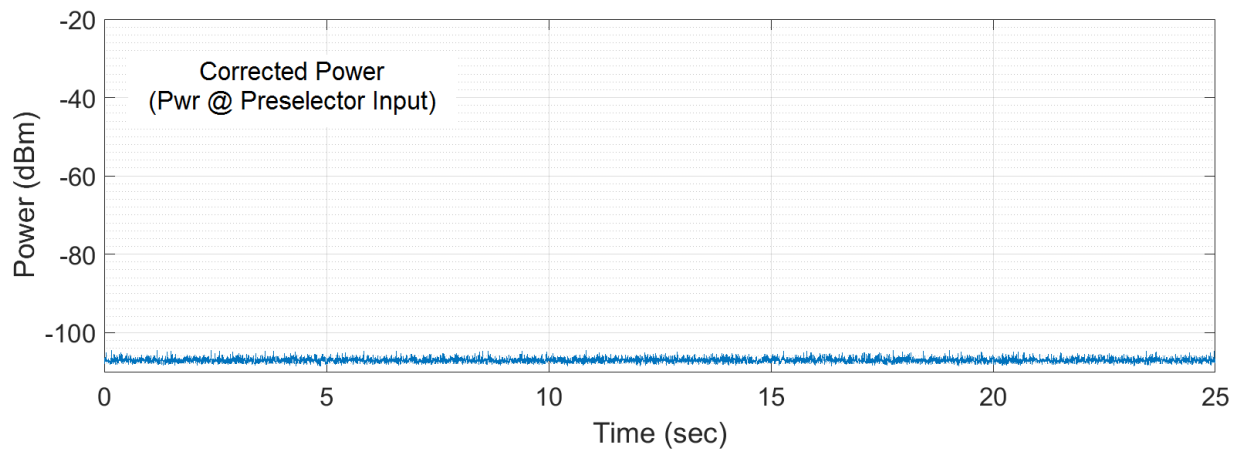


Figure 7. Over-the-air system noise floor of the measurement system at 1327 MHz in a 300-kHz RBW using peak detection with the low-noise amplifier (AC power via measurement vehicle’s internal DC to AC power inverter).

A summary of the median peak over-the-air system noise power in a given RBW for each preselector path (referenced to the RF input of the preselector) both with and without the low-noise amplifier is given in Table 1.

Table 1. Median peak over-the-air system noise power for each preselector path.

Preselector Path	Median Peak Over-The-Air System Noise Power (dBm)
ASR-9 without low-noise amplifier	-61.2 (3 MHz RBW)
ASR-9 with low-noise amplifier	-92.8 (3 MHz RBW)
CARSR without low-noise amplifier	-77.6 (300 kHz RBW)
CARSR with low-noise amplifier	-106.9 (300 kHz RBW)

The over-the-air noise floor performance of this measurement system in the 1300 MHz band represents a significant improvement over the measurement system used in the Colorado measurements. The improvement is due to using the PSCR measurement van instead of the Cargo Van for housing the measurement system. The diesel engine and the built-in DC to AC power inverter in the PSCR measurement van exhibit significantly less radiated noise in the 1300 MHz band than the built-in gasoline generator in the Cargo Van (used to house the measurement system for the Colorado measurements).

3. MEASUREMENT LOCATION SELECTION

3.1 Previous Measurement Location Selection Methodology

Measurement site selection for the Colorado measurements was done by using radials emanating from the transmitter locations as a guide. Predictions of received signal power along these radials were made using the Irregular Terrain Model (ITM) [1]. Specific site locations along these radials were chosen with consideration of predicted received signal power at potential locations, predicted propagation modes at potential locations (such as line-of-sight, diffracted, tropospheric scatter, etc.), the availability of suitable roads for access in the area, and the suitability of places to park the measurement vehicle to conduct measurements. An attempt was made to select four or five potential measurement locations along each radial for each transmitter where the predicted received signal power varied from a relatively strong to weak (but still detectable) level. An attempt was also made to select potential measurement locations along the radials where as many different propagation modes as possible could be represented.

The actual measurements were taken at locations as close to the potential measurement locations as possible given the practical constraints of roads, significant obstructions (such as large trees, power lines, buildings, etc.), and the ability to safely park the measurement vehicle.

This radial-based method of measurement site selection resulted in selection of sites that required a disproportionate amount of time driving on small, rural, dirt roads to access locations. In an effort to reduce the amount of driving time and maximize the number of measurement locations to be measured, a new methodology of selecting measurement sites, more closely based on existing roads, was used.

3.2 New Measurement Location Selection Methodology

The new methodology of measurement location selection consisted of several steps. First, expected propagation loss (from which expected received signal power can be determined) and propagation mode over an area surrounding the radar transmitter were determined using ITM at points along concentric circles with radii of increasing distance from the radar transmitter. The predicted propagation loss and propagation mode at points along the concentric circles were used as a rough guide to select candidate measurement sites along actual existing roads. An attempt was made to choose candidate measurement locations likely to have predicted received signal power levels 10 dB or more above the peak measurement system noise floor. Because of this, candidate measurement locations tended to be significantly closer to the radar transmitter than the spectrum usage contours were to the radar transmitter. Google My Maps[®] was used to manually add to a map candidate measurement locations that were on small roads just slightly off major roads or along major roads if appropriate places to park the vehicle were available. If at all possible, candidate measurement locations were selected at roughly 1 km intervals traveling generally away from the transmitter.

The next step was to save the manually added candidate measurement locations to a .csv file using Google My Maps[®]. The expected propagation loss at these candidate measurement

locations was then determined from ITM. Potential measurement locations were selected from the candidate measurement locations based on several criteria.

- Predicted received signal power levels that are 10 dB or more above the peak measurement system noise floor
- Predicted received signal power variation from a relatively strong to weak (but still detectable) level
- Representation from as many different propagation modes as possible
- Avoidance of any significant obstructions (such as large trees, power lines, buildings, etc.) that could be determined a priori

Actual measurements were taken at locations as close to these potential measurement locations as possible given the practical constraints of roads, significant obstructions (such as large trees, power lines, buildings, etc.), and the ability to safely park the measurement vehicle. The potential (and actual) measurement locations were organized into various zones about each radar transmitter. Each measurement location is identified by a Zone and Location Number. The actual measurement locations used, identified by their Zone and Location Number along with their coordinates, are listed in Tables 2 and 3 for the ASR-9 in Trout Creek, Utah, and the CARSR in Cedar City, Utah, respectively. Measurements were taken at a total of 49 measurement locations for the ASR-9 and a total of 63 measurement locations for the CARSR.

Figure 8 shows a map of the predicted spectrum usage contour, radar transmitter location, and all of the actual measurement locations for the ASR-9 in Trout Creek, Utah. An expanded view of this map, showing the area inside the rectangle, is given in Figure 9. Figure 10 shows a map with the predicted spectrum usage contour, radar transmitter location, and all of the actual measurement locations for the CARSR in Cedar City, Utah. An expanded view of this map, showing the area inside the rectangle, is given in Figure 11. The intent of the maps is to give a general idea of where the measurement locations are with respect to the radar transmitter and the spectrum usage contour. Because of this, the scale of the maps is such that the identification of each individual measurement location is not possible, but the Zones are identified on the maps showing the expanded view.

While measurements ideally would be made at locations around the contour, typically the signal level at the contours is either not detectable or only rarely detectable. Therefore, in these measurements, the measurement locations were selected to both represent all of the various propagation modes that could be expected (line-of-sight, diffracted, tropospheric scatter, etc.) and yet still have a predicted received signal power level 10 dB or more above the measurement system noise floor. Thus, the measurement locations were significantly closer to the radar transmitter than the spectrum usage contours; measurements at or near the spectrum usage contours were not made.

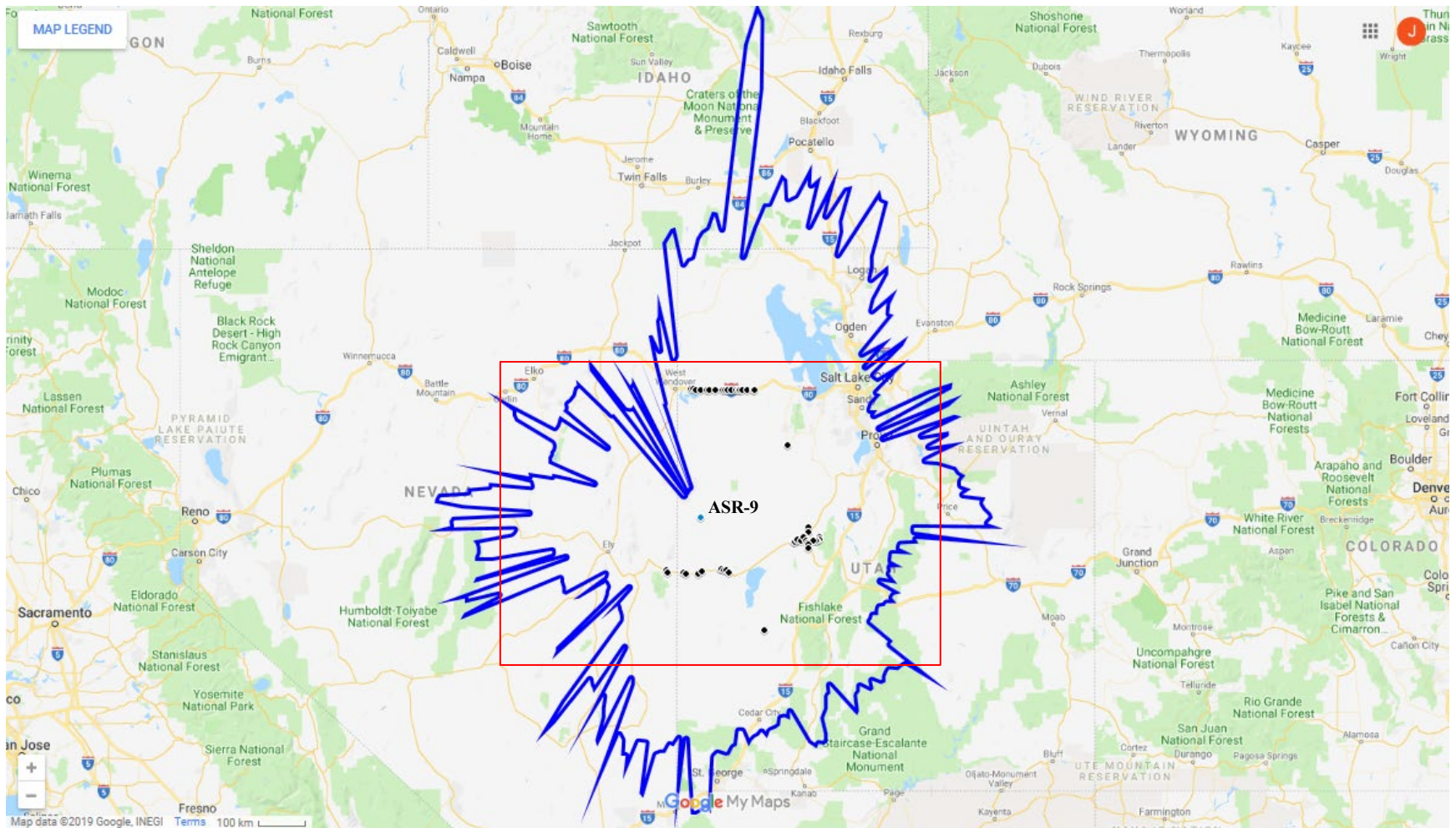


Figure 8. Spectrum usage contour, radar transmitter, and actual measurement locations for the ASR-9 in Trout Creek, Utah. An expanded view of the map showing the area inside the rectangle is given in Figure 9.



Figure 9. Expanded view of the map showing actual measurement locations for the ASR-9 in Trout Creek, Utah.

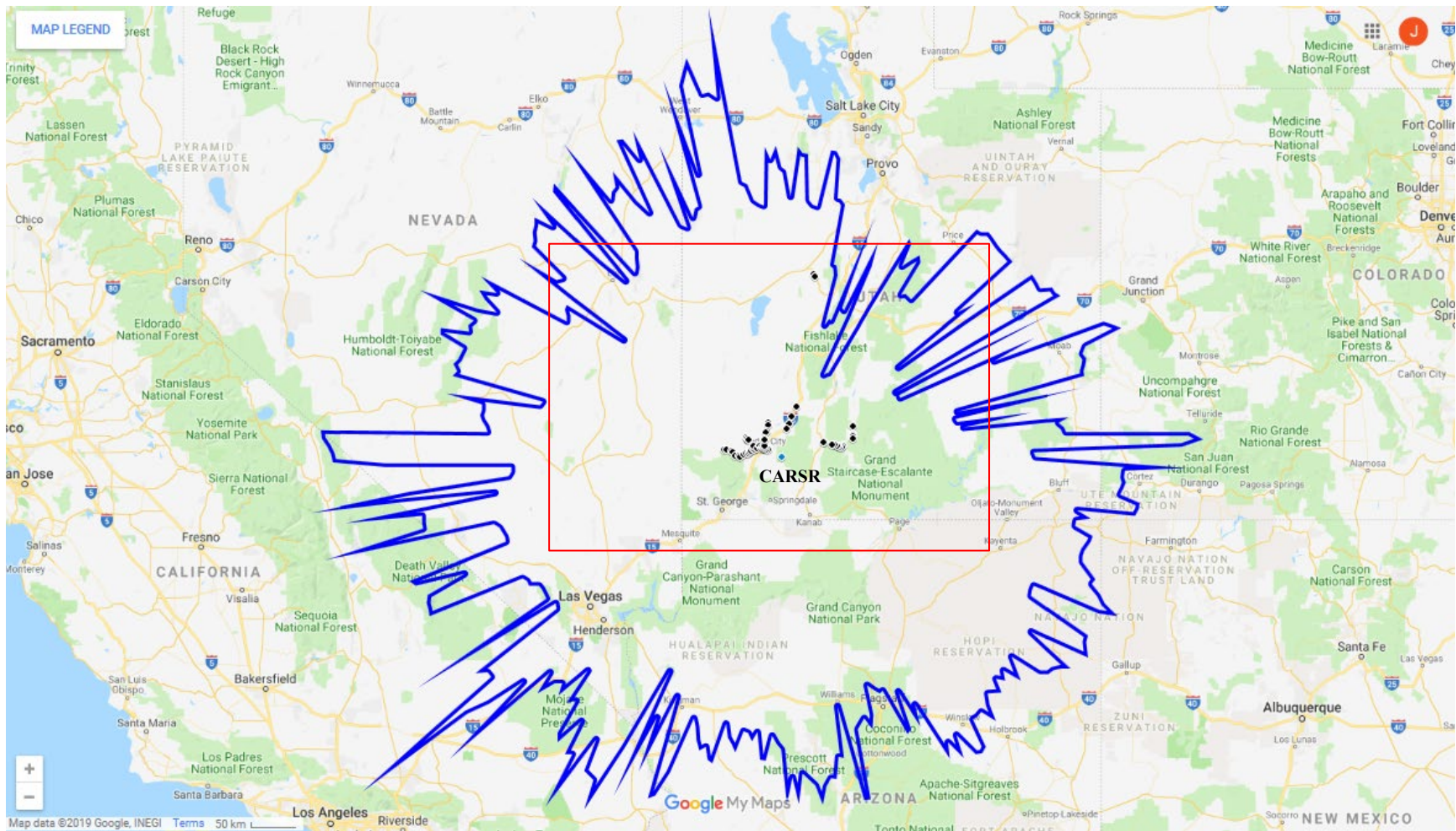


Figure 10. Spectrum usage contour, radar transmitter, and actual measurement locations for the CARSR in Cedar City, Utah. An expanded view of the map showing the area inside the rectangle is given in Figure 11.

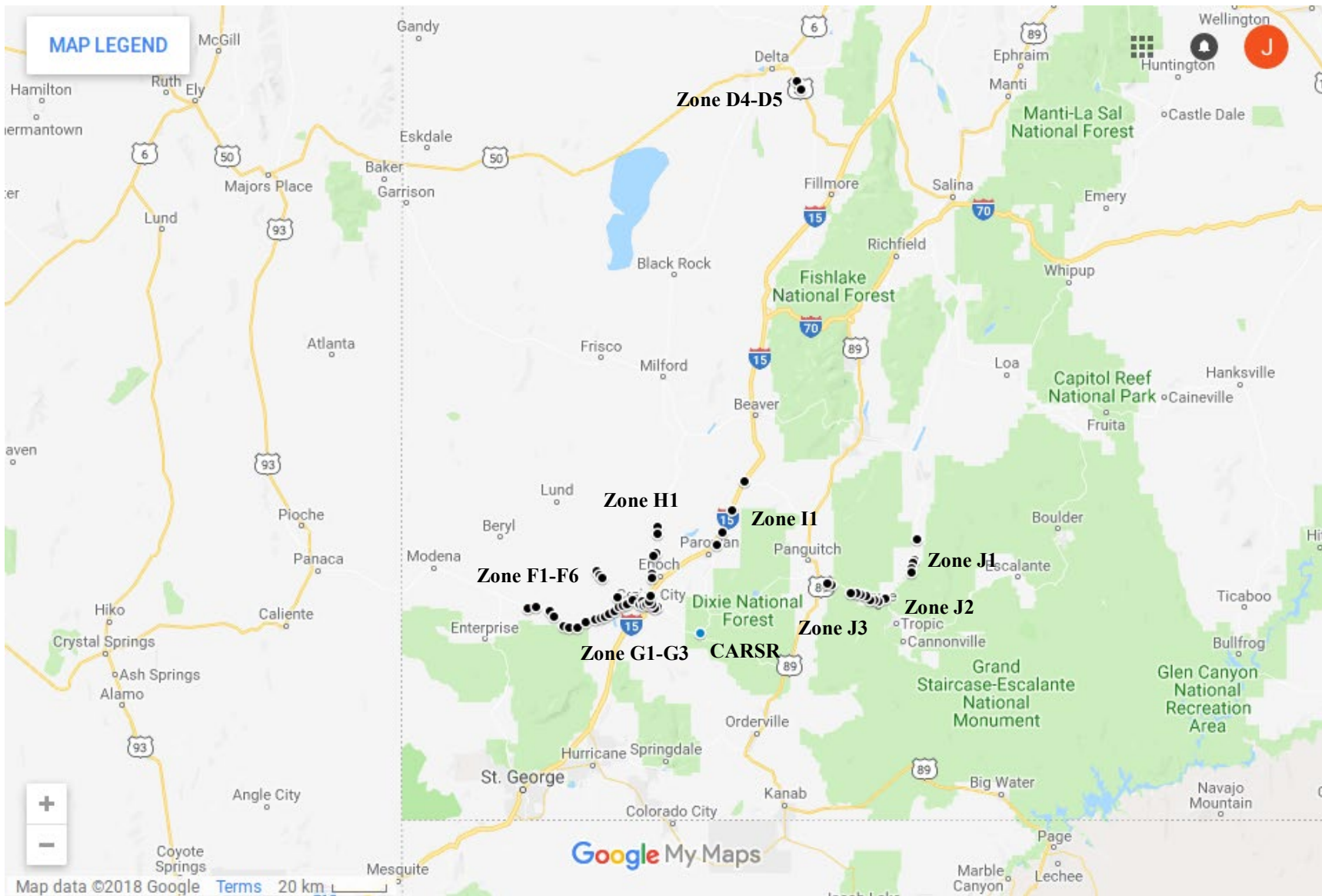


Figure 11. Expanded view of the map showing actual measurement locations for the CARSR in Cedar City, Utah.

4. MEASUREMENT PROCEDURE

At each measurement location, the following general procedure was followed:

- 1) Set preselector path to use the appropriate tunable bandpass filter for the radar to be measured.
- 2) Determine if the low-noise amplifier is to be used or not based on the expected received signal power. No amplifier is used if the received signal power is expected to be greater than -40 dBm at the preselector input.
- 3) Perform a noise diode calibration with the current preselector settings. The noise diode calibration uses the traditional Y-factor method (where the calibration measurement is performed twice, once with the diode turned on and once with the diode turned off; the gain and noise figure are determined by Y , the difference between the measured power in decibels with the diode on and the measured power in decibels with the diode off). This calibration provides assurance that the measurement system is operating properly and provides measurements of the preselector gain and system noise figure. The preselector gain is subtracted from the received power measured at the RF input of the spectrum analyzer to provide calibrated power measurements referenced to the preselector input RF connector.
- 4) Start the radar measurement (details of the radar measurement are described in Section 5 below).
- 5) Observe the received signal power data being collected on the measurement controller computer display.
 - a) The data are observed to ensure that the radar signal is detectible, to determine the appropriate spectrum analyzer attenuation to use,⁵ to determine if the preselector low-noise amplifier should be used, and to determine if any measurement system overload conditions exist.
 - b) Based on the results of this data observation, data collection is either allowed to continue to completion (signifying that the choice of using the amplifier or not was correct and the selection of spectrum analyzer attenuation was correct) or is terminated. If data collection is terminated, the preselector settings are changed. (The initial choice of using the amplifier or not is reversed and the spectrum analyzer attenuation is modified if needed.) Then the noise diode calibration is redone and the radar measurement is redone.

⁵ Note that the default spectrum analyzer attenuation for the measurements was set to 10 dB. While this attenuation could be changed, it was not changed for the measurements discussed in this report. The option for increasing the attenuation exists to accommodate measuring very high signal levels when not using the amplifier. Decreasing the attenuation does not have a significant advantage for this measurement system since it will not significantly improve the system sensitivity and will slightly degrade the measurement accuracy. The reason that the system sensitivity is not significantly improved is that the low-noise amplifier gain in the preselector is high enough that the noise figure of the low-noise amplifier dominates the overall measurement system noise figure even with 10 dB of spectrum analyzer attenuation invoked.

5. RADAR MEASUREMENTS

The radar measurements were made using the swept-measurement mode of the Radio Spectrum Measurement System Fifth Generation (RSMS-5G) software. The spectrum analyzer was set up in the zero-span mode (providing time-domain measurements) using peak detection with a sweep time set slightly longer than two times the rotation period⁶ of the radar to be measured. This ensures data capture of at least two rotations of the radar. Capturing at least two rotations of the radar allows for easier identification of the radar and permits the peak received power of the radar to be measured. The rotation period of the ASR-9 is roughly 4.6 seconds and a spectrum analyzer sweep time of 10 seconds was chosen. The rotation period of the CARSR is roughly 12 seconds and a spectrum analyzer sweep time of 25 seconds was chosen. The number of spectrum analyzer display points per sweep for each radar was determined so that the display bin width of the spectrum analyzer is greater than the maximum pulse repetition interval of the radar. This is done to ensure that the peak of at least one radar pulse (if it is detectable) will be captured for each spectrum analyzer display point. Therefore, the number of spectrum analyzer display points per sweep N needs to satisfy

$$\text{Display Bin Width} = \frac{\text{Sweep Time}}{N-1} > \text{Maximum Pulse Repetition Interval} \quad (1)$$

Since the sweep time for each radar was already chosen, selecting N requires the maximum pulse repetition interval to be known. The maximum pulse repetition interval for each radar was determined as the maximum of that observed from preliminary field measurements of the radars and that listed in the frequency assignment records. As listed in the frequency assignment records for the ASR-9, this maximum pulse repetition interval was

$$\frac{1}{prp} = \frac{1}{928 \text{ pps}} \cong 1.078 \text{ ms},$$

where prp is the pulse repetition rate and pps is the number of pulses per second. Selecting $N = 6500$ for the ASR-9 results in a display bin width of 1.539 ms which satisfies (1). For the CARSR, the maximum pulse repetition interval was 3.474 ms as seen during the preliminary field measurements. Therefore, selecting $N = 6250$ for the CARSR results in a display bin width of 4.001 ms that satisfies (1).

Note that while the selection of N produces an aesthetically pleasing peak-detected time domain capture, it is the peak detection on the spectrum analyzer that ensures that the maximum power of the received radar signal is not missed.

The RBW to use for the measurements was determined empirically by the preliminary field measurements of signals from both radars. During the preliminary field measurements, measurements of peak received power from the radar transmissions were made at varying RBWs from 51 kHz to 8 MHz. Using this method, RBWs that are too narrow do not capture all of the

⁶ The ASR-9 and CARSR utilize mechanically rotated antennas that produce radiation beams that are narrow in azimuth but broad in elevation. They do not form pencil beams or perform any electronic beam steering or frequency hopping that would otherwise complicate the measurements.

power of the received radar emissions. RBWs that are too wide, while capturing all of the power of the received radar emissions, also include more noise (both internal measurement system noise and external noise) in the power measurement than is necessary or desirable. Additionally, in the case of the CARSR, bandwidths that are too wide include power from the nearby paired transmission of the radar thus providing inaccurate results. Using this method, a 3 MHz RBW for the ASR-9 and a 300 kHz RBW for the CARSR were determined to be optimal.

Seventy-five spectrum analyzer sweeps were taken at each location. The number of sweeps was chosen to be as large as practical to provide statistically significant results of peak received signal power. Measurement time at each location was limited due to the relatively large number of measurement locations, measurement setup time, the need for occasional measurement system troubleshooting, and the need for calibration at each location. Since the data collection is asynchronous (i.e., the radar transmissions are not synchronized with the start of the sweeps in the spectrum analyzer) and the sweep time is long enough to always capture at least two main beam radar transmissions, the 75 sweeps provide the opportunity to capture at least 150 received radar signal power measurements per location.

Figure 12 shows an example captured sweep of a relatively strong signal received from the ASR-9 transmitter at Location 1 in Zone C2. Note the two peaks that show the peak power of the ASR-9 as it rotates. The maximum of each peak provides the peak received power of the radar as measured at the RF input of the preselector. Note that the time between the peaks is the rotation period of the radar, approximately 4.6 seconds. Figure 13 shows a magnified view of the first peak in the signal seen in Figure 12. This magnified view illustrates the “peak detected time signature” of the radar, which is simply the shape of the received signal power of the radar as the radar rotates and is captured with the spectrum analyzer sweep in zero-span mode.⁷ Figure 13 shows the shape of the radar’s main beam, roughly 20 milliseconds wide at its 3 dB points. Each data point in the sweep is clearly seen in Figure 13. Each data point represents the peak received power over an interval of

$$\frac{\text{Sweep Time (sec)}}{N - 1} = \frac{10 \text{ sec}}{6500 - 1} \cong 1.539 \text{ msec.}$$

Since the maximum period of the individual pulses of the ASR-9, 1.078 ms, is less than the time interval used to determine each data point, every data point in the sweep will show the peak received power of at least one individual radar pulse if detectable. This results in the relatively smooth, monotonically increasing and decreasing waveform seen in Figure 13 as the radar rotates.

⁷ The peak detected time signature of the radar signal is important since the area under this signature is used to automatically detect the radar signals in the data processing (as discussed in Section 6).

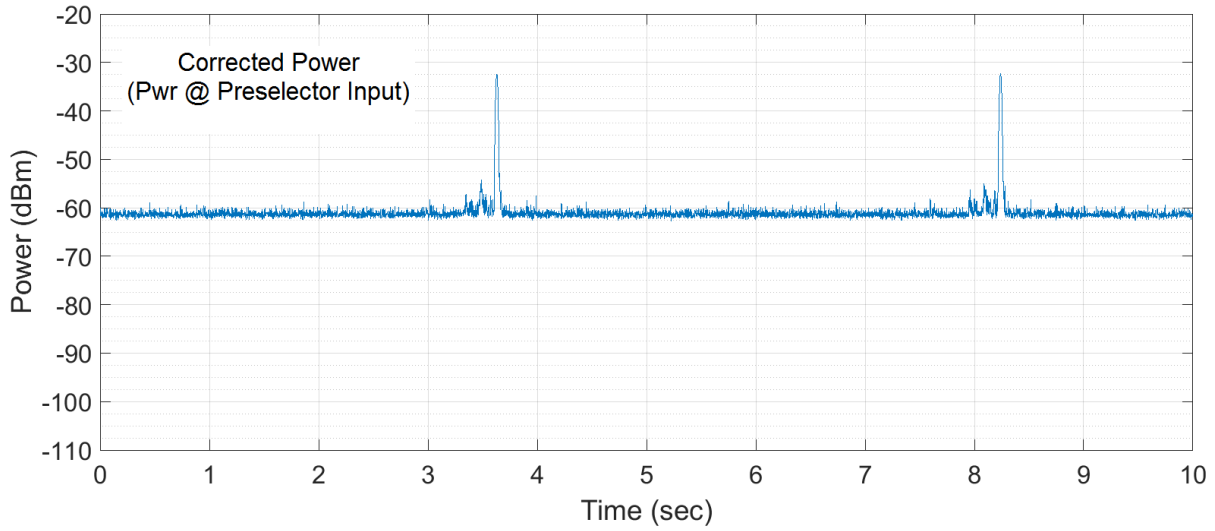


Figure 12. Example of a relatively strong signal received at Location 1 in Zone C2 for the ASR-9.

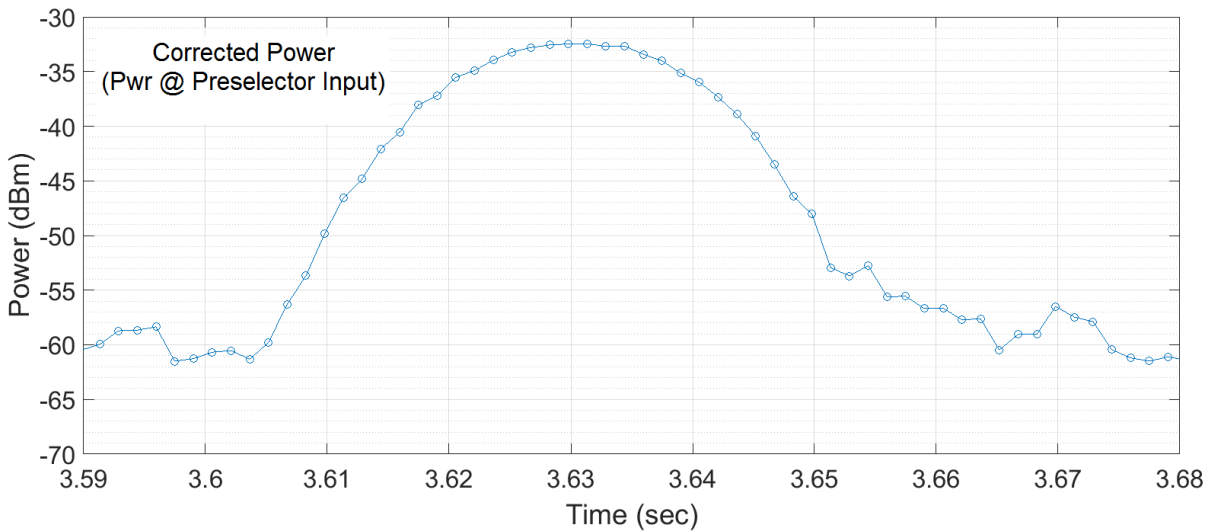


Figure 13. Magnified view of the first peak of the signal received at Location 1 in Zone C2 for the ASR-9.

Figure 14 shows an example captured sweep of a relatively strong signal received from the CARSR transmitter at Location 2 in Zone F4. The two peaks show the peak power of the CARSR as it rotates. Again, the maximum of each peak provides the peak received power of the radar as measured at the RF input of the preselector. Note that the time between the peaks is the rotation period of the radar, approximately 12 seconds. Figure 15 shows a magnified view of the first peak in the signal seen in Figure 14 illustrating the “peak detected time signature” of the radar. Each data point represents the peak received power over an interval of

$$\frac{\text{Sweep Time (sec)}}{N - 1} = \frac{25 \text{ sec}}{6250 - 1} \cong 4.001 \text{ msec.}$$

Since the maximum period of the individual pulses of the CARSR, 3.474 ms, is less than the time interval used to determine each data point, every data point in the sweep will show the peak received power of at least one individual radar pulse if detectable. This results in the relatively smooth, monotonically increasing and decreasing waveform seen in Figure 15 as the radar rotates. As in Figure 13 for the ASR-9, Figure 15 shows the roughly 60-millisecond wide main beam of the CARSR.

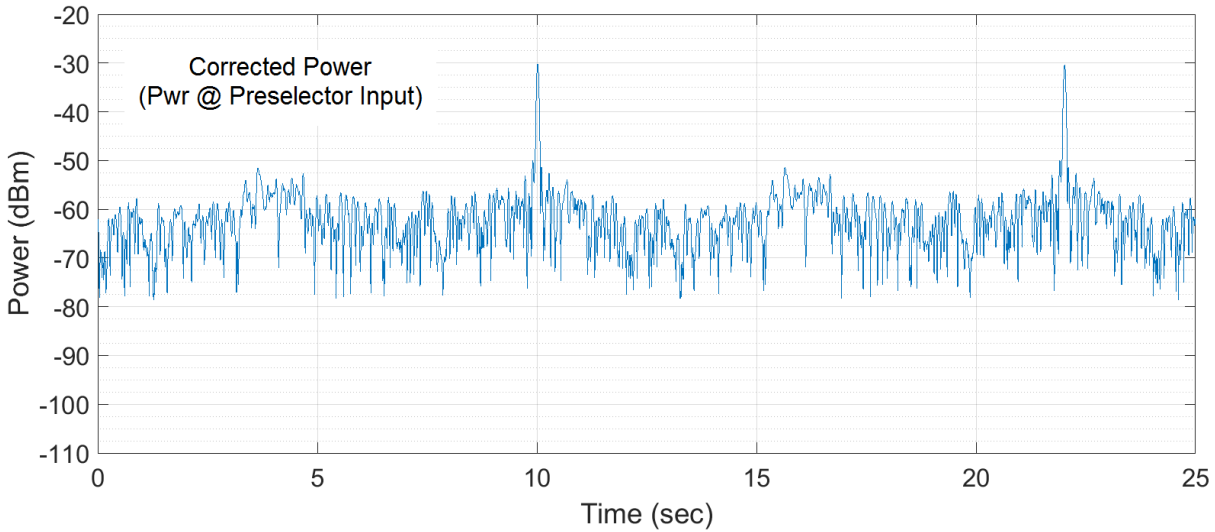


Figure 14. Example of a relatively strong signal received at Location 2 in Zone F4 for the CARSR.

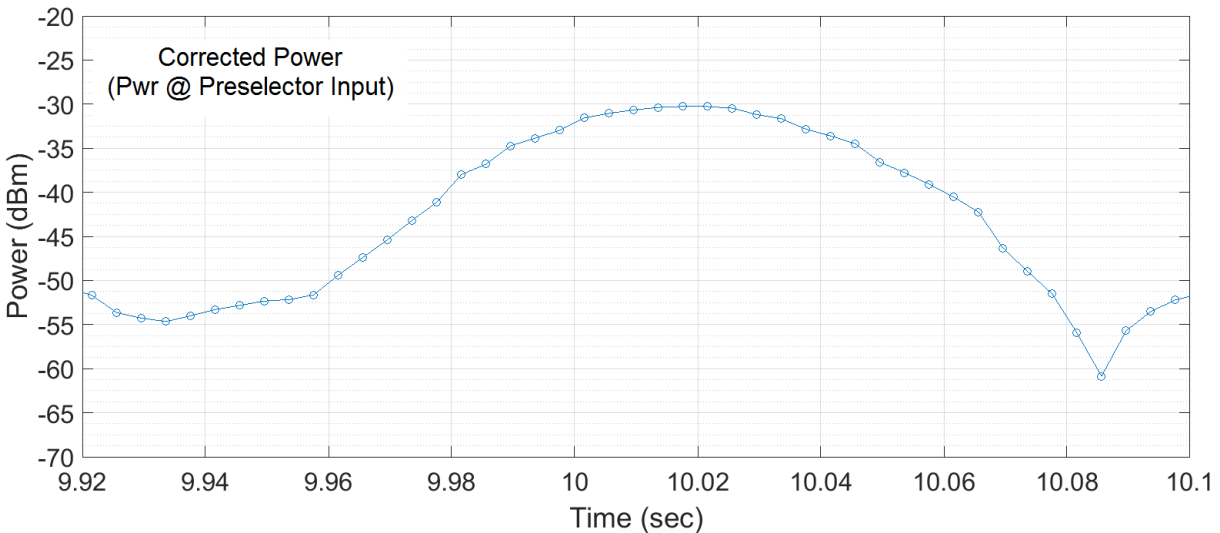


Figure 15. Magnified view of the first peak in the signal received at Location 2 in Zone F4 for the CARSR.

Figures 12–15 show relatively strong received radar transmissions where multipath (multiple received copies of the transmitted radar signal) effects on the radar signal are not prominent. Received radar signals at many of the measurement locations showed lower power signals and/or multipath effects more prominently. Figures 16 and 17 show examples of received radar transmissions for the ASR-9 and CARSR, respectively, where the radar signals were significantly weaker and multipath effects are more prominent. The signals seen in these two figures were some of the weakest signals seen at all of the measurement locations during the measurement campaign; the received power levels were typically higher than seen here for most of the measurement locations.

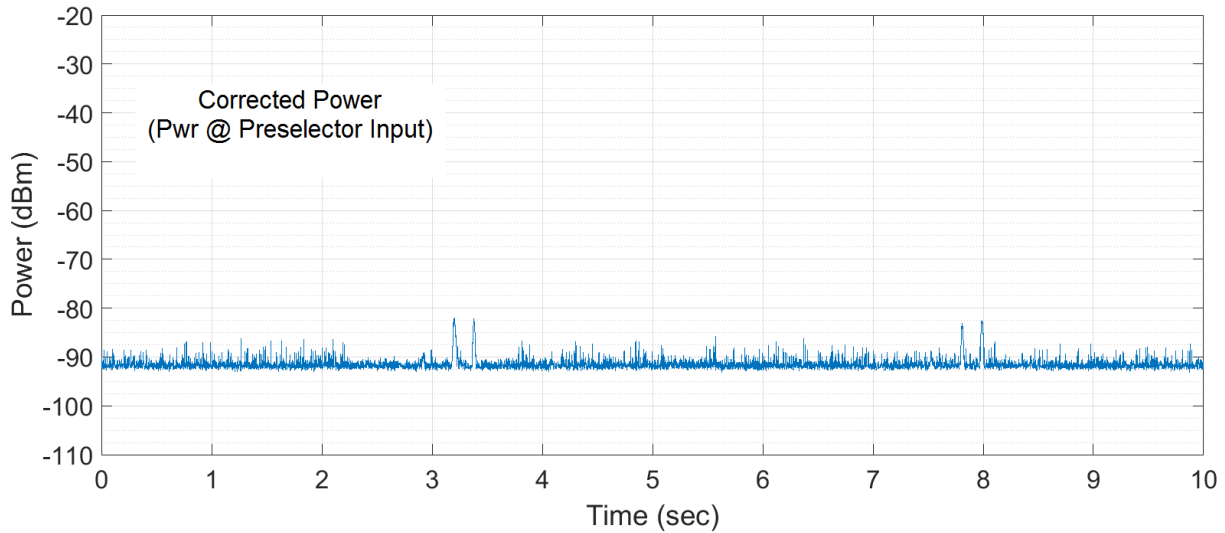


Figure 16. Example of a relatively weak signal received at Location 5 in Zone D1 for the ASR-9.

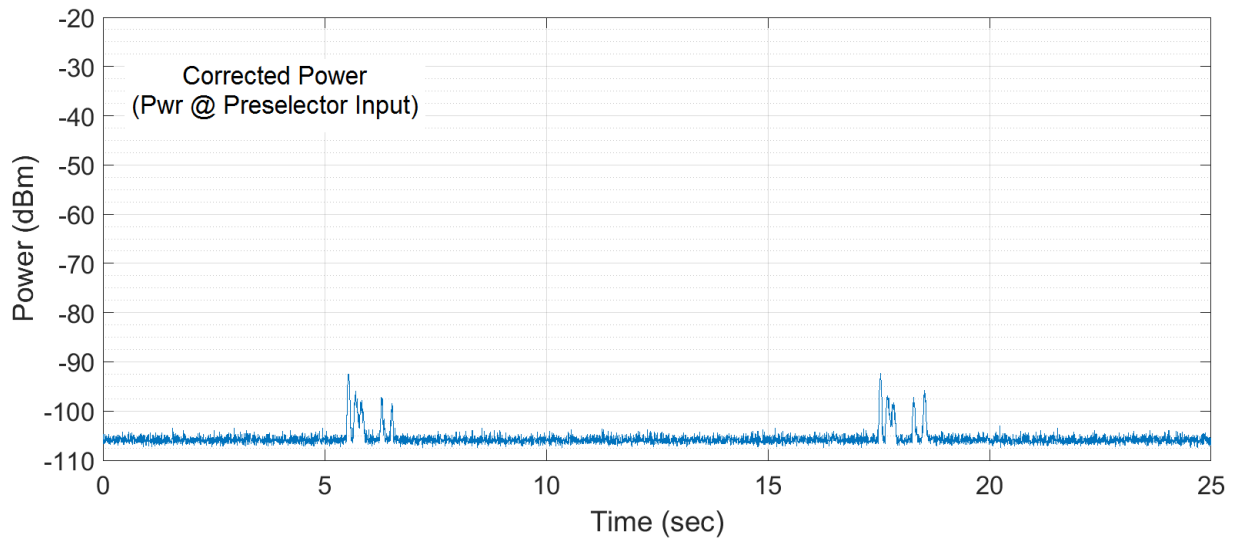


Figure 17. Example of a relatively weak signal received at Location 5 in Zone D1 for the CARSR.

Both of these figures illustrate multipath. Multipath can occur from several phenomena: 1) direct reception of emissions from the main radar transmitter antenna beam, 2) direct reception of emissions from the radar transmitter antenna sidelobes and backlobe, 3) emissions from the main radar transmitter beam reflecting off objects as the radar rotates, and 4) emissions from the radar transmitter sidelobes and backlobe reflecting off objects as the radar rotates. Note that the sidelobes and the backlobe have significantly lower gain (roughly 25 dB or more lower) than the main beam for the radar antennas causing received emissions from the sidelobes and backlobe to be significantly lower in power than received emissions from the main beam.

The received signal seen at the measurement locations in this measurement campaign from the radar transmitter can be quite complicated. Figures 18 and 19 show examples of measurement locations where severe multipath was observed. These locations represent the worst-case multipath seen. Significant variability in the number of received copies of the radar transmissions seen and the power levels of these received copies were observed over all the measurement locations.

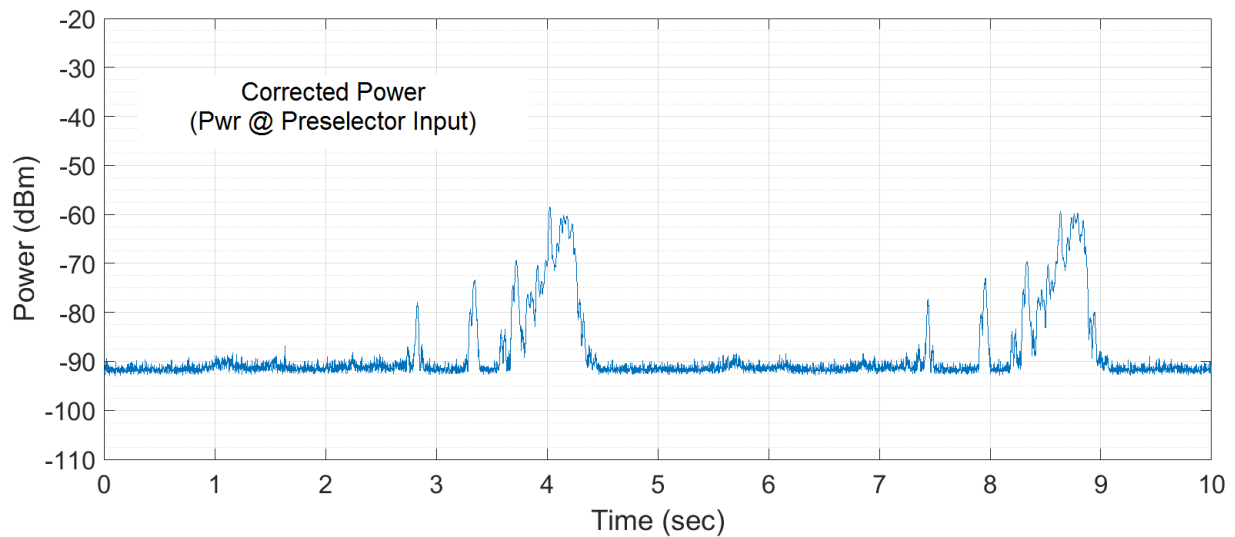


Figure 18. Example of a received radar transmission showing severe multipath at Location 1 in Zone C1 for the ASR-9.

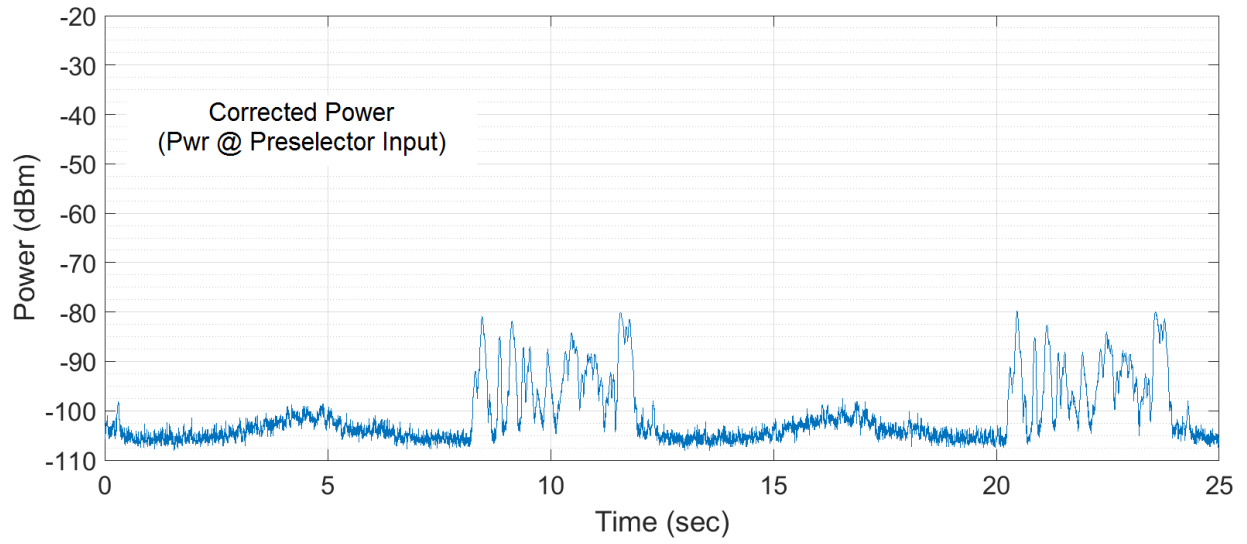


Figure 19. Example of a received radar transmission showing severe multipath at Location 6 in Zone H1 for the CARSR.

6. DATA PROCESSING AND ANALYSIS

Accurate peak power measurements of the ASR-9 and CARSR radars at the various measurement locations are required. To accomplish this, the radar signals in each sweep of the raw measured data must be accurately identified and then the peak power in those signals must be determined. An automated data processing algorithm was developed that post-processes the raw measured data collected at each measurement location. The algorithm identifies the radar signals in each sweep, determines the peak power of these signals, and generates received signal power statistics for all sweeps taken at that measurement location.

The data processing is performed over all 75 sweeps taken at each measurement location. For each of the 75 sweeps taken at each measurement location, the first step in the data processing is to accurately detect the presence of any radar signals. Initially auto- and cross-correlation techniques were investigated to detect the radar signals. The performance of these techniques proved to be inadequate, however. A radar detection technique was developed based on exploitation of the peak detected time signature of the radar. Looking at the peak detected time signatures of the ASR-9 and the CARSR (Figures 13 and 15, respectively) it is seen that these signatures exhibit a significantly larger area under the curve than noise emissions. Therefore a technique was implemented to look for the largest sum of n contiguous data points of each sweep which directly correlates to the area under the curve. This identifies a potential radar signal.

The number of data points to sum, n , is chosen to be 8 for both the ASR-9 and CARSR. This represents the number of data points in the peak detected time signature that fall roughly within 1 to 2 dB of the peak of the radar signal. Once the largest sum of n contiguous data points is found for a sweep, indicating a potential radar signal, the processing algorithm exploits the known rotation period of the radar and looks for other possible radar signals in the sweep.

Recall from Section 5 that data collection is an asynchronous process and therefore, the initially identified potential radar signal can occur at any time in the sweep. Based on when in time this first identified potential radar signal occurs, a search is performed for other potential radar signals in the sweep. The search is performed in small regions around plus and minus one or two radar rotation periods away from the originally identified potential radar signal. Here, the technique of looking for the largest sum of n contiguous data points within a specific region of the sweep is employed again to identify any other potential radar signals in the sweep. Once all potential radar signals in a sweep have been identified (there can be up to three), an additional test is performed on the potential radar signals to determine if they are valid radar signals.

To be considered a valid radar signal, all n data points of a potential radar signal must be above a threshold. The threshold is set to a certain amount (6 dB) above the median peak over-the-air system noise power level. The median peak over-the-air system noise power levels are determined by taking the median of the dB values and are shown in Table 1 in Section 2.2. This represents a conservative approach; radar signals can certainly be identified using a lower threshold. However, the power levels determined using a lower threshold may not be accurate.

Once valid radar signals are identified, the received power level of each valid received radar signal is determined. First the n data points for each valid radar signal are examined. Any potential noise spikes that appear on these n data points (noise spikes were observed only very

rarely in the entire measurement data set) are eliminated from the identification of the maximum received power of the radar. A noise spike is defined here as a data point whose power is more than 3 dB greater than both the previous and the next data points. After any noise spikes are removed from the n data points for each radar signal, the maximum power of the remaining data points is used as a measurement of the peak received power of the radar signal.

Recall that the raw measured data provides the peak received power at the RF input to the preselector. These power values are further corrected to provide the peak received power at the RF output of the antenna. The antenna cable loss was measured from the RF output of the antenna to the RF input of the preselector. The antenna cable loss was measured as 0.8 dB for the ASR-9 and 0.5 dB for the CARSR. The peak received power at the RF output of the antenna is found by adding the antenna cable loss to the peak received power at the RF input of the preselector.

For each measurement location, statistics are computed of the peak received power values (referenced to the RF output of the antenna) for all of the valid radar signals over all 75 sweeps. These statistics include a histogram and maximum, minimum, median, 75% quartile, and 25% quartile values. Seventy-five percent of the power values in the data set fall below the 75% quartile. Similarly, 25% of the power values in the data set fall below the 25% quartile. The histograms for each measurement location for both the ASR-9 and CARSR are shown in Appendices A and B. Tables 2 and 3 provide a statistical summary of the peak received power measured at each measurement location for the ASR-9 and the CARSR, respectively.

For each location in Tables 2 and 3, the number of valid radar signals that were determined over all 75 sweeps is provided along with the received power statistics. The latitude and longitude of the location are given as well as the distance from the radar transmitter. The columns for the propagation mode and peak predicted ITM power are provided for future use to provide a convenient way to compare the measured results with ITM predictions. To further facilitate this comparison, Tables 4 and 5 provide radar transmitter and receiver parameters that would be required to perform the ITM predictions for both the ASR-9 and CARSR, respectively.

All measurement locations for both the ASR-9 and CARSR had a large number of valid radar signals, ranging from 150 to 163 at each location, except for one CARSR measurement location, Zone D4 Location 1, where still 143 valid radar signals were measured. Therefore, statistically significant results were obtained for all measurement locations.

Figures 20 and 21 show plots of the median peak received signal power values as a function of distance between the radar transmitter and the receiver location for all measurement locations for the ASR-9 and CARSR, respectively. The ASR-9 data in Figure 20 show that while the largest median peak received signal power values occurred at the measurement locations generally closer to the radar transmitter, in general, median peak received signal power is not closely correlated with distance from the transmitter.

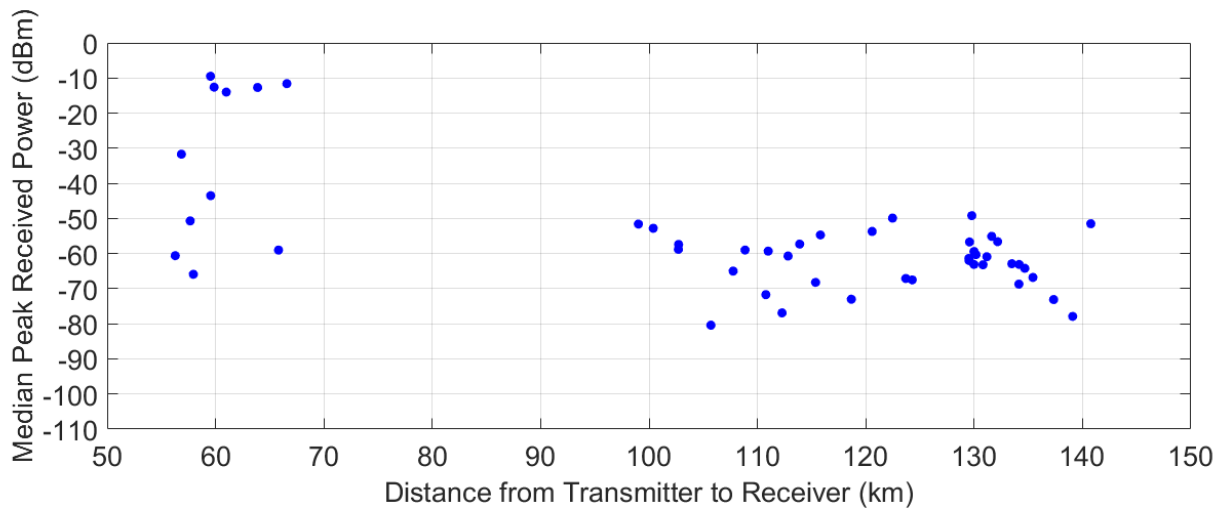


Figure 20. Median peak received signal power vs. distance between the radar transmitter and the receiver for all measurement locations for the ASR-9.

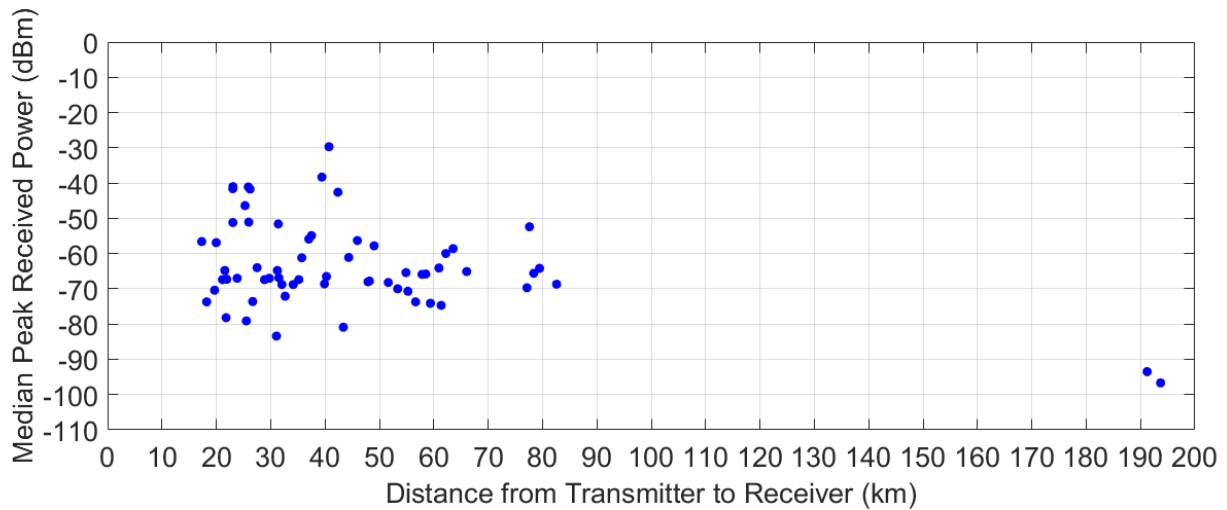


Figure 21. Median peak received signal power vs. distance between the radar transmitter and the receiver for all measurement locations for the CARSR.

As would be expected due to differences in terrain, median peak received signal power does not simply decrease with distance from the transmitter. The CARSR data in Figure 21 show that the smallest median peak received signal power values occurred at the two measurement locations farthest away from the radar transmitter.⁸ The CARSR data also show that median peak received signal power is not closely correlated with distance from the transmitter.

As seen from Figure 20 and Table 2, the distance from the transmitter to the measurement locations for the ASR-9 varied from roughly 56 km to 141 km. Median peak received power levels varied from -9.5 dBm to -80.4 dBm over all the ASR-9 measurement locations. Similarly,

⁸ These two measurement locations are ones where tropospheric scatter propagation mode was expected.

as seen from Figure 21 and Table 3, the distance from the transmitter to the measurement locations for the CARSR varied from roughly 17 km to 194 km, while median peak received power levels varied from -29.7 dBm to -96.7 dBm.

In looking at the ASR-9 data in Table 2, comparing the median peak received power at different locations within each Zone, it is observed that relatively small changes in receiver location can result in significantly different median peak received power levels. For example, in Zone C1, the median peak received signal power was -59.0 dBm at Location 1 but -11.6 dBm at Location 2, roughly 2 km away. This phenomenon, perhaps not quite as marked, was also observed in the CARSR data in Table 3.

From the histograms in Appendix A and B (or the received power statistics in Tables 2 and 3), depending on the location, the variation in power levels at a given location over all 75 sweeps can be small or large. Very few locations exhibited very large (10 dB or more) variation in power levels. Those locations tended to exhibit severe multipath and not a single, clearly defined peak for each rotation of the radar. Figures 18 and 19 show examples of locations where the received signal illustrates this phenomenon.

Locations that exhibit only a very small variation in power levels over all 75 sweeps (say 1 or 2 dB) typically exhibited a single, clearly defined peak for each rotation of the radar with very little substantial multipath. Any multipath that did exist in these cases was relatively low in power compared to the peak (10 to 20 dB or more below the peak). Figures 12 and 14 show examples of locations where the received signal illustrates this phenomenon. In addition, the very small variation in power levels over all 75 sweeps at these locations provides further confidence in the capability of the measurement system to provide precise and repeatable power measurements.

Table 2. Measured received power statistics at measurement locations for the ASR-9 radar in Trout Creek, Utah.

Zone	Location	Lat (deg)	Lon (deg)	Num Valid Signals	Measured Peak Power					Distance from Tx (km)	Prop_Mode	ITM_PeakPwr
					Max (dBm)	75% Quart (dBm)	Median (dBm)	25% Quart (dBm)	Min (dBm)			
A1	Loc1	40.73561	-113.87439	160	-58.7	-59.9	-60.3	-60.8	-61.6	130.16568		
A1	Loc2	40.73516	-113.85127	160	-58.4	-59.1	-59.4	-59.8	-60.7	129.98246		
A1	Loc3	40.73453	-113.82074	162	-48.7	-49.0	-49.2	-49.3	-49.8	129.78213		
A1	Loc4	40.73322	-113.75820	160	-61.1	-61.7	-62.0	-62.3	-63.4	129.53175		
A1	Loc5	40.73168	-113.68575	161	-59.9	-60.9	-61.4	-61.9	-66.0	129.51227		
A1	Loc6	40.73109	-113.65932	160	-55.1	-56.4	-56.7	-57.2	-58.2	129.57596		
A2	Loc1	40.72948	-113.58378	160	-61.3	-62.5	-63.1	-63.9	-66.5	129.98026		
A2	Loc2	40.72750	-113.49745	160	-60.9	-62.5	-63.2	-63.9	-66.0	130.81435		
A2	Loc3	40.72682	-113.46928	160	-57.6	-60.3	-60.9	-61.6	-65.1	131.17125		
A2	Loc4	40.72606	-113.43814	159	-53.9	-54.7	-55.1	-55.5	-56.2	131.61466		
A2	Loc5	40.72527	-113.40406	160	-55.3	-56.2	-56.6	-57.1	-58.2	132.16364		
A2	Loc6	40.72355	-113.33380	160	-61.4	-62.7	-62.9	-63.2	-64.0	133.47894		
A3	Loc1	40.72276	-113.30224	160	-60.6	-62.5	-63.1	-63.7	-65.3	134.15056		
A3	Loc2	40.72373	-113.28562	161	-62.1	-63.7	-64.2	-64.7	-68.3	134.67154		
A3	Loc3	40.72420	-113.25886	160	-65.2	-66.3	-66.8	-67.4	-68.9	135.42195		
A3	Loc4	40.72719	-113.20212	158	-67.3	-71.8	-73.1	-73.9	-76.7	137.33298		
A3	Loc5	40.72627	-113.14211	157	-73.7	-77.7	-77.9	-78.2	-79.5	139.08885		
A3	Loc6	40.73395	-113.11493	159	-50.2	-51.1	-51.5	-51.9	-60.9	140.76526		
B1	Loc1	40.23209	-112.72338	161	-66.4	-67.5	-68.2	-69.1	-70.7	115.36476		

Zone	Location	Lat (deg)	Lon (deg)	Num Valid Signals	Measured Peak Power					Distance from Tx (km)	Prop_Mode	ITM_PeakPwr
					Max (dBm)	75% Quart (dBm)	Median (dBm)	25% Quart (dBm)	Min (dBm)			
C1	Loc1	39.06869	-114.17349	163	-55.6	-58.5	-59.0	-59.5	-61.4	65.81359		
C1	Loc2	39.05399	-114.16000	161	-10.8	-11.5	-11.6	-11.6	-11.9	66.58189		
C1	Loc3	39.05089	-113.96191	160	-12.4	-12.6	-12.6	-12.7	-12.8	59.86553		
C1	Loc4	39.04825	-113.93667	158	-43.1	-43.4	-43.5	-43.6	-43.7	59.55050		
C1	Loc5	39.04556	-113.79842	156	-63.8	-65.7	-65.9	-66.1	-67.4	57.95178		
C1	Loc6	39.05972	-113.75750	161	-58.8	-60.2	-60.6	-61.0	-62.7	56.28244		
C2	Loc1	39.08620	-113.53142	160	-31.5	-31.6	-31.7	-31.7	-31.9	56.85061		
C2	Loc2	39.08469	-113.51031	160	-49.5	-50.3	-50.7	-50.9	-51.4	57.66151		
C2	Loc3	39.07679	-113.47862	160	-9.3	-9.4	-9.5	-9.5	-9.6	59.53470		
C2	Loc4	39.06949	-113.45858	161	-13.2	-13.8	-14.0	-14.6	-14.9	60.99143		
C2	Loc5	39.05328	-113.42502	161	-12.3	-12.5	-12.7	-12.8	-13.1	63.87912		
D1	Loc1	39.33085	-112.65002	160	-50.6	-51.5	-51.6	-51.9	-58.2	99.01890		
D1	Loc2	39.33065	-112.63361	160	-51.9	-52.7	-52.8	-53.0	-53.4	100.38713		
D1	Loc3	39.34502	-112.60088	161	-56.9	-58.1	-58.8	-59.3	-60.7	102.70591		
D1	Loc4	39.35979	-112.59603	161	-56.7	-57.2	-57.4	-57.7	-58.4	102.72215		
D1	Loc5	39.35272	-112.56257	156	-77.4	-80.1	-80.4	-81.0	-82.8	105.70917		
D2	Loc1	39.47369	-112.47674	160	-69.0	-70.9	-71.7	-72.9	-80.6	110.77874		
D2	Loc2	39.43033	-112.46611	162	-71.8	-75.1	-76.9	-77.7	-81.2	112.27052		
D2	Loc3	39.38842	-112.51529	160	-55.8	-58.6	-59.0	-59.5	-61.1	108.86132		
D2	Loc4	39.37698	-112.53126	159	-62.9	-64.4	-65.0	-65.6	-67.0	107.75982		
D2	Loc5	39.35309	-112.49954	160	-58.4	-58.9	-59.3	-59.8	-67.1	110.99268		
D2	Loc6	39.32794	-112.48538	160	-59.7	-60.5	-60.7	-60.8	-61.3	112.82511		

Zone	Location	Lat (deg)	Lon (deg)	Num Valid Signals	Measured Peak Power					Distance from Tx (km)	Prop_Mode	ITM_PeakPwr
					Max (dBm)	75% Quart (dBm)	Median (dBm)	25% Quart (dBm)	Min (dBm)			
D3	Loc1	39.37473	-112.33648	161	-66.3	-67.1	-67.5	-68.0	-69.9	124.28471		
D3	Loc2	39.36382	-112.34615	160	-65.9	-66.7	-67.1	-67.5	-68.3	123.68896		
D3	Loc3	39.35509	-112.36285	159	-49.2	-49.6	-49.9	-50.2	-50.7	122.46574		
D3	Loc4	39.35479	-112.38519	160	-53.1	-53.6	-53.7	-54.0	-54.7	120.58619		
D3	Loc5	39.35453	-112.40802	160	-67.3	-72.1	-73.0	-73.7	-75.8	118.66523		
D4	Loc1	39.31170	-112.47787	161	-56.4	-57.2	-57.3	-57.5	-58.0	113.90104		
D5	Loc1	39.28706	-112.46358	160	-53.3	-54.0	-54.7	-55.2	-73.6	115.81462		
E1	Loc1	38.51750	-112.99124	160	-64.6	-67.3	-68.7	-70.2	-71.3	134.12393		

Table 3. Measured received power statistics at measurement locations for the CARSR radar in Cedar City, Utah.

Zone	Location	Lat (deg)	Lon (deg)	Num Valid Signals	Measured Peak Power					Distance from Tx (km)	Prop_Mode	ITM_PeakPwr
					Max (dBm)	75% Quart (dBm)	Median (dBm)	25% Quart (dBm)	Min (dBm)			
F1	Loc1	37.67244	-113.55102	161	-72.7	-74.3	-74.7	-75.1	-76.2	61.35700		
F1	Loc2	37.67506	-113.51821	156	-65.0	-65.7	-65.8	-65.9	-66.5	58.53532		
F1	Loc3	37.66107	-113.46151	156	-68.6	-69.7	-70.0	-70.3	-71.6	53.36040		
F1	Loc4	37.64593	-113.44401	153	-67.6	-68.1	-68.2	-68.3	-69.0	51.61986		

Zone	Location	Lat (deg)	Lon (deg)	Num Valid Signals	Measured Peak Power					Distance from Tx (km)	Prop_Mode	ITM_PeakPwr
					Max (dBm)	75% Quart (dBm)	Median (dBm)	25% Quart (dBm)	Min (dBm)			
F1	Loc5	37.61496	-113.40777	161	-66.9	-67.5	-67.8	-68.4	-70.0	48.15927		
F2	Loc1	37.61127	-113.38293	160	-54.1	-56.0	-56.3	-56.7	-58.2	45.94996		
F2	Loc2	37.60930	-113.35369	151	-78.7	-80.4	-80.9	-81.4	-82.7	43.36173		
F2	Loc3	37.62527	-113.31722	150	-65.3	-66.3	-66.5	-66.7	-67.2	40.25694		
F2	Loc4	37.63652	-113.27874	156	-54.6	-55.7	-55.9	-56.1	-57.7	37.01205		
F2	Loc5	37.63972	-113.25718	152	-65.6	-67.1	-67.4	-67.6	-70.1	35.17547		
F3	Loc1	37.64553	-113.24411	160	-67.1	-68.4	-68.8	-69.3	-72.0	34.13629		
F3	Loc2	37.65445	-113.22498	160	-70.2	-71.8	-72.1	-72.3	-73.6	32.66243		
F3	Loc3	37.66399	-113.20556	156	-64.2	-64.7	-64.8	-64.9	-65.6	31.23413		
F3	Loc4	37.67323	-113.18490	150	-65.7	-66.8	-67.0	-67.2	-67.8	29.76056		
F3	Loc5	37.67959	-113.17168	152	-64.4	-67.3	-67.4	-67.6	-70.9	28.87379		
F4	Loc1	37.78831	-113.27606	155	-42.4	-42.5	-42.6	-42.7	-43.1	42.36992		
F4	Loc2	37.77406	-113.26476	156	-27.7	-29.7	-29.7	-29.8	-29.9	40.71712		
F4	Loc3	37.76478	-113.25442	153	-37.1	-38.0	-38.3	-38.6	-39.6	39.42032		
F4	Loc4	37.70432	-113.19027	150	-49.0	-51.4	-51.6	-51.8	-54.7	31.39420		
F4	Loc5	37.68531	-113.15234	150	-63.2	-63.9	-64.0	-64.2	-64.6	27.49755		
G1	Loc1	37.70955	-113.10942	150	-44.3	-46.0	-46.4	-47.0	-48.5	25.27910		
G1	Loc2	37.70966	-113.11826	157	-46.6	-50.2	-51.1	-51.5	-55.5	25.95961		
G1	Loc3	37.70222	-113.12244	154	-40.2	-40.8	-41.1	-41.3	-42.2	25.88526		
G1	Loc4	37.69794	-113.12926	150	-39.6	-41.3	-41.7	-42.0	-42.5	26.20575		
G1	Loc5	37.68557	-113.10697	151	-60.1	-66.3	-67.0	-67.9	-70.2	23.83853		

Zone	Location	Lat (deg)	Lon (deg)	Num Valid Signals	Measured Peak Power					Distance from Tx (km)	Prop_Mode	ITM_PeakPwr
					Max (dBm)	75% Quart (dBm)	Median (dBm)	25% Quart (dBm)	Min (dBm)			
G2	Loc1	37.69988	-113.08719	150	-49.3	-51.1	-51.2	-51.4	-52.5	23.04572		
G2	Loc2	37.69614	-113.09011	159	-39.7	-40.7	-41.0	-41.1	-52.6	23.05998		
G2	Loc3	37.69080	-113.09351	150	-40.9	-41.4	-41.6	-41.7	-42.2	23.03713		
G2	Loc4	37.68140	-113.08534	153	-65.4	-66.8	-67.3	-67.7	-69.8	21.91949		
G2	Loc5	37.68433	-113.07885	150	-61.8	-64.3	-64.8	-65.2	-66.6	21.55777		
G3	Loc1	37.67423	-113.03082	152	-56.1	-56.4	-56.6	-56.8	-57.3	17.31773		
G3	Loc2	37.67282	-113.04385	150	-73.1	-73.5	-73.7	-73.9	-74.4	18.23435		
G3	Loc3	37.68003	-113.06146	160	-54.3	-55.9	-56.9	-58.6	-61.8	19.98152		
G3	Loc4	37.68214	-113.05613	155	-69.7	-70.1	-70.4	-70.5	-71.2	19.68641		
G3	Loc5	37.69154	-113.06830	153	-64.6	-66.8	-67.4	-67.7	-68.8	21.14100		
G3	Loc6	37.71169	-113.06011	152	-77.6	-78.0	-78.2	-78.6	-79.4	21.79325		
H1	Loc1	37.92690	-113.03153	158	-65.9	-68.3	-68.6	-68.9	-69.7	39.88917		
H1	Loc2	37.90360	-113.03179	161	-54.3	-54.7	-54.9	-55.1	-55.8	37.51085		
H1	Loc3	37.84536	-113.04103	150	-67.9	-68.6	-68.8	-69.1	-74.3	32.07345		
H1	Loc4	37.83504	-113.05036	150	-66.0	-66.7	-66.9	-67.1	-67.4	31.50325		
H1	Loc5	37.77933	-113.05481	159	-69.2	-73.3	-73.6	-73.8	-76.4	26.68780		
H1	Loc6	37.76548	-113.05489	151	-75.7	-78.9	-79.1	-79.3	-85.9	25.52251		
I1	Loc1	38.07075	-112.68587	157	-68.7	-70.4	-70.7	-71.0	-72.5	55.23821		
I1	Loc2	37.98012	-112.73624	153	-59.2	-60.4	-61.1	-61.5	-63.8	44.35964		
I1	Loc3	37.90746	-112.77490	150	-59.9	-61.1	-61.2	-61.3	-61.7	35.72068		
I1	Loc4	37.86838	-112.79798	155	-81.0	-82.9	-83.4	-84.0	-90.2	31.06167		

Zone	Location	Lat (deg)	Lon (deg)	Num Valid Signals	Measured Peak Power					Distance from Tx (km)	Prop_Mode	ITM_PeakPwr
					Max (dBm)	75% Quart (dBm)	Median (dBm)	25% Quart (dBm)	Min (dBm)			
J1	Loc1	37.88827	-112.00273	153	-63.7	-67.5	-68.7	-69.6	-73.3	82.59309		
J1	Loc2	37.82388	-112.01002	158	-62.3	-64.1	-64.2	-64.5	-66.0	79.45284		
J1	Loc3	37.81207	-112.01797	153	-62.2	-64.5	-65.6	-66.5	-68.8	78.37920		
J1	Loc4	37.79755	-112.02147	151	-51.4	-52.2	-52.4	-52.6	-53.8	77.60697		
J1	Loc5	37.78292	-112.02168	160	-66.3	-68.9	-69.7	-70.2	-71.9	77.13707		
J2	Loc1	37.70135	-112.12700	160	-62.5	-64.3	-65.1	-65.8	-67.6	66.05494		
J2	Loc2	37.69261	-112.15378	150	-56.9	-57.5	-58.6	-61.5	-64.0	63.56082		
J2	Loc3	37.69581	-112.17003	150	-58.0	-59.7	-60.0	-60.2	-62.1	62.21087		
J2	Loc4	37.69770	-112.18505	161	-62.9	-63.8	-64.1	-64.6	-66.1	60.94750		
J2	Loc5	37.70877	-112.20609	159	-72.1	-73.6	-74.1	-74.8	-76.5	59.37393		
J3	Loc1	37.71439	-112.22565	152	-64.8	-65.8	-65.9	-66.1	-69.5	57.82950		
J3	Loc2	37.71778	-112.24038	151	-71.9	-73.4	-73.7	-74.2	-76.1	56.65543		
J3	Loc3	37.72033	-112.26186	152	-64.6	-65.2	-65.4	-65.6	-66.3	54.89032		
J3	Loc4	37.74622	-112.34179	150	-56.5	-57.7	-57.8	-58.1	-58.8	49.01908		
J3	Loc5	37.74763	-112.35592	150	-66.5	-67.8	-68.0	-68.3	-69.0	47.90736		
D4	Loc1	39.31170	-112.47786	143	-86.9	-96.1	-96.7	-97.1	-98.6	193.6879		
D5	Loc1	39.28704	-112.46358	151	-86.9	-92.9	-93.5	-94.0	-96.1	191.2165		

Table 4. ASR-9 radar transmitter and receiver parameters for ITM predicted power.

Tx Pwr	1000000 W
Tx Freq	2860.00 MHz
Tx Ant Gain	33.0 dBi
Rx Ant Gain	-2.2 dBi
Tx Lat	39.566667°
Tx Lon	-113.759444°
Tx Height	6.0 m
Rx Height	2.2 m

Table 5. CARSR radar transmitter and receiver parameters for ITM predicted power.

Tx Pwr	75000 W
Tx Freq	1318.59 MHz
Tx Ant Gain	33.7 dBi
Rx Ant Gain	-2.8 dBi
Tx Lat	37.593333°
Tx Lon	-112.863056°
Tx Height	15.0 m
Rx Height	2.2 m

7. SUMMARY

The objective of this work was to conduct received signal power measurements on select air traffic control radars and provide measured data results that can be used (in a separate effort) to validate spectrum usage contours and the Quantitative Assessments of Spectrum Usage methodology used to generate them, as developed by OSM.

Initially, to address this objective, ITS performed received signal power measurements in May 2017 on the CARSR operating in the 1300–1370 MHz band in Parker, Colorado and the ASR-9 operating in the 2700–2900 MHz band in Platteville, Colorado. Those measurements, referred to as the Colorado measurements, are described in detail in a different report [2].

Continuing to address this objective, this report describes received signal power measurements performed by ITS on two new radars during April and May 2018: the CARSR operating in the 1300–1370 MHz band in Cedar City, Utah and the ASR-9 operating in the 2700–2900 MHz band in Trout Creek, Utah. Received signal power measurements were taken at a received antenna height of 2.2m AGL at a set of fixed locations along accessible roads at varying distances from the transmitter locations. Multiple received signal power measurements at each fixed location were made to provide statistically significant results.

The measurement system consisted of an antenna, an ITS custom-built preselector, a spectrum analyzer, a GPS antenna and receiver, and an ITS custom-built measurement controller. For these measurements, the measurement system was installed in the ITS PSCR measurement van. Automated control of the preselector and spectrum analyzer is provided by the measurement controller. The spectrum analyzer, GPS antenna and receiver, and measurement controller combination collects the received signal RF peak power measured data tagged with location information, formats the data, and saves the data to a local hard drive on the measurement controller.

Measurement site selection for the Colorado measurements was done by using propagation loss and propagation mode predictions along radials emanating from the transmitter locations. Sites chosen in this manner tended to be far from major roads and required a disproportional amount of time driving on small, rural, dirt roads to access locations. In an effort to reduce the amount of driving time and maximize the number of measurement locations to be measured, a new methodology of selecting measurement sites more closely based on existing roads was used.

The new methodology of measurement location selection was based on points along concentric circles with radii of increasing distance from the radar transmitter. The predicted propagation loss and propagation mode at points along the concentric circles were used as a rough guide to select candidate measurement sites along actual existing roads. Candidate measurement sites were chosen on small roads just slightly off major roads or along major roads if appropriate places to park the vehicle were available. Sites were chosen to represent different predicted propagation modes (such as line-of-sight, diffracted, tropospheric scatter, etc.) and predicted received signal powers that varied from strong to weak.

The radar measurements were made using the swept-measurement mode of the RSMS-5G software. The spectrum analyzer was set up in the zero-span mode (providing time-domain measurements) using peak detection and with a sweep time set slightly longer than two times the

rotation period of the radar to be measured. The RBW to use for the measurements was determined empirically by measurements of signals from both radars as measured in the field. A 3 MHz RBW was used for the ASR-9 and a 300-kHz RBW was used for the CARSR.

Seventy-five spectrum analyzer sweeps were taken at each location. The number of sweeps was chosen to be as large as practicable to provide statistically significant results of peak received signal power.

An automated data processing algorithm was developed that processes the raw measured data taken at each measurement location. The algorithm identifies the radar signals in each sweep, determines the peak power of these signals (referenced to the RF output of the antenna), and generates peak received signal power statistics for all seventy-five sweeps taken at that measurement location.

All measurement locations for both the ASR-9 and CARSR had a large number of valid radar signals, ranging from 150 to 163 at each location, except for one CARSR measurement location, Zone D4 Location 1, where still 143 valid radar signals were measured. Therefore, statistically significant results were obtained for all measurement locations. This represented a significant improvement in measured data results compared to the Colorado measurements.

The ASR-9 data show that while the largest median peak received signal power values occurred at the measurement locations generally closer to the radar transmitter, in general median peak received signal power is not closely correlated with distance from the transmitter. As would be expected due to differences in terrain, median peak received signal power does not simply decrease with distance from the transmitter.

The CARSR data show that the smallest median peak received signal power values occurred at the two measurement locations farthest away from the radar transmitter. The CARSR data also show that median peak received signal power is not closely correlated with distance from the transmitter. Relatively small changes in receiver location can result in significantly different median peak received power levels. For example, in Zone C1, the median peak received signal power was -59.0 dBm at Location 1 but -11.6 dBm at Location 2, roughly 2 km away.

8. ACKNOWLEDGEMENTS

The authors would like to thank the following individuals for their efforts in helping complete this project. Frank Sanders, drawing on his experience and expertise on radar systems, provided the basis for developing the measurement methodology used. Stephen McCormick of First RF Corporation was instrumental in teaching us the use of the antenna turntable for performing the antenna gain and pattern measurements at Table Mountain. Additional thanks go to Erik Hill and Robert Johnk for their assistance in performing the antenna measurements at Table Mountain. Finally, special thanks go to Michael Cotton for his assistance and guidance during all phases of this project. Without the assistance of these individuals, this work would not have been possible.

9. REFERENCES

- [1] National Telecommunications and Information Administration, *Quantitative Assessments of Spectrum Usage* (Nov. 17, 2016), available at <https://www.ntia.doc.gov/report/2016/quantitative-assessments-spectrum-usage>.
- [2] J. A. Wepman, E .F. Drocella, A. Lundy, P. M. McKenna, H .E. Ottke, and Y. Lo, “Received Signal Power Measurements on Select Air Traffic Control Radars in Colorado,” NTIA Report TR-19-542, August 2019, available at <https://its.bldrdoc.gov/publications/3223.aspx>
- [3] E.B. Larsen, R.L. Ehret, D.G. Camell, and G.H. Koepke, “Calibration of antenna factor at a ground screen field site using an automatic network analyzer,” in *Proc. of the 1989 IEEE National Symposium on EMC*, Denver, CO, May 23-25, 1989, pp. 19-24.
- [4] Anita G. Longley; Philip L. Rice, “Prediction of tropospheric radio transmission loss over irregular terrain: a computer method - 1968,” ESSA Technical Report ERL 79-ITS 67, July 1968, available at <https://www.its.bldrdoc.gov/publications/2784.aspx>

APPENDIX A: RECEIVED POWER HISTOGRAMS FOR ASR-9 MEASUREMENTS

This appendix contains the received radar signal power histograms and maximum, median, minimum, 75% quartile, and 25% quartile statistics for each measurement location for the ASR-9 measurements.

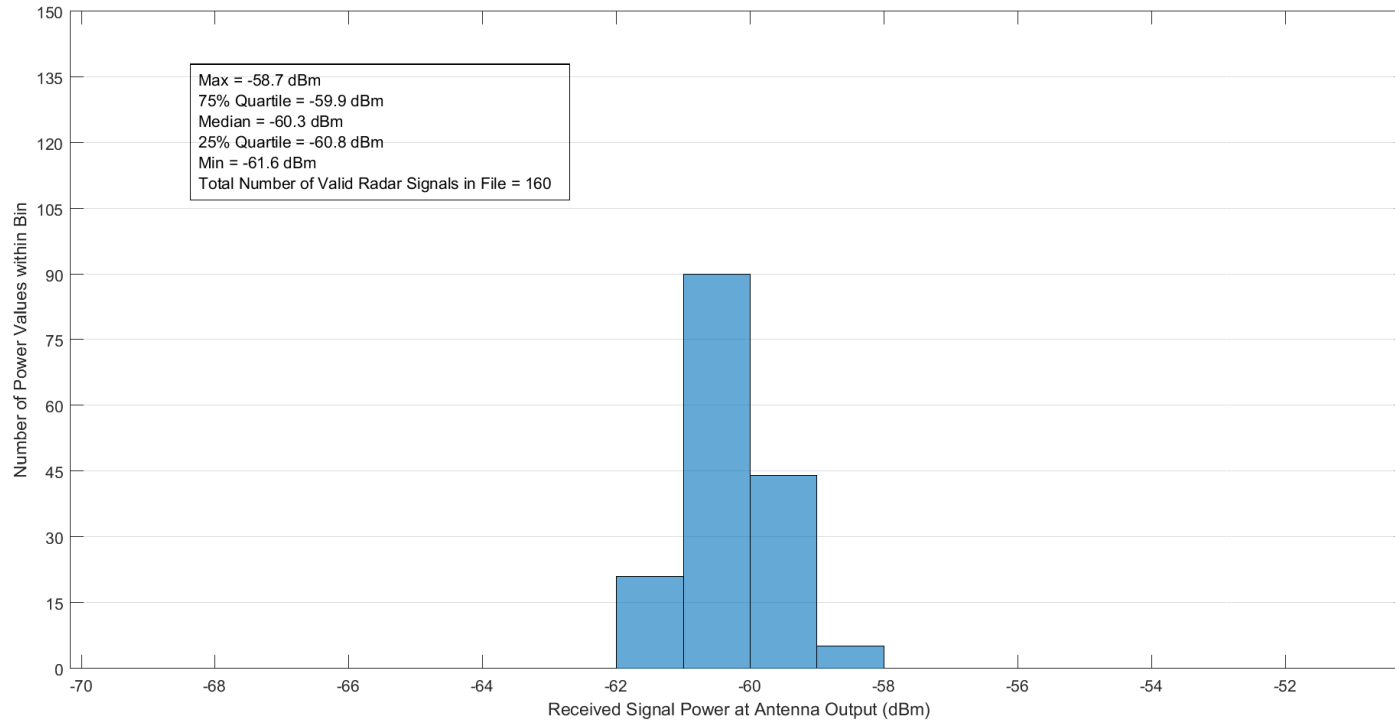


Figure A-1. Received radar signal power statistics at Location 1 in Zone A1 for the ASR-9.

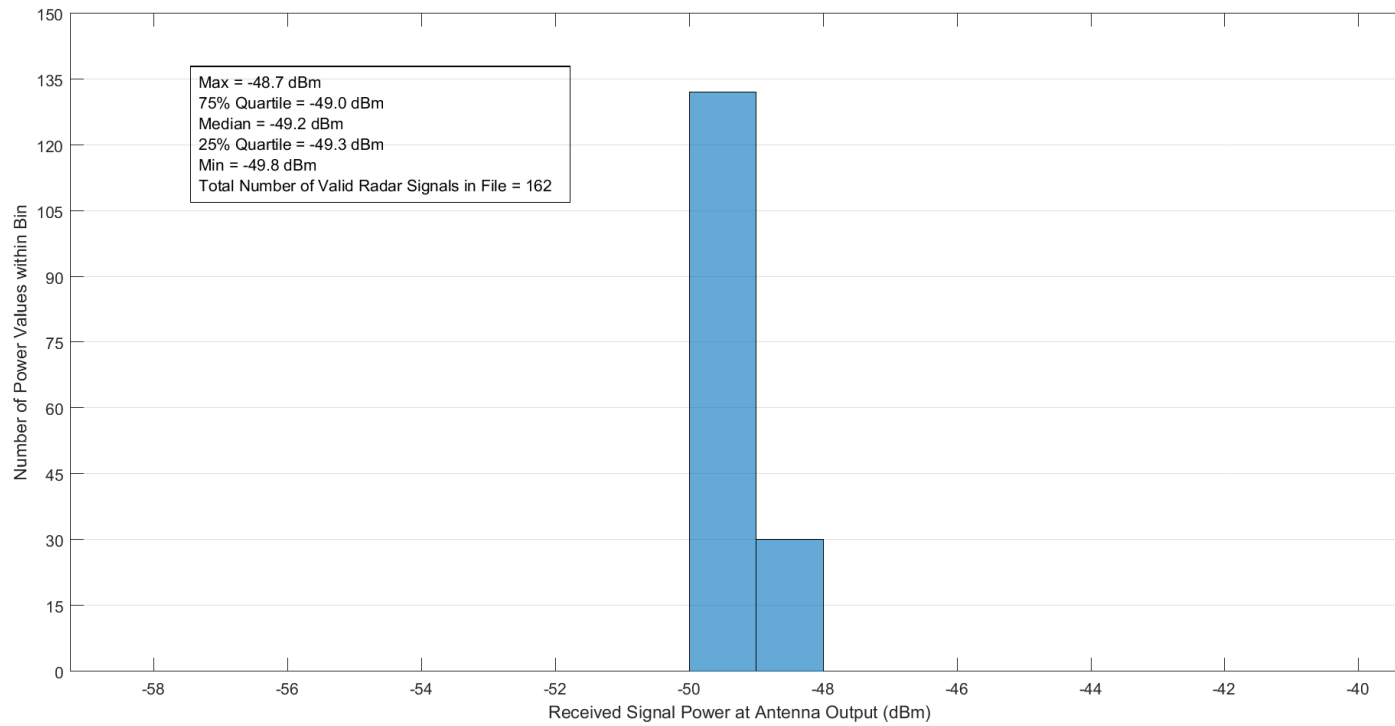


Figure A-2. Received radar signal power statistics at Location 2 in Zone A1 for the ASR-9.

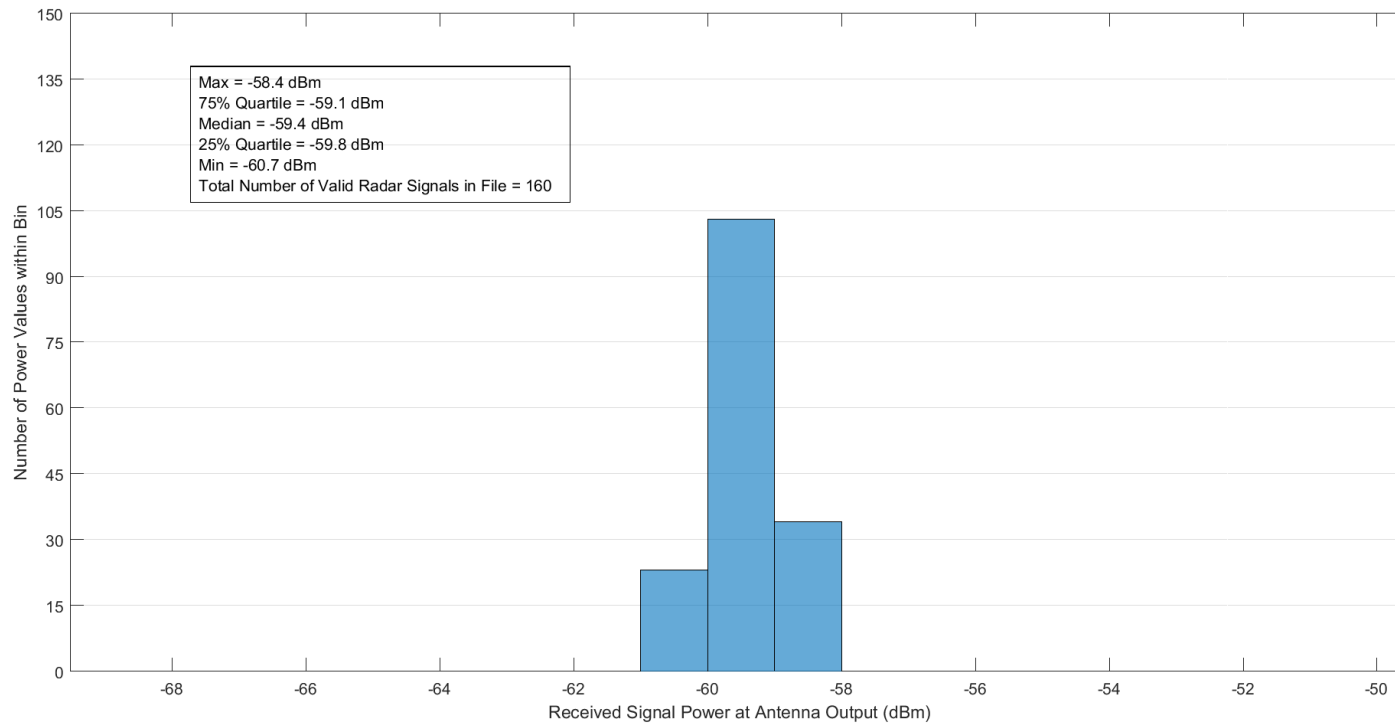


Figure A-3. Received radar signal power statistics at Location 3 in Zone A1 for the ASR-9.

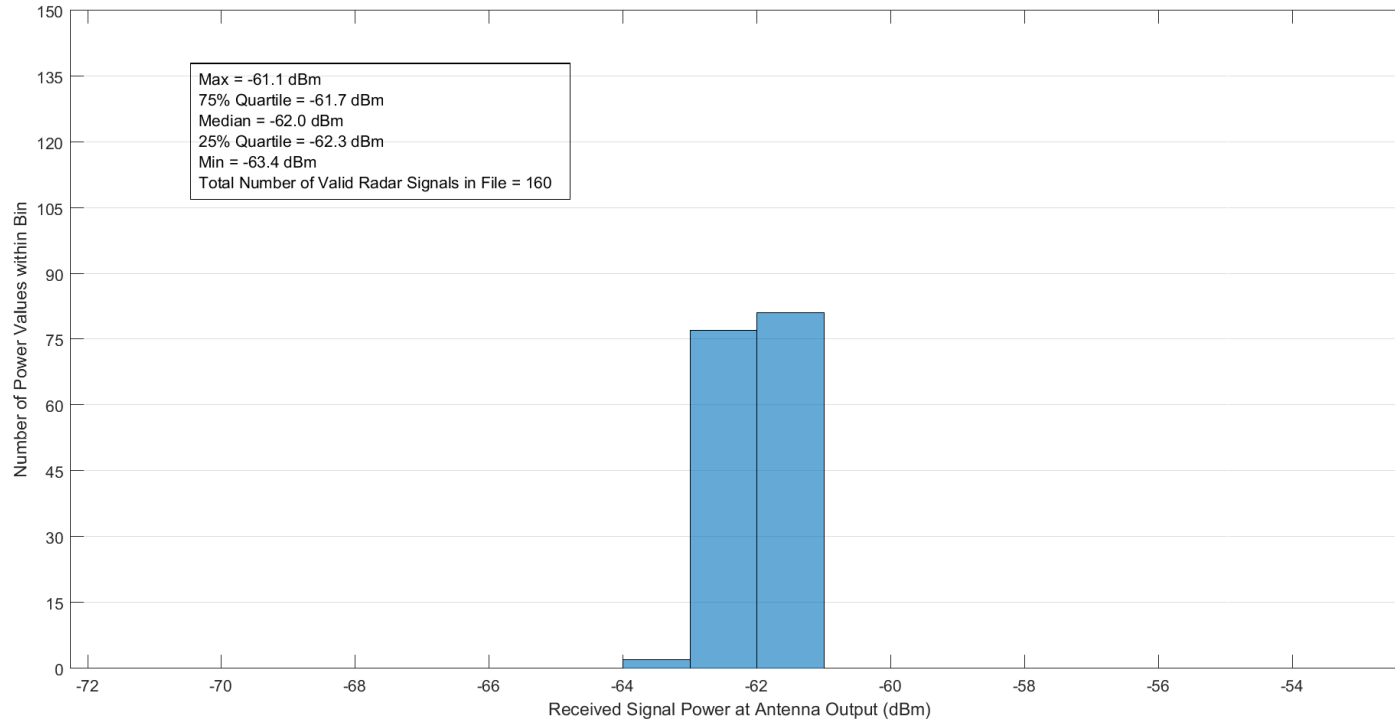


Figure A-4. Received radar signal power statistics at Location 4 in Zone A1 for the ASR-9.

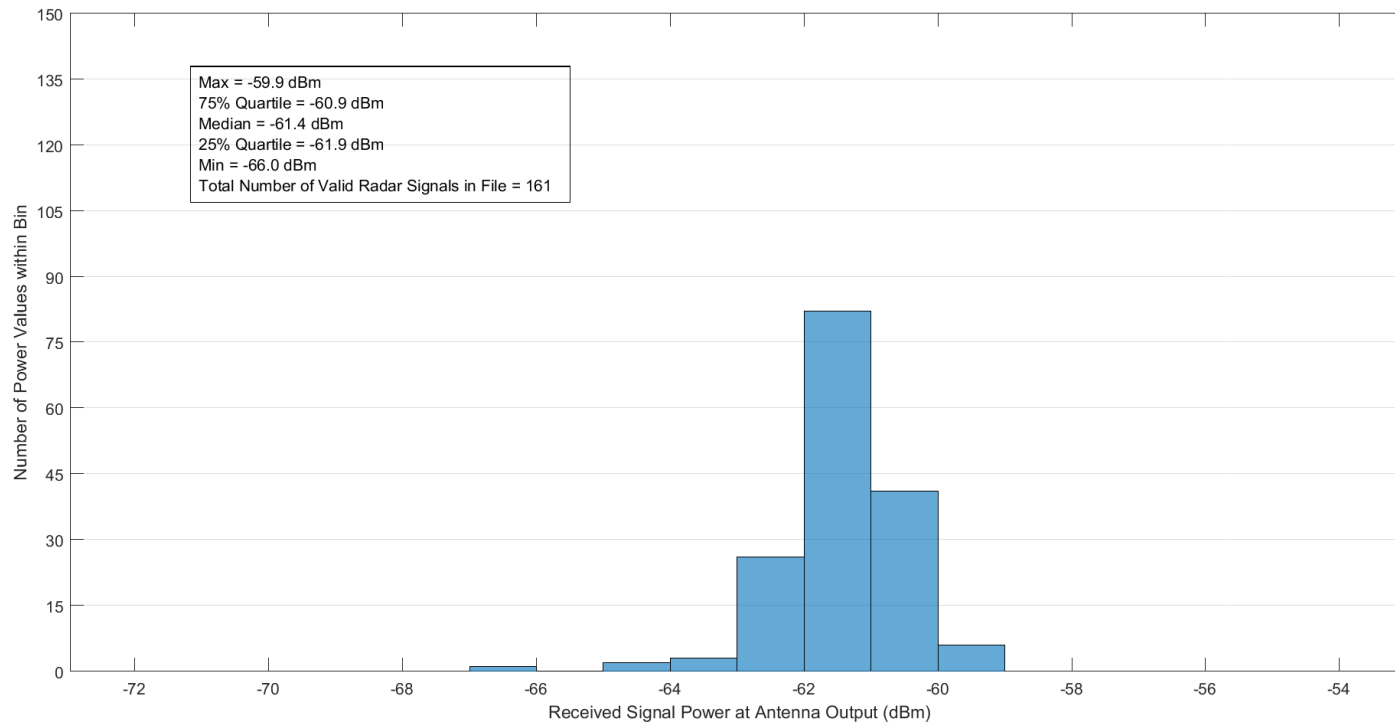


Figure A-5. Received radar signal power statistics at Location 5 in Zone A1 for the ASR-9.

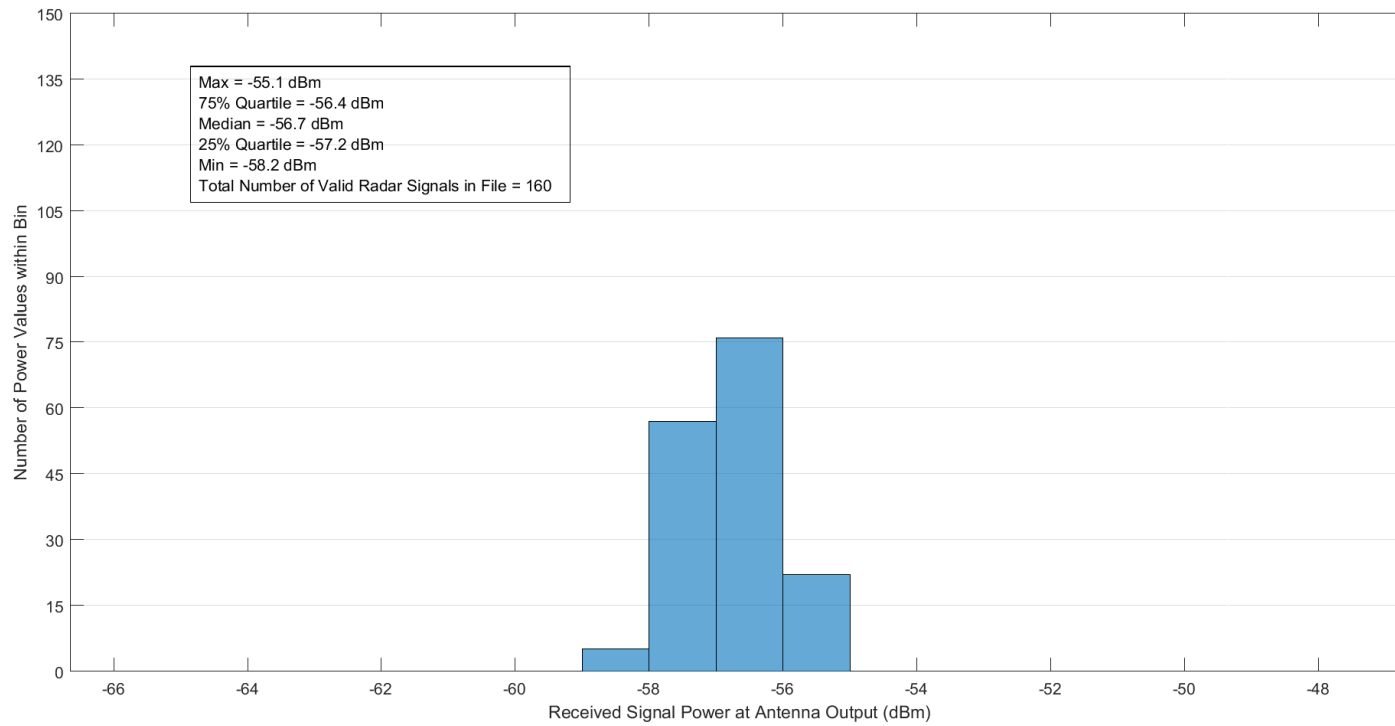


Figure A-6. Received radar signal power statistics at Location 6 in Zone A1 for the ASR-9.

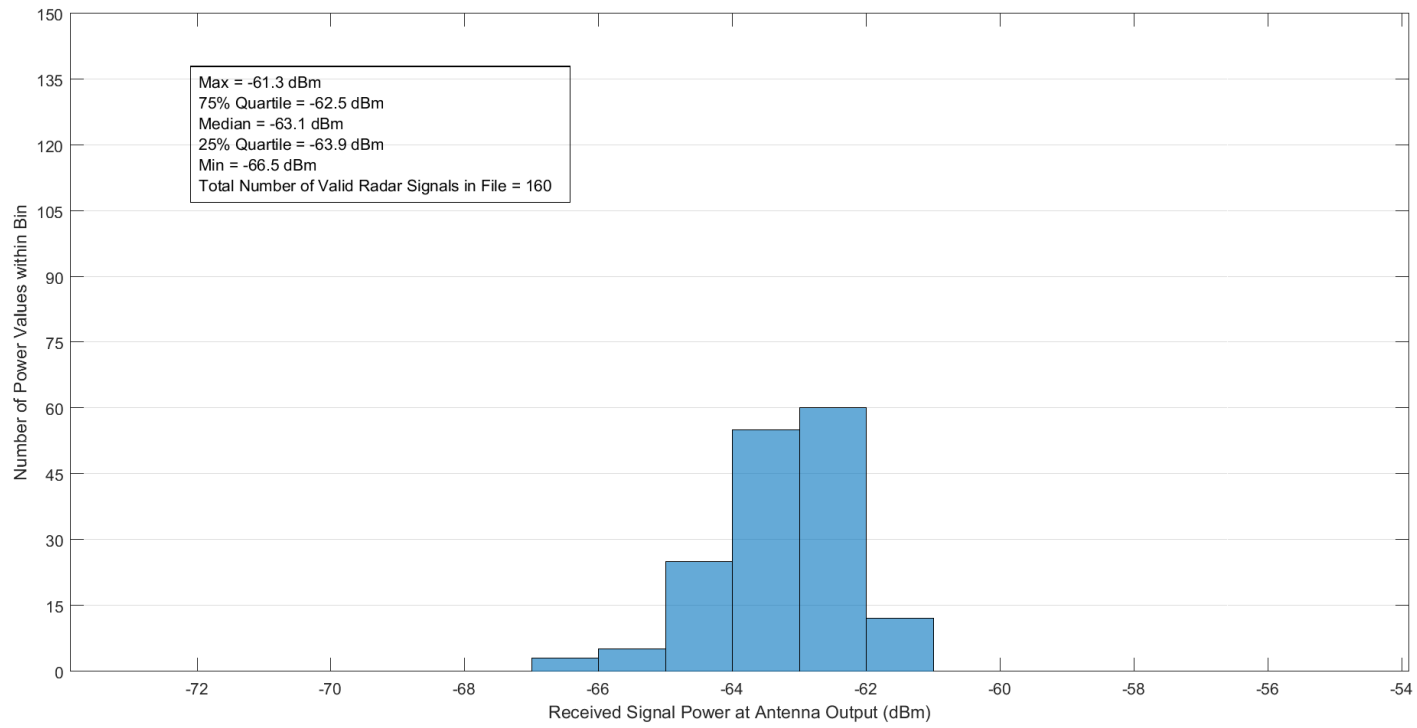


Figure A-7. Received radar signal power statistics at Location 1 in Zone A2 for the ASR-9.

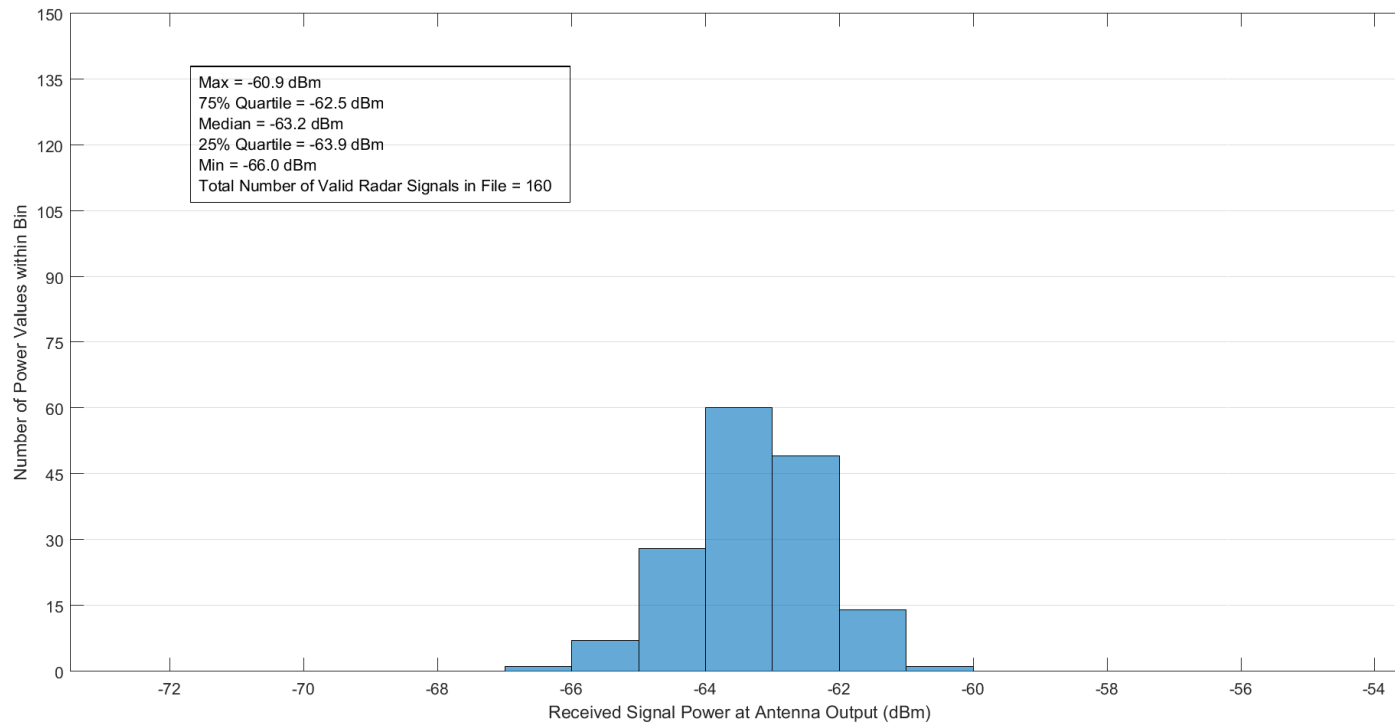


Figure A-8. Received radar signal power statistics at Location 2 in Zone A2 for the ASR-9.

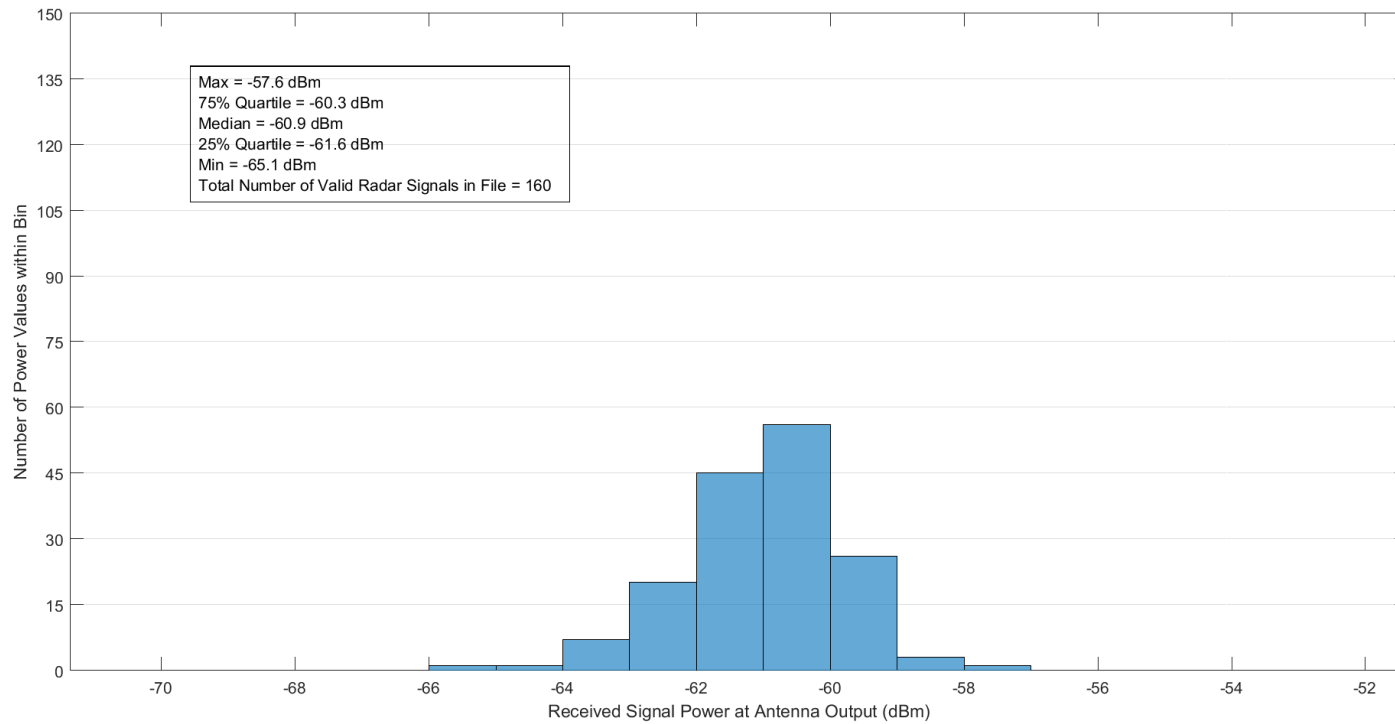


Figure A-9. Received radar signal power statistics at Location 3 in Zone A2 for the ASR-9.

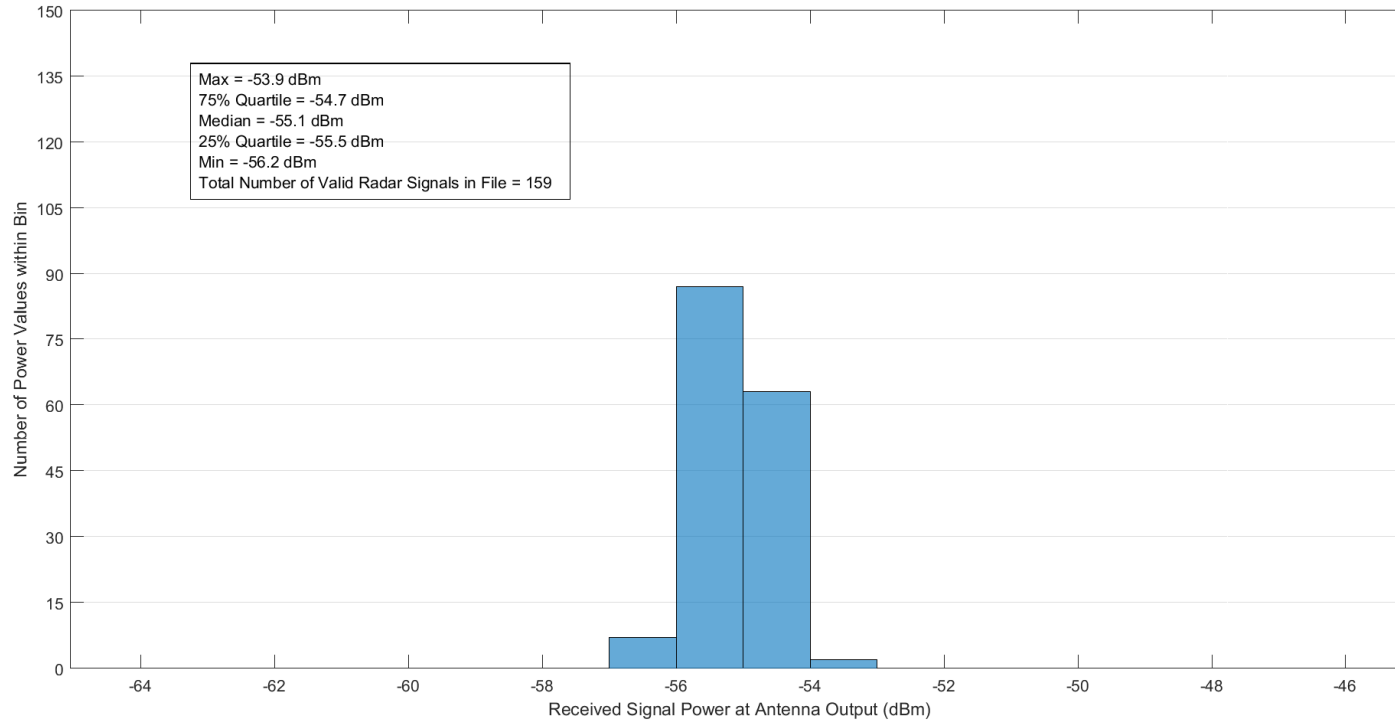


Figure A-10. Received radar signal power statistics at Location 4 in Zone A2 for the ASR-9.

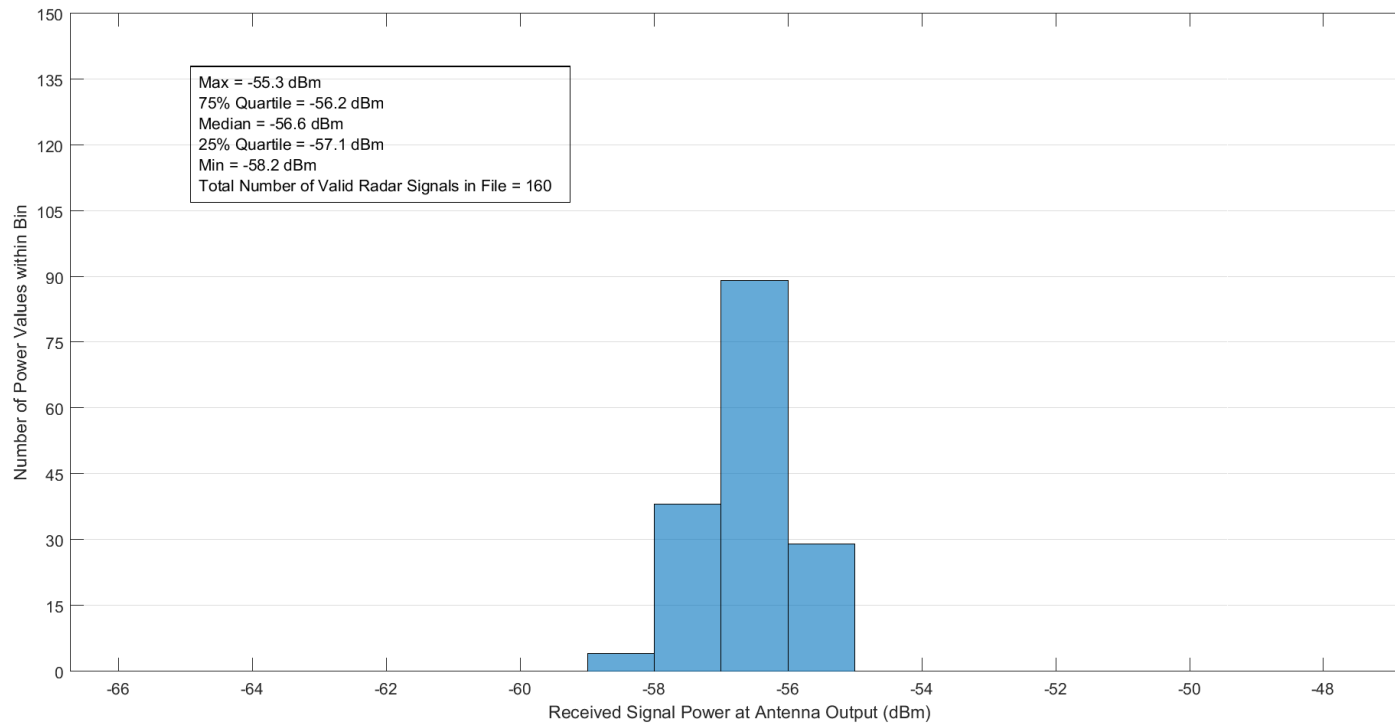


Figure A-11. Received radar signal power statistics at Location 5 in Zone A2 for the ASR-9.

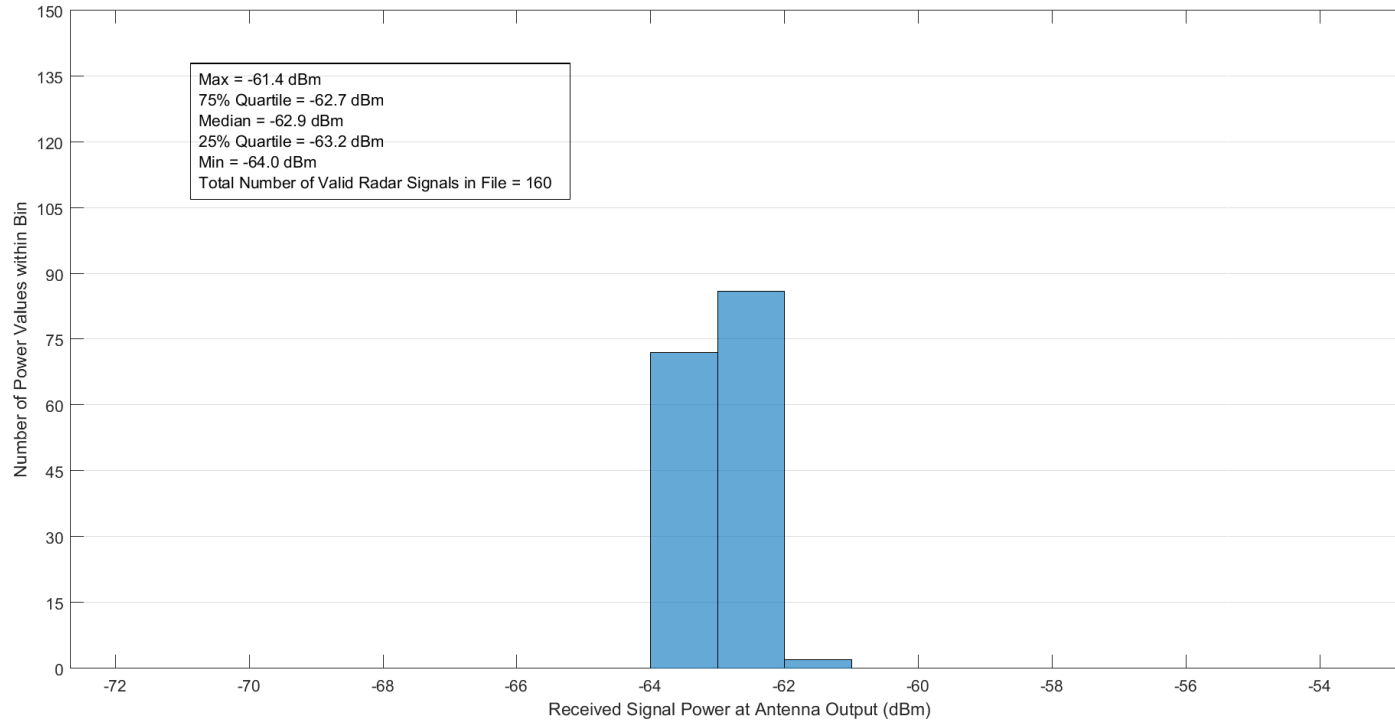


Figure A-12. Received radar signal power statistics at Location 6 in Zone A2 for the ASR-9.

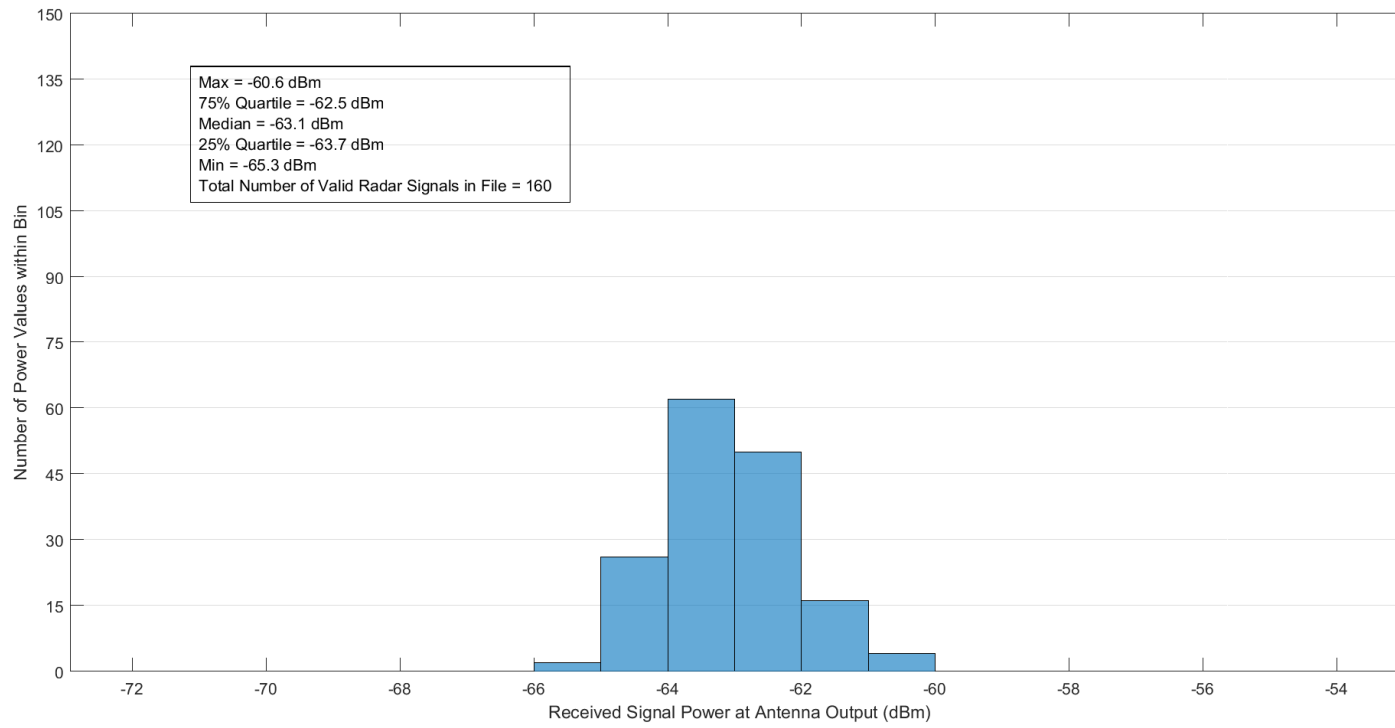


Figure A-13. Received radar signal power statistics at Location 1 in Zone A3 for the ASR-9.

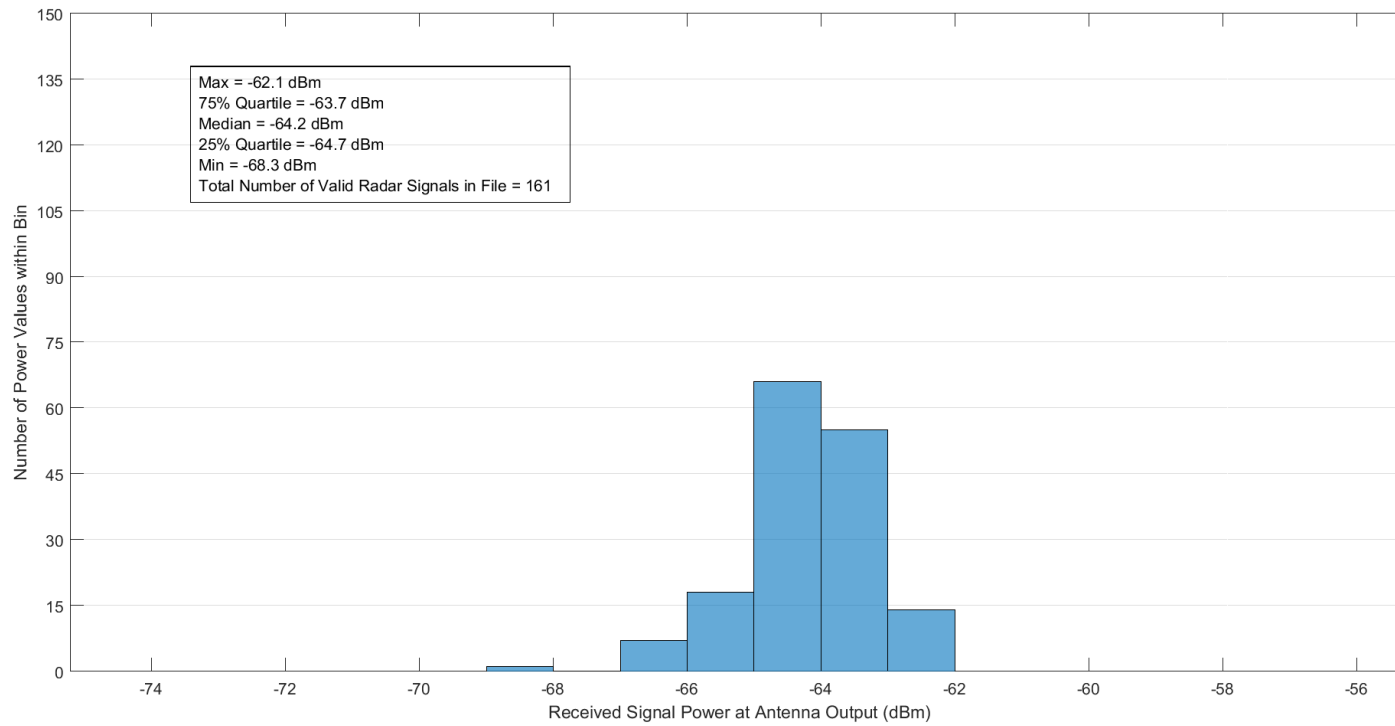


Figure A-14. Received radar signal power statistics at Location 2 in Zone A3 for the ASR-9.

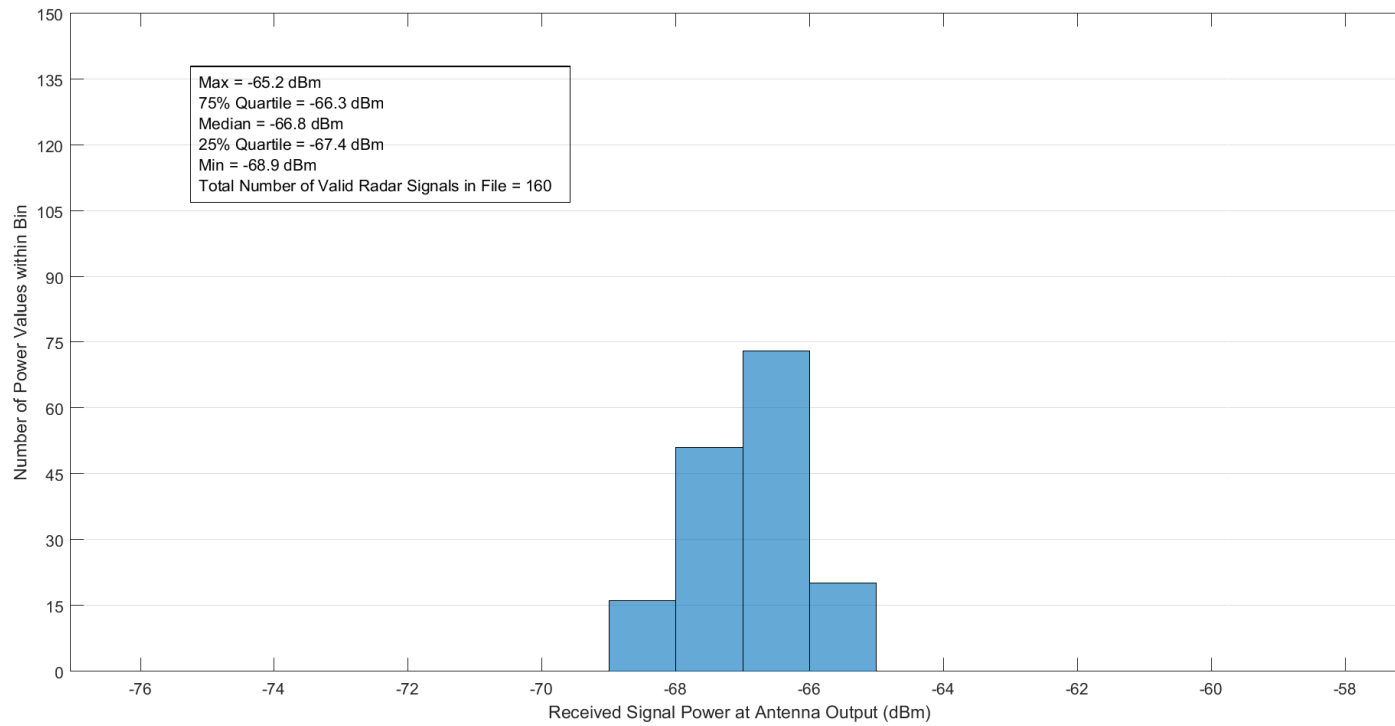


Figure A-15. Received radar signal power statistics at Location 3 in Zone A3 for the ASR-9.

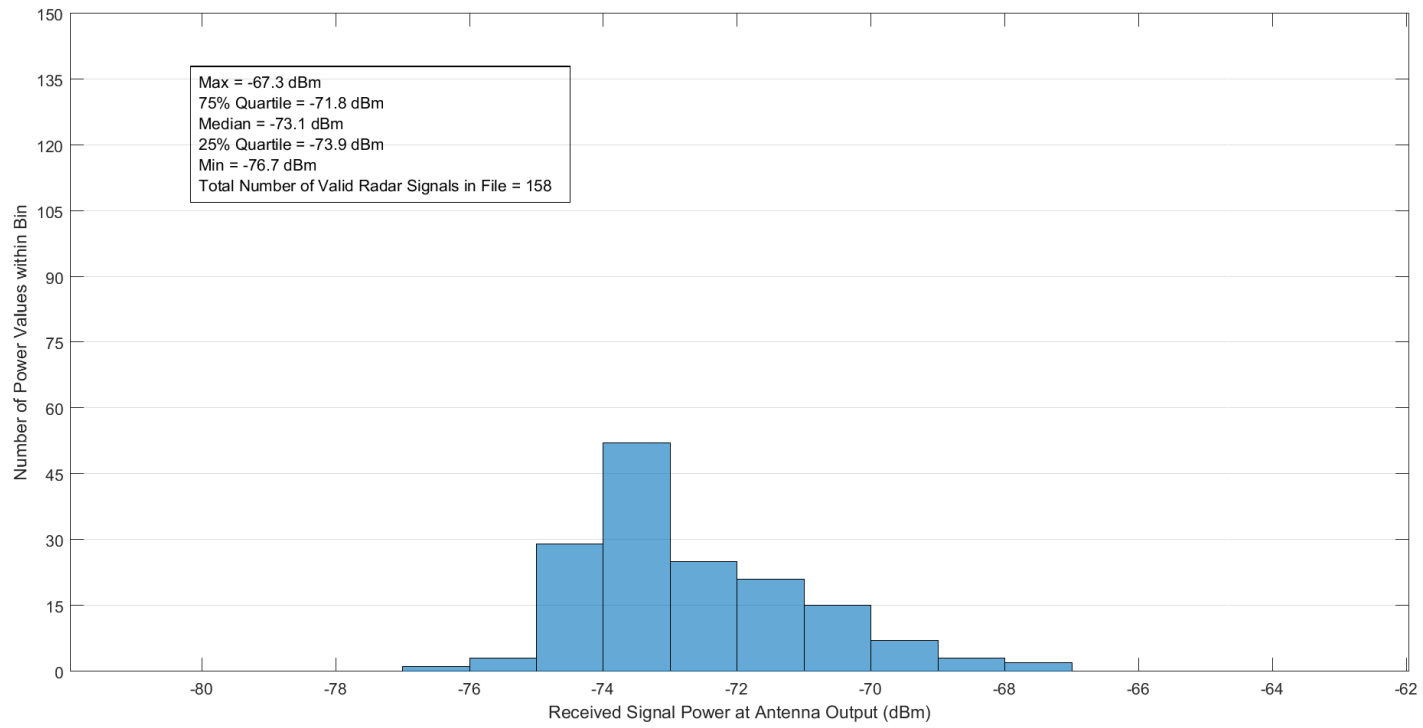


Figure A-16. Received radar signal power statistics at Location 4 in Zone A3 for the ASR-9.

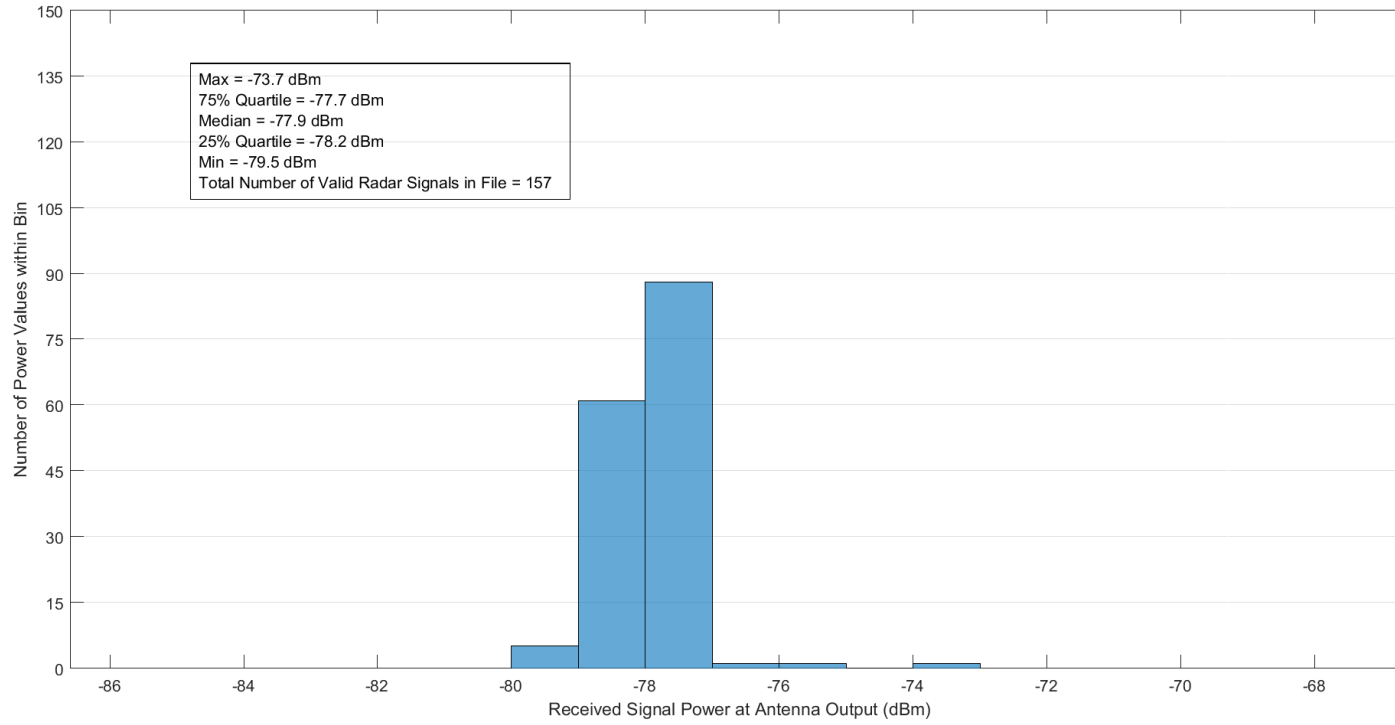


Figure A-17. Received radar signal power statistics at Location 5 in Zone A3 for the ASR-9.

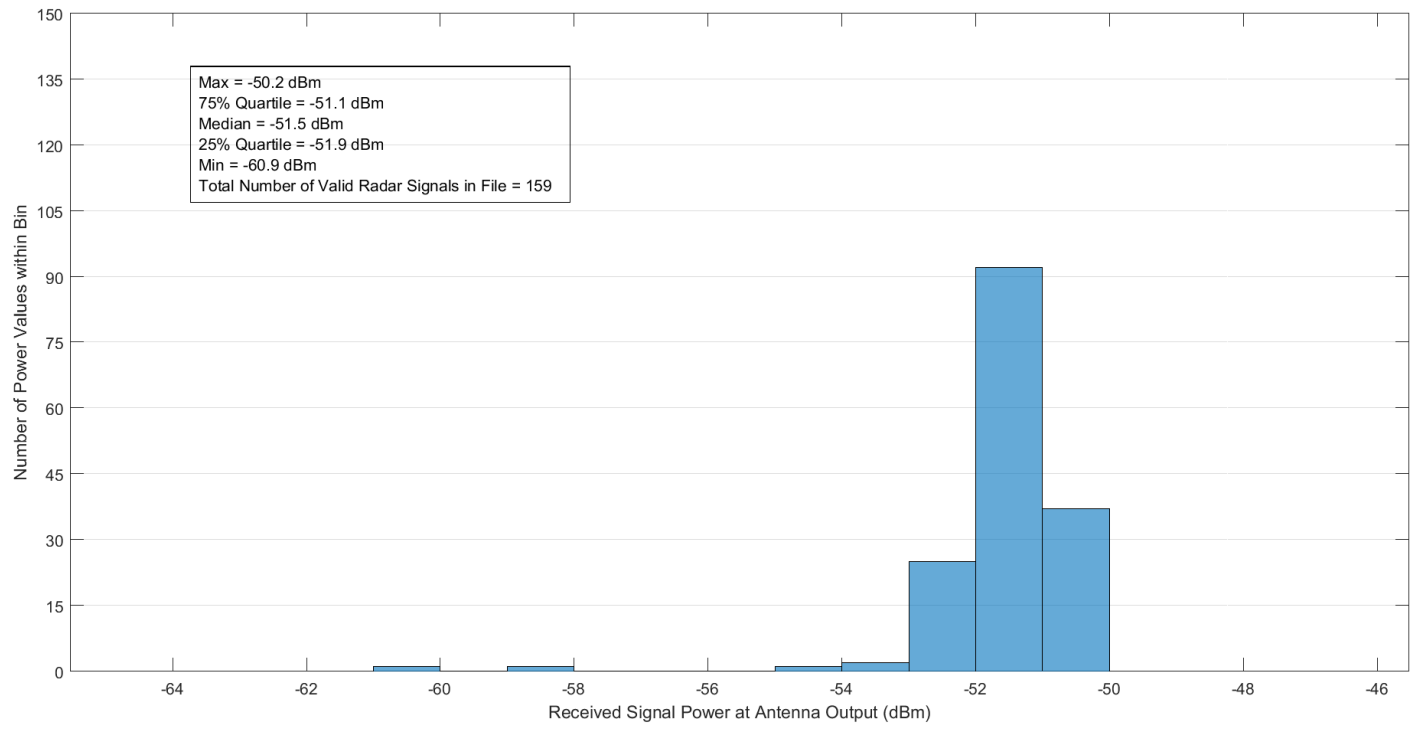


Figure A-18. Received radar signal power statistics at Location 6 in Zone A3 for the ASR-9.

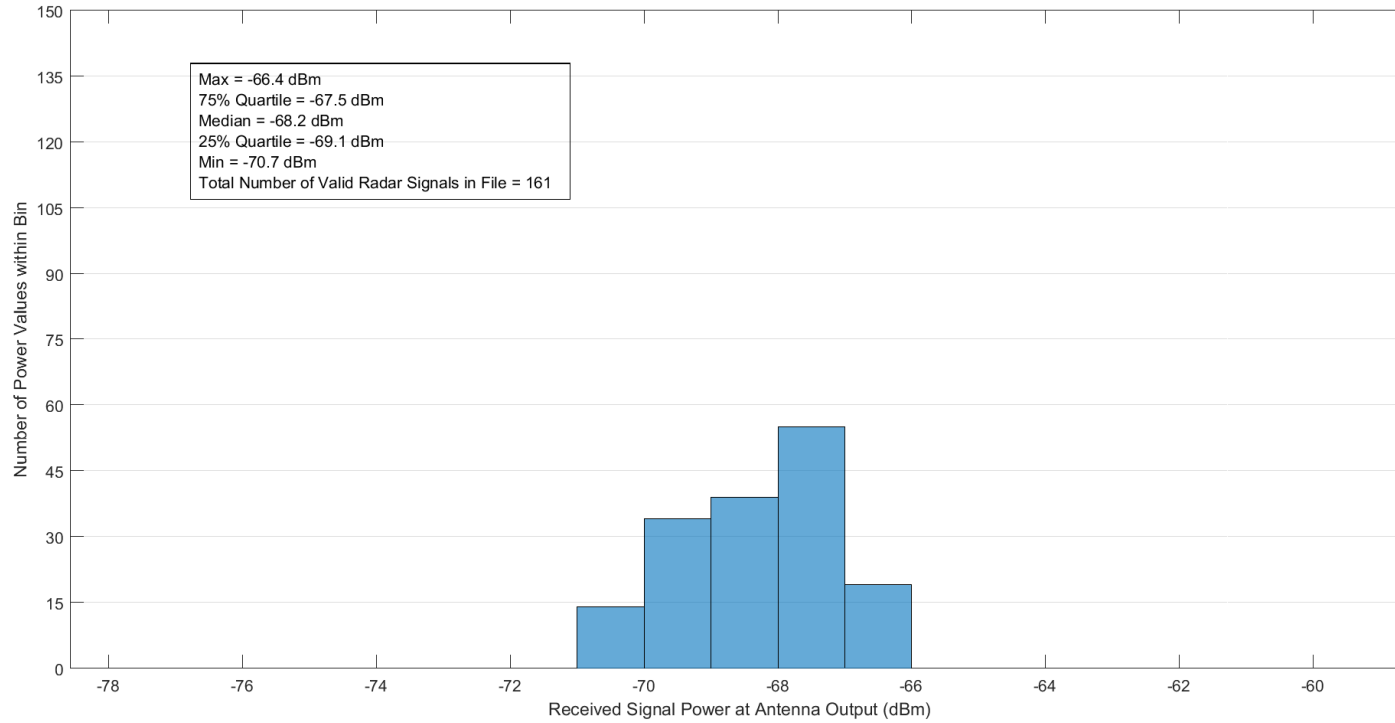


Figure A-19. Received radar signal power statistics at Location 1 in Zone B1 for the ASR-9.

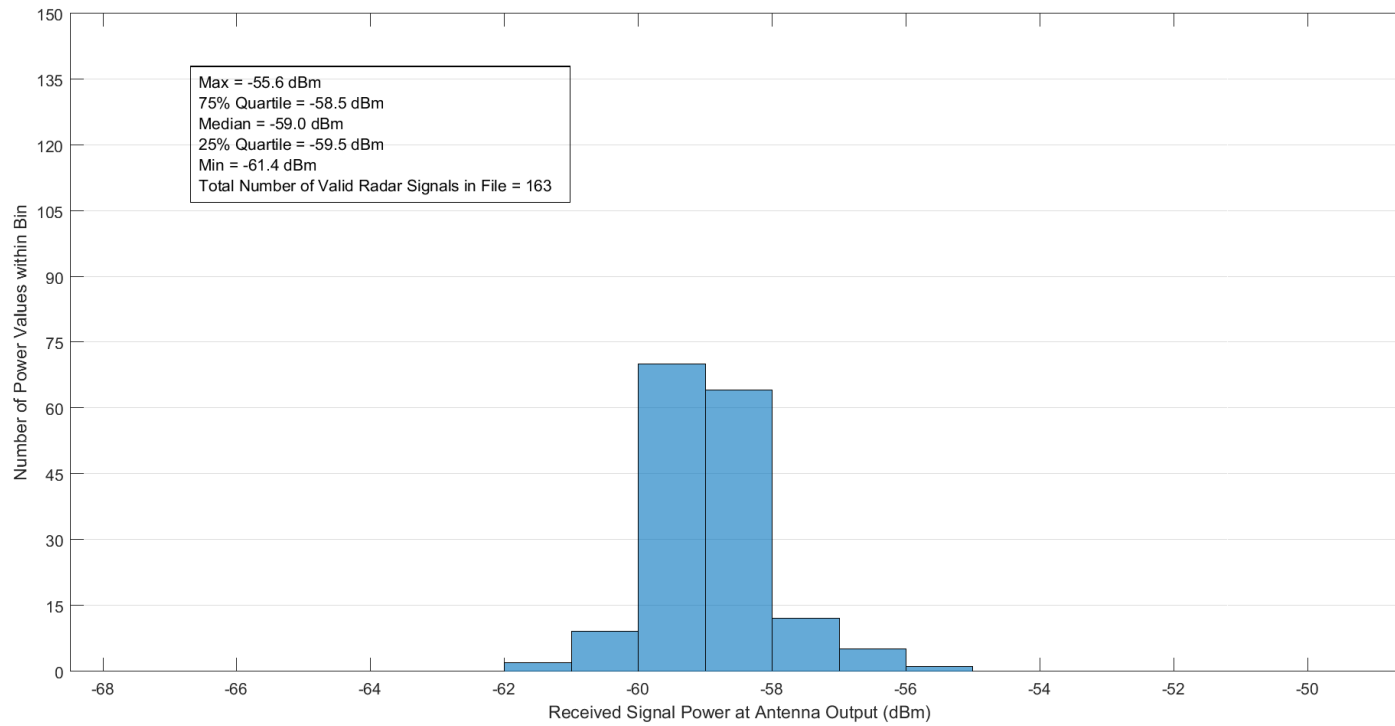


Figure A-20. Received radar signal power statistics at Location 1 in Zone C1 for the ASR-9.

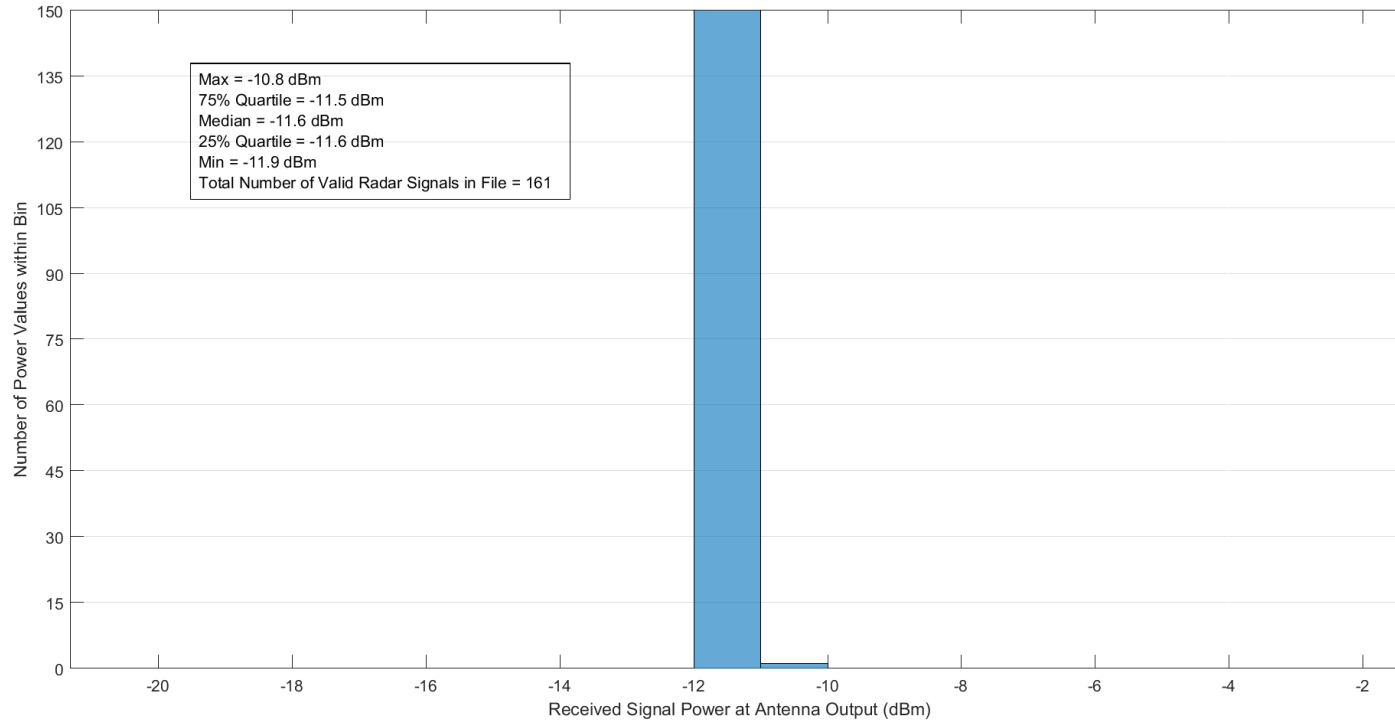


Figure A-21. Received radar signal power statistics at Location 2 in Zone C1 for the ASR-9.

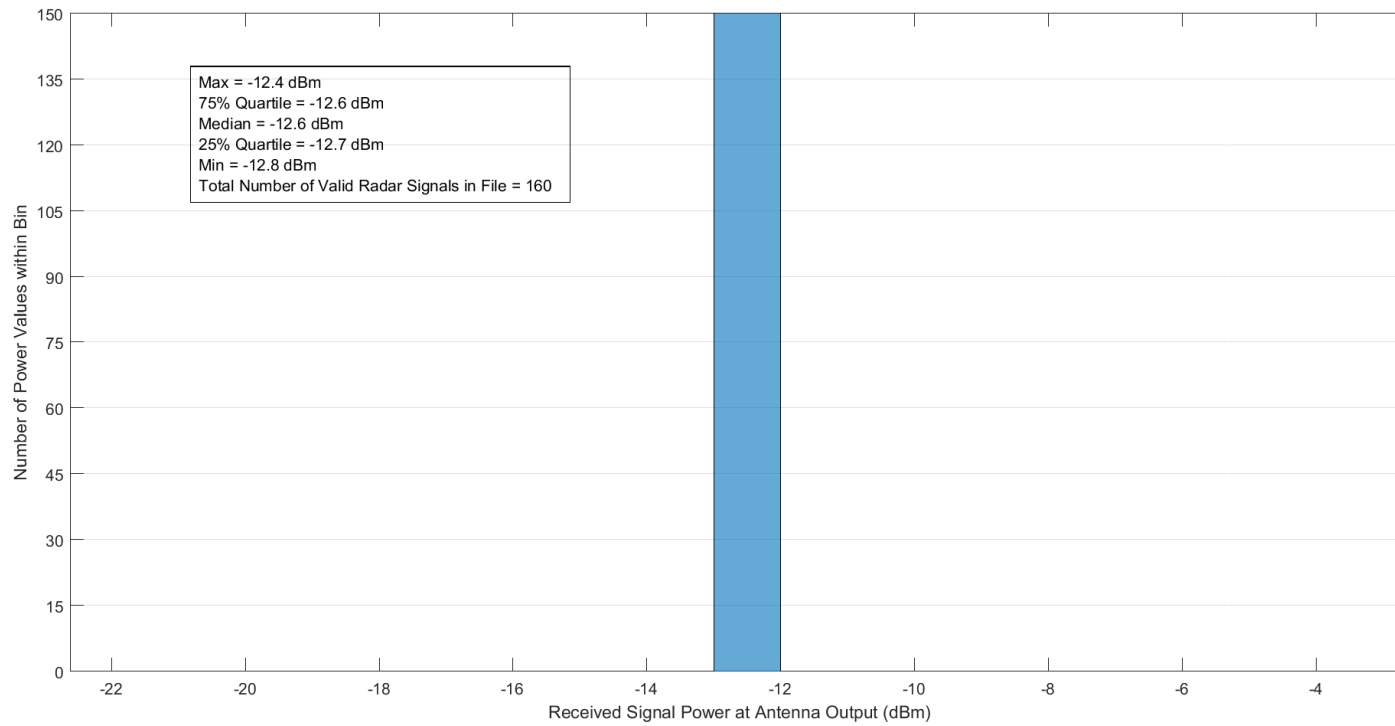


Figure A-22. Received radar signal power statistics at Location 3 in Zone C1 for the ASR-9.

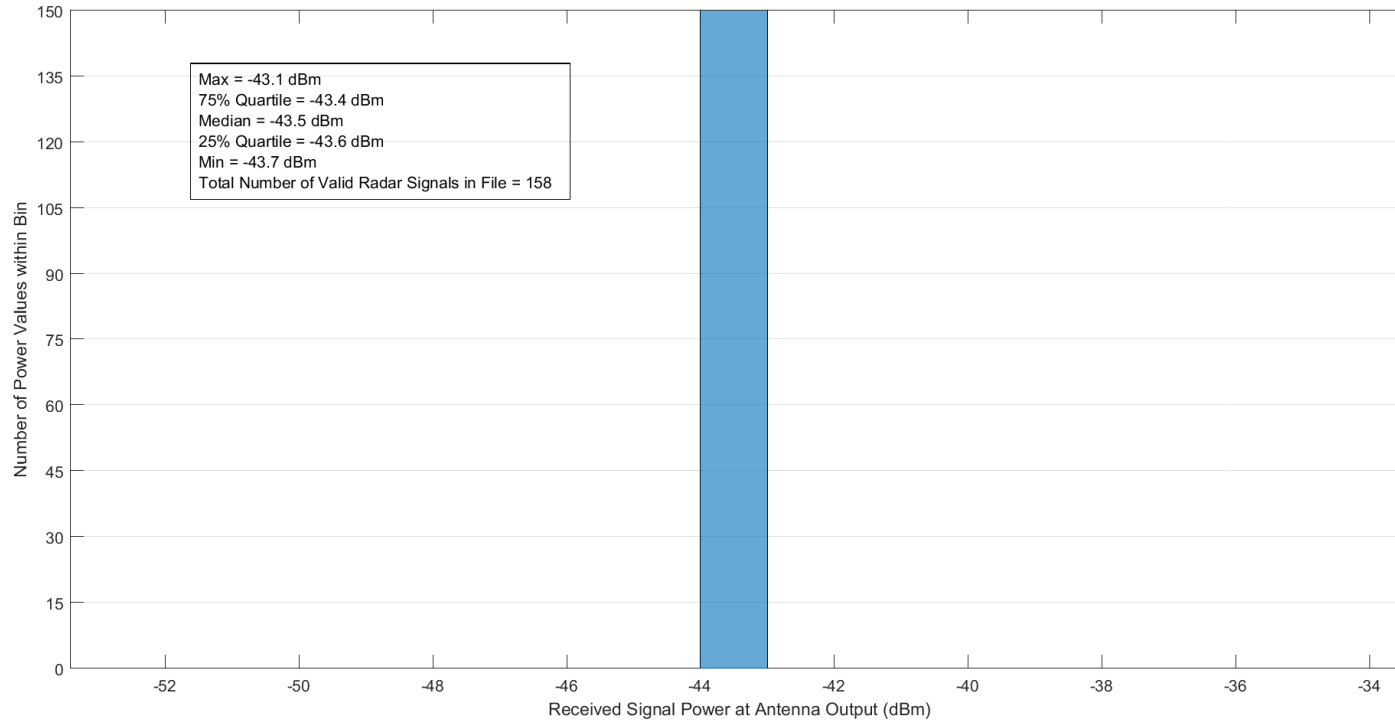


Figure A-23. Received radar signal power statistics at Location 4 in Zone C1 for the ASR-9.

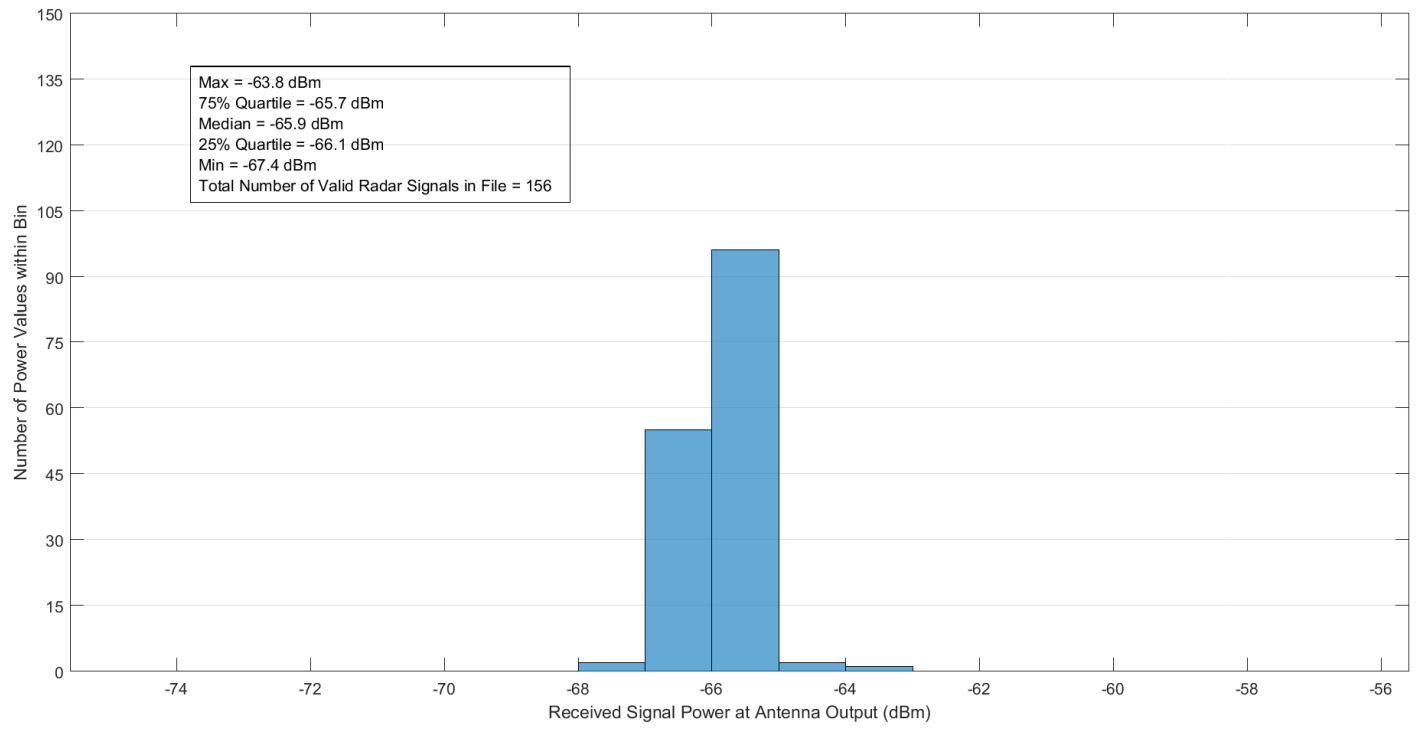
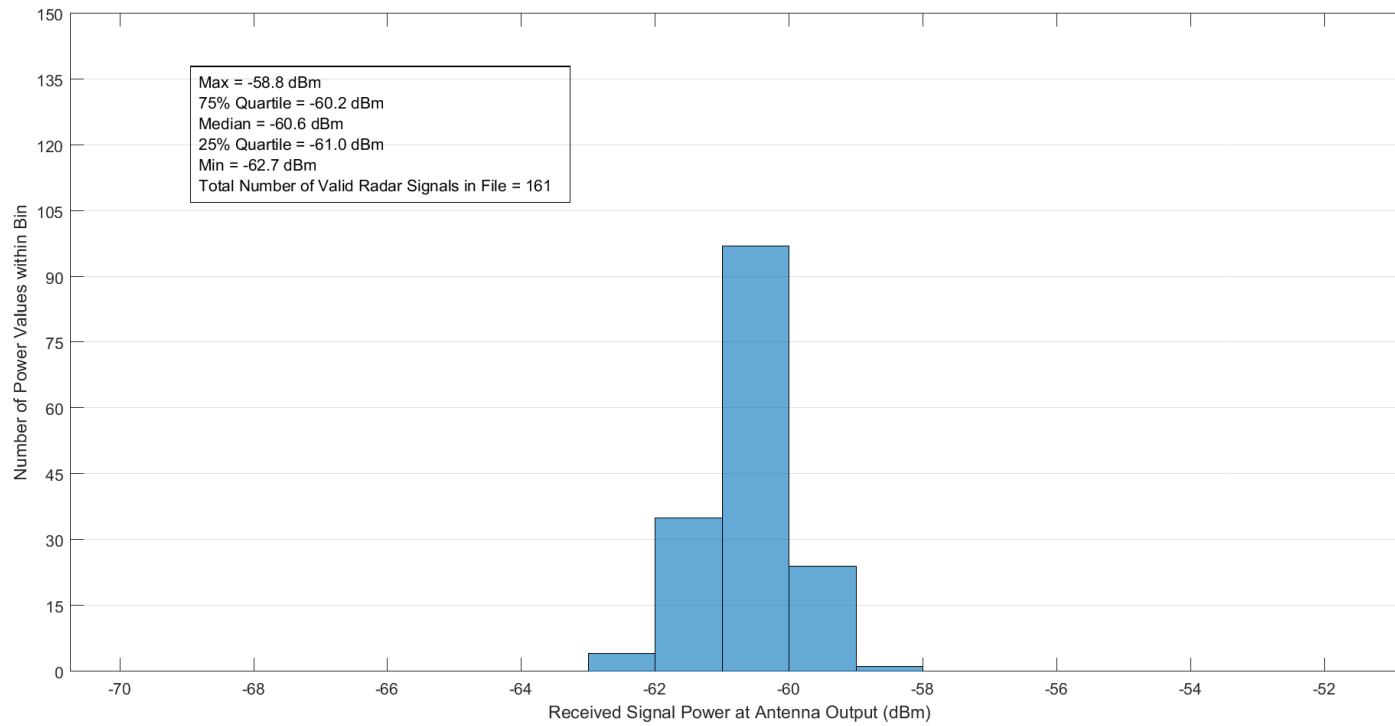


Figure A-24. Received radar signal power statistics at Location 5 in Zone C1 for the ASR-9.



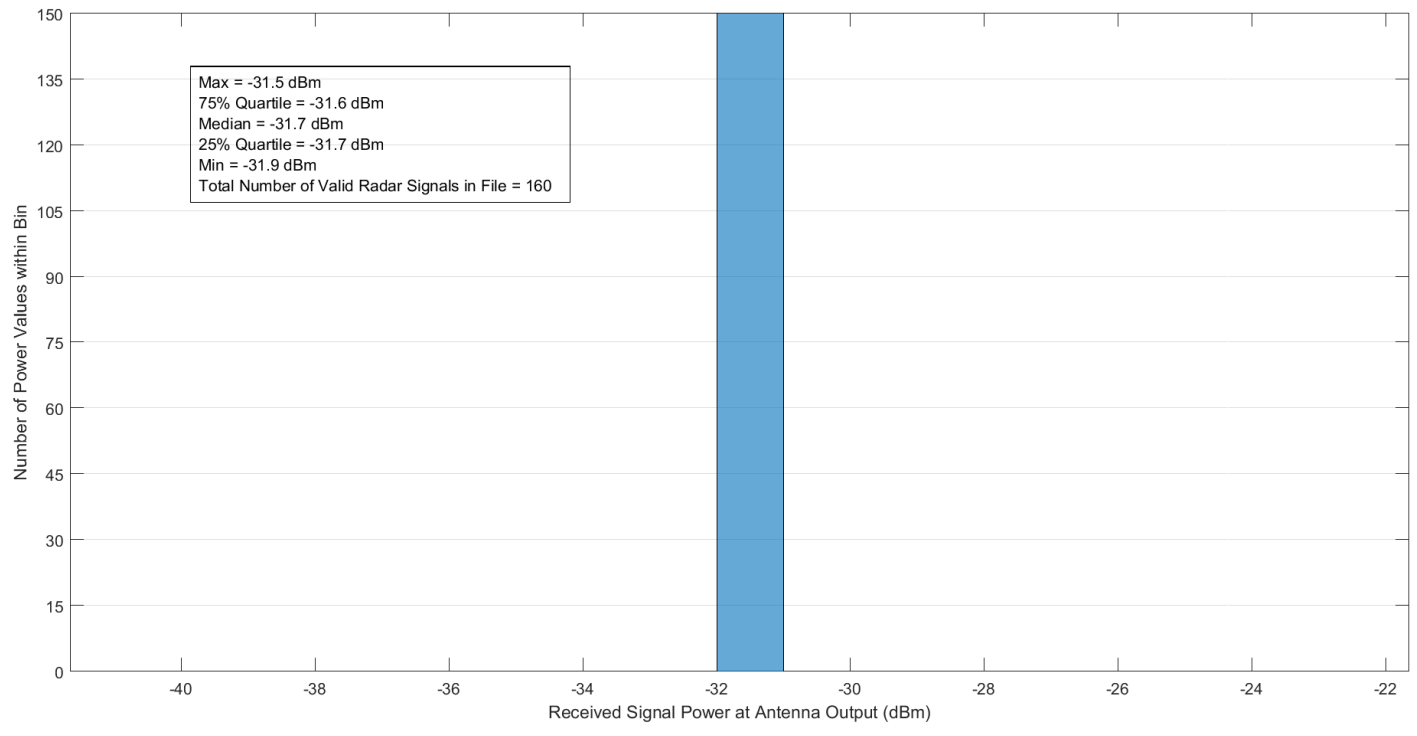


Figure A-26. Received radar signal power statistics at Location 1 in Zone C2 for the ASR-9.

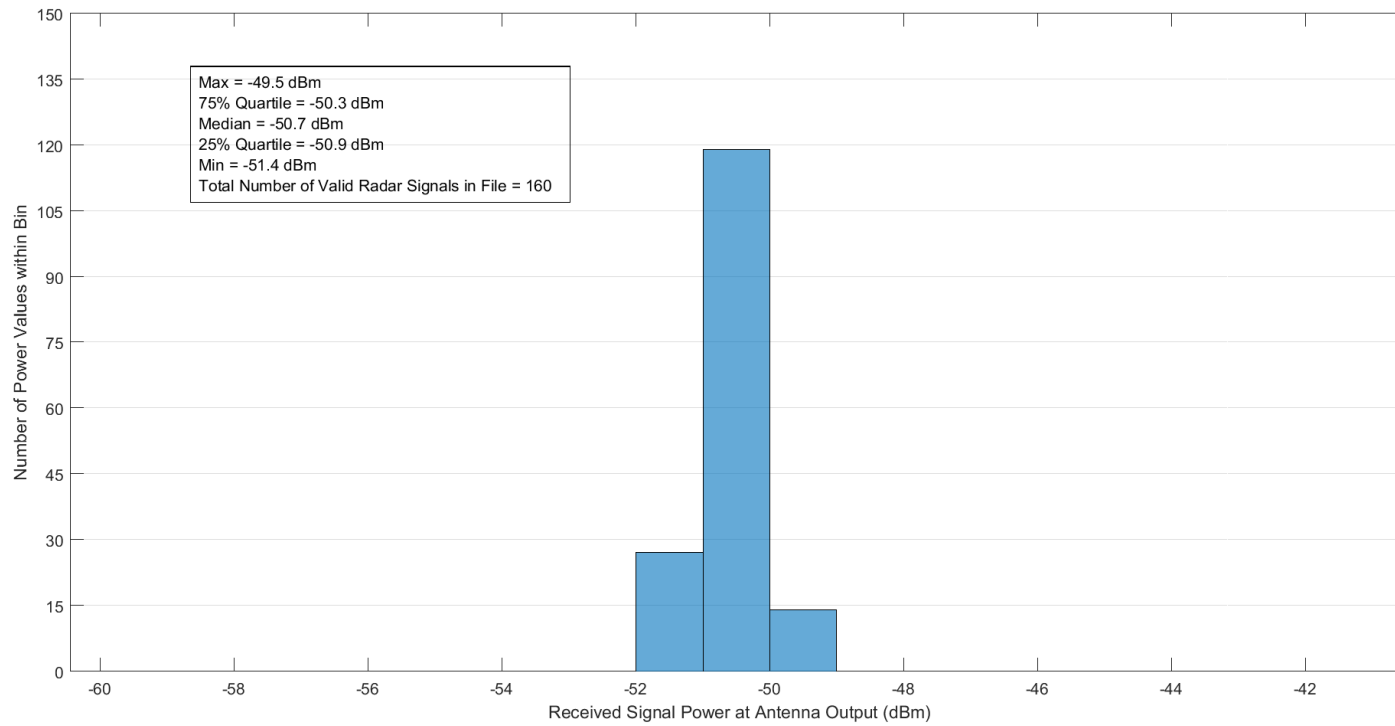


Figure A-27. Received radar signal power statistics at Location 2 in Zone C2 for the ASR-9.

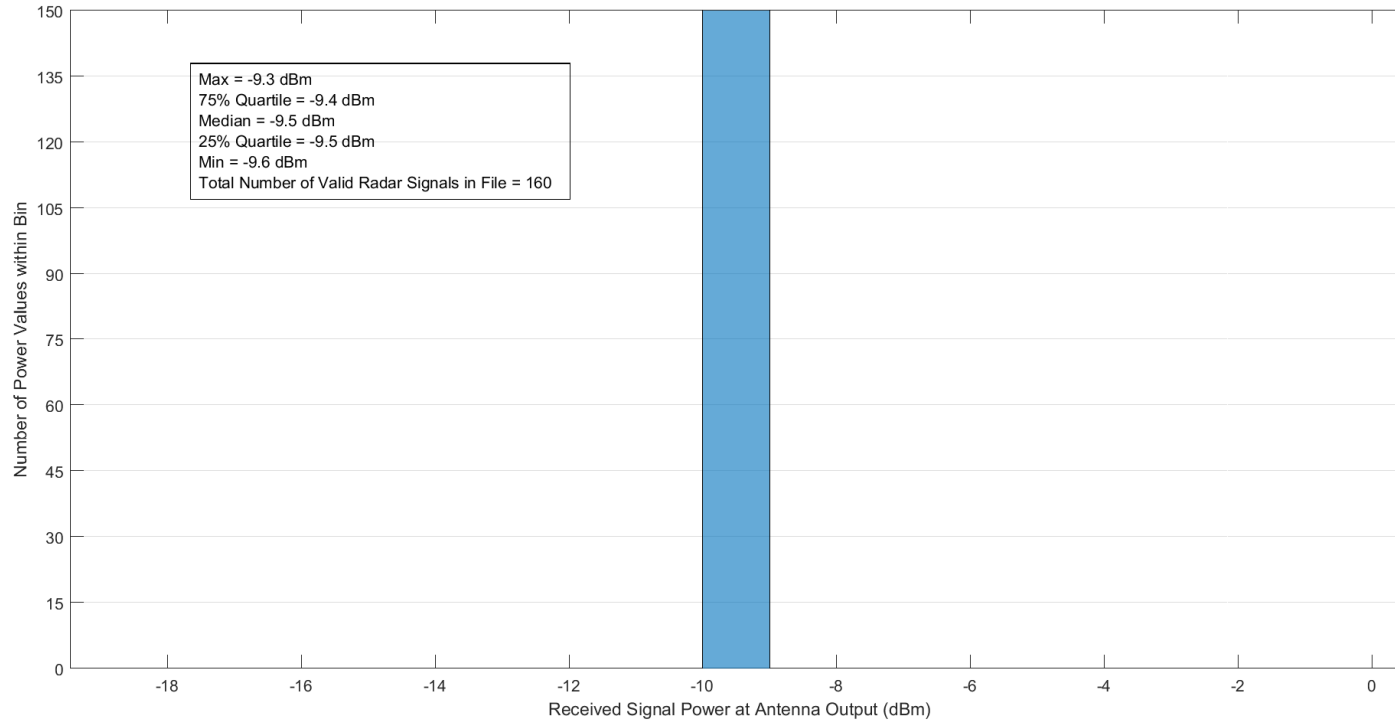


Figure A-28. Received radar signal power statistics at Location 3 in Zone C2 for the ASR-9.

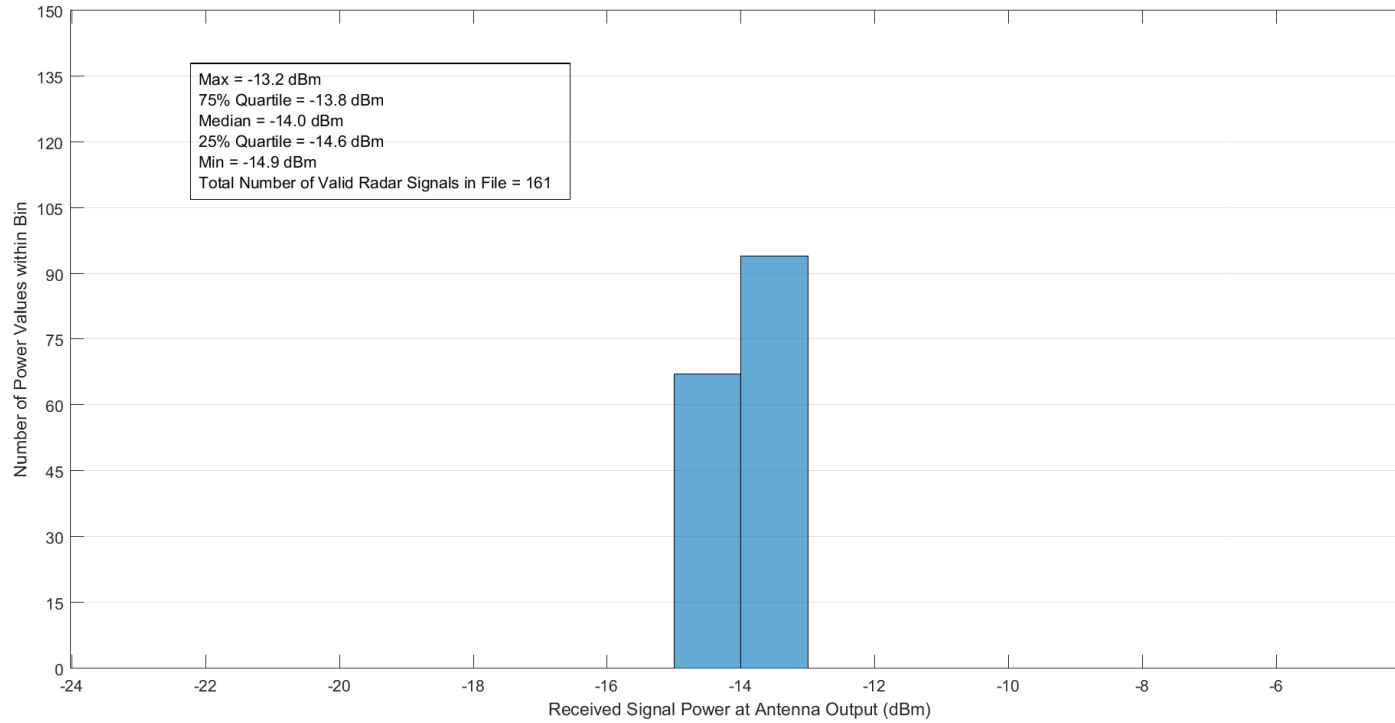


Figure A-29. Received radar signal power statistics at Location 4 in Zone C2 for the ASR-9.

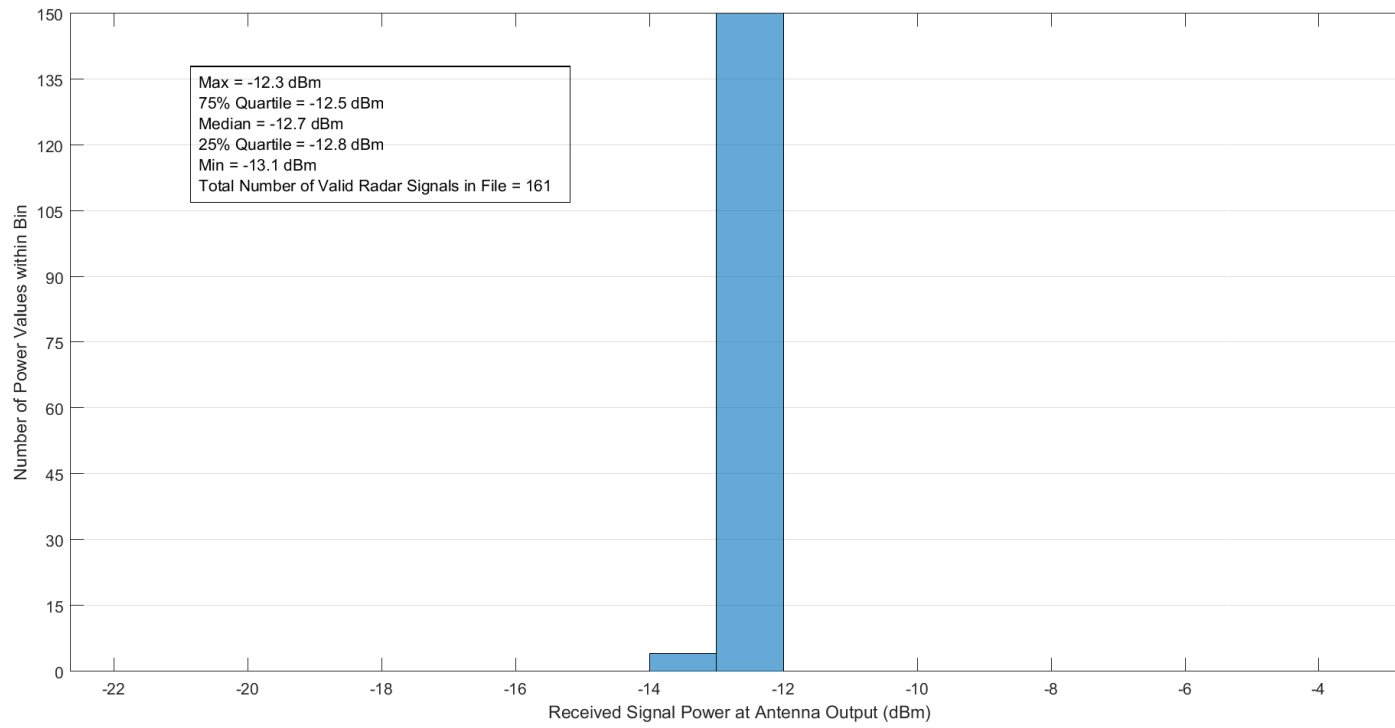


Figure A-30. Received radar signal power statistics at Location 5 in Zone C2 for the ASR-9.

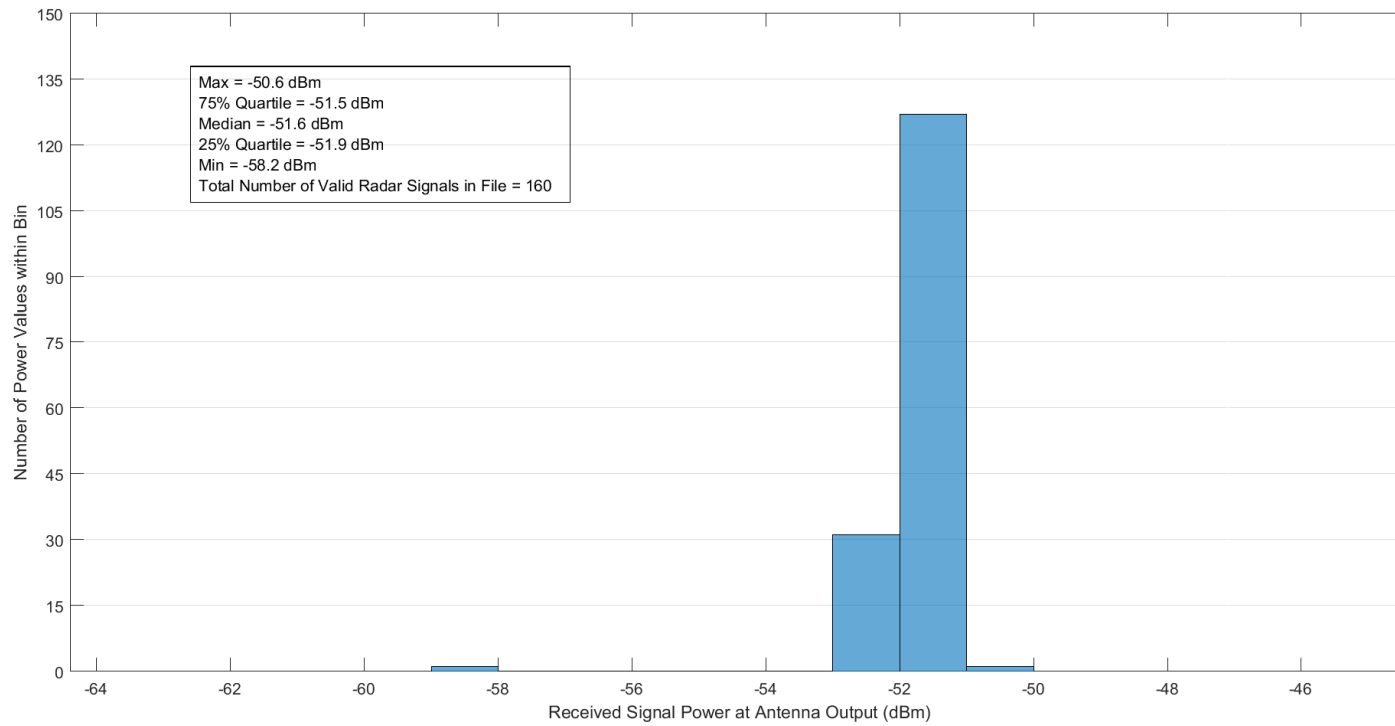


Figure A-31. Received radar signal power statistics at Location 1 in Zone D1 for the ASR-9.

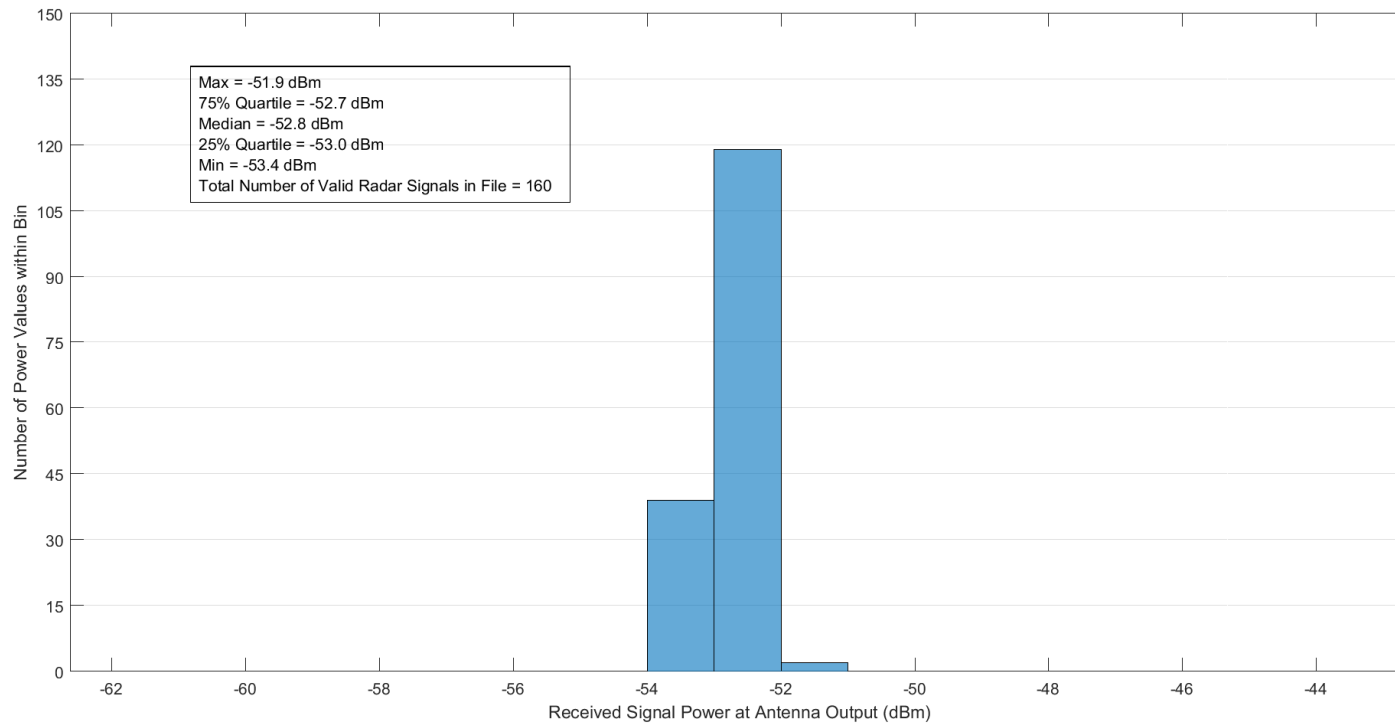


Figure A-32. Received radar signal power statistics at Location 2 in Zone D1 for the ASR-9.

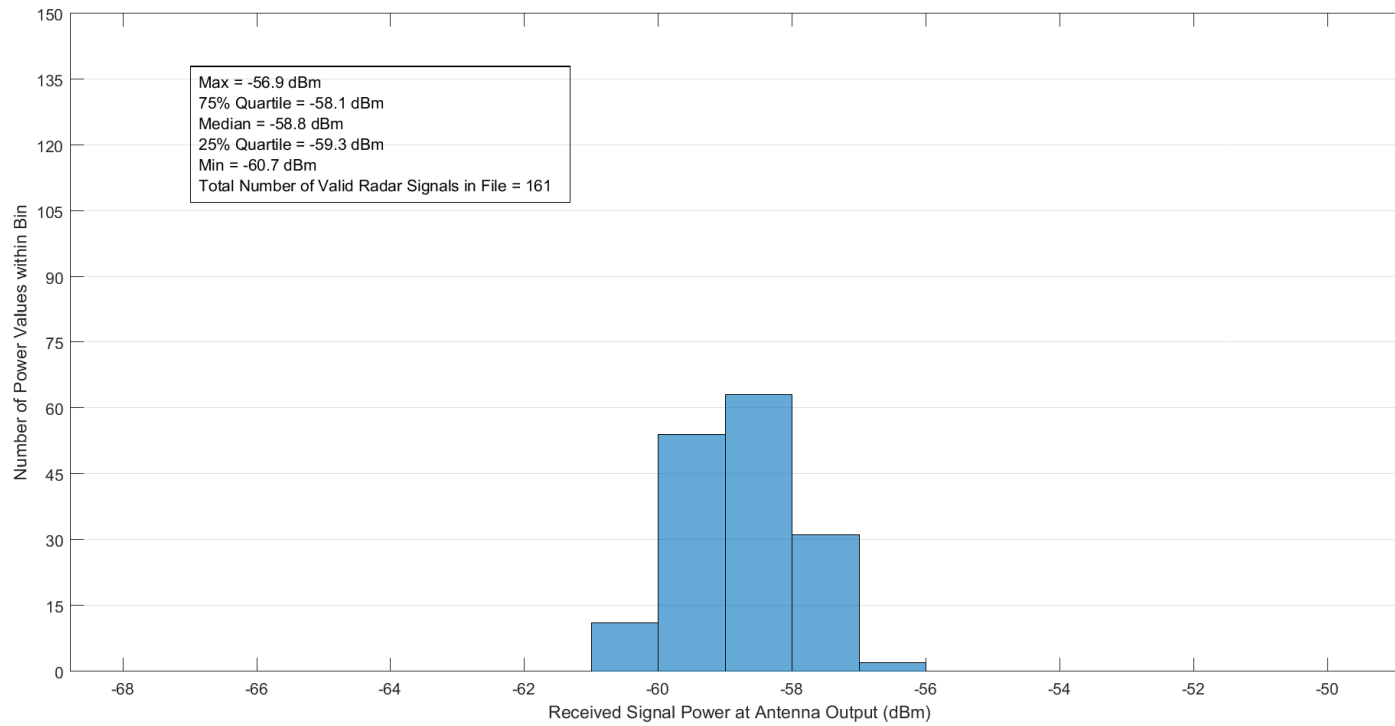


Figure A-33. Received radar signal power statistics at Location 3 in Zone D1 for the ASR-9.

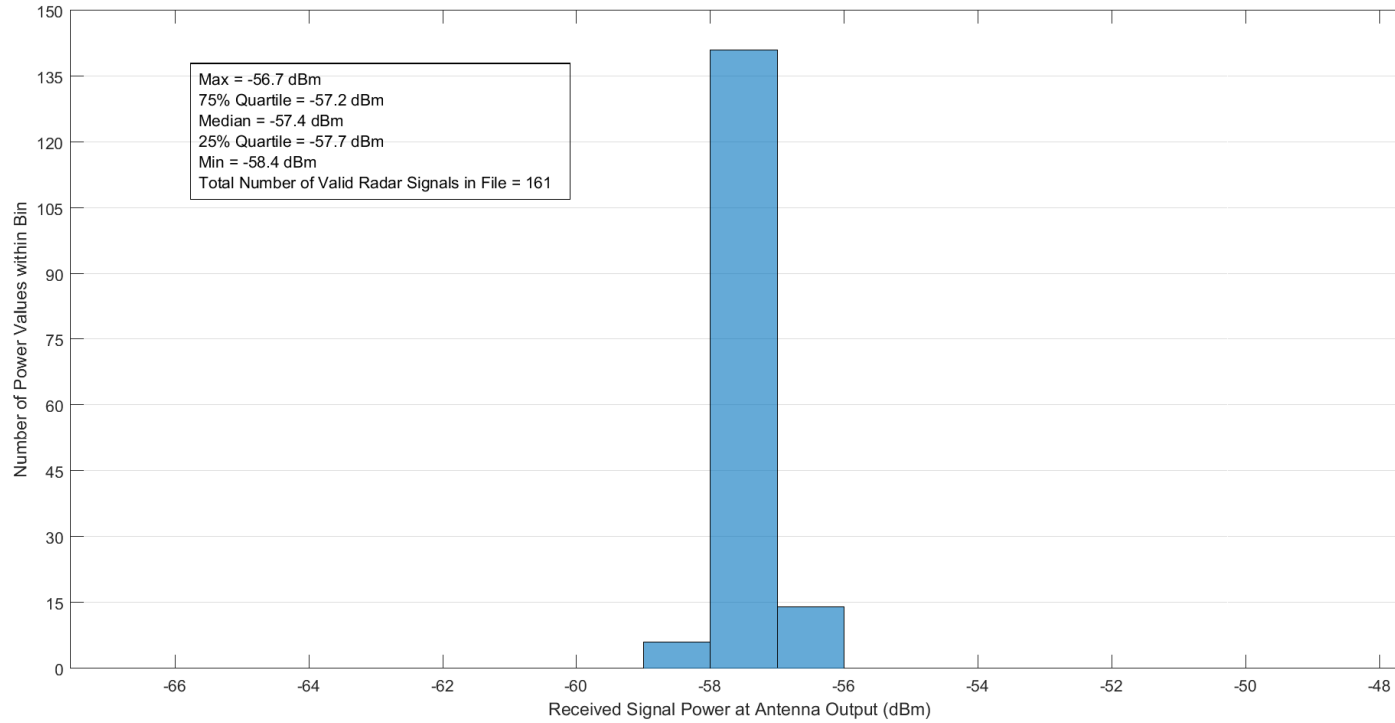


Figure A-34. Received radar signal power statistics at Location 4 in Zone D1 for the ASR-9.

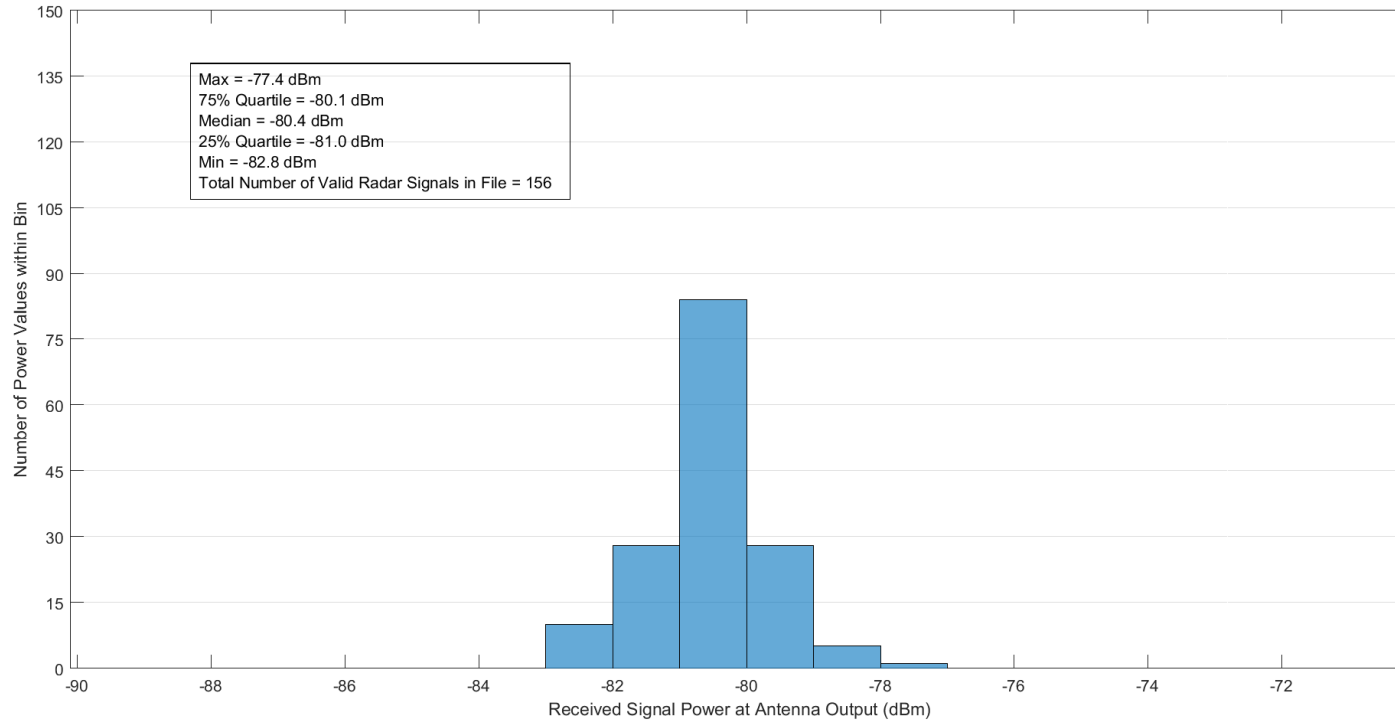


Figure A-35. Received radar signal power statistics at Location 5 in Zone D1 for the ASR-9.

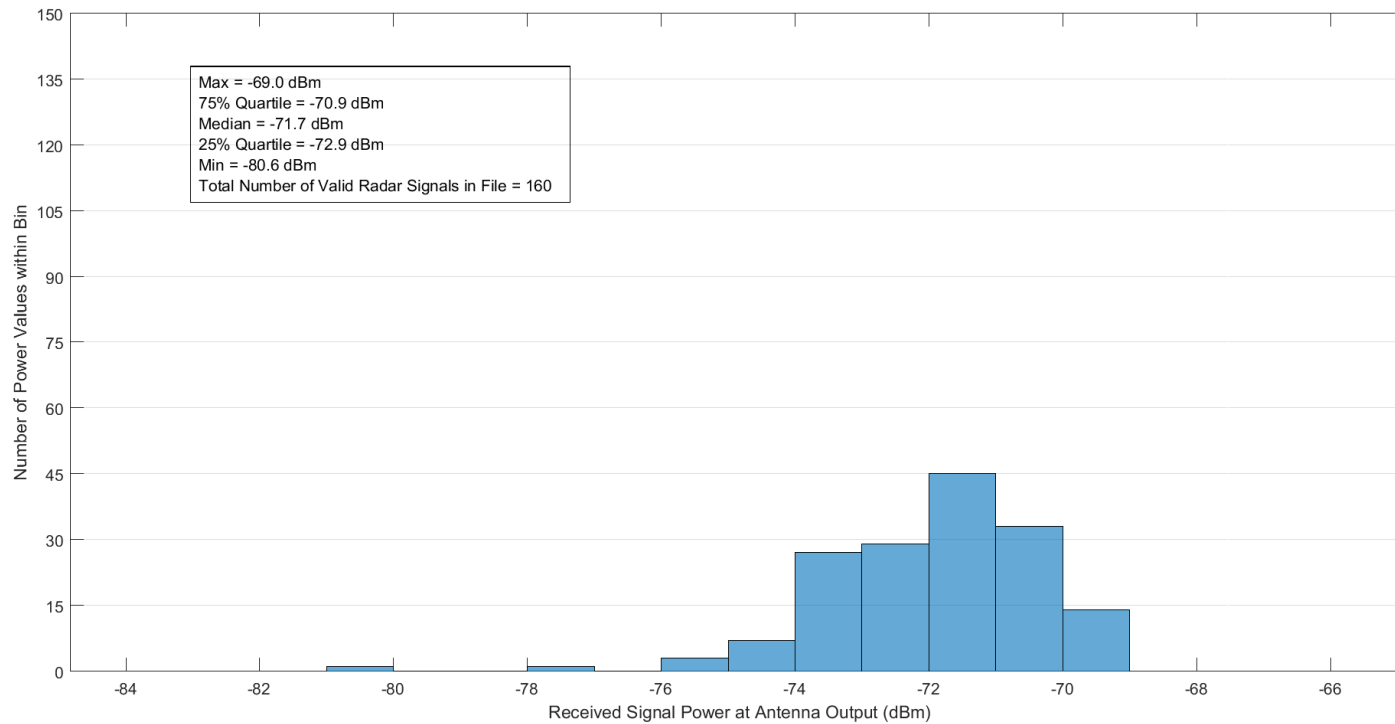


Figure A-36. Received radar signal power statistics at Location 1 in Zone D2 for the ASR-9.

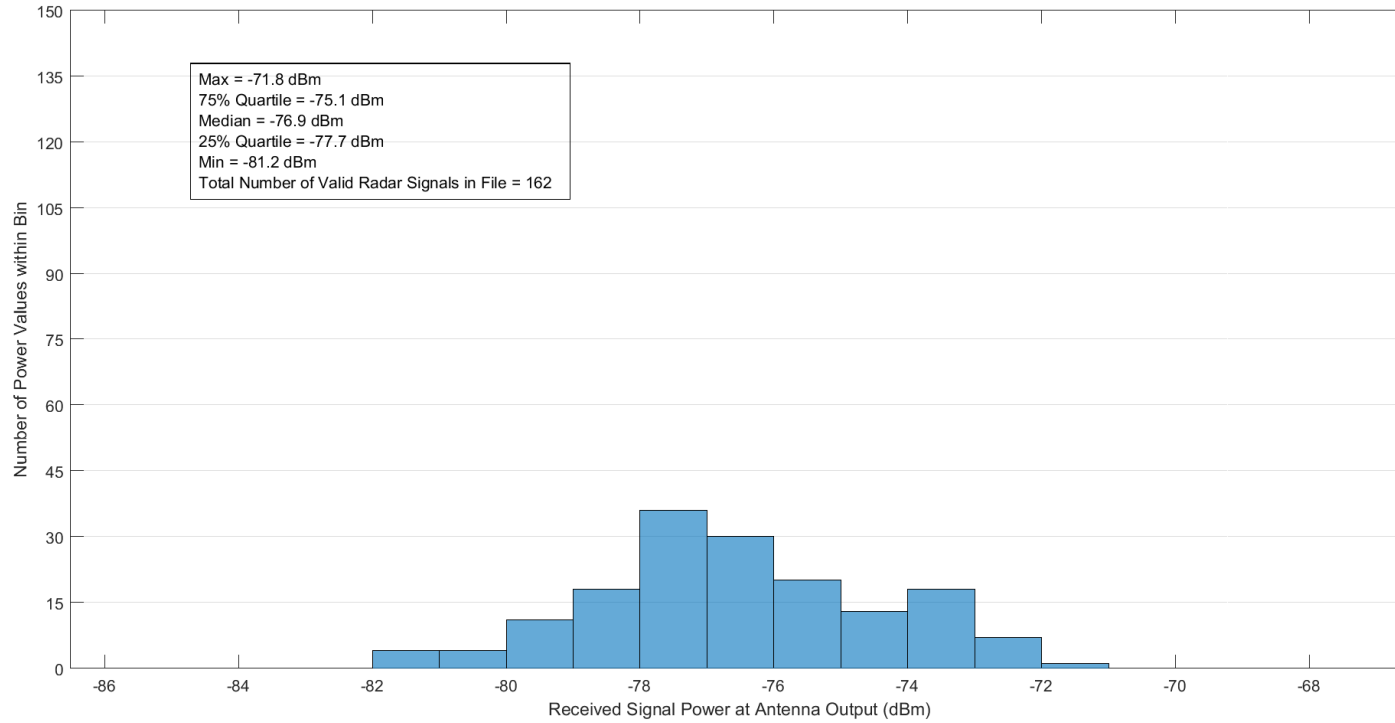


Figure A-37. Received radar signal power statistics at Location 2 in Zone D2 for the ASR-9.

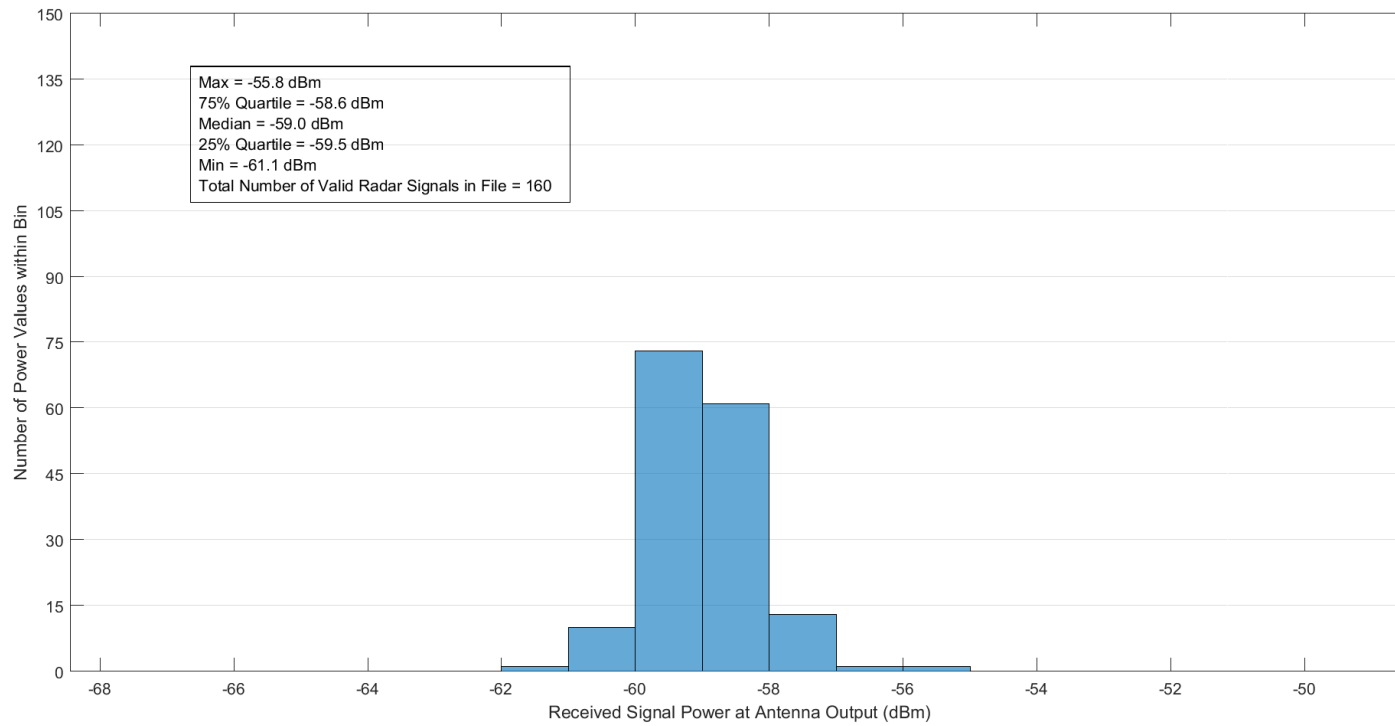


Figure A-38. Received radar signal power statistics at Location 3 in Zone D2 for the ASR-9.

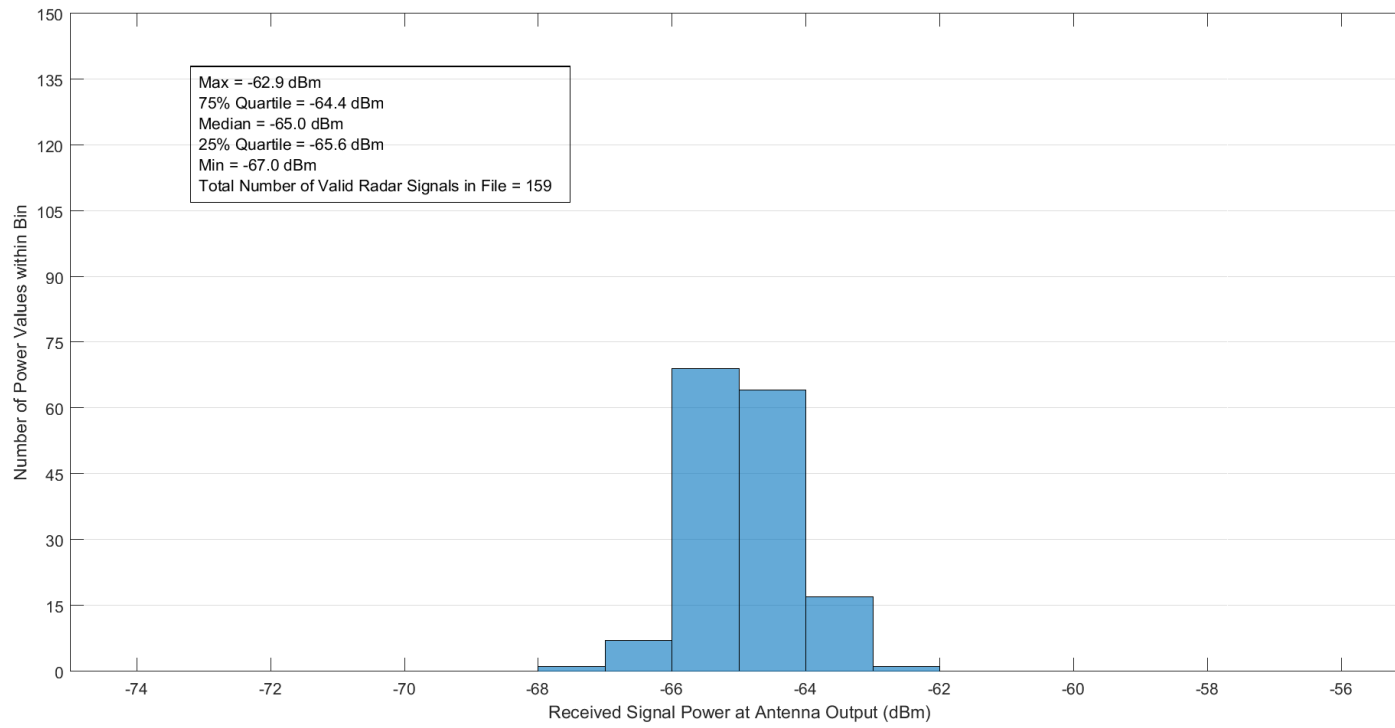


Figure A-39. Received radar signal power statistics at Location 4 in Zone D2 for the ASR-9.

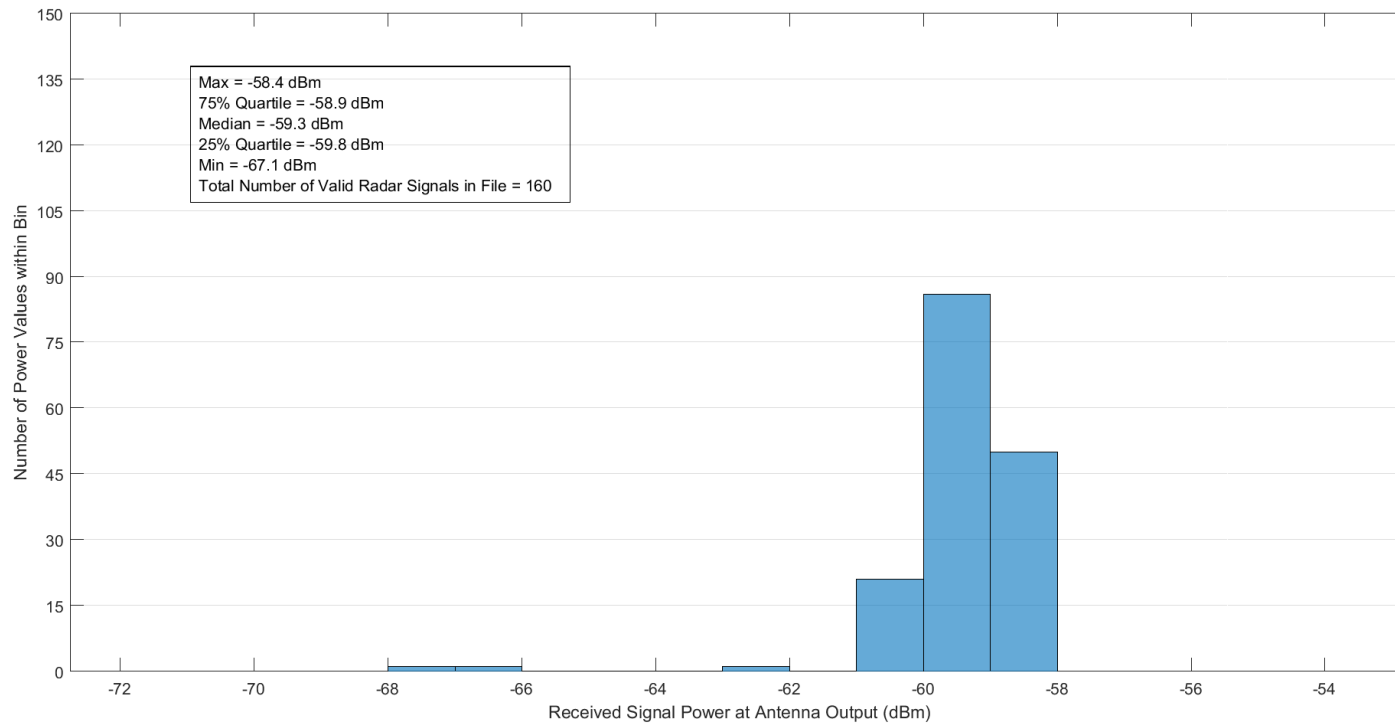


Figure A-40. Received radar signal power statistics at Location 5 in Zone D2 for the ASR-9.

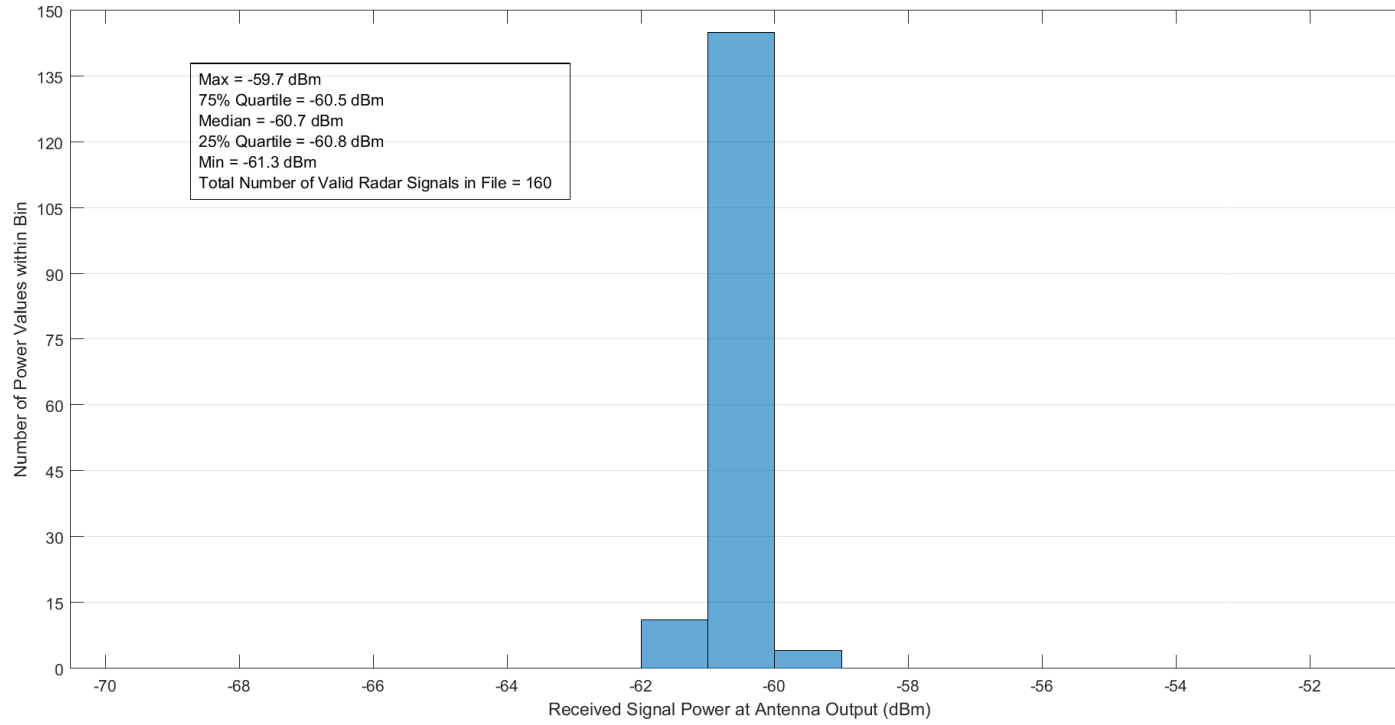


Figure A-41. Received radar signal power statistics at Location 6 in Zone D2 for the ASR-9.

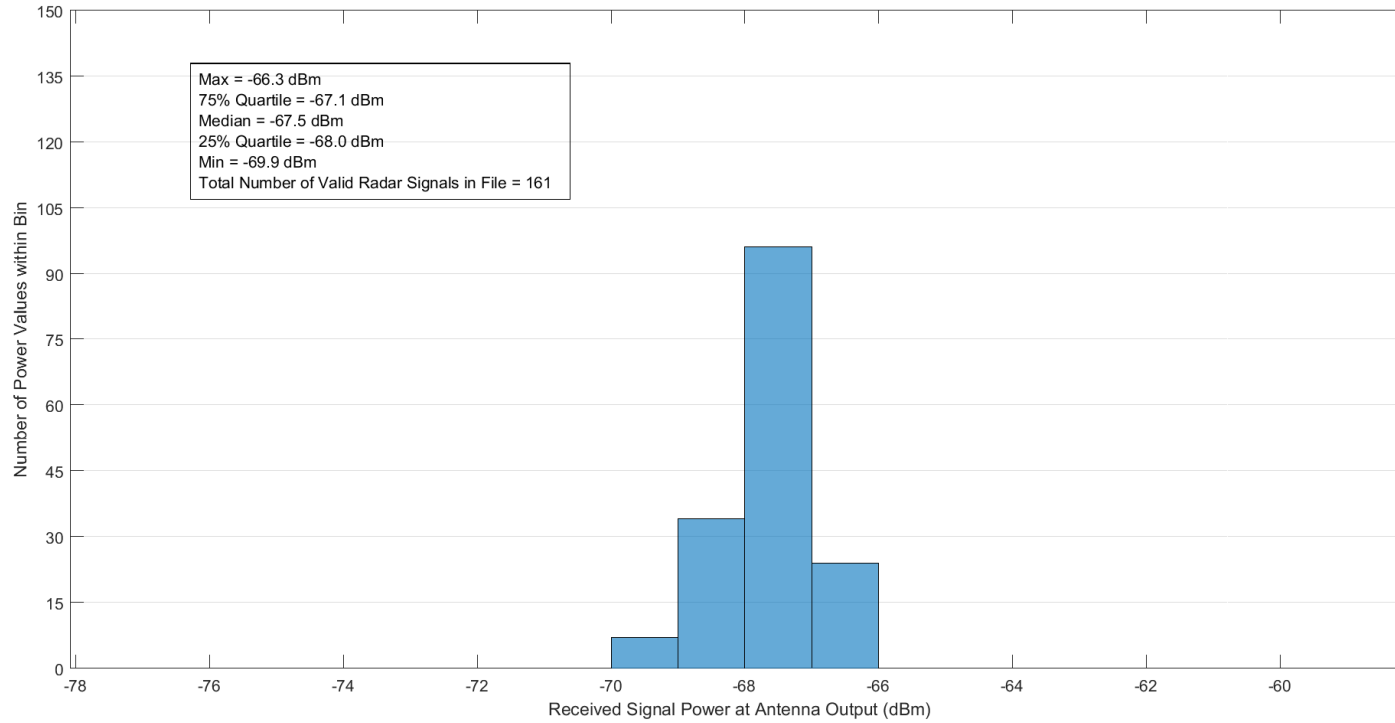


Figure A-42. Received radar signal power statistics at Location 1 in Zone D3 for the ASR-9.

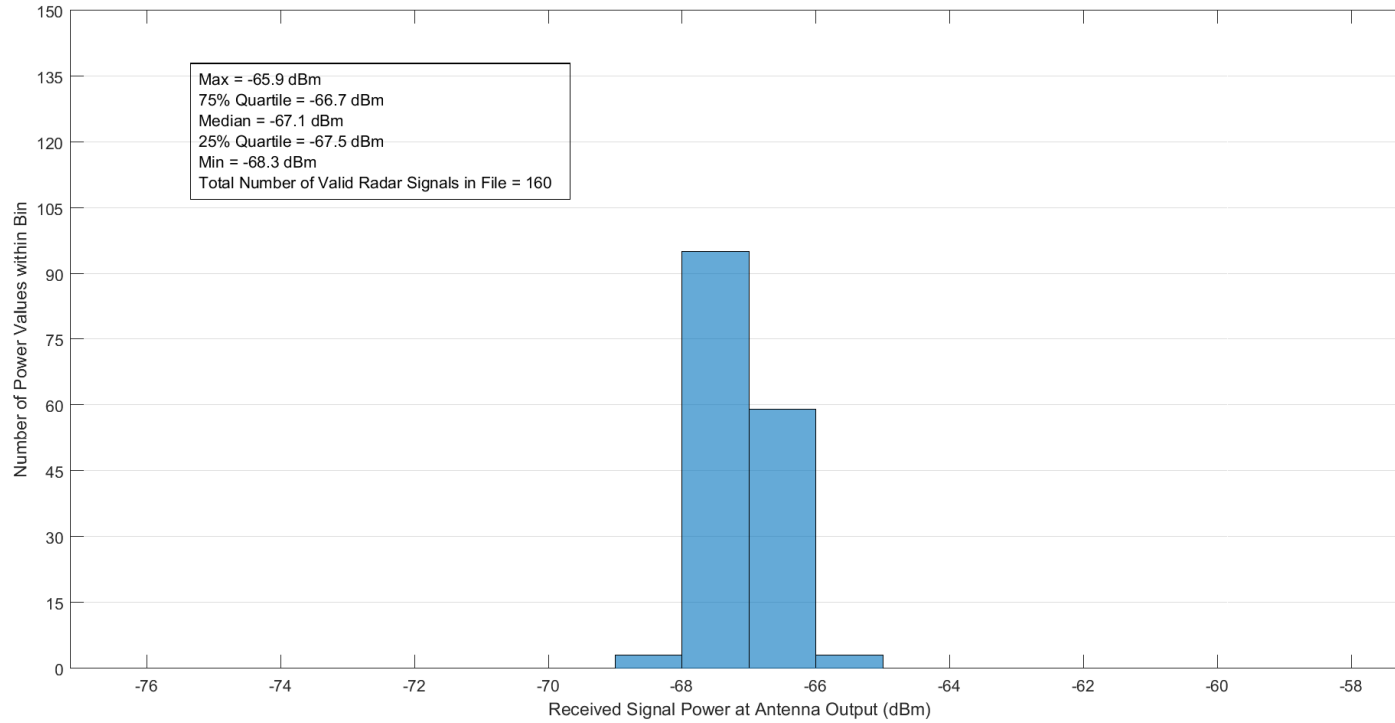


Figure A-43. Received radar signal power statistics at Location 2 in Zone D3 for the ASR-9.

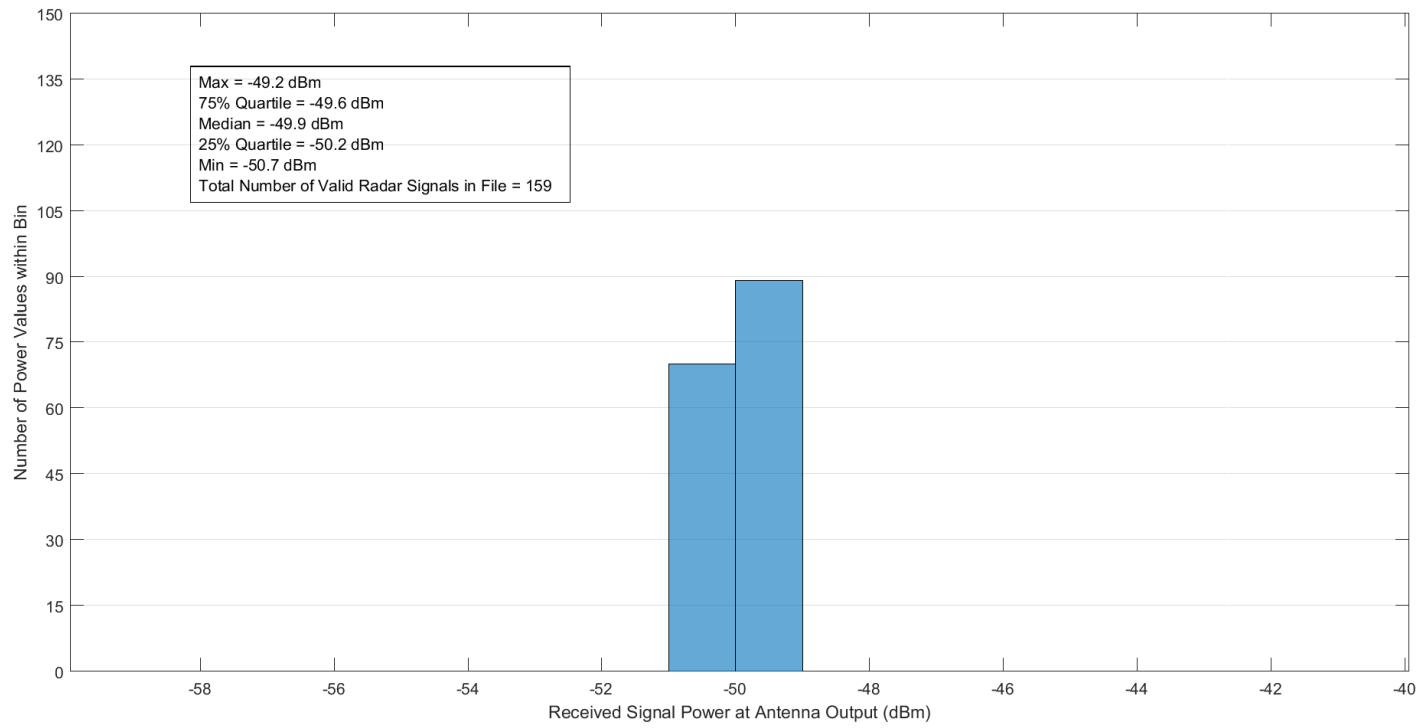


Figure A-44. Received radar signal power statistics at Location 3 in Zone D3 for the ASR-9.

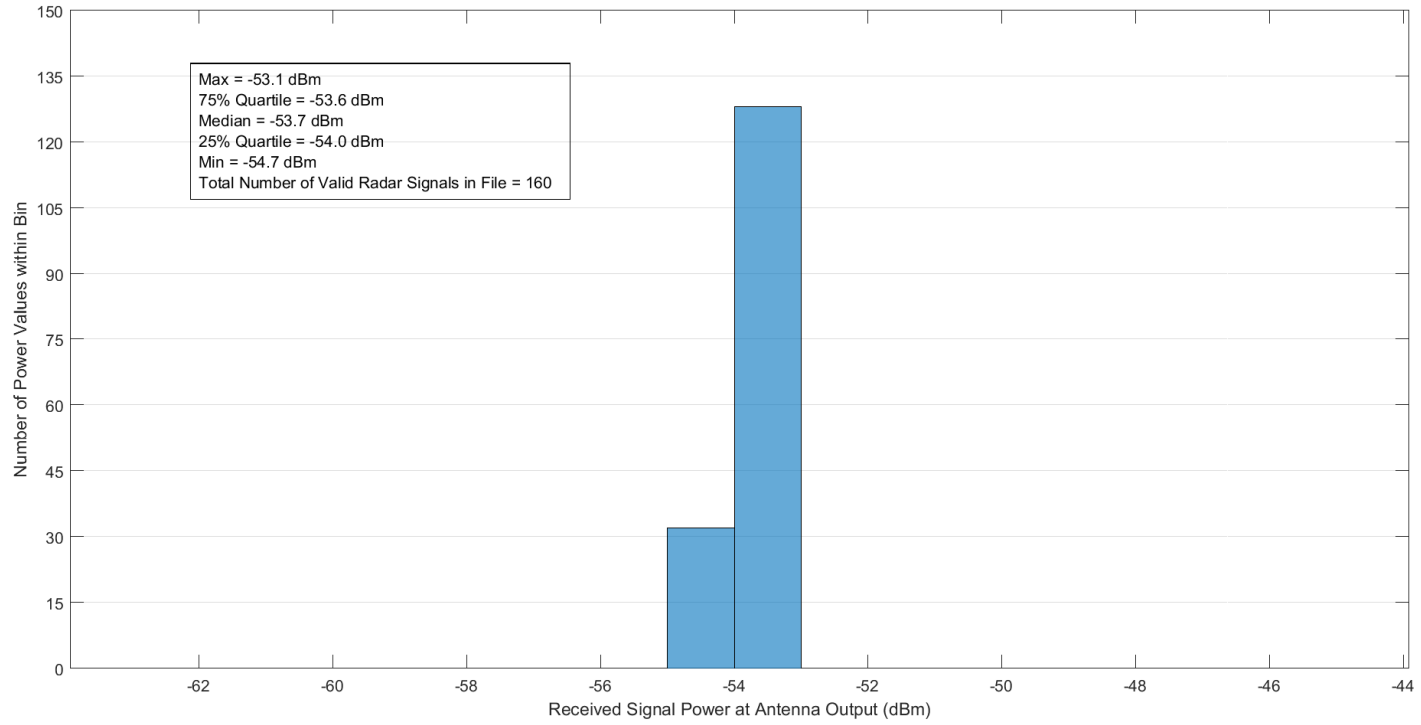


Figure A-45. Received radar signal power statistics at Location 4 in Zone D3 for the ASR-9.

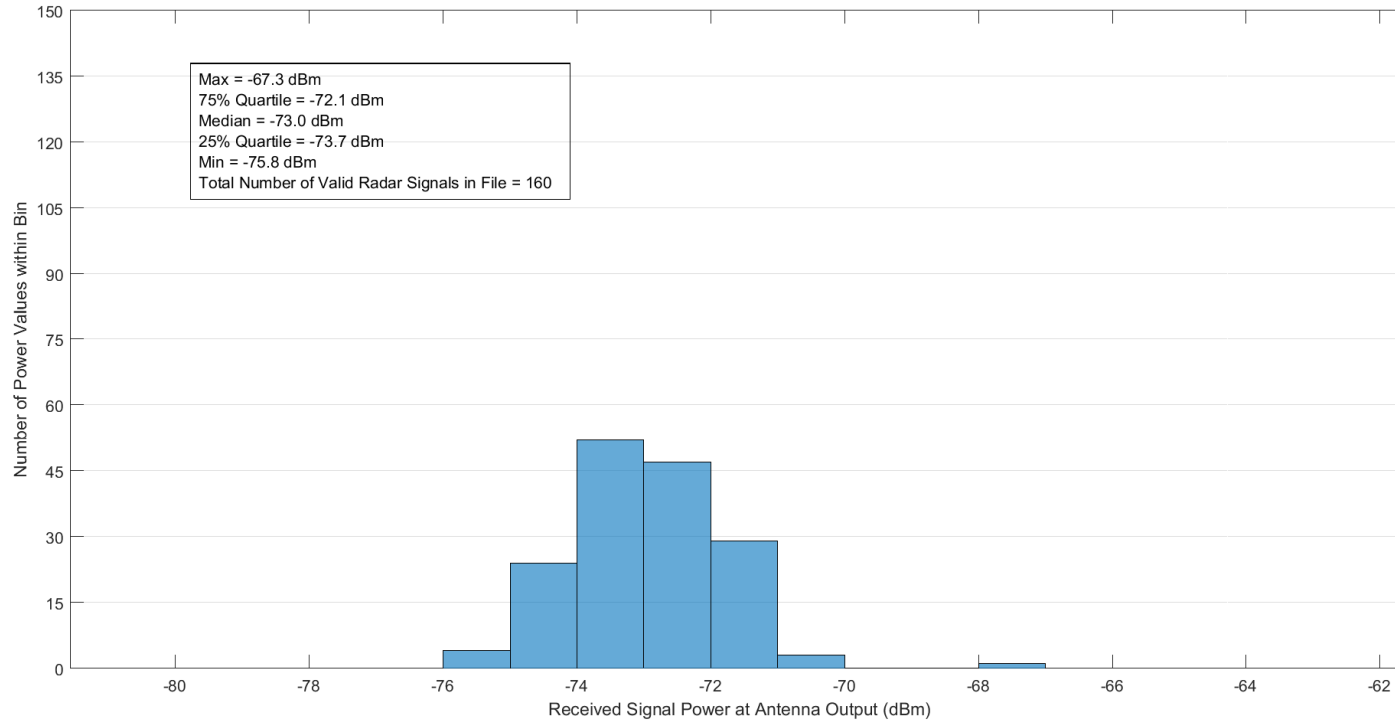


Figure A-46. Received radar signal power statistics at Location 5 in Zone D3 for the ASR-9.

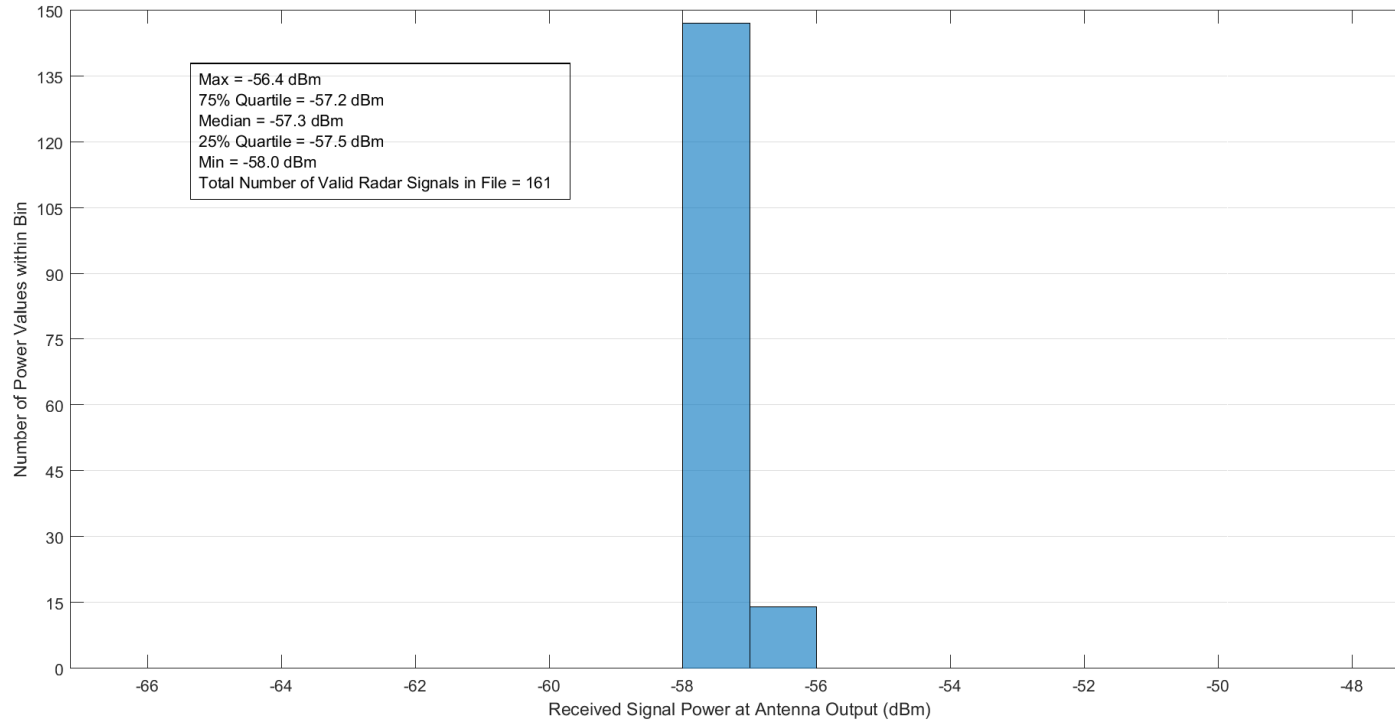


Figure A-47. Received radar signal power statistics at Location 1 in Zone D4 for the ASR-9.

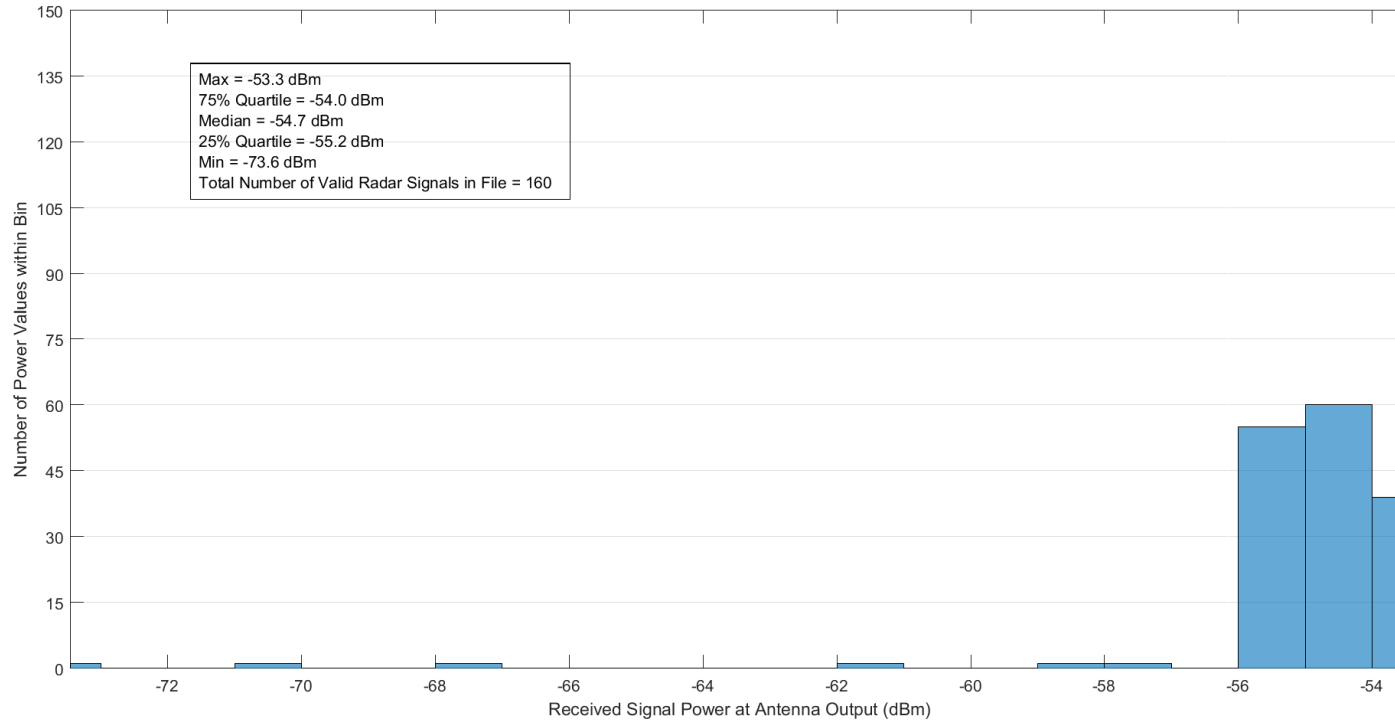


Figure A-48. Received radar signal power statistics at Location 1 in Zone D5 for the ASR-9.

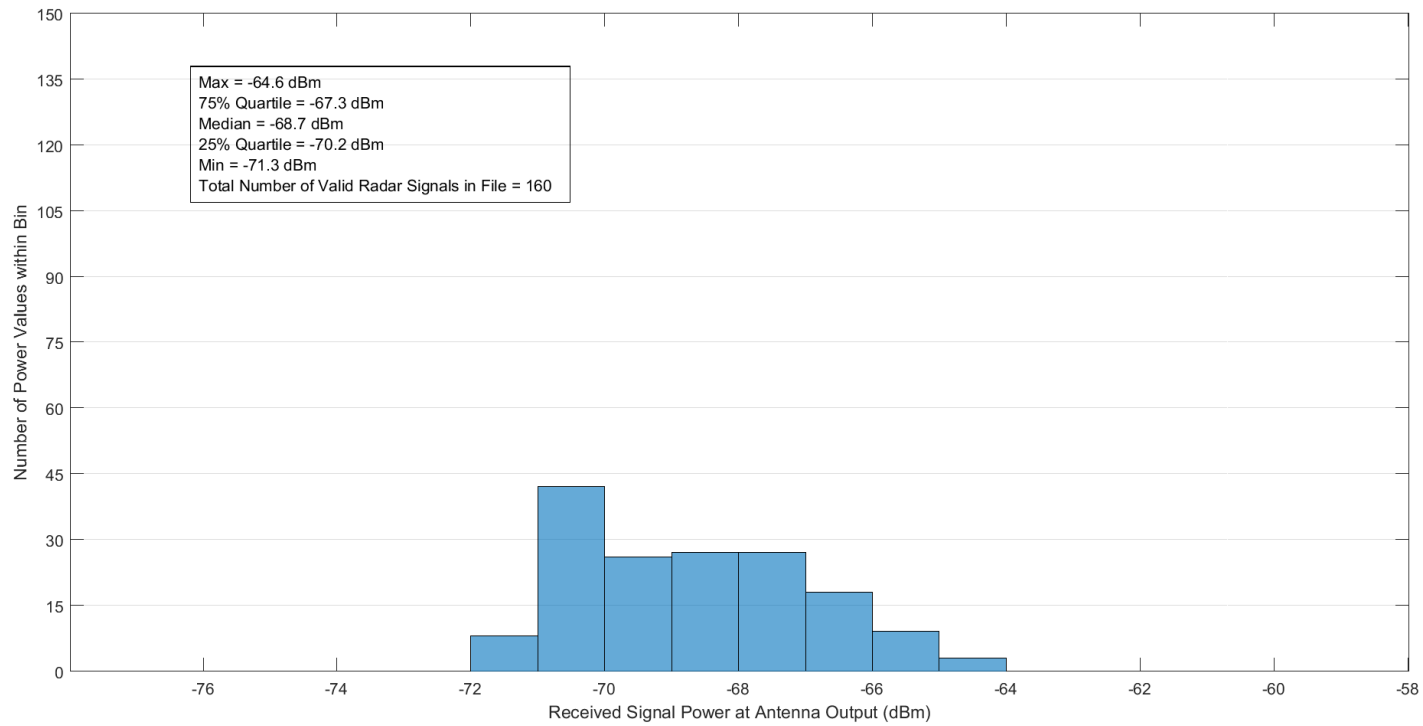


Figure A-49. Received radar signal power statistics at Location 1 in Zone E1 for the ASR-9.

APPENDIX B: RECEIVED POWER HISTOGRAMS FOR CARSR MEASUREMENTS

This appendix contains the received radar signal power histograms and maximum, median, minimum, 75% quartile, and 25% quartile statistics for each measurement location for the CARSR measurements.

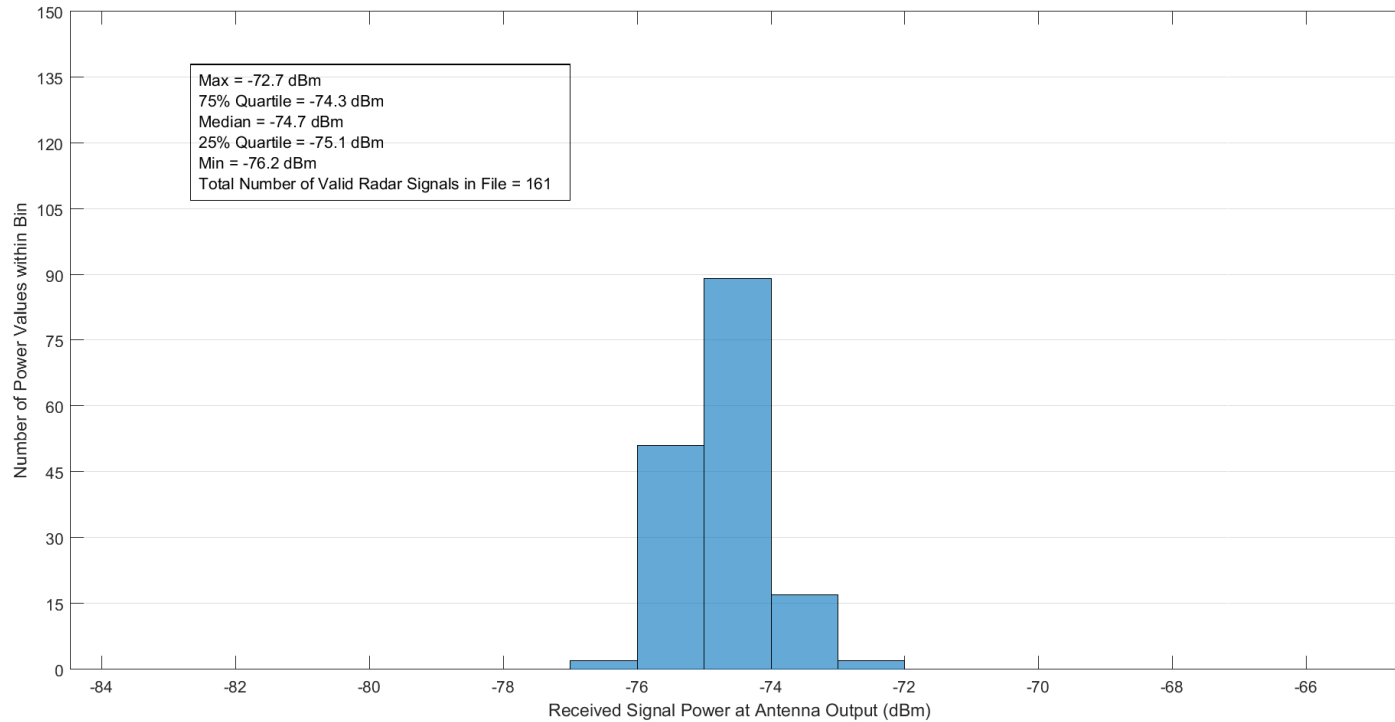


Figure B-1. Received radar signal power statistics at Location 1 in Zone F1 for the CARSR.

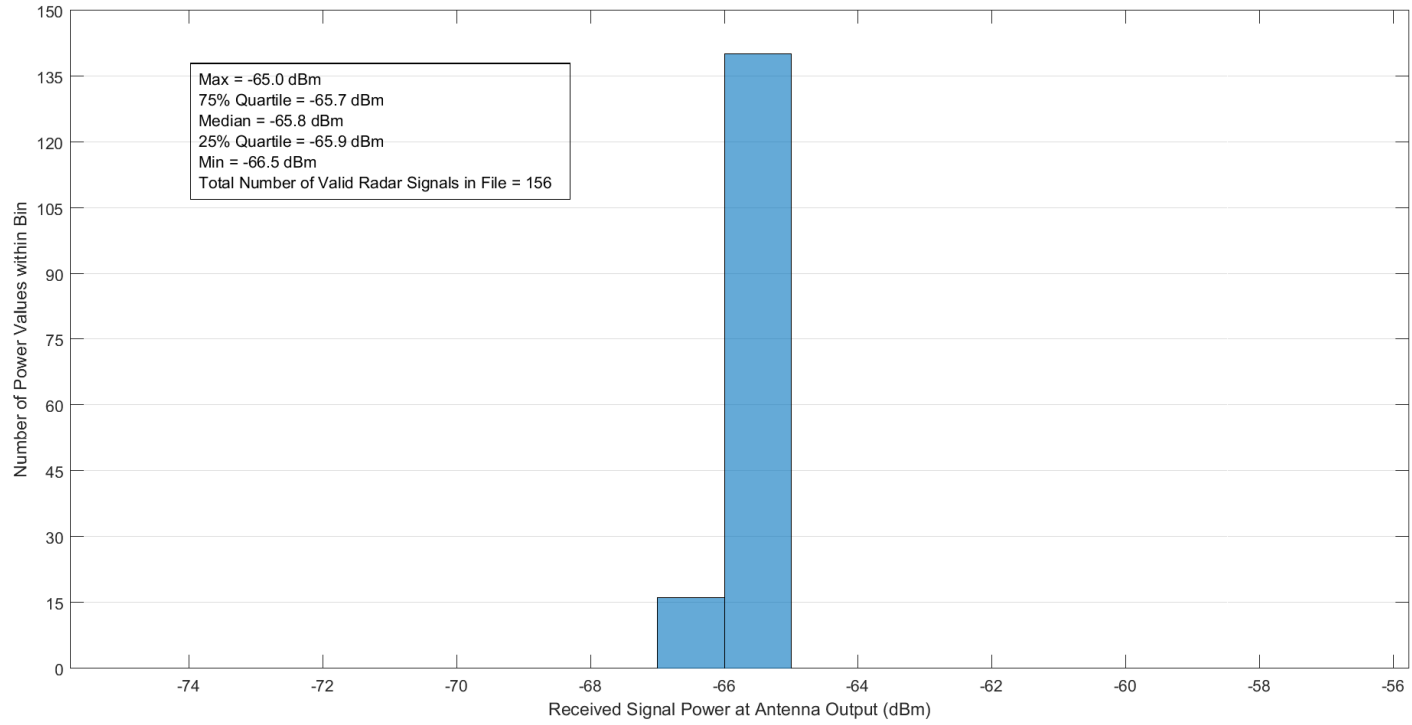


Figure B-2. Received radar signal power statistics at Location 2 in Zone F1 for the CARSR.

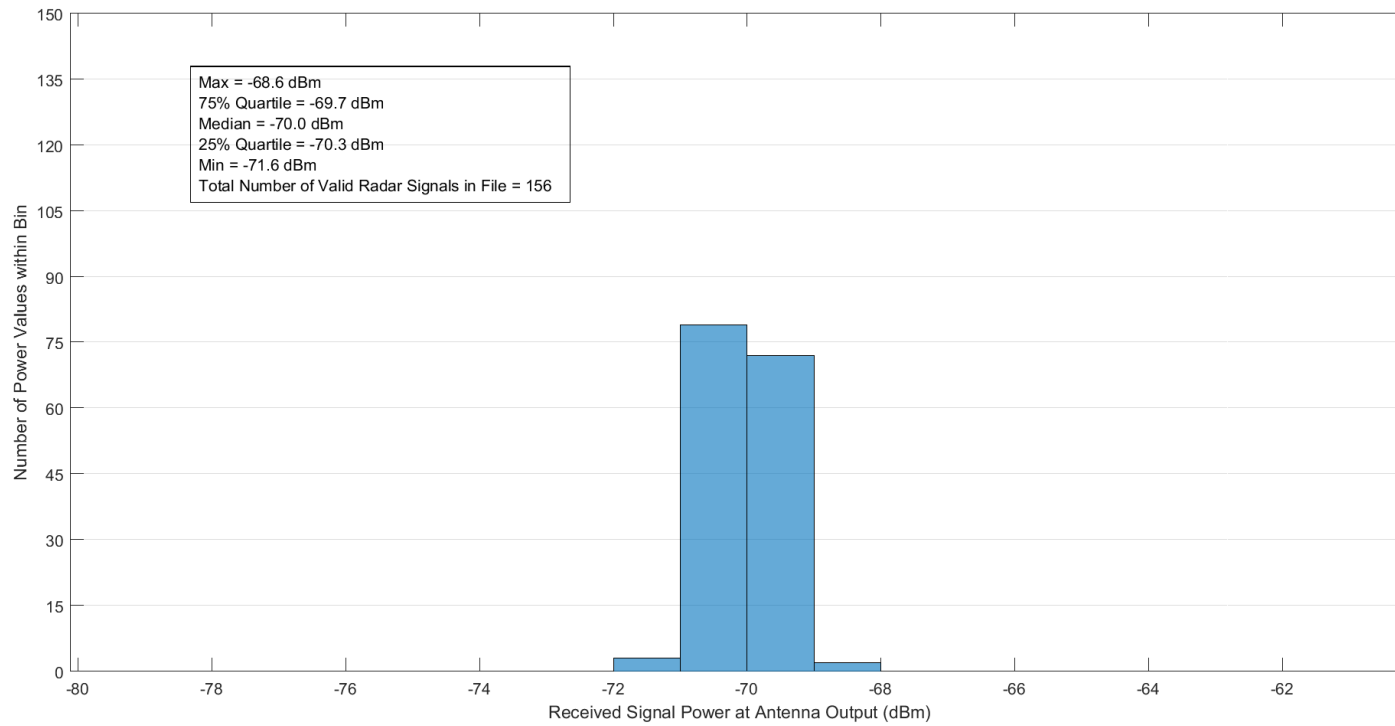


Figure B-3. Received radar signal power statistics at Location 3 in Zone F1 for the CARSR.

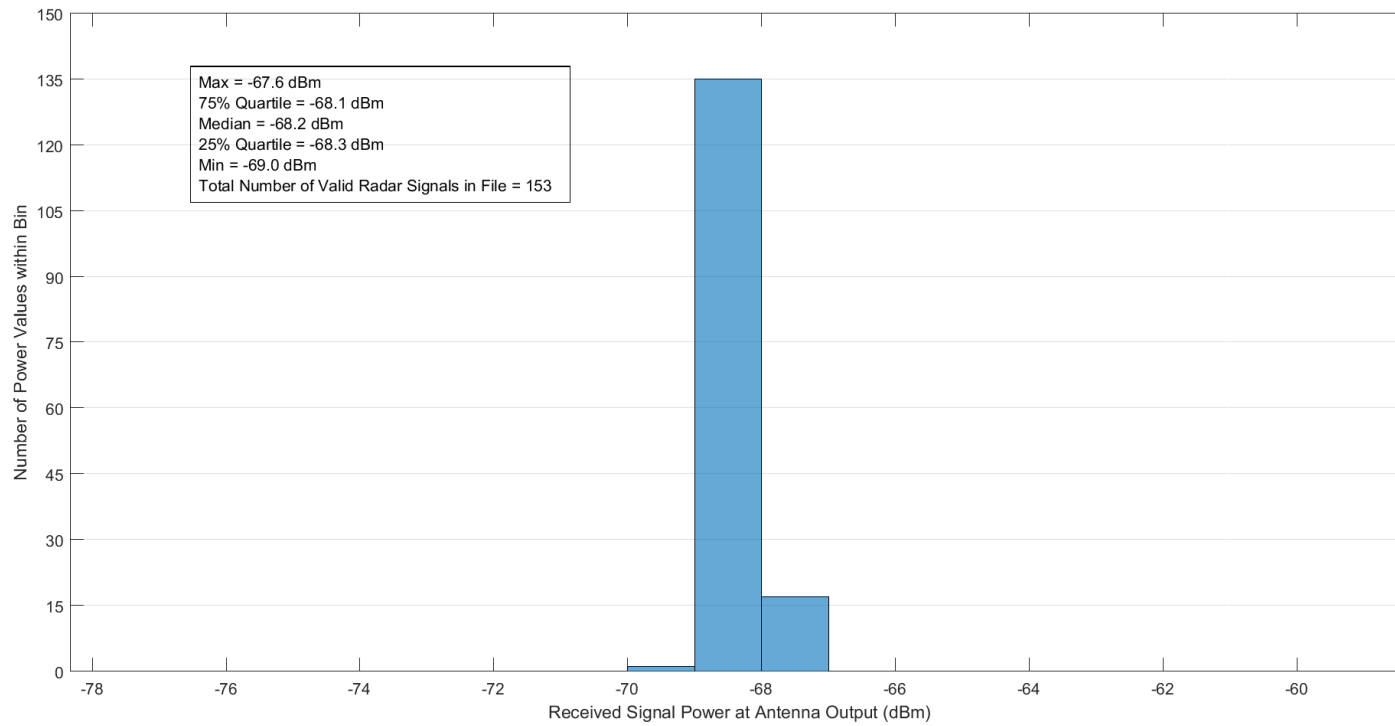


Figure B-4. Received radar signal power statistics at Location 4 in Zone F1 for the CARSR.

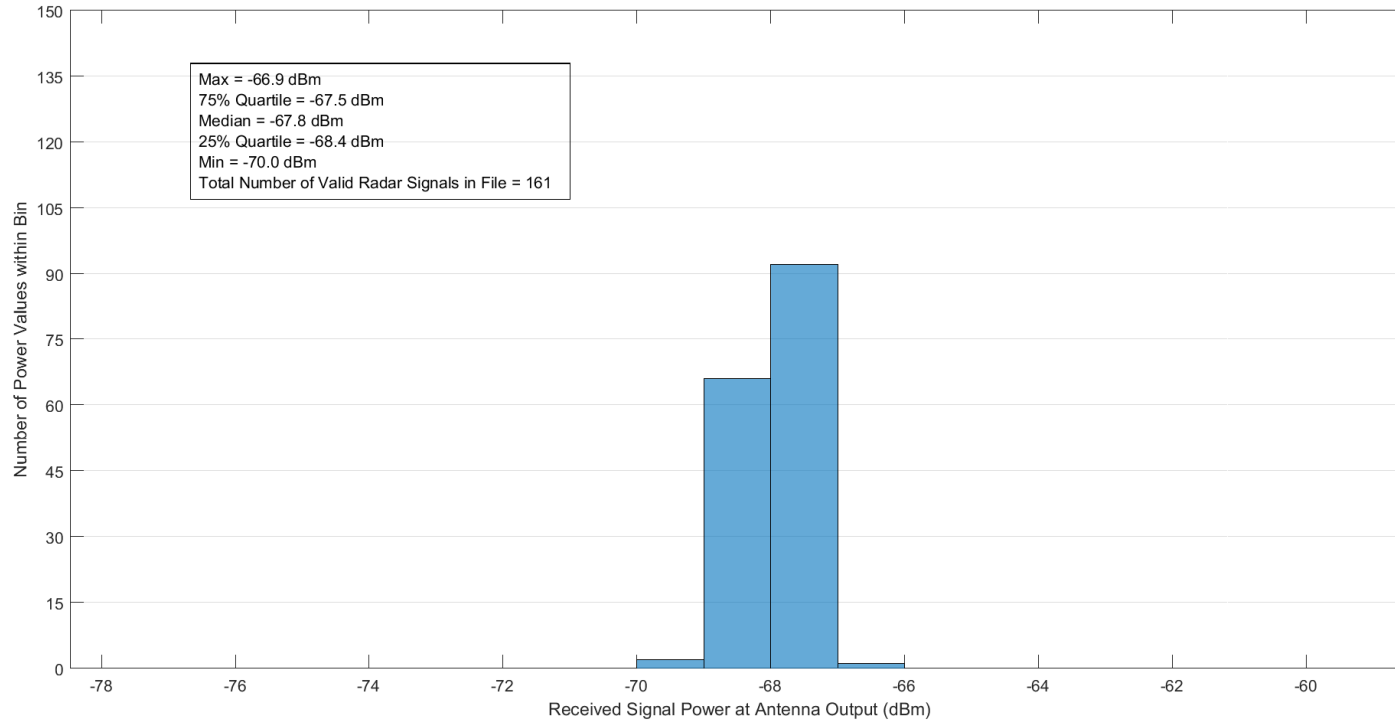


Figure B-5. Received radar signal power statistics at Location 5 in Zone F1 for the CARSR.

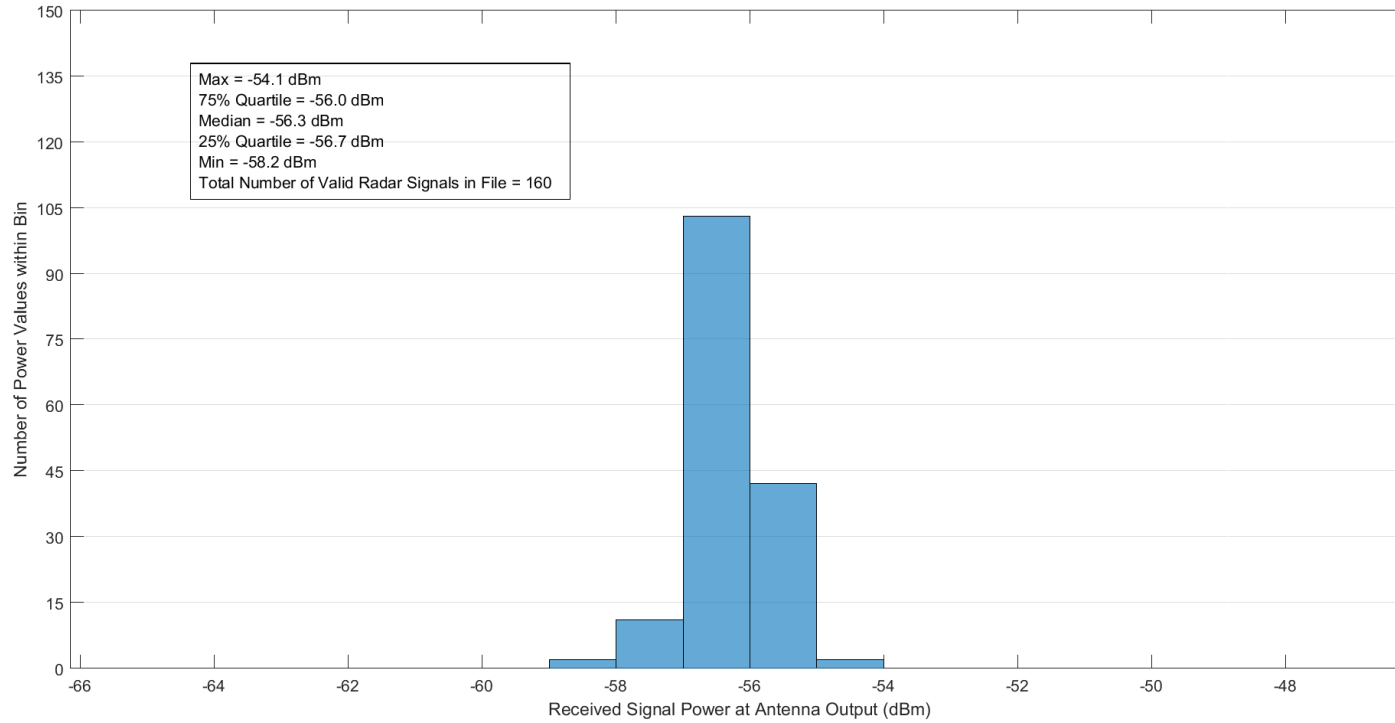


Figure B-6. Received radar signal power statistics at Location 1 in Zone F2 for the CARSR.

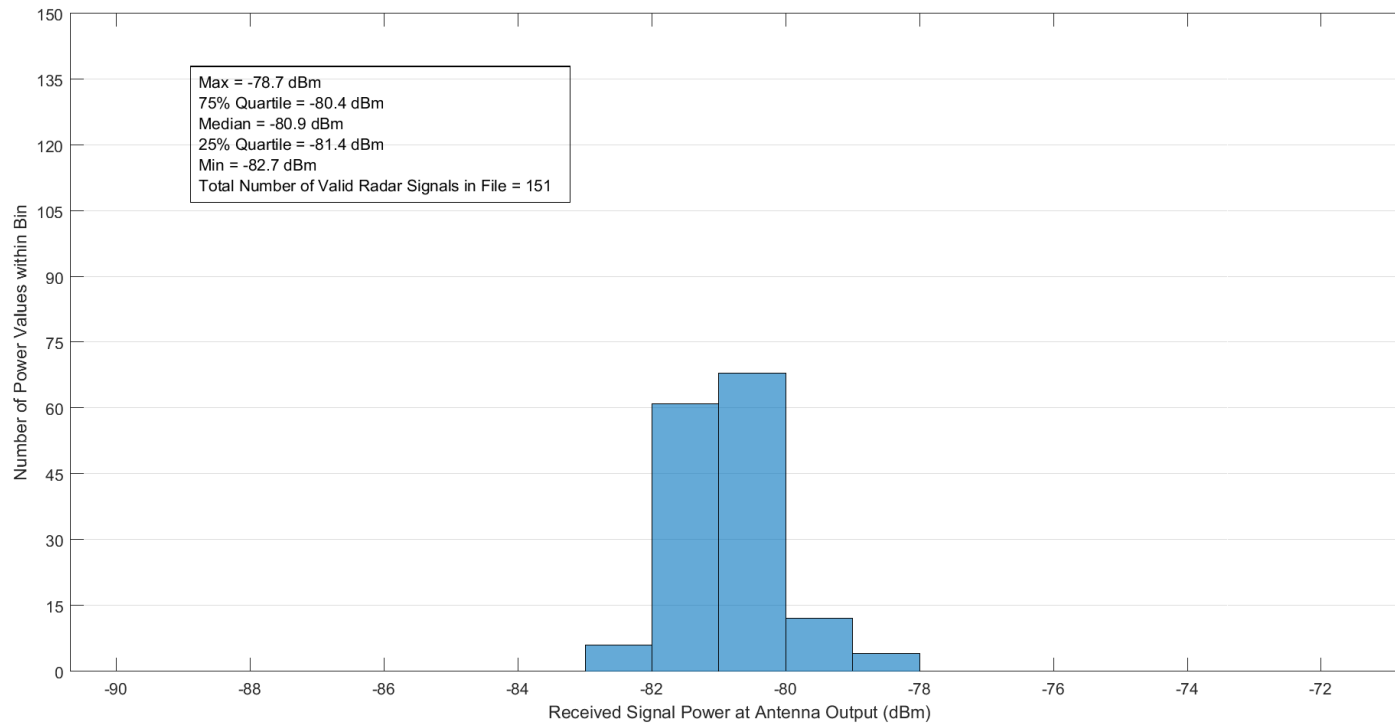


Figure B-7. Received radar signal power statistics at Location 2 in Zone F2 for the CARSR.

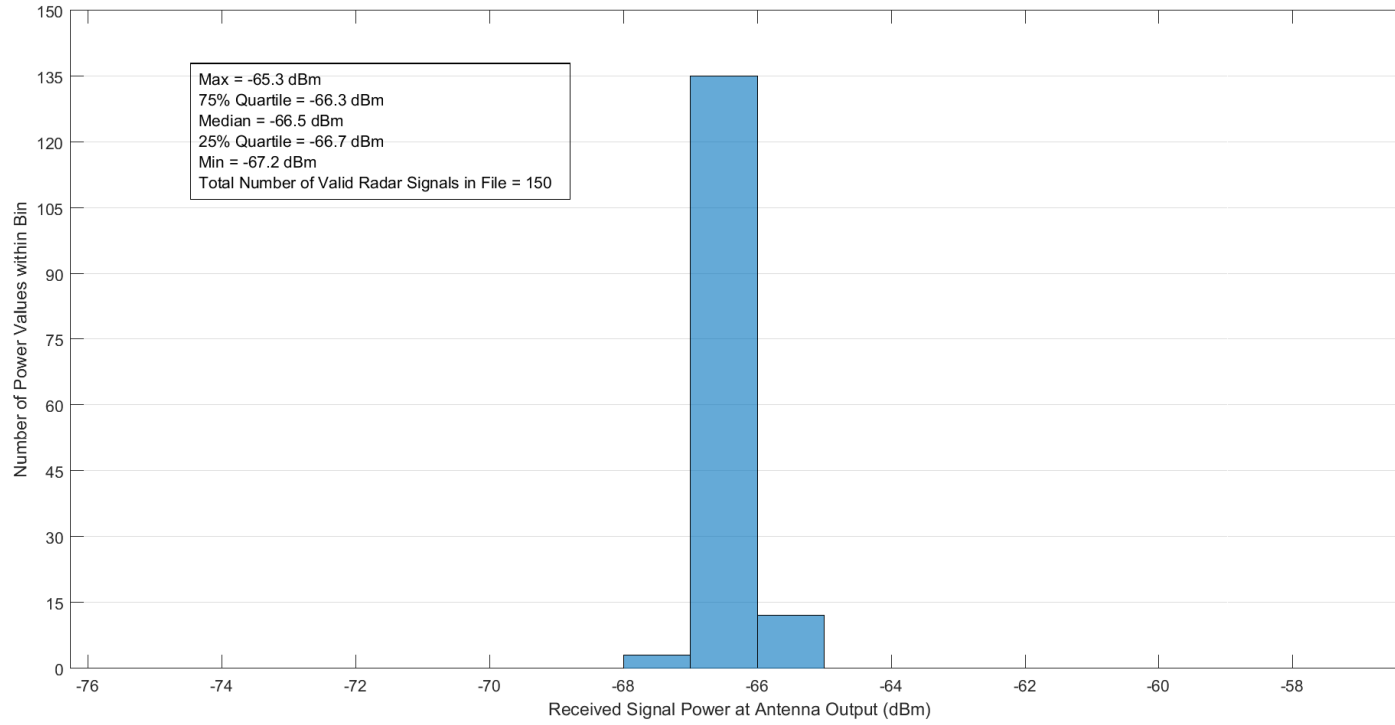


Figure B-8. Received radar signal power statistics at Location 3 in Zone F2 for the CARSR.

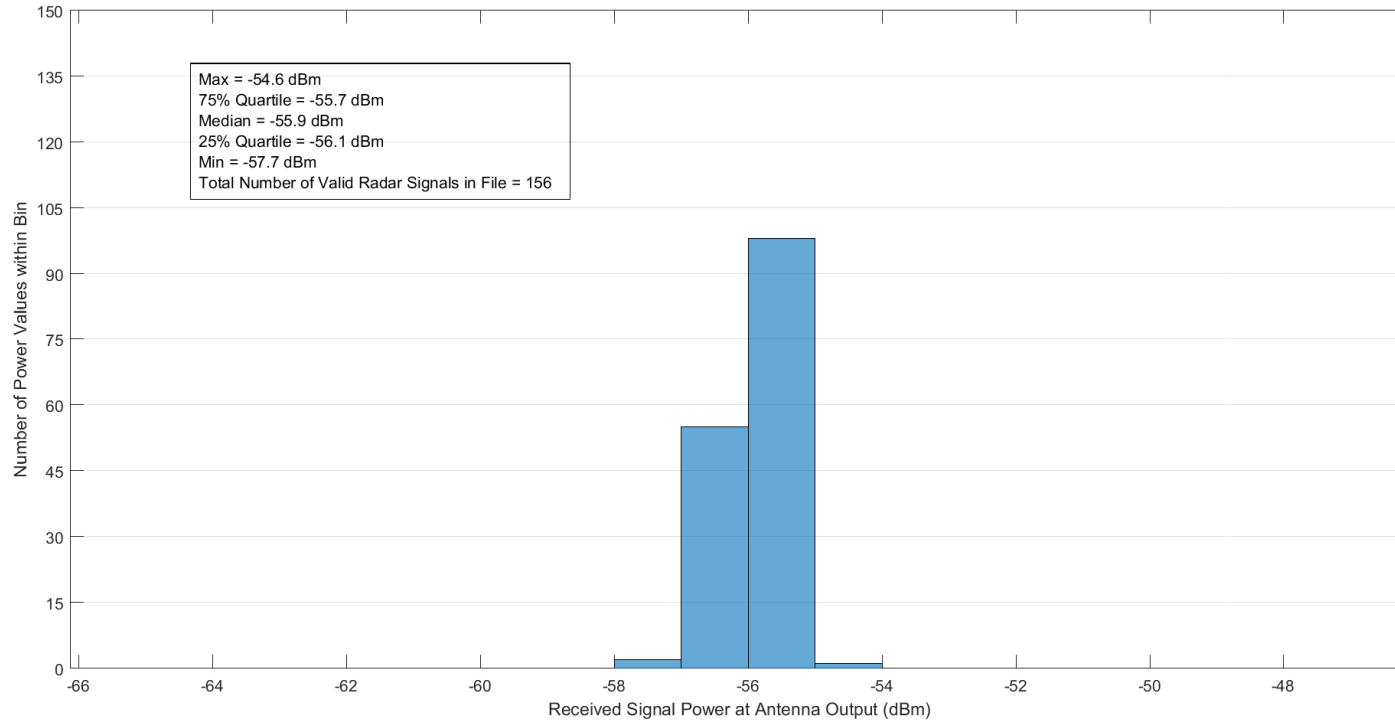


Figure B-9. Received radar signal power statistics at Location 4 in Zone F2 for the CARSR.

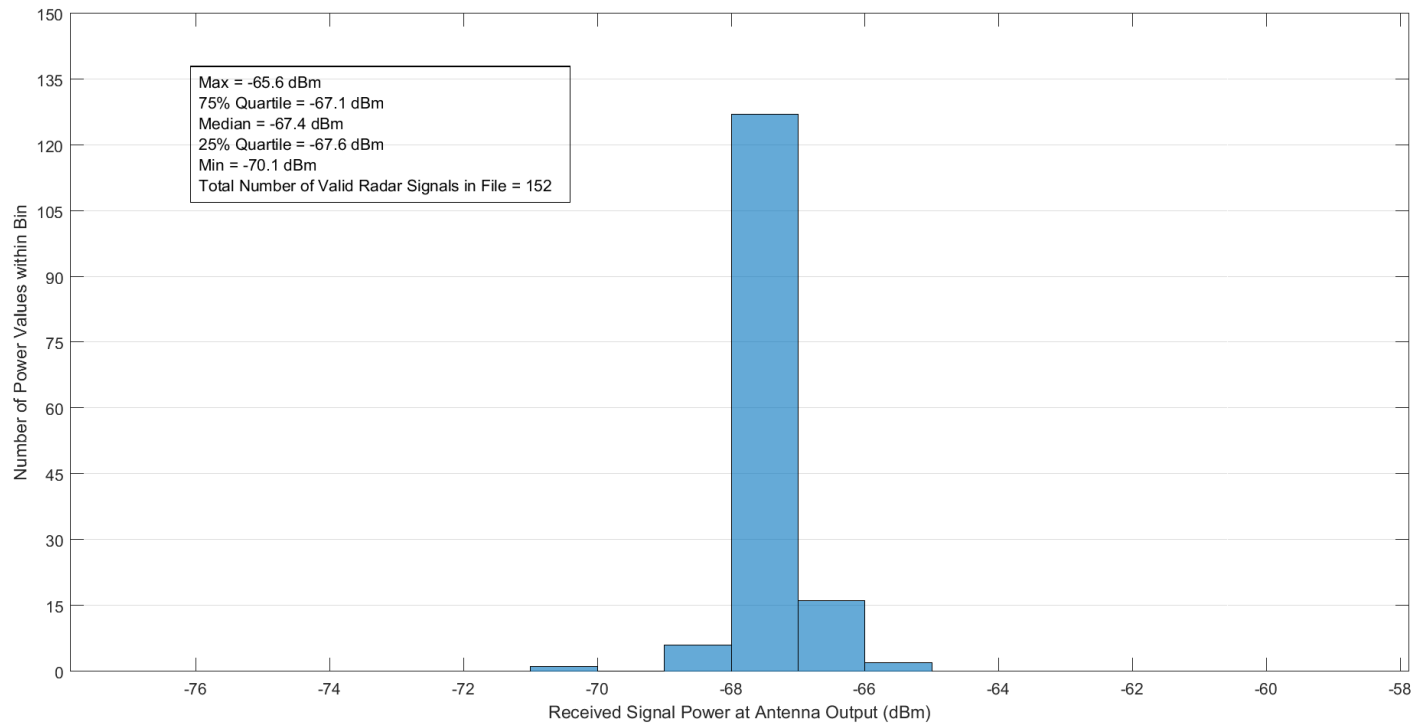


Figure B-10. Received radar signal power statistics at Location 5 in Zone F2 for the CARSR.

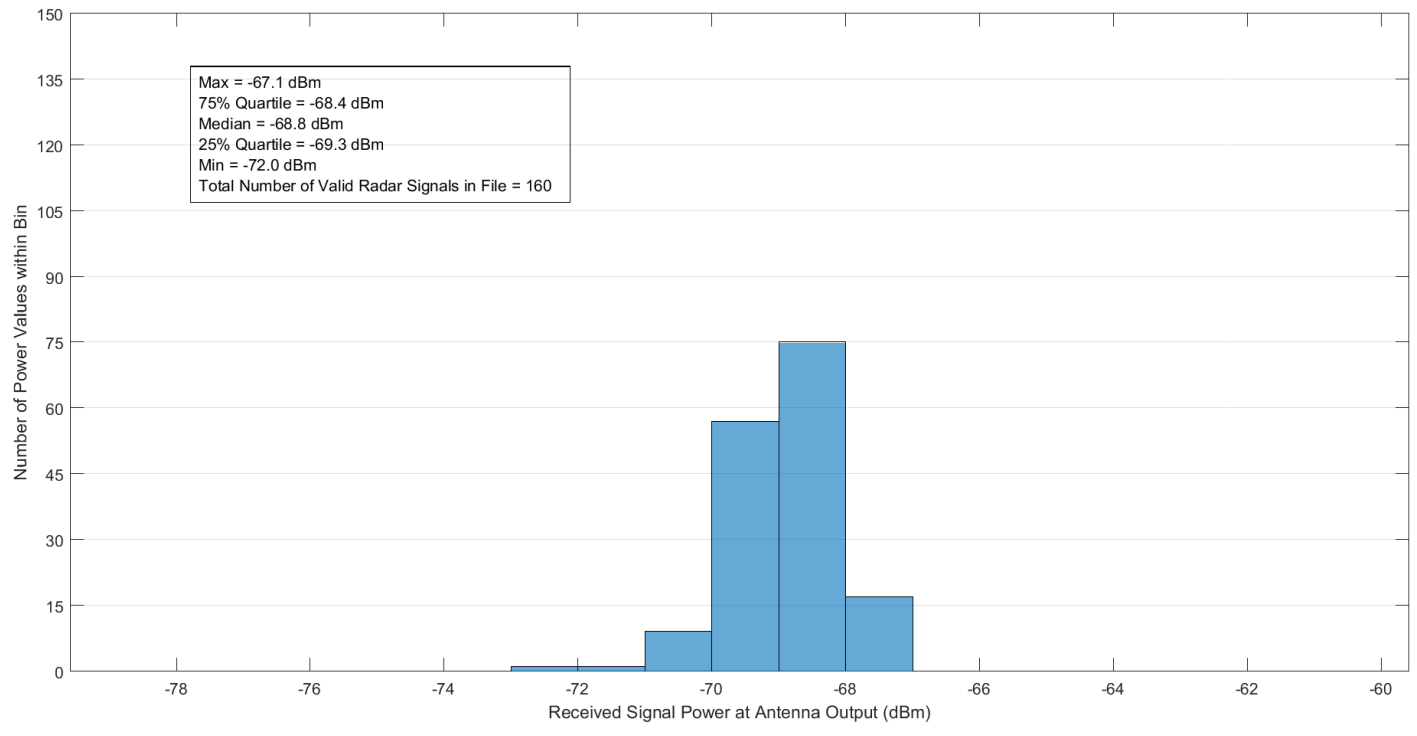


Figure B-11. Received radar signal power statistics at Location 1 in Zone F3 for the CARSR.

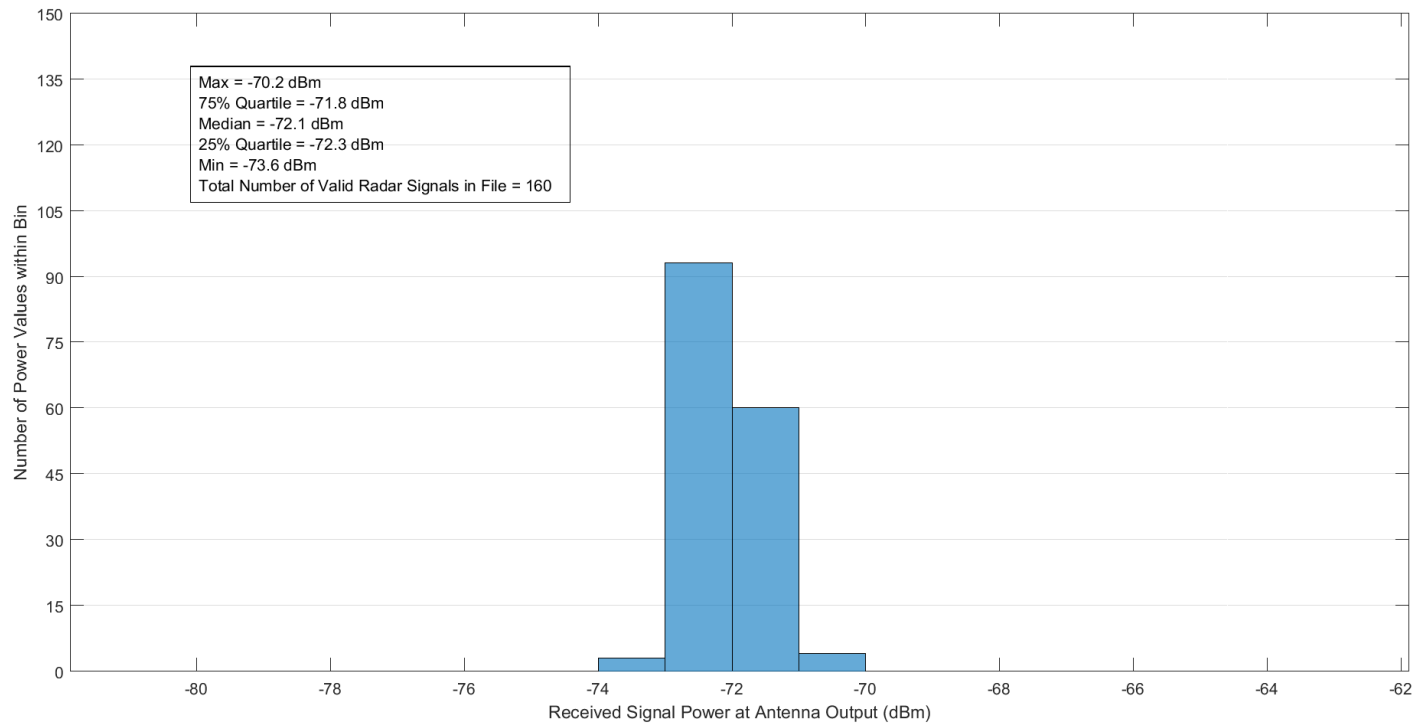


Figure B-12. Received radar signal power statistics at Location 2 in Zone F3 for the CARSR.

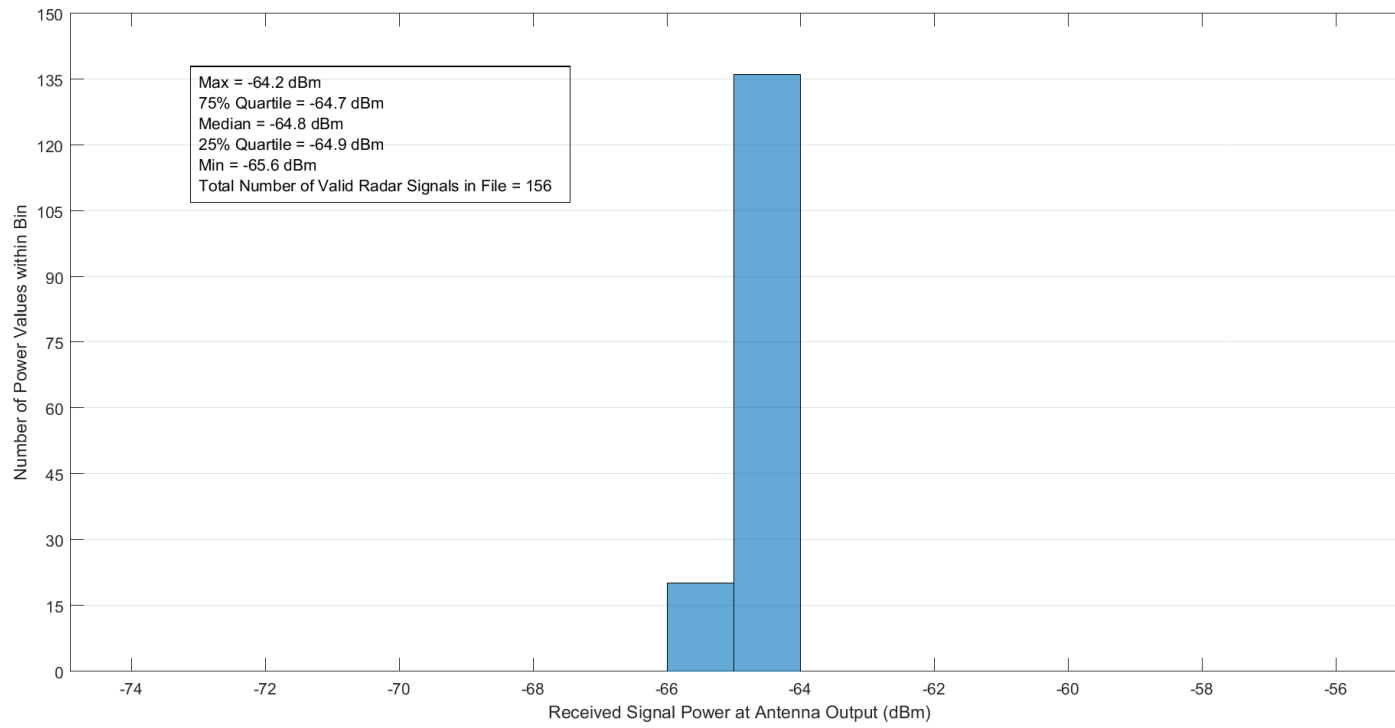


Figure B-13. Received radar signal power statistics at Location 3 in Zone F3 for the CARSR.

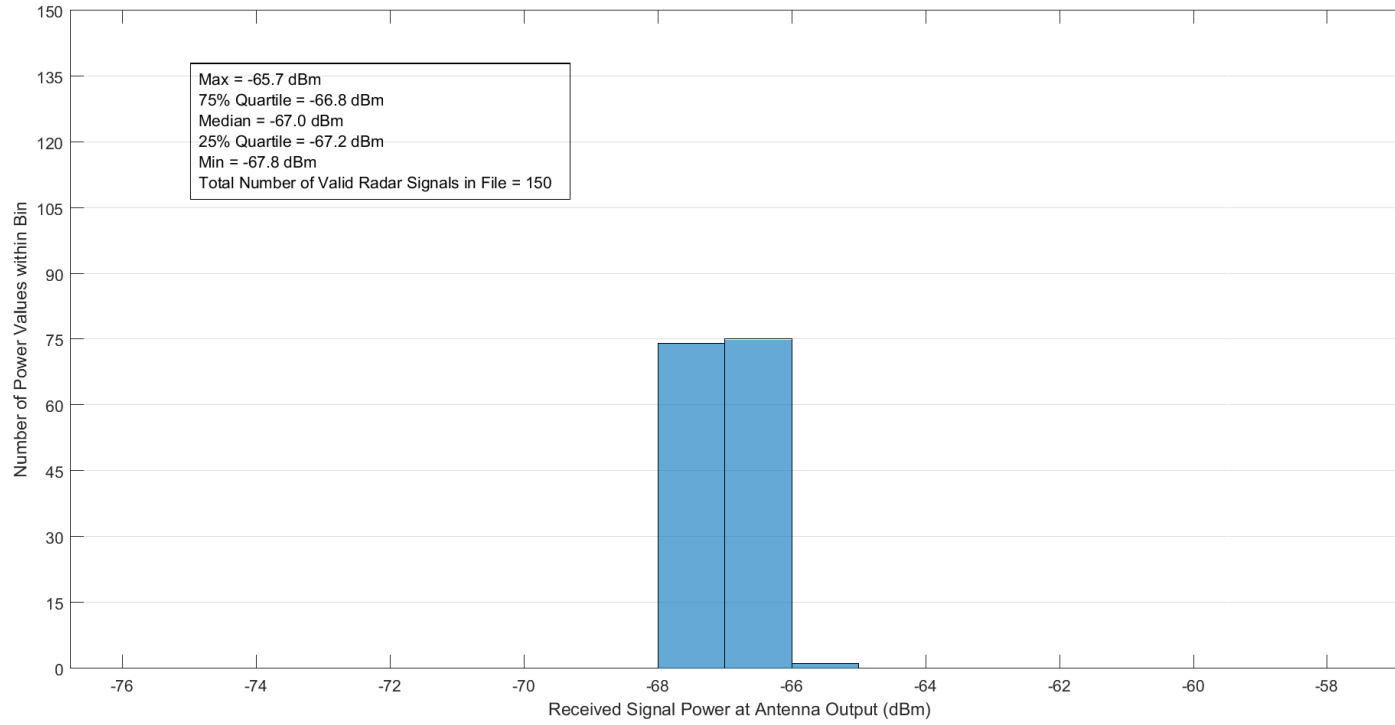


Figure B-14. Received radar signal power statistics at Location 4 in Zone F3 for the CARSR.

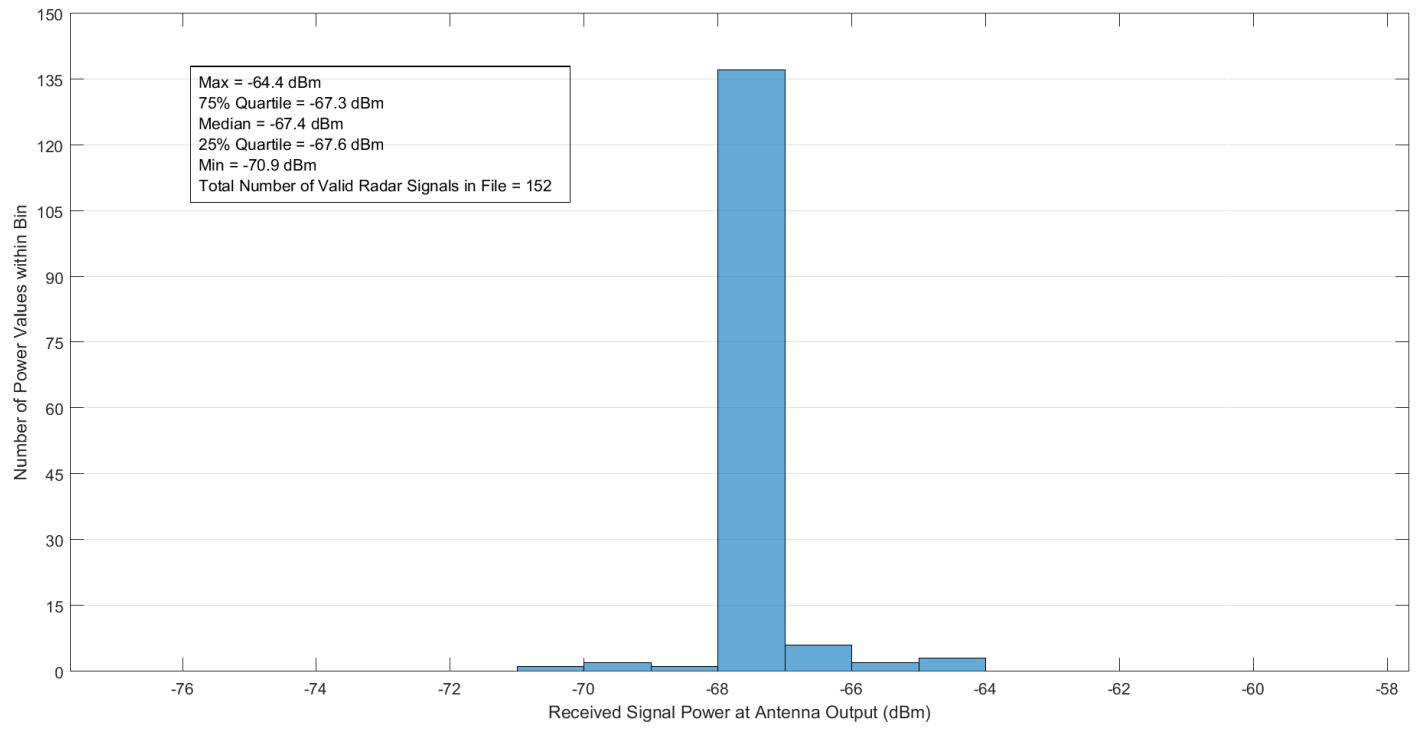


Figure B-15. Received radar signal power statistics at Location 5 in Zone F3 for the CARSR.

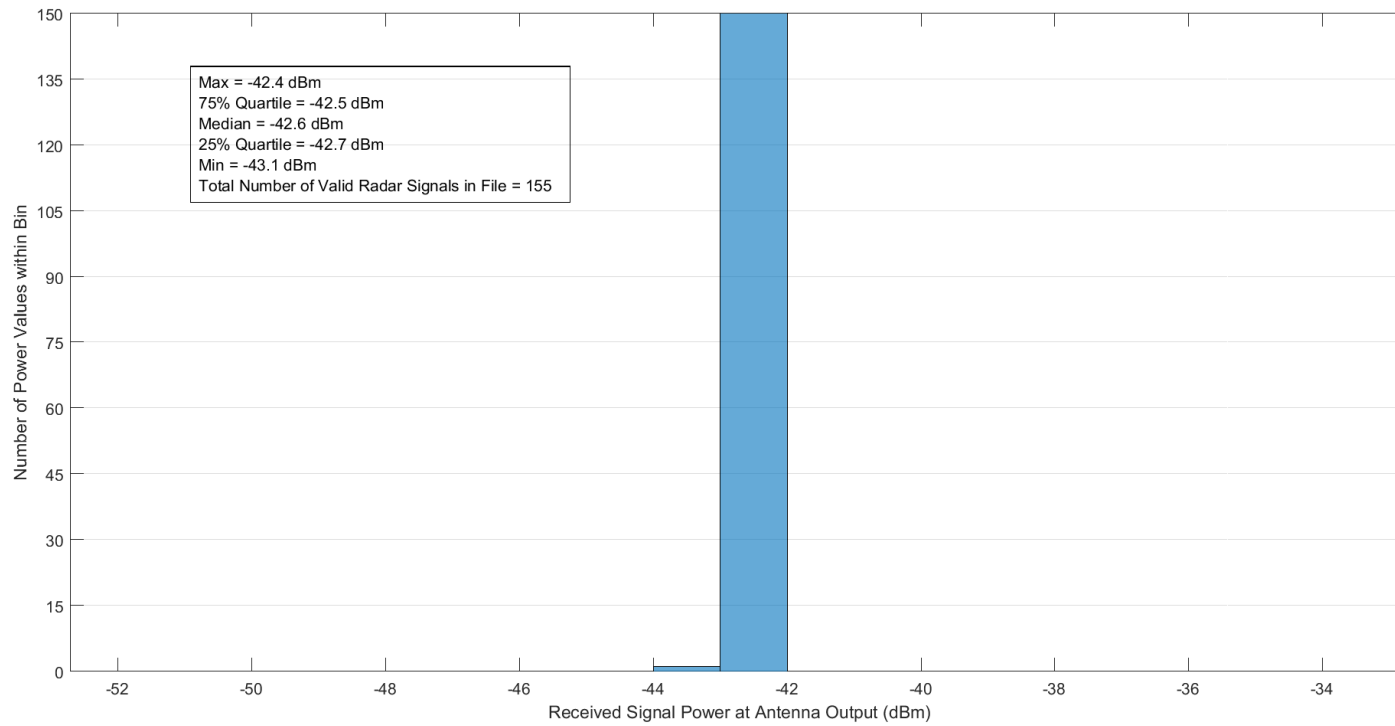


Figure B-16. Received radar signal power statistics at Location 1 in Zone F4 for the CARSR.

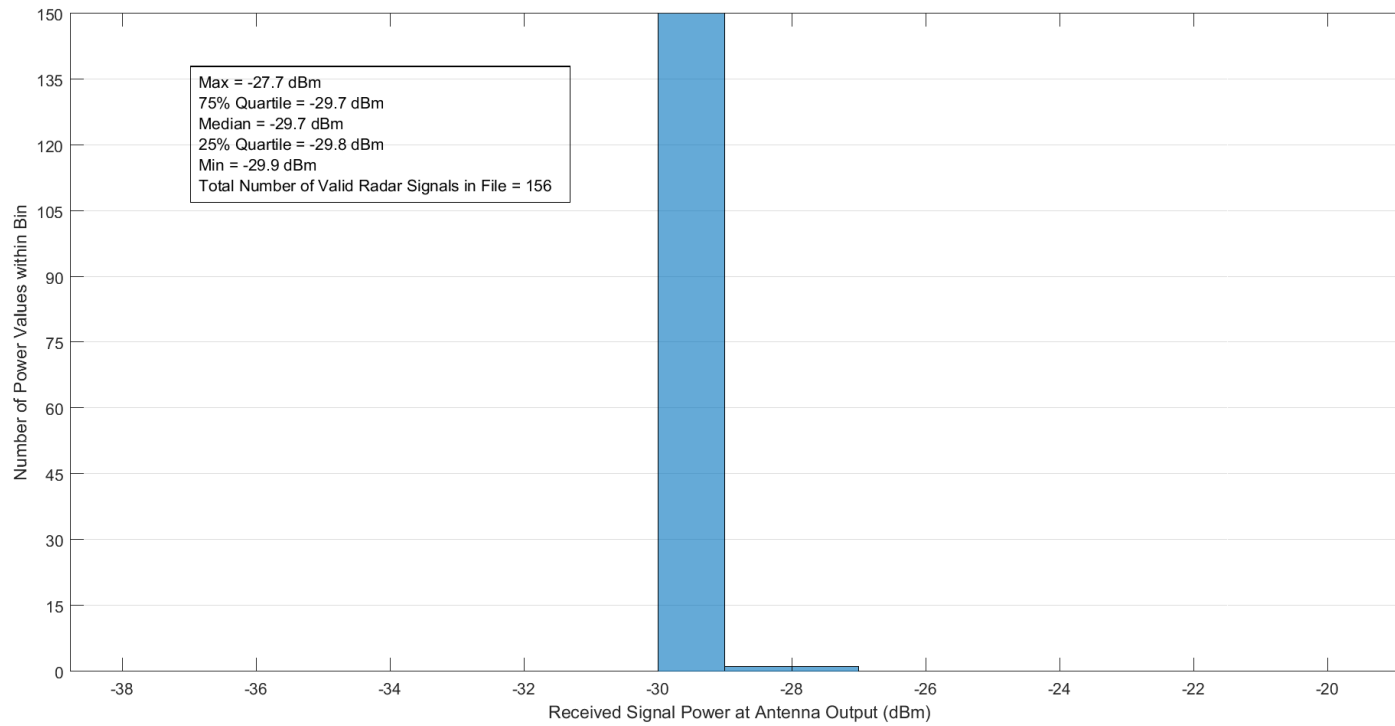


Figure B-17. Received radar signal power statistics at Location 2 in Zone F4 for the CARSR.

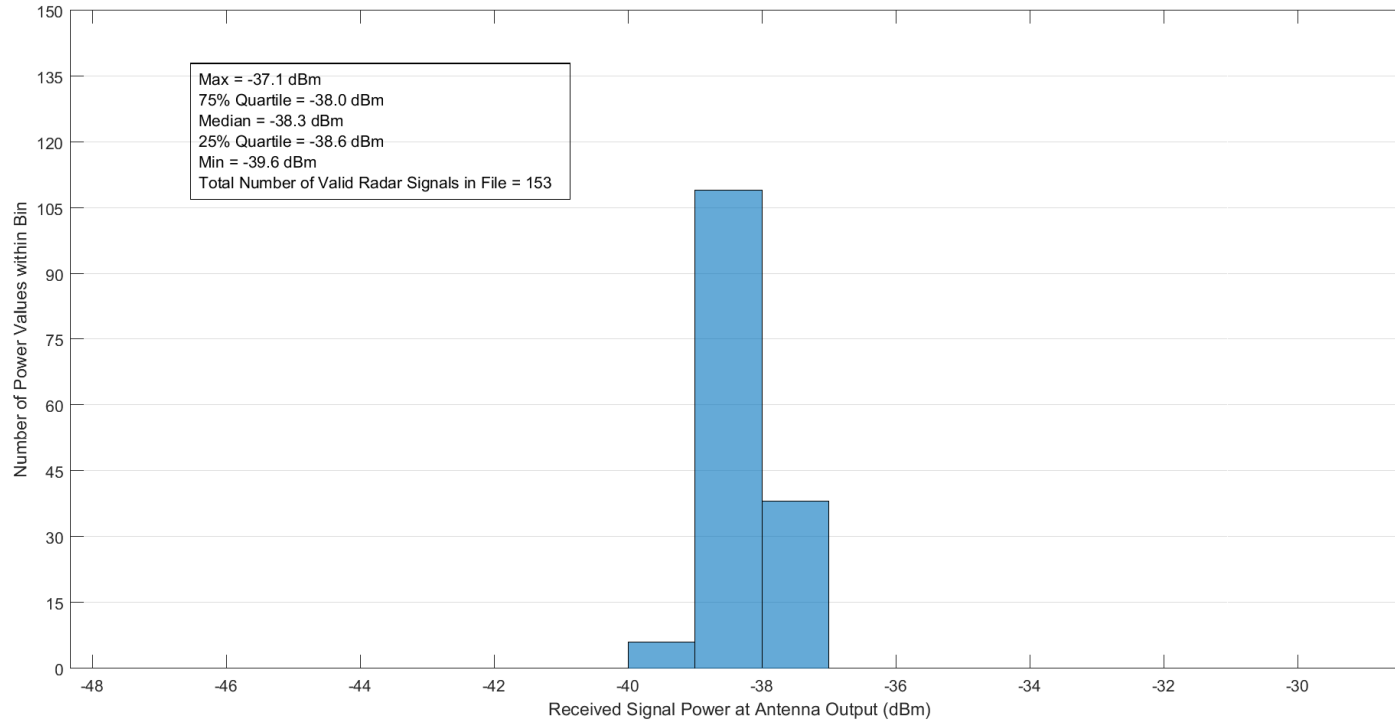


Figure B-18. Received radar signal power statistics at Location 3 in Zone F4 for the CARSR.

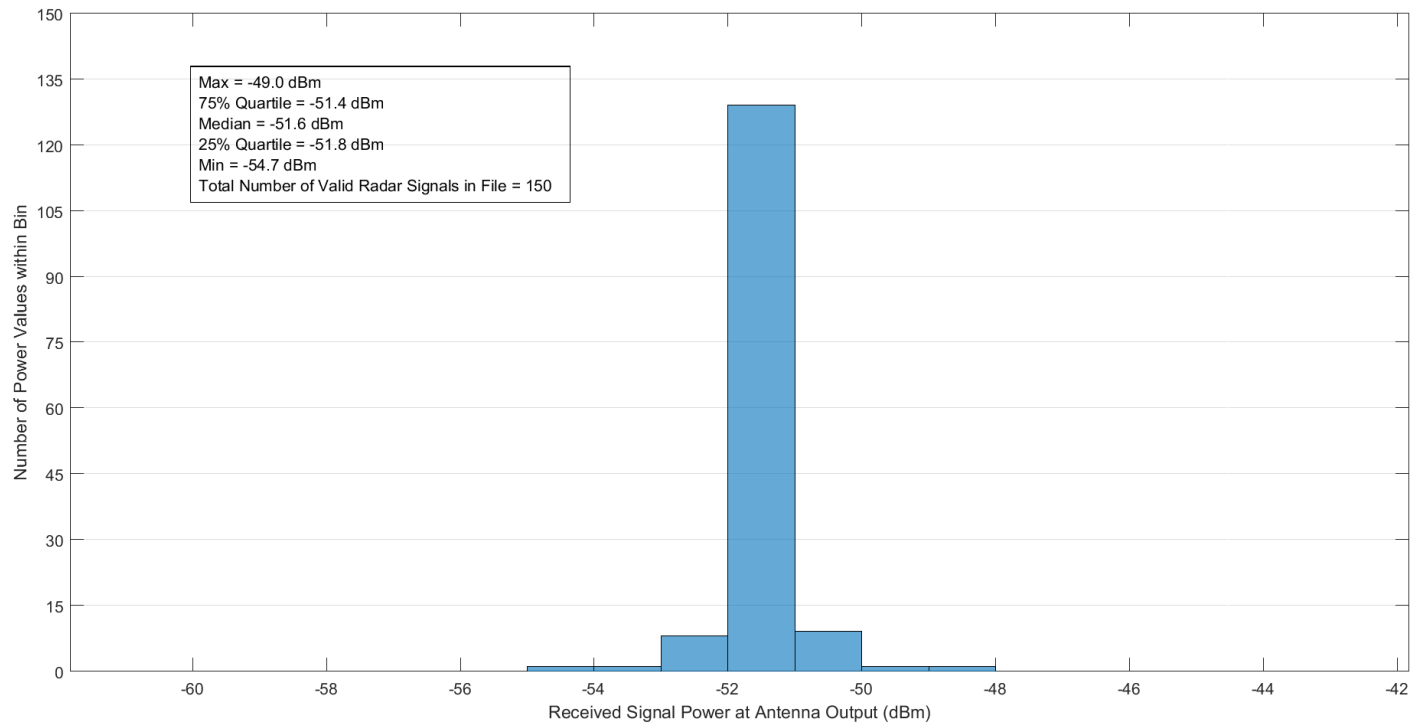


Figure B-19. Received radar signal power statistics at Location 4 in Zone F4 for the CARSR.

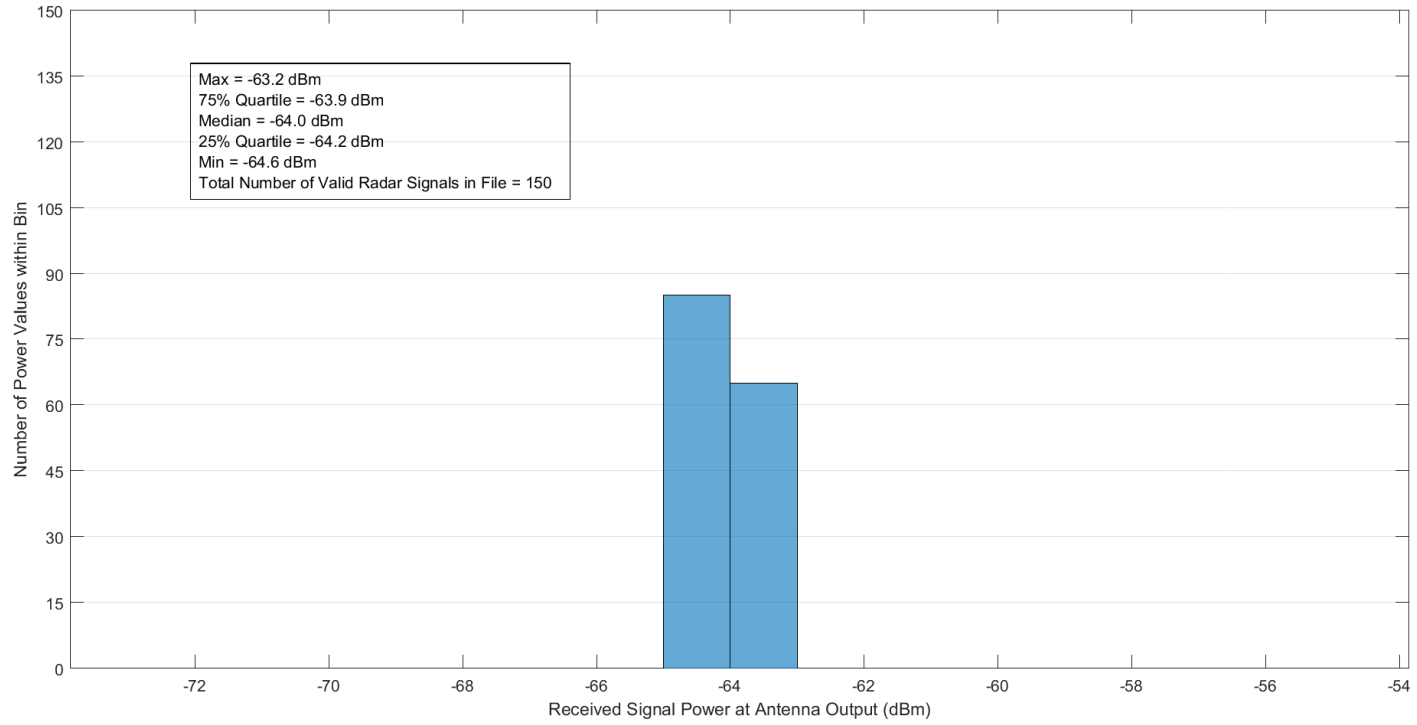


Figure B-20. Received radar signal power statistics at Location 5 in Zone F4 for the CARSR.

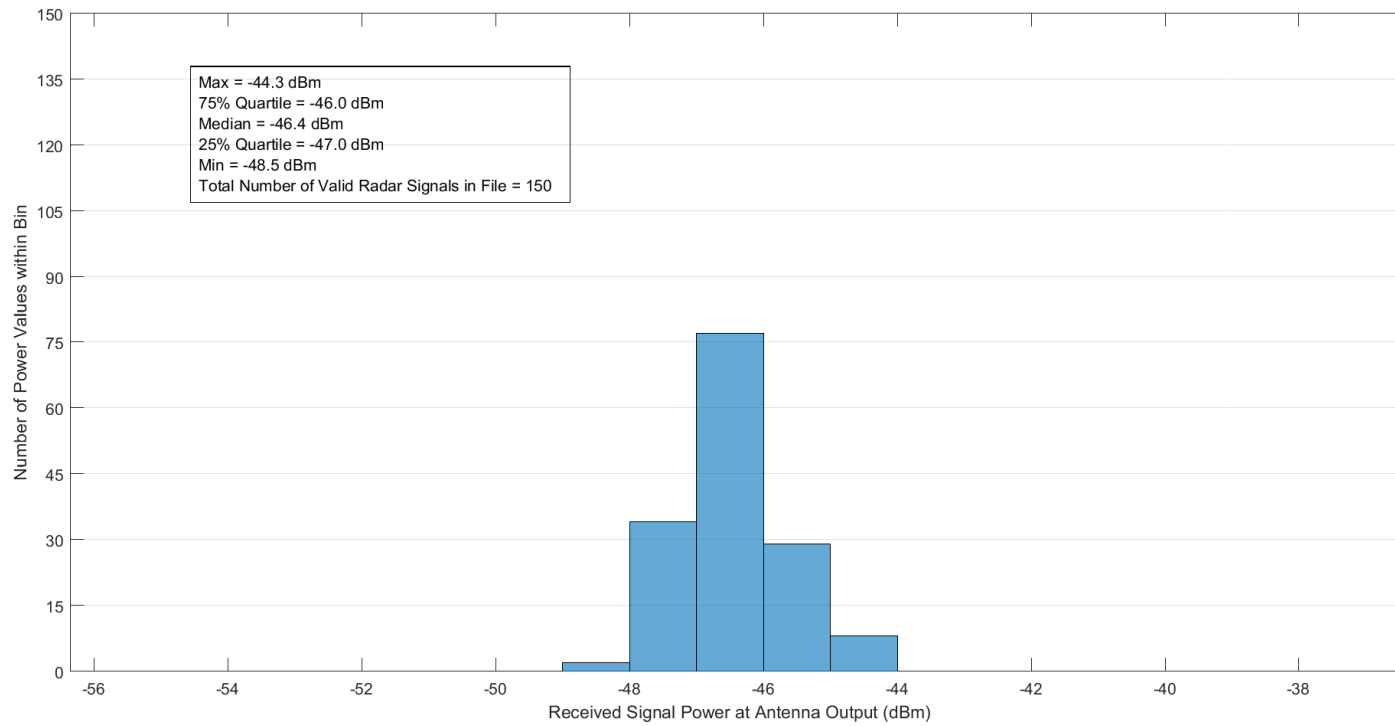


Figure B-21. Received radar signal power statistics at Location 1 in Zone G1 for the CARSR.

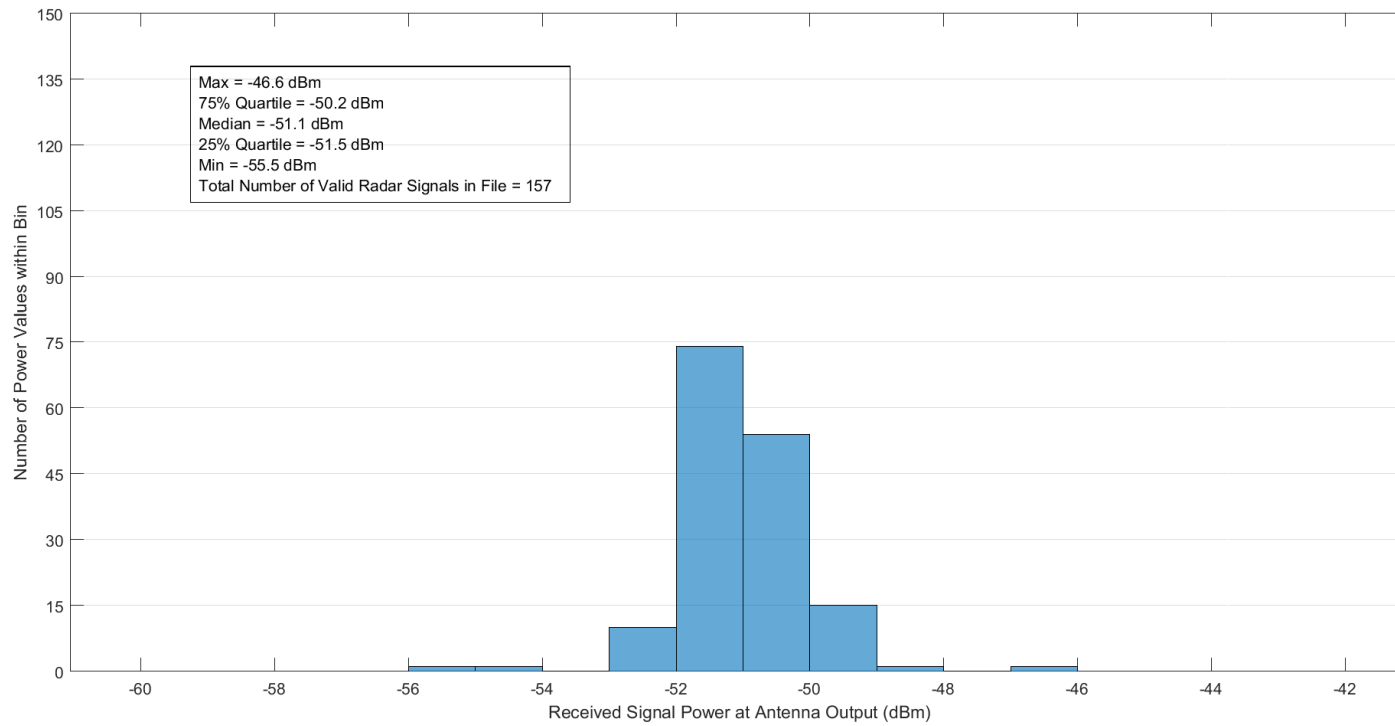


Figure B-22. Received radar signal power statistics at Location 2 in Zone G1 for the CARSR.

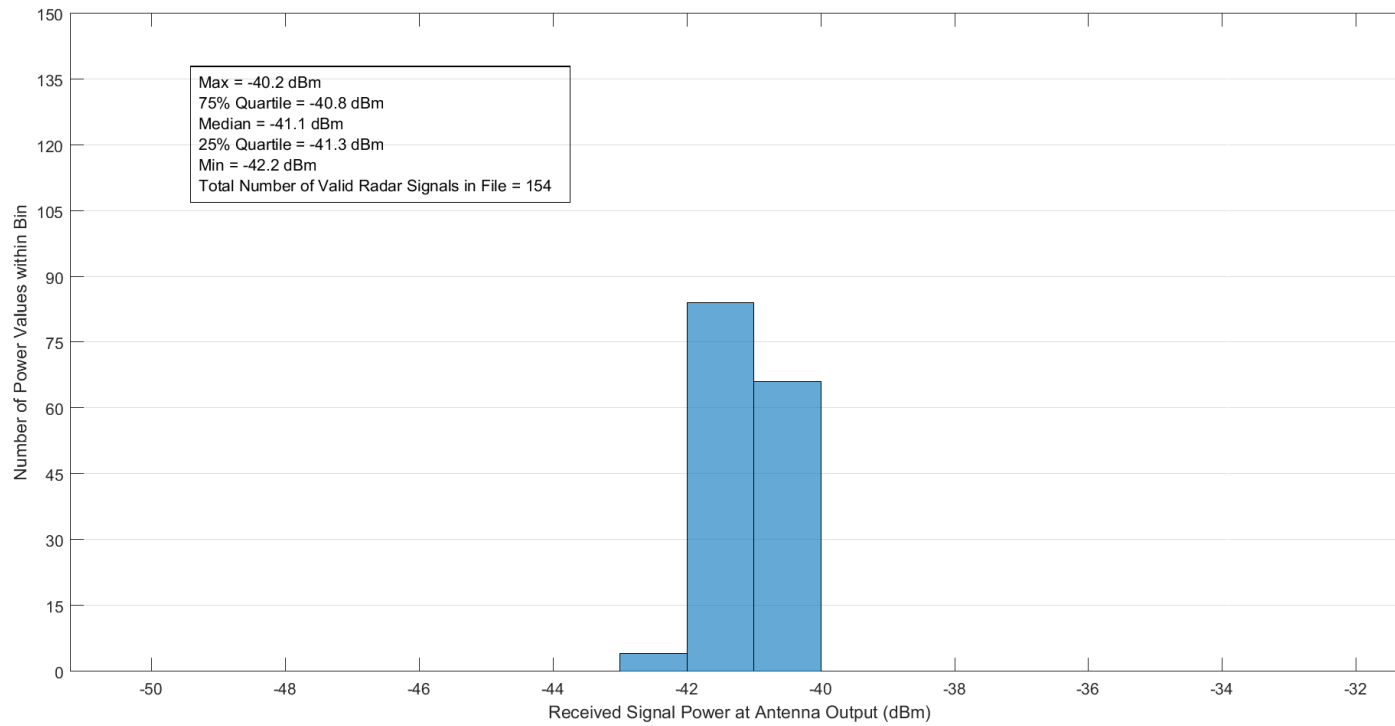


Figure B-23. Received radar signal power statistics at Location 3 in Zone G1 for the CARSR.

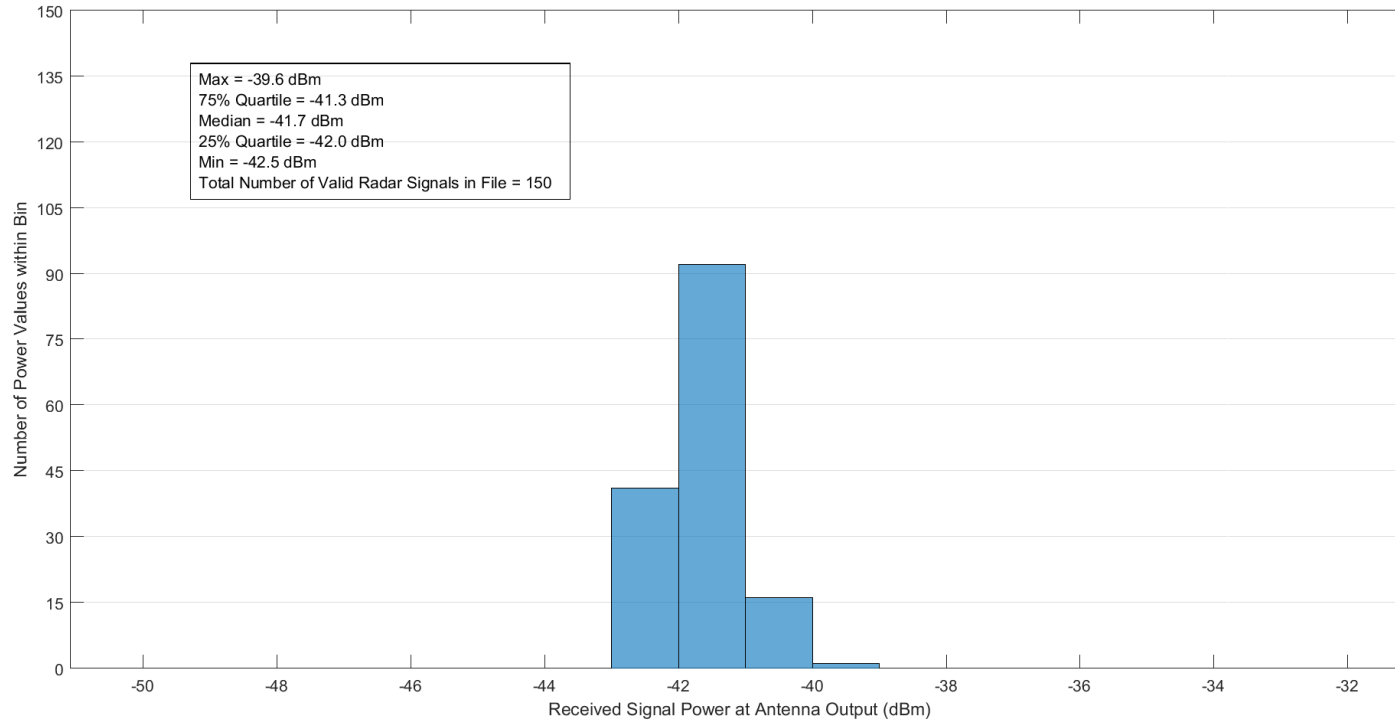


Figure B-24. Received radar signal power statistics at Location 4 in Zone G1 for the CARSR.

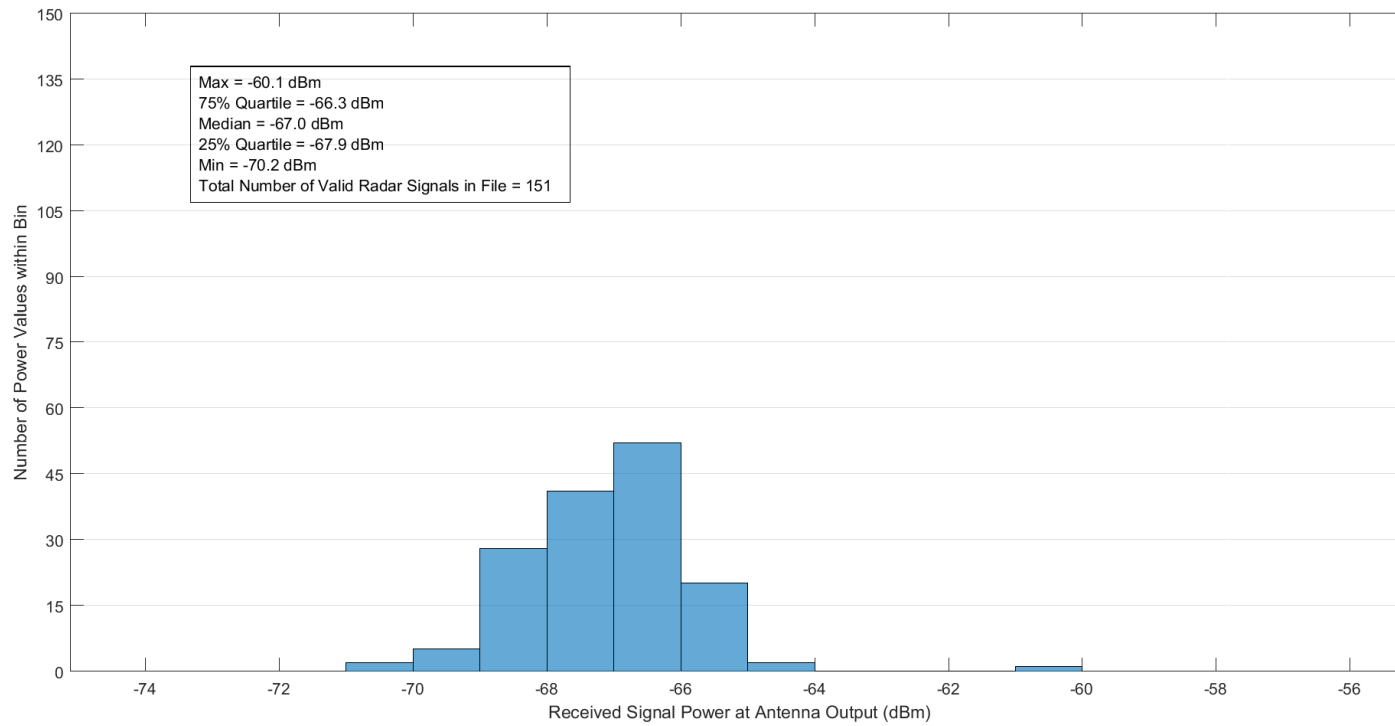


Figure B-25. Received radar signal power statistics at Location 5 in Zone G1 for the CARSR.

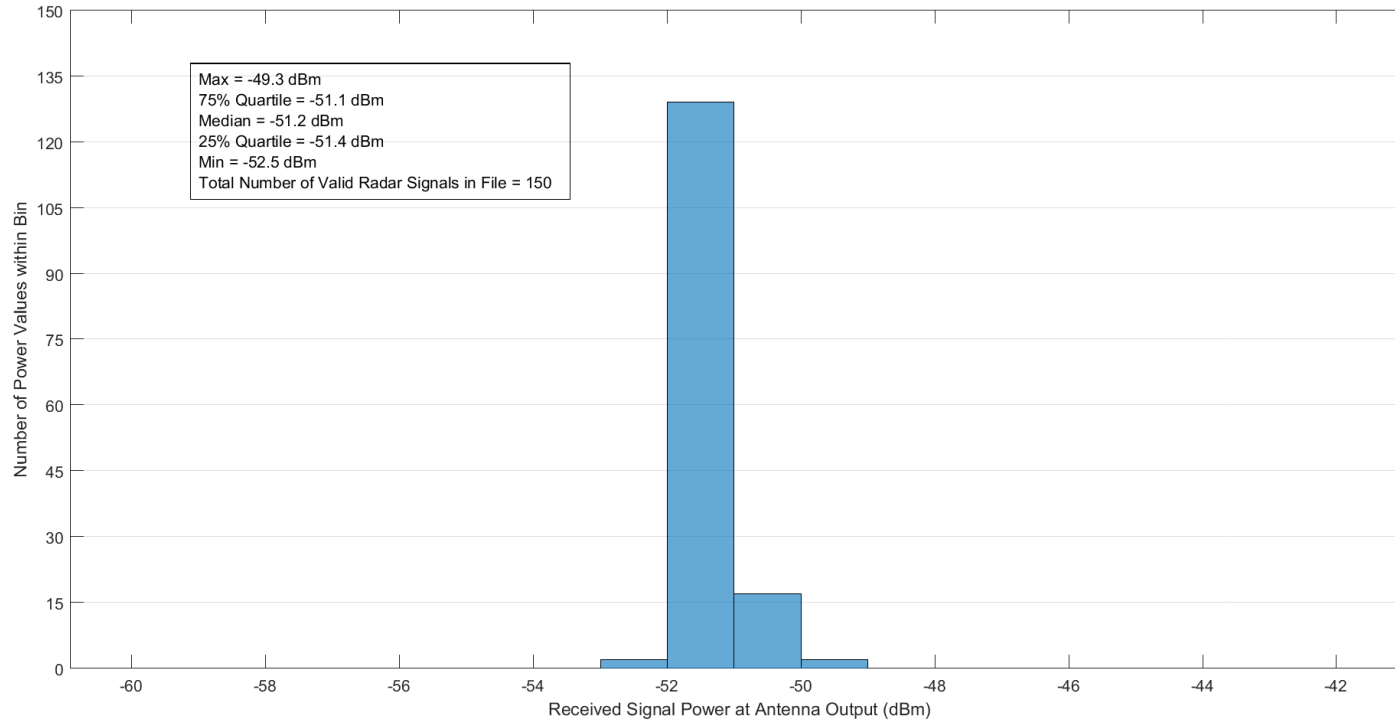


Figure B-26. Received radar signal power statistics at Location 1 in Zone G2 for the CARSR.

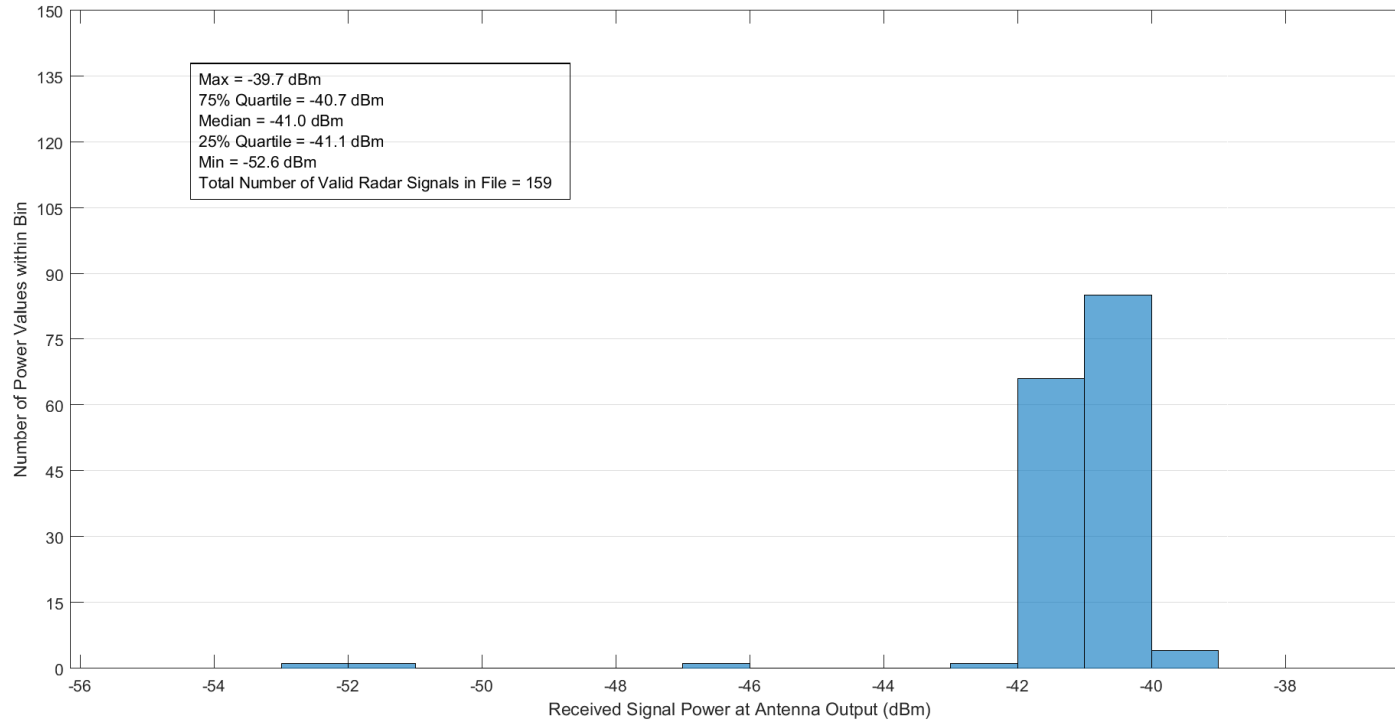


Figure B-27. Received radar signal power statistics at Location 2 in Zone G2 for the CARSR.

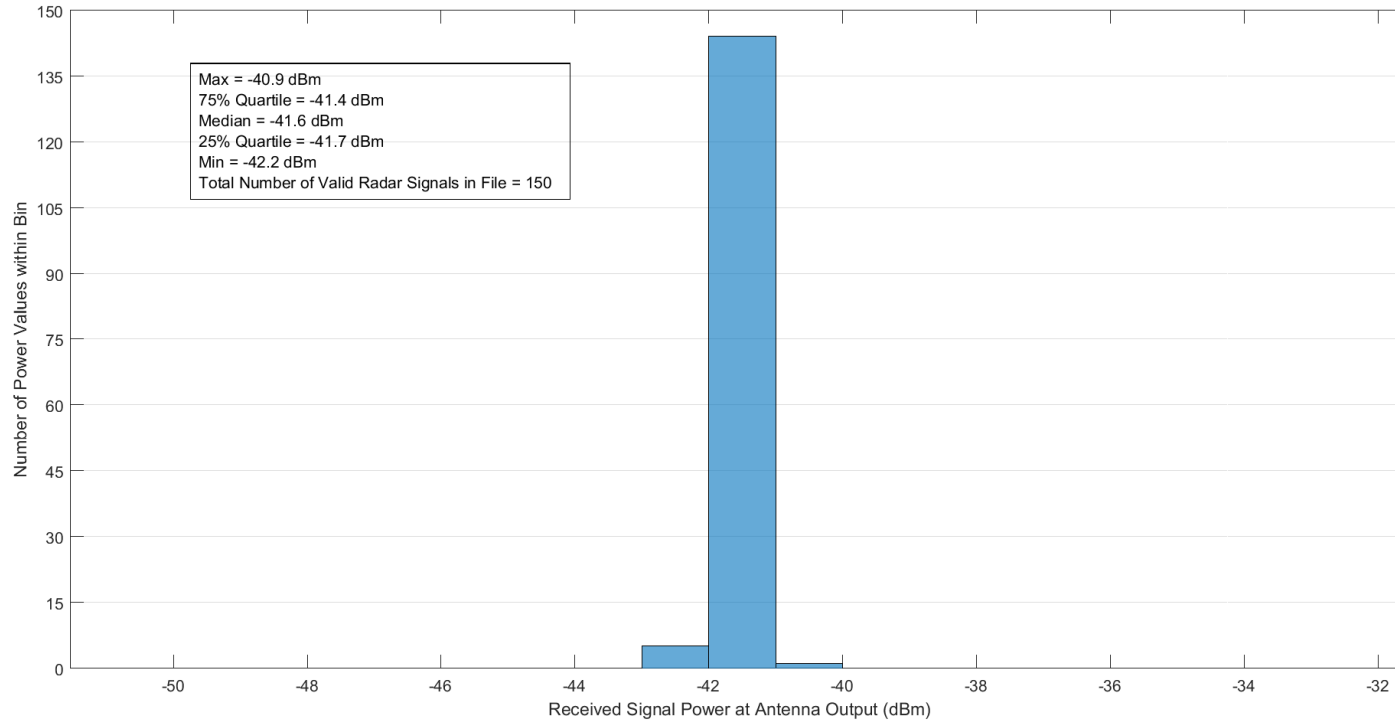


Figure B-28. Received radar signal power statistics at Location 3 in Zone G2 for the CARSR.

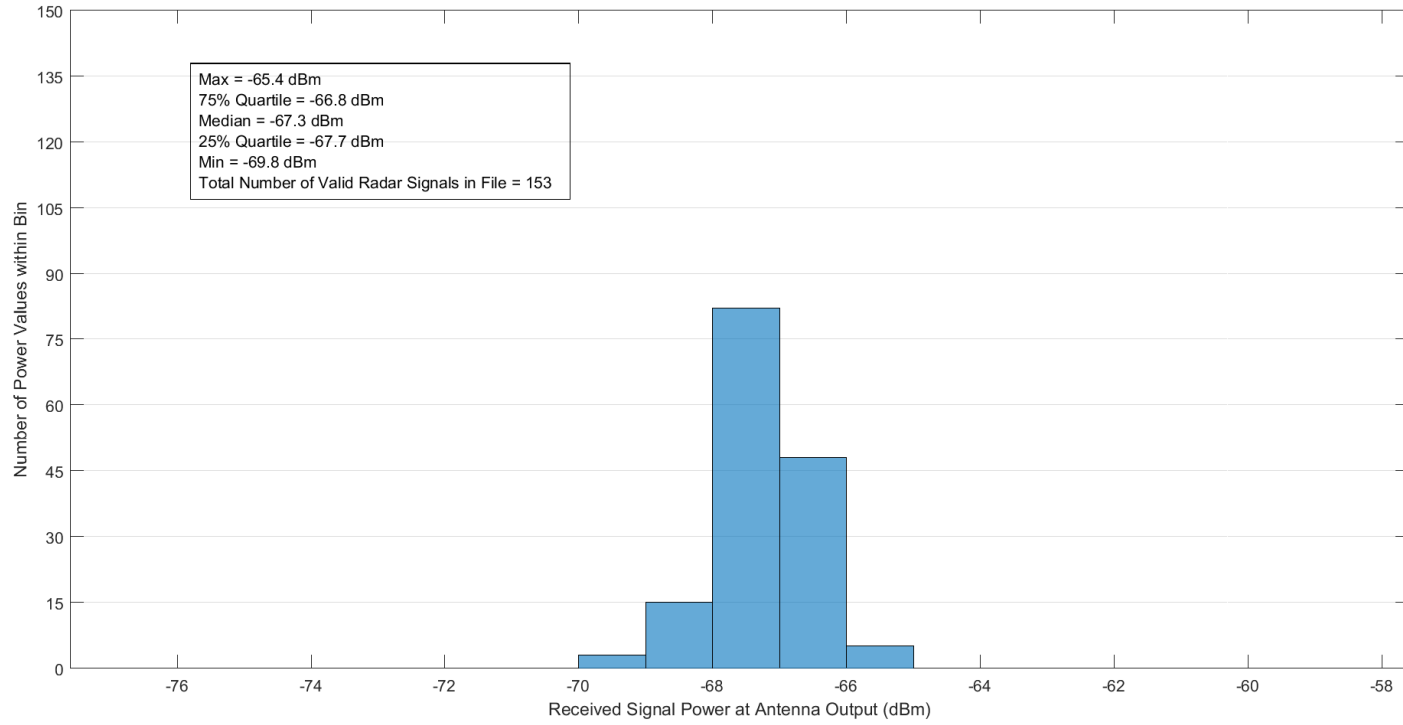


Figure B-29. Received radar signal power statistics at Location 4 in Zone G2 for the CARSR.

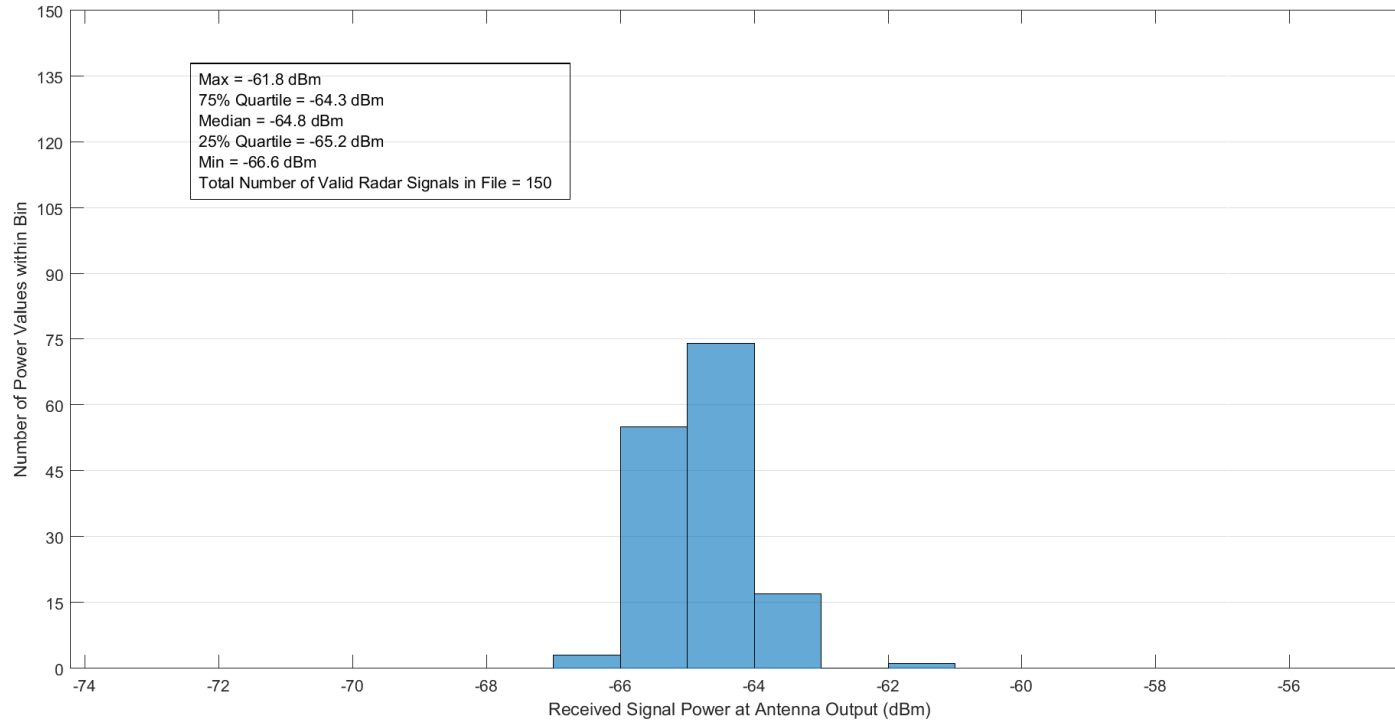


Figure B-30. Received radar signal power statistics at Location 5 in Zone G2 for the CARSR.

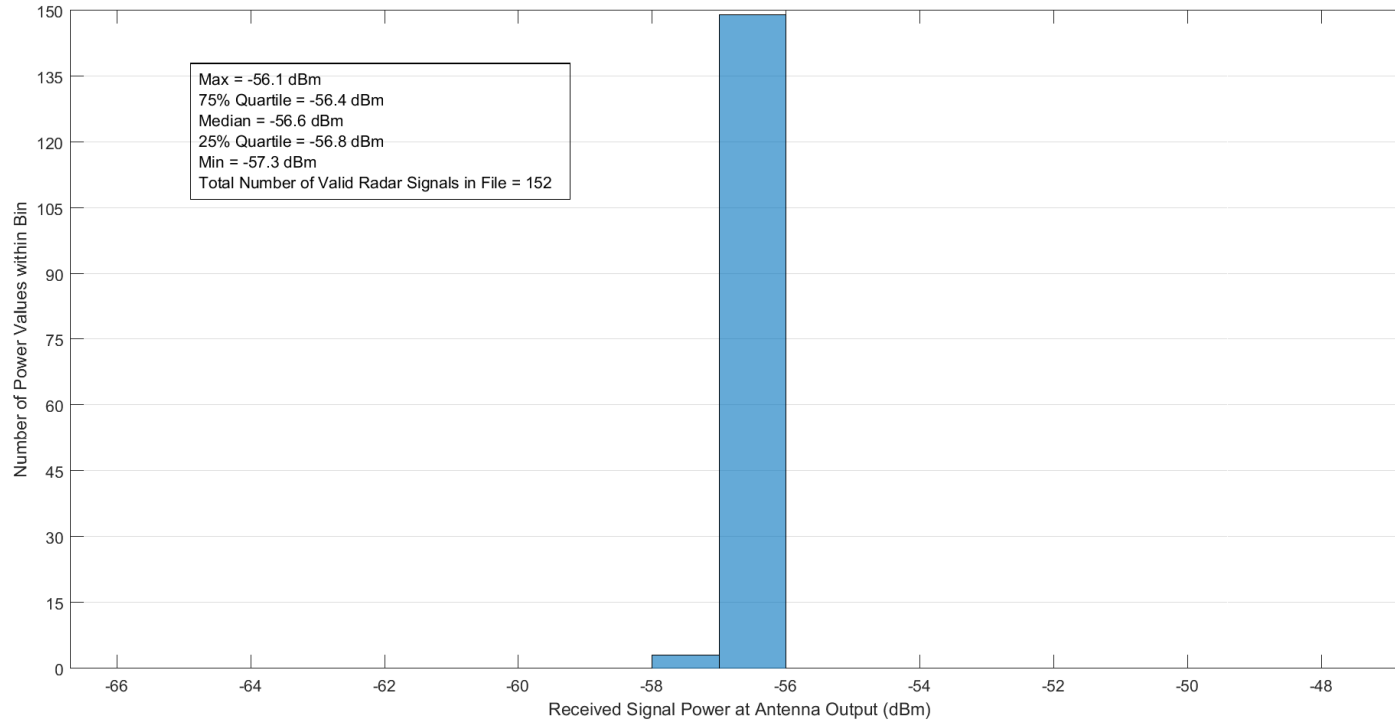


Figure B-31. Received radar signal power statistics at Location 1 in Zone G3 for the CARSR.

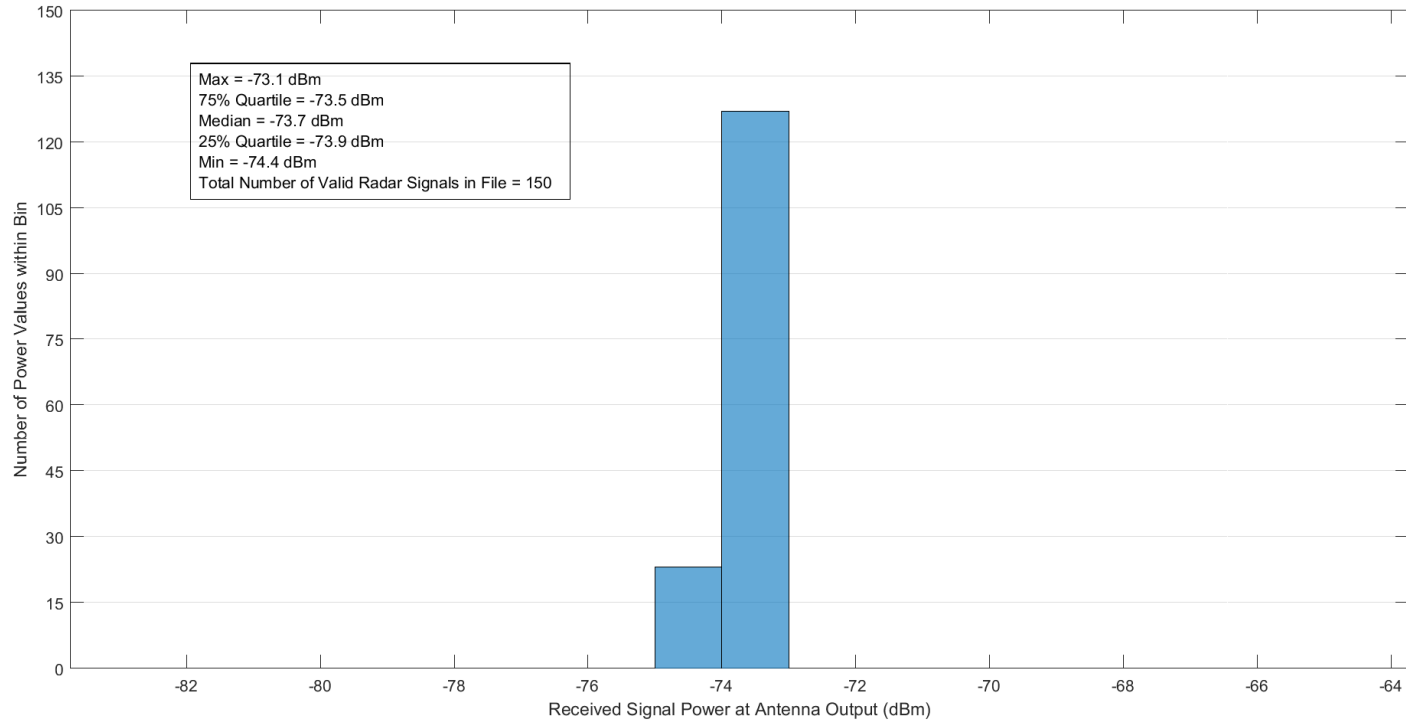


Figure B-302. Received radar signal power statistics at Location 2 in Zone G3 for the CARSR.

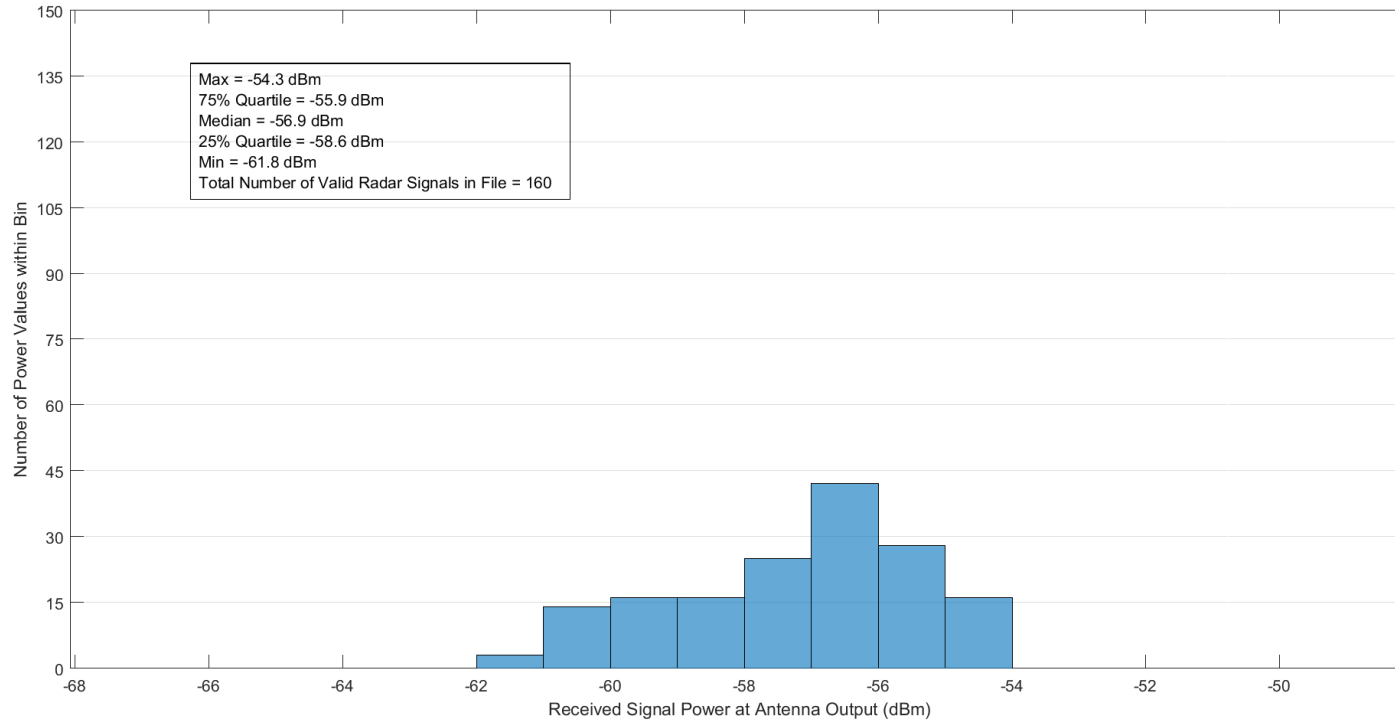


Figure B-33. Received radar signal power statistics at Location 3 in Zone G3 for the CARSR.

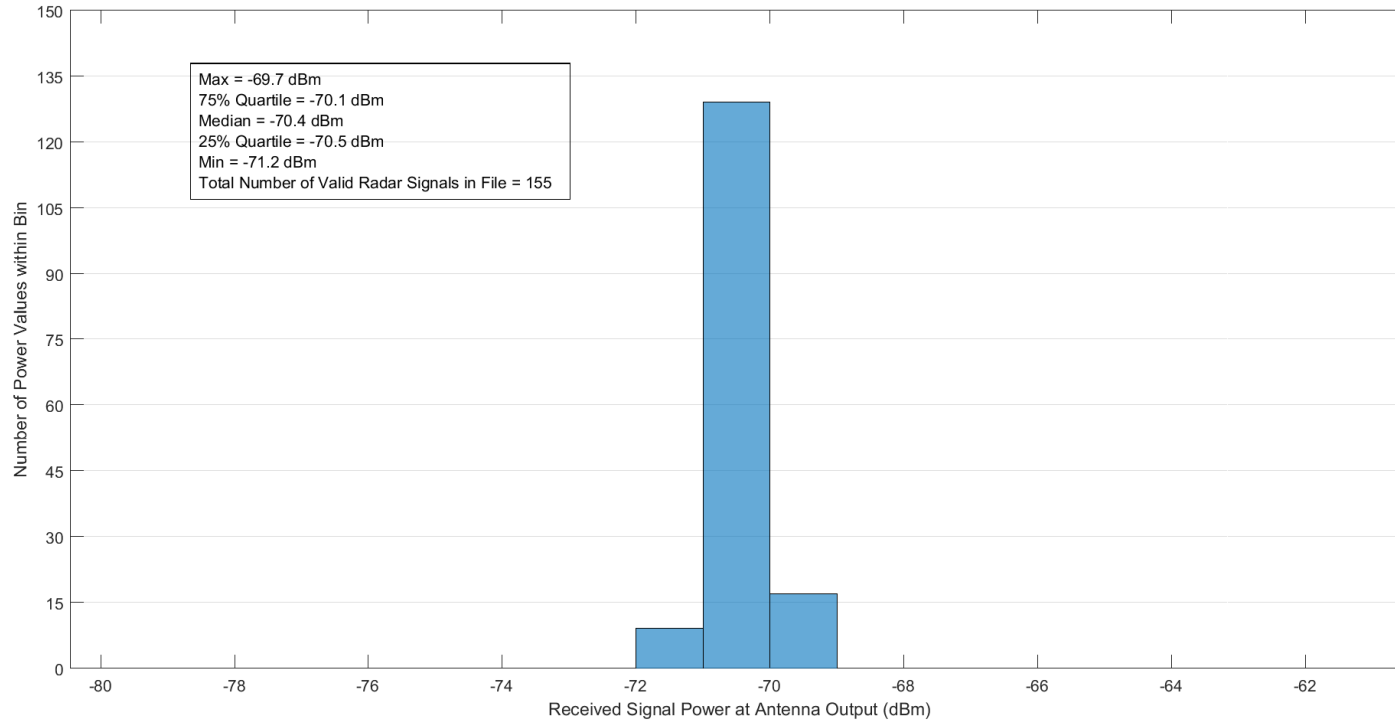


Figure B-34. Received radar signal power statistics at Location 4 in Zone G3 for the CARSR.

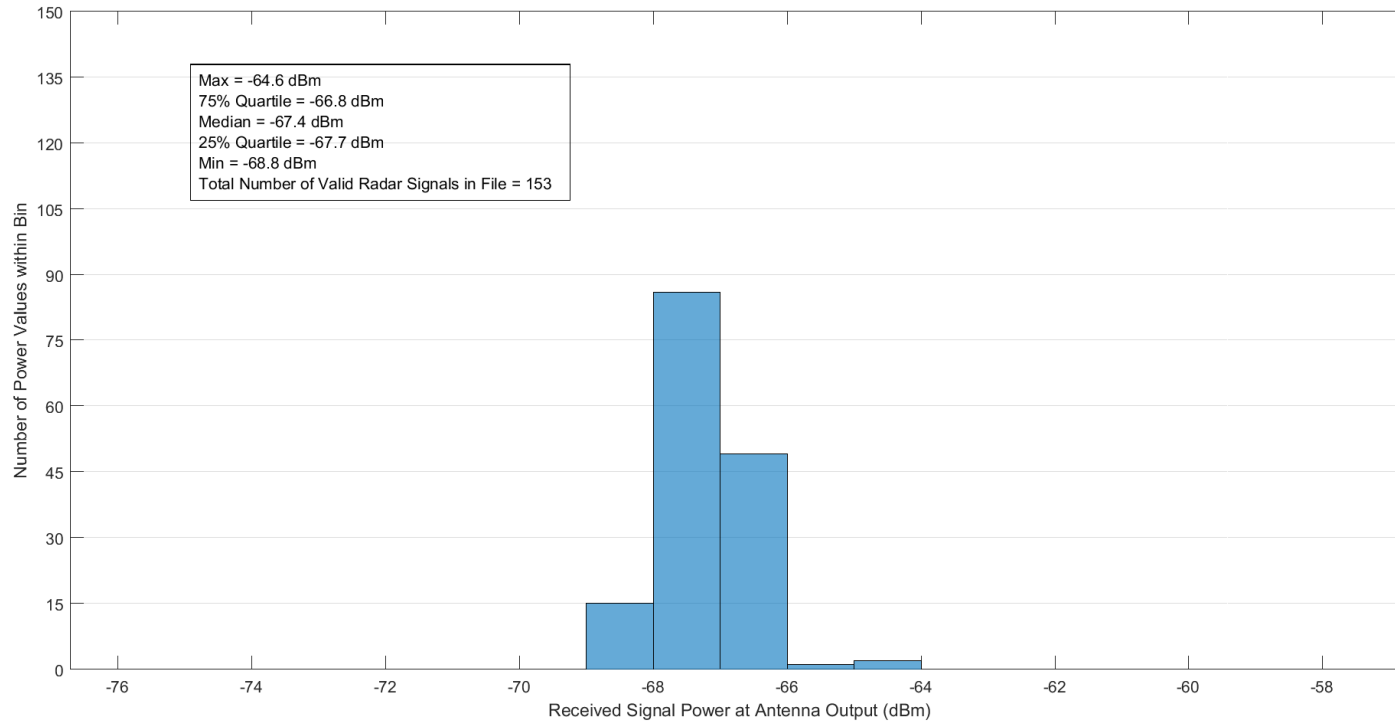


Figure B-35. Received radar signal power statistics at Location 5 in Zone G3 for the CARSR.

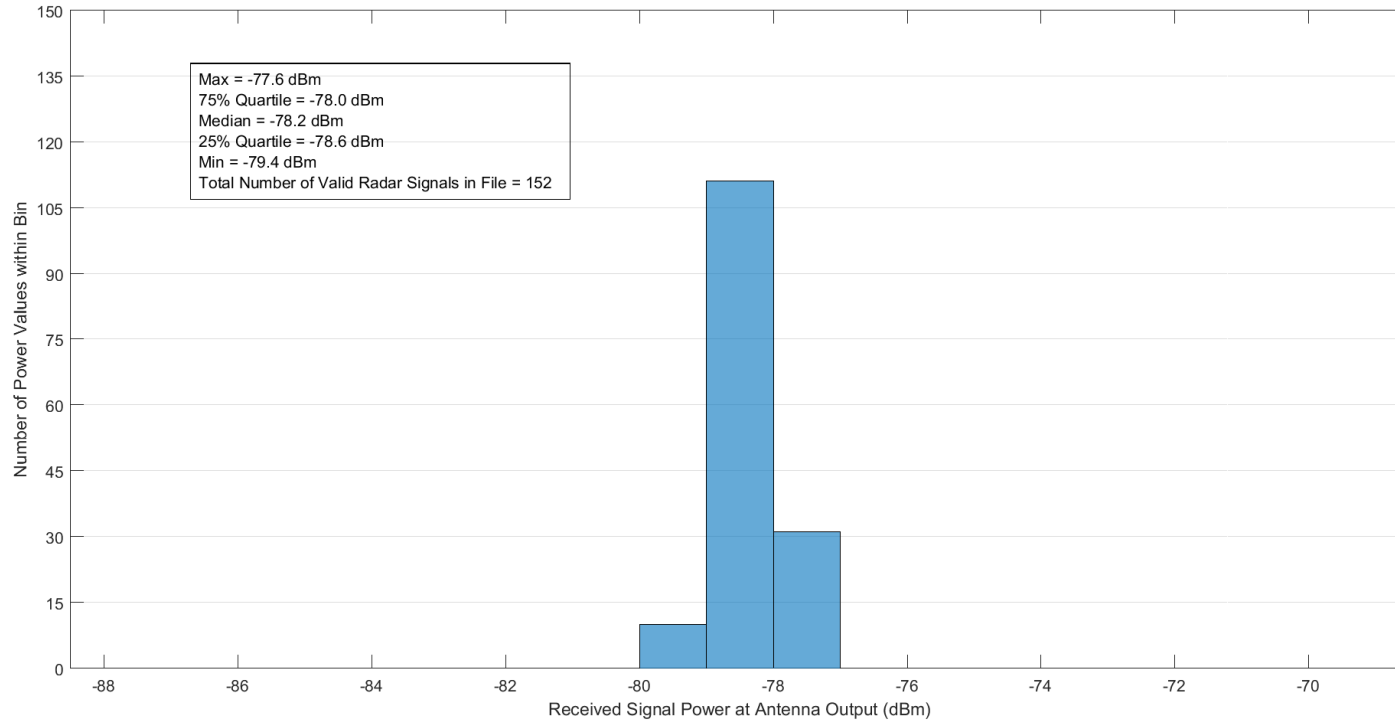


Figure B-36. Received radar signal power statistics at Location 6 in Zone G3 for the CARSR.

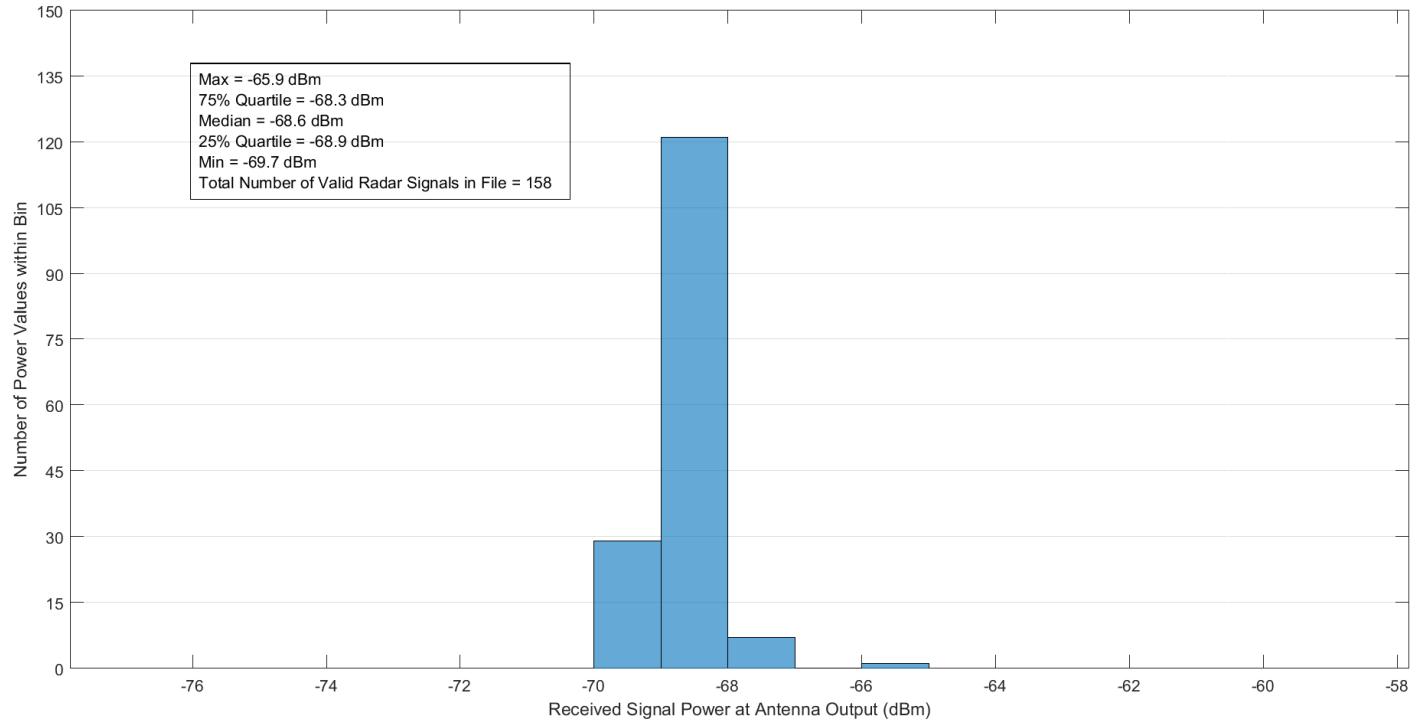


Figure B-37. Received radar signal power statistics at Location 1 in Zone H1 for the CARSR.

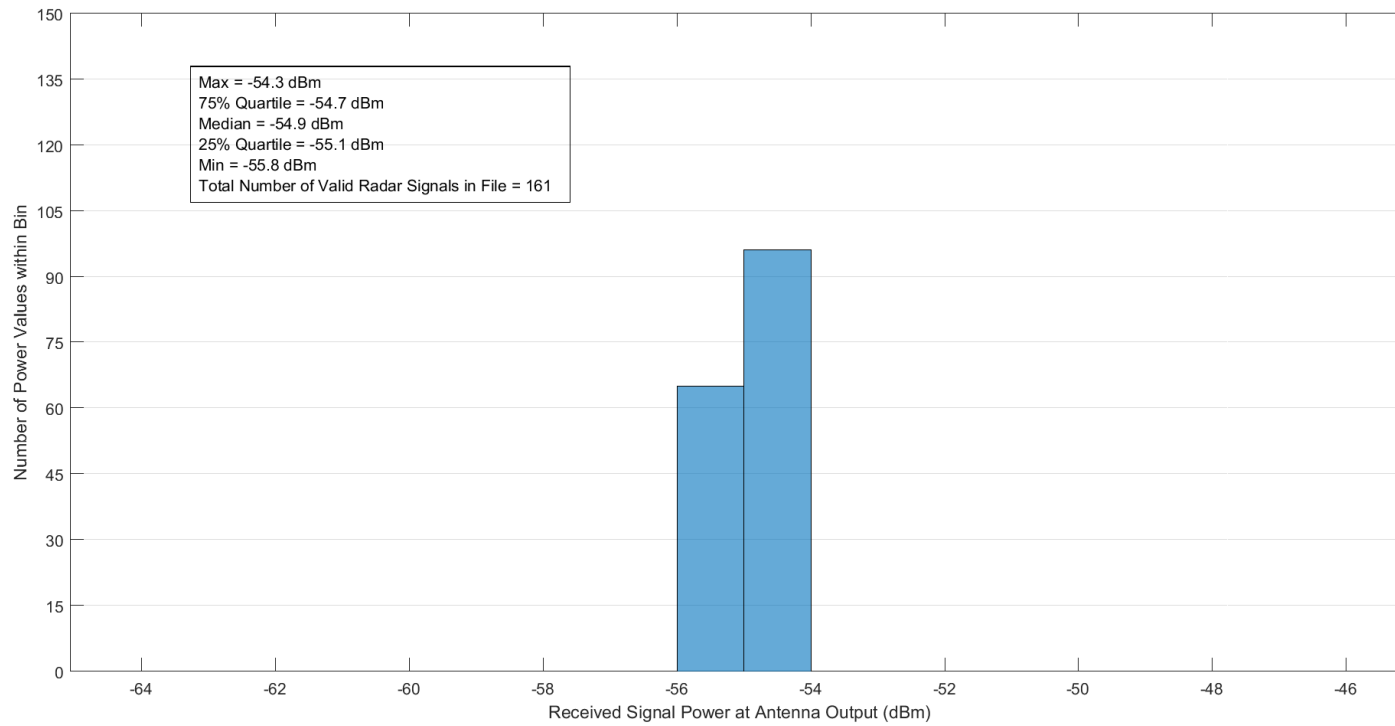


Figure B-38. Received radar signal power statistics at Location 2 in Zone H1 for the CARSR.

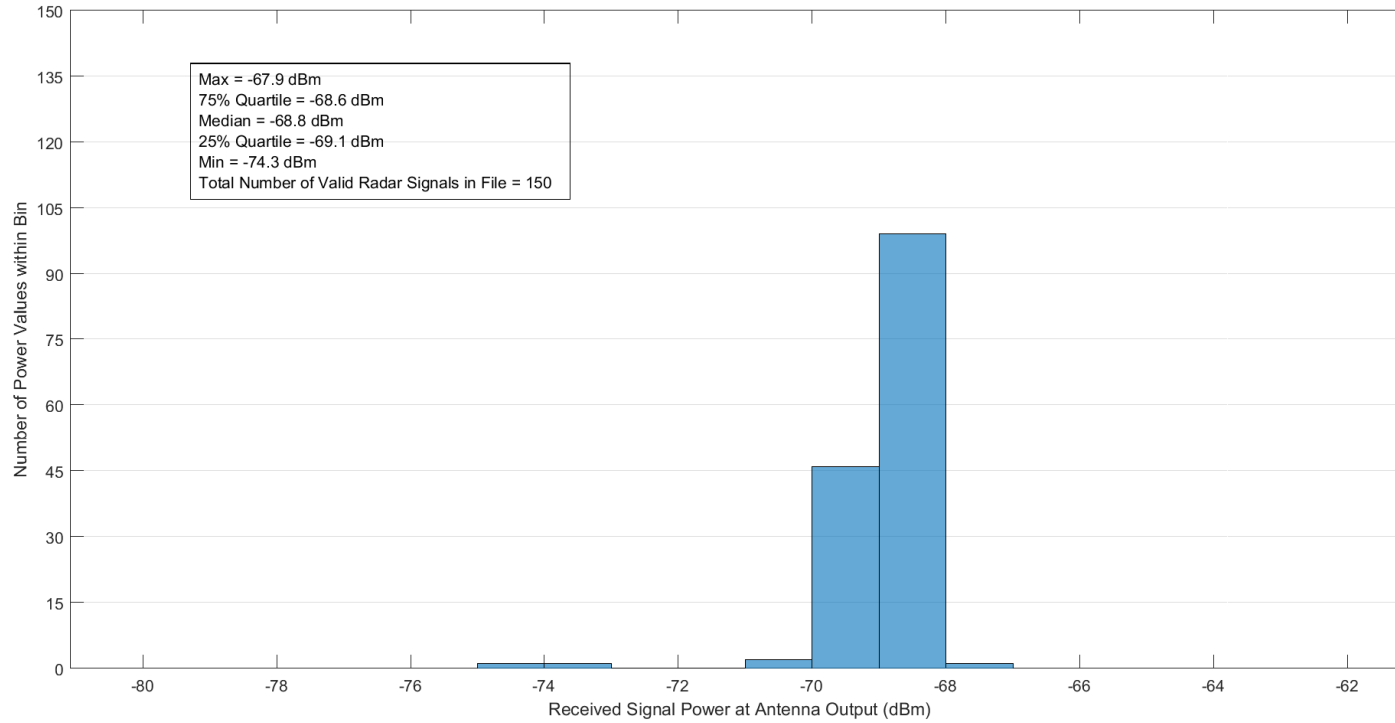


Figure B-39. Received radar signal power statistics at Location 3 in Zone H1 for the CARSR.

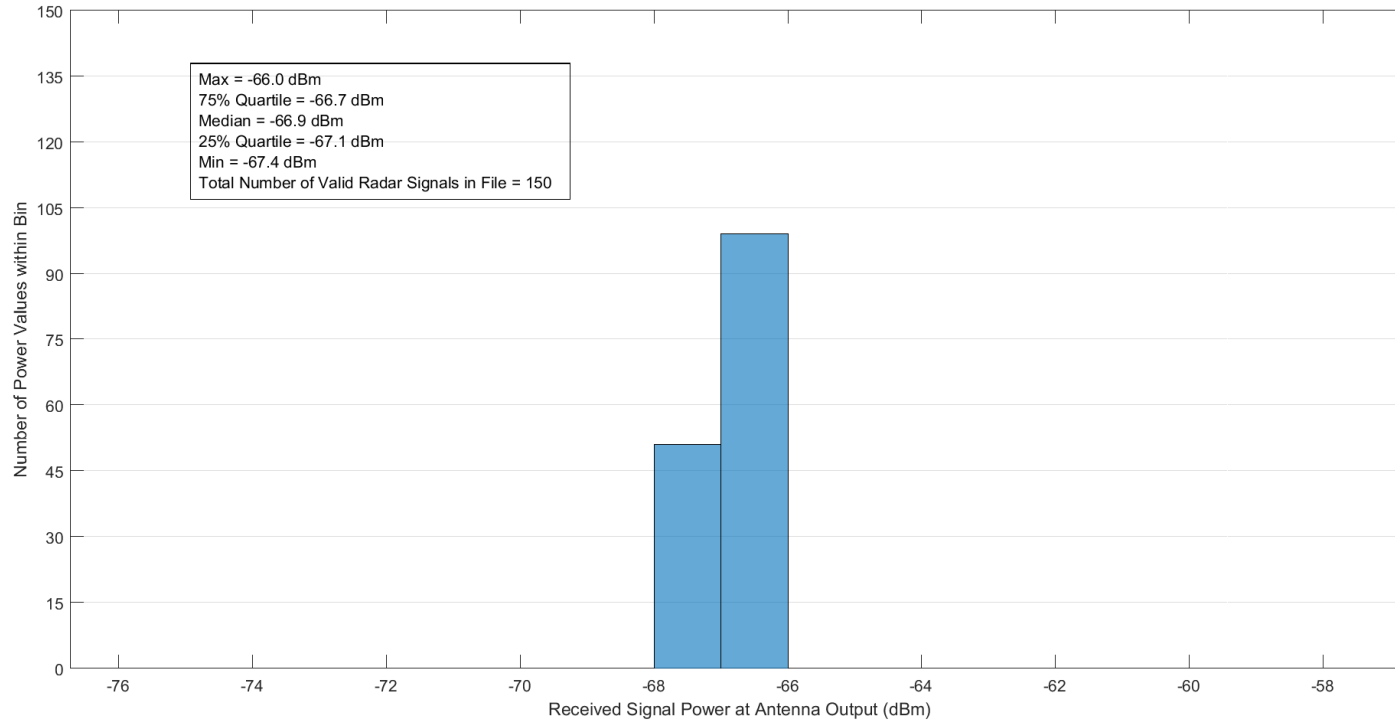


Figure B-40. Received radar signal power statistics at Location 4 in Zone H1 for the CARSR.

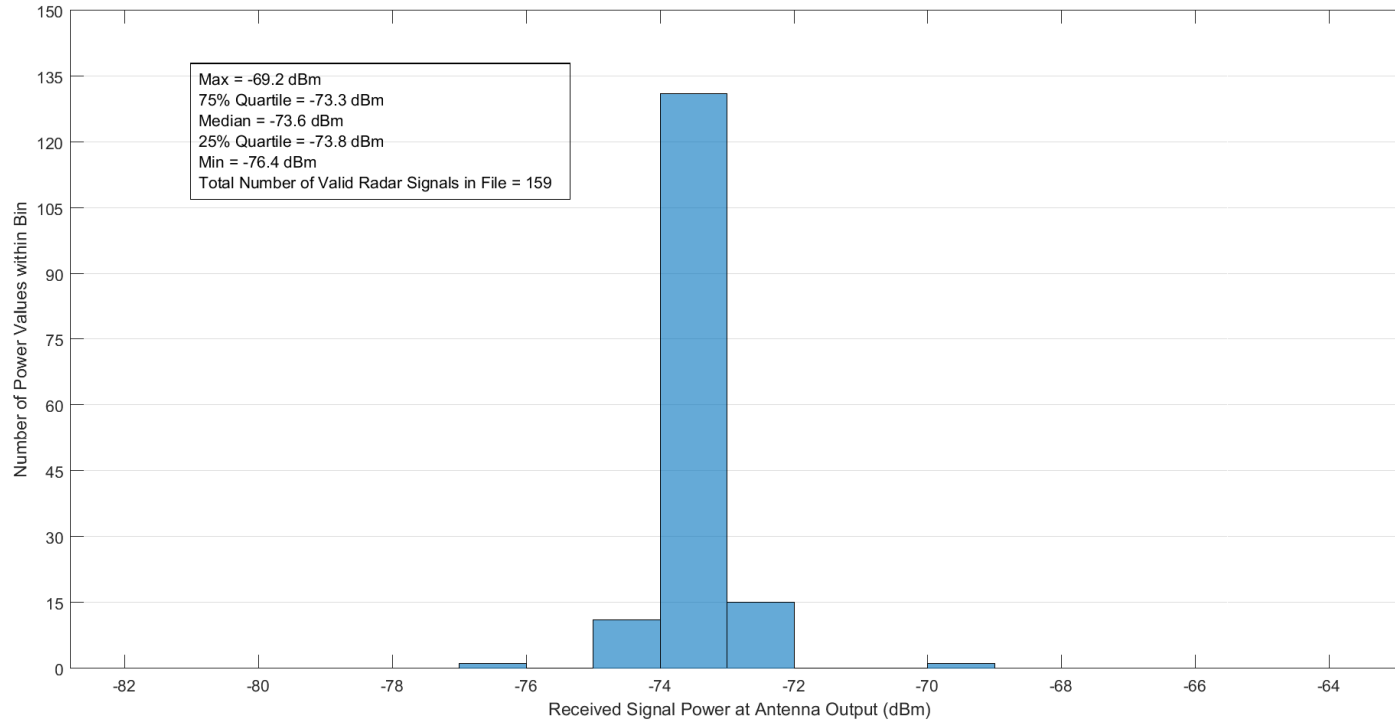


Figure B-41. Received radar signal power statistics at Location 5 in Zone H1 for the CARSR.

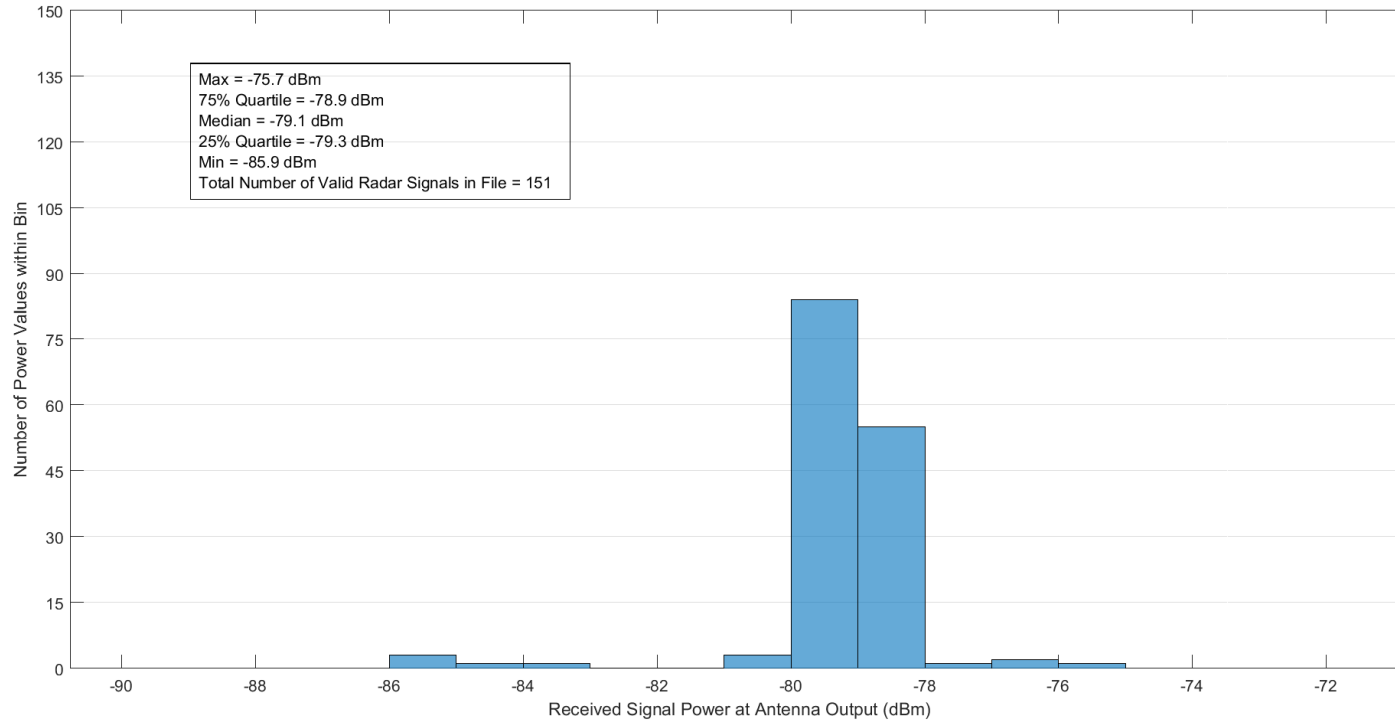


Figure B-42. Received radar signal power statistics at Location 6 in Zone H1 for the CARSR.

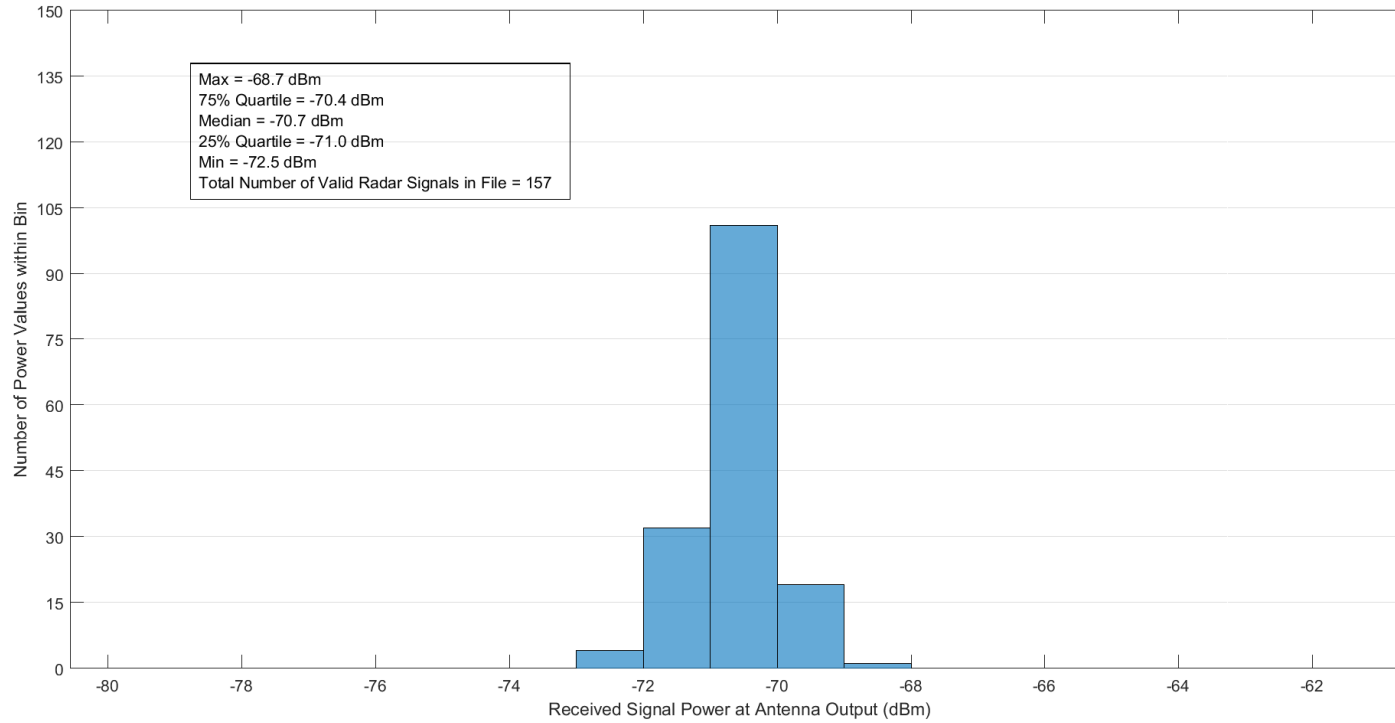


Figure B-43. Received radar signal power statistics at Location 1 in Zone I1 for the CARSR.

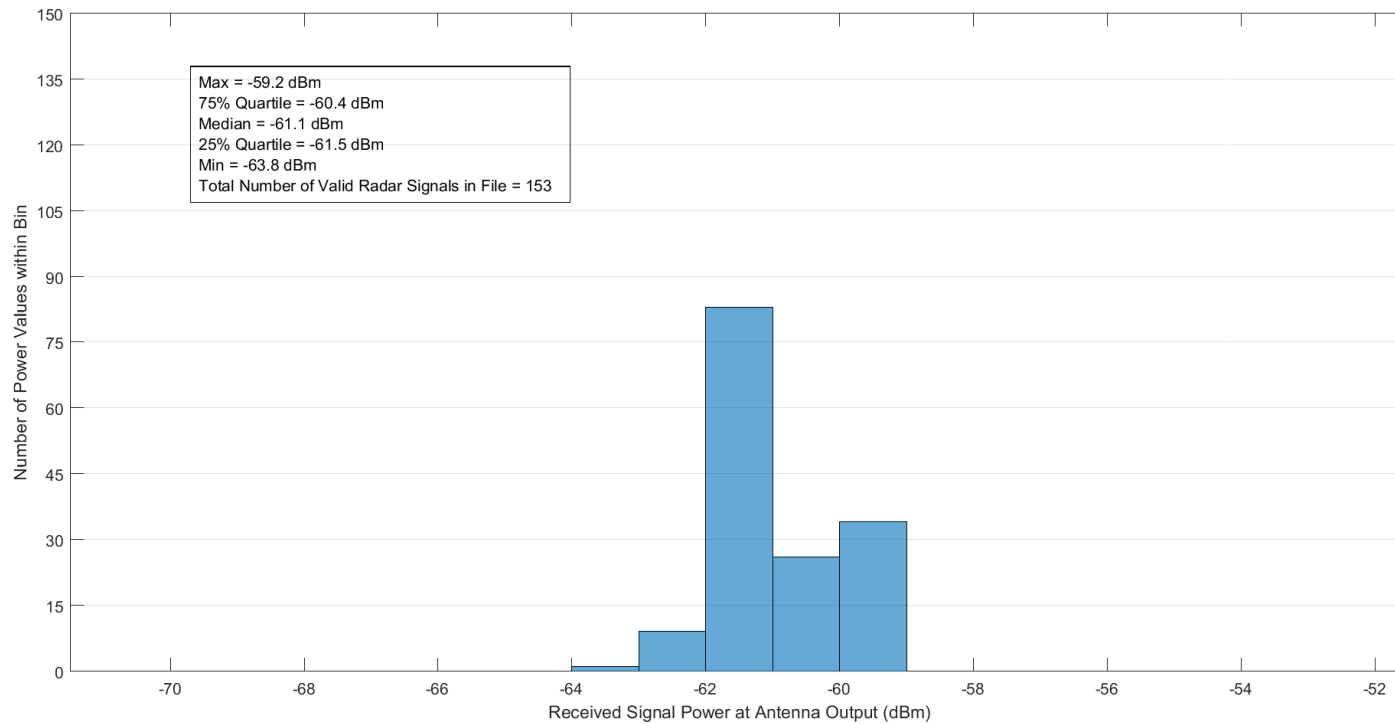


Figure B-44. Received radar signal power statistics at Location 2 in Zone I1 for the CARSR.

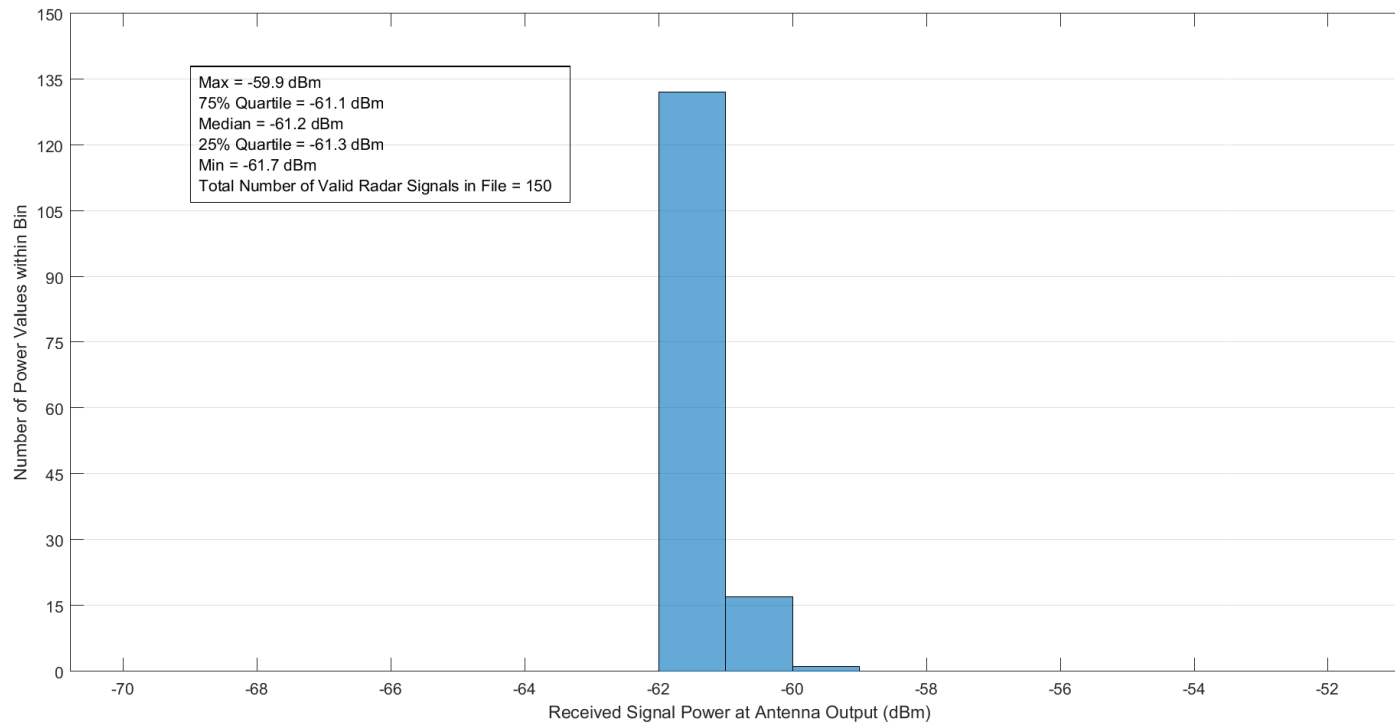


Figure B-45. Received radar signal power statistics at Location 3 in Zone I1 for the CARSR.

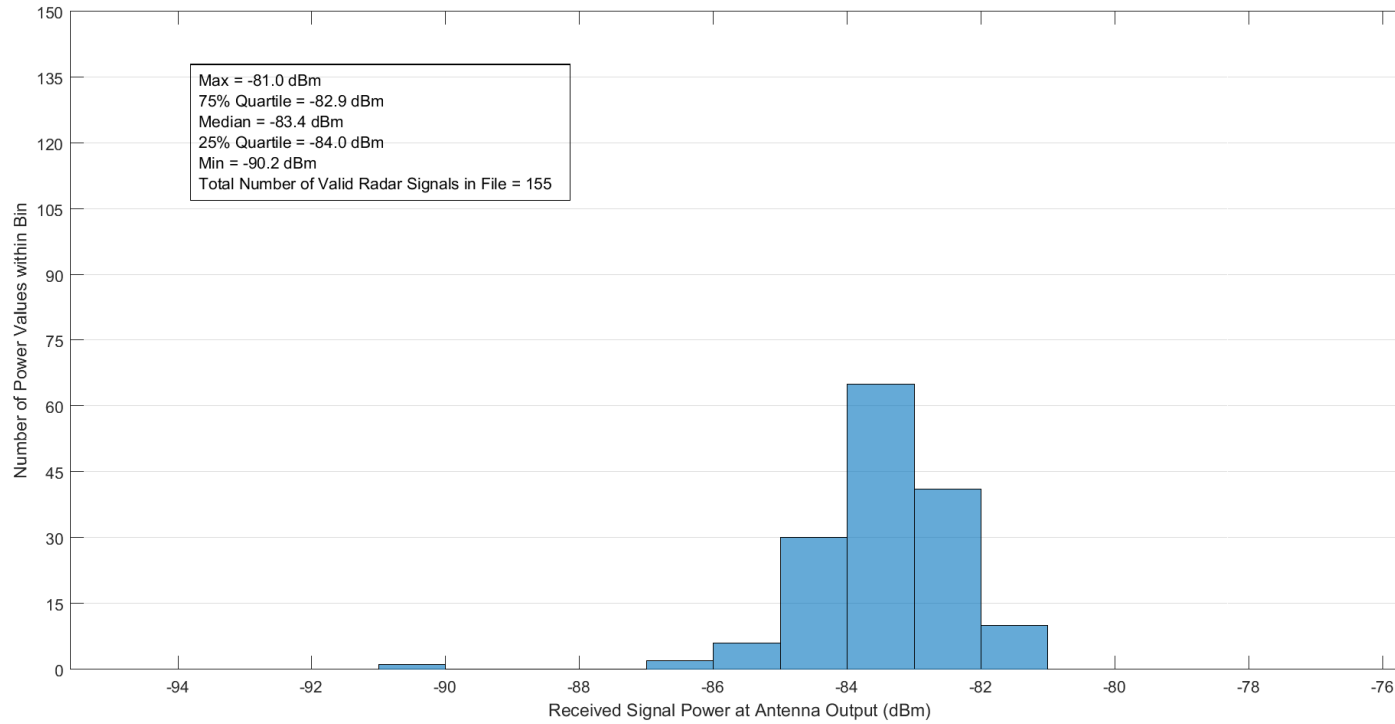


Figure B-46. Received radar signal power statistics at Location 4 in Zone I1 for the CARSR.

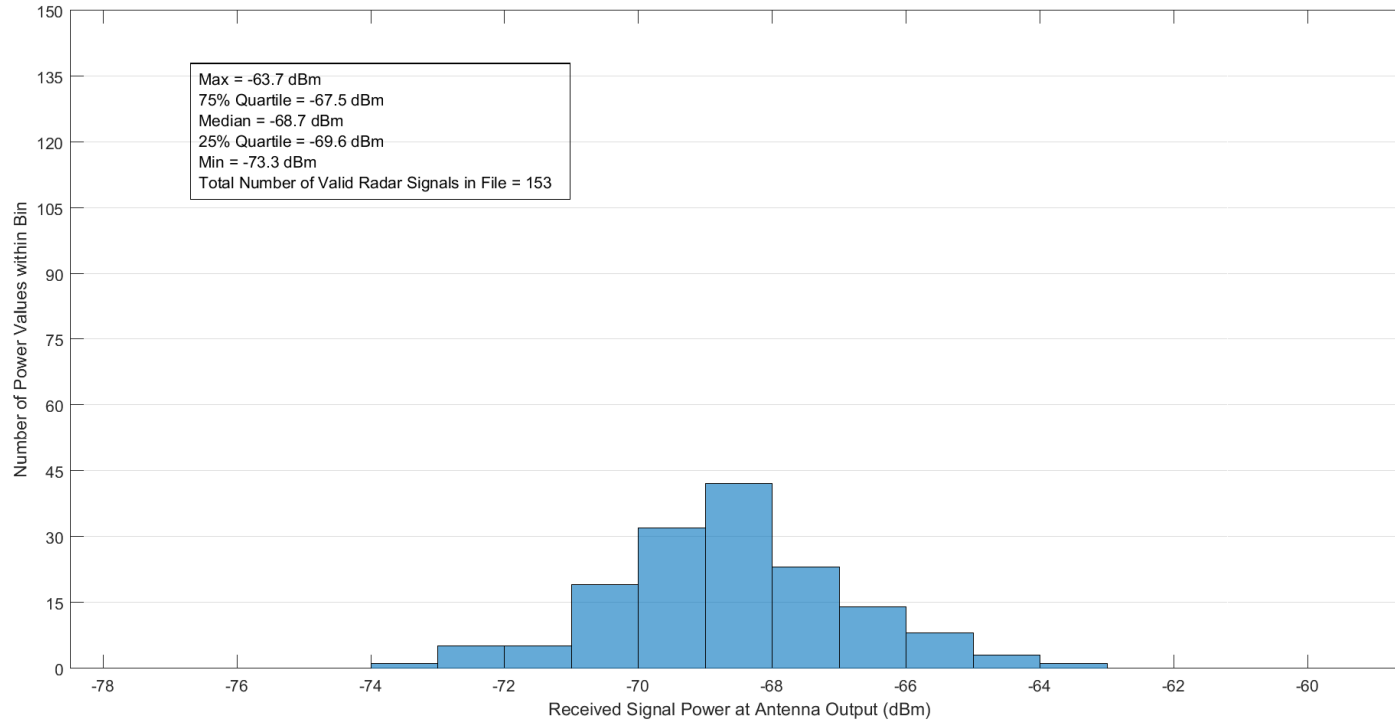


Figure B-47. Received radar signal power statistics at Location 1 in Zone J1 for the CARSR.

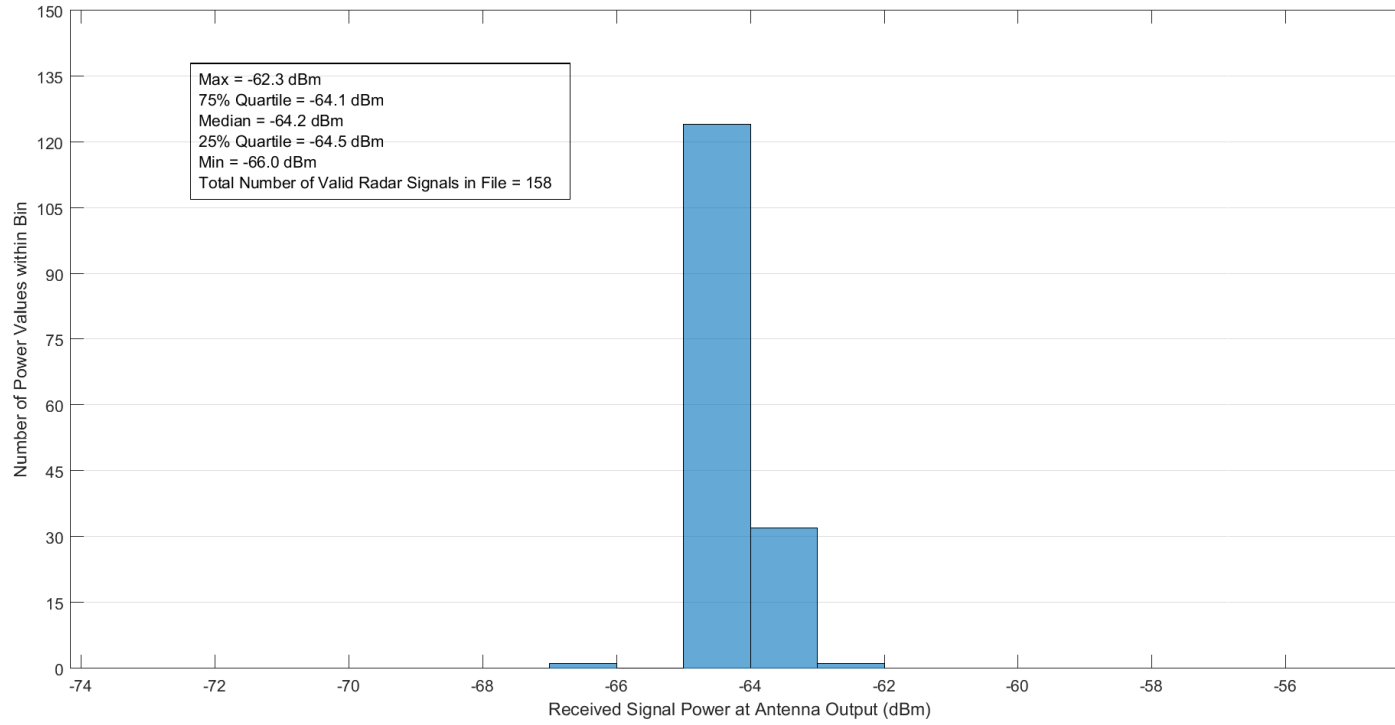


Figure B-48. Received radar signal power statistics at Location 2 in Zone J1 for the CARSR.

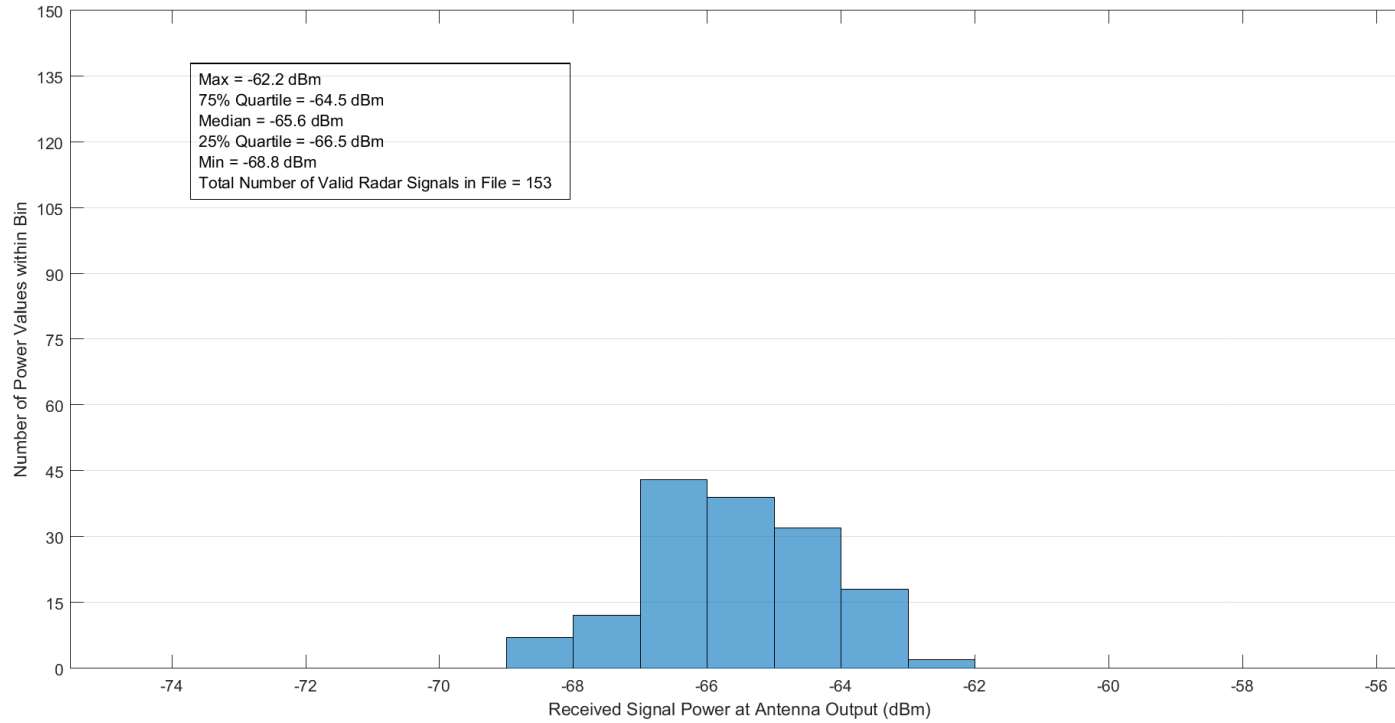


Figure B-49. Received radar signal power statistics at Location 3 in Zone J1 for the CARSR.

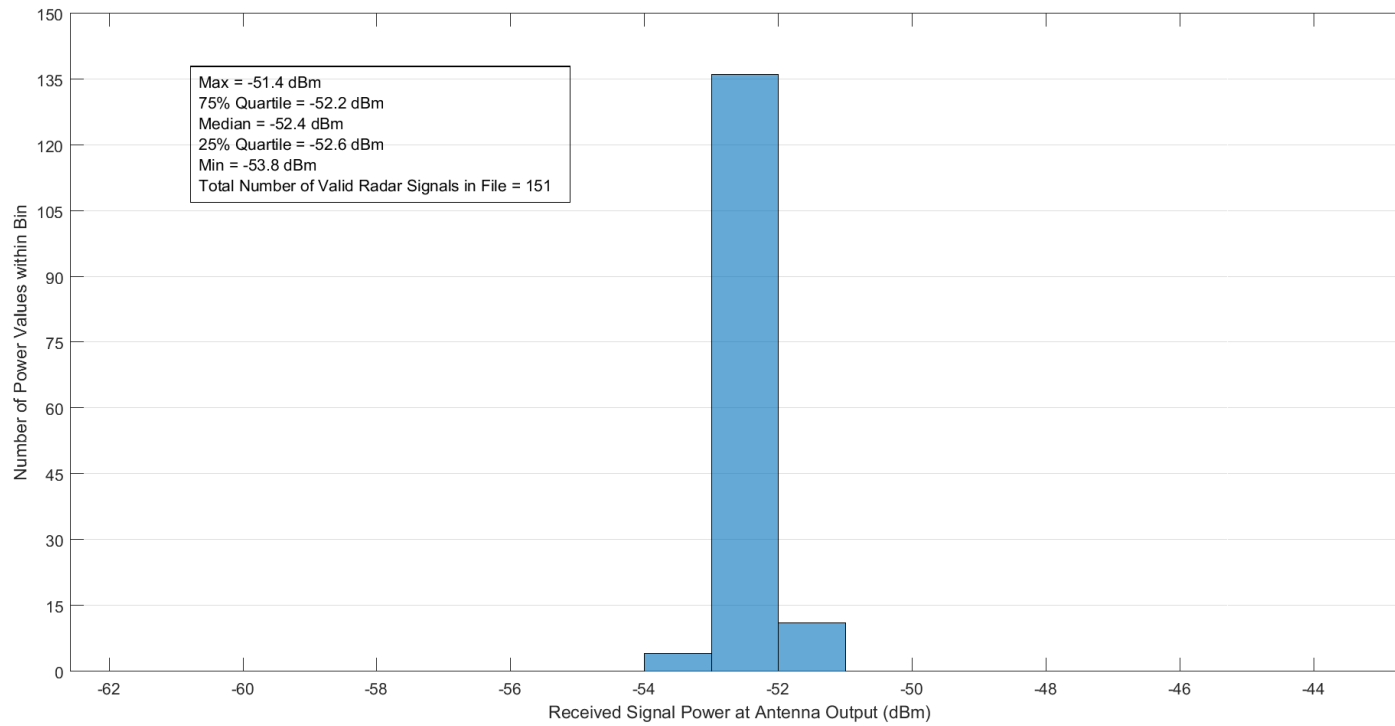


Figure B-50. Received radar signal power statistics at Location 4 in Zone J1 for the CARSR.

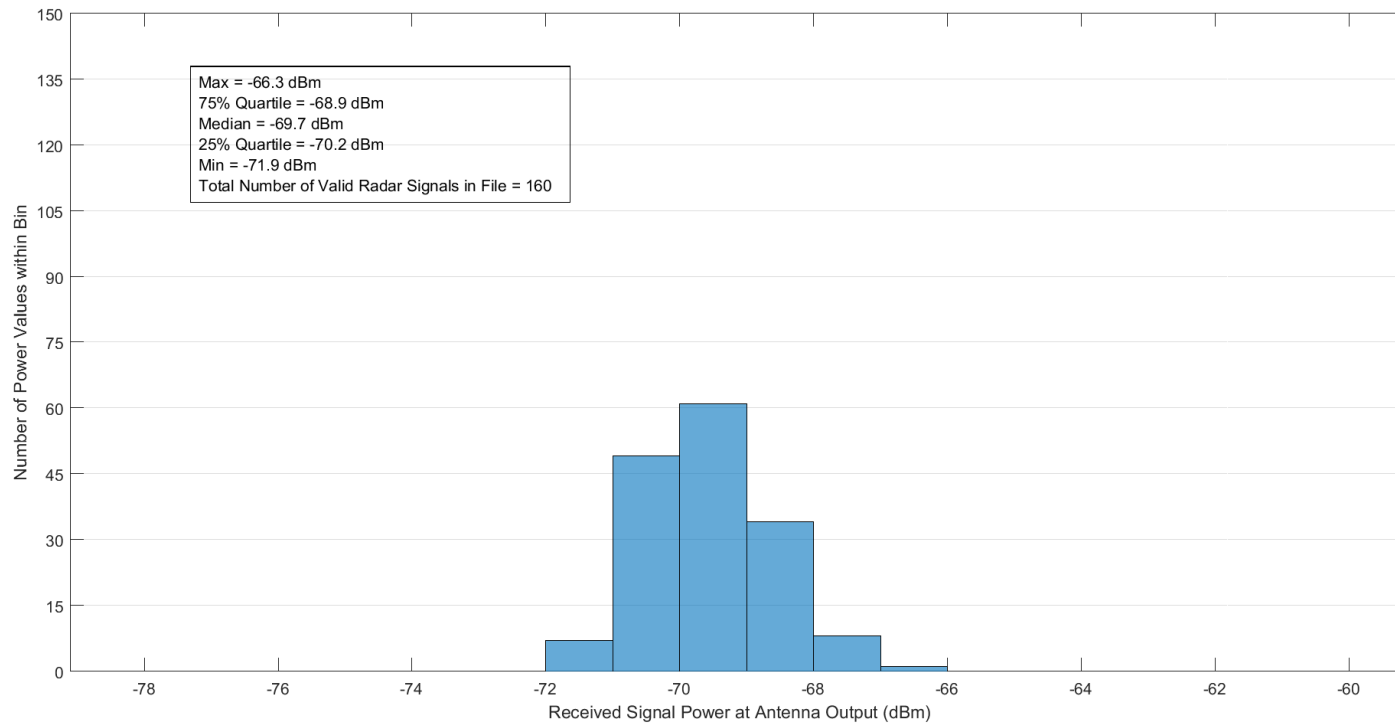


Figure B-51. Received radar signal power statistics at Location 5 in Zone J1 for the CARSR.

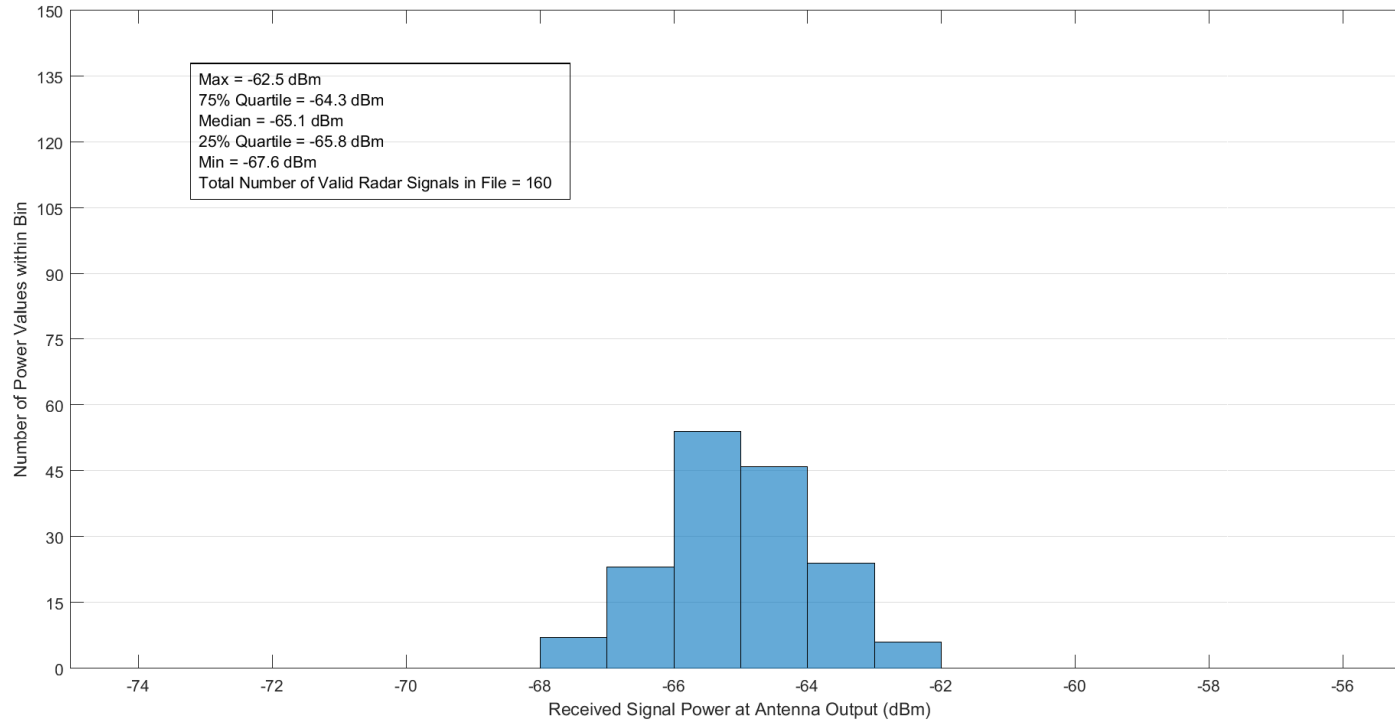


Figure B-52. Received radar signal power statistics at Location 1 in Zone J2 for the CARSR.

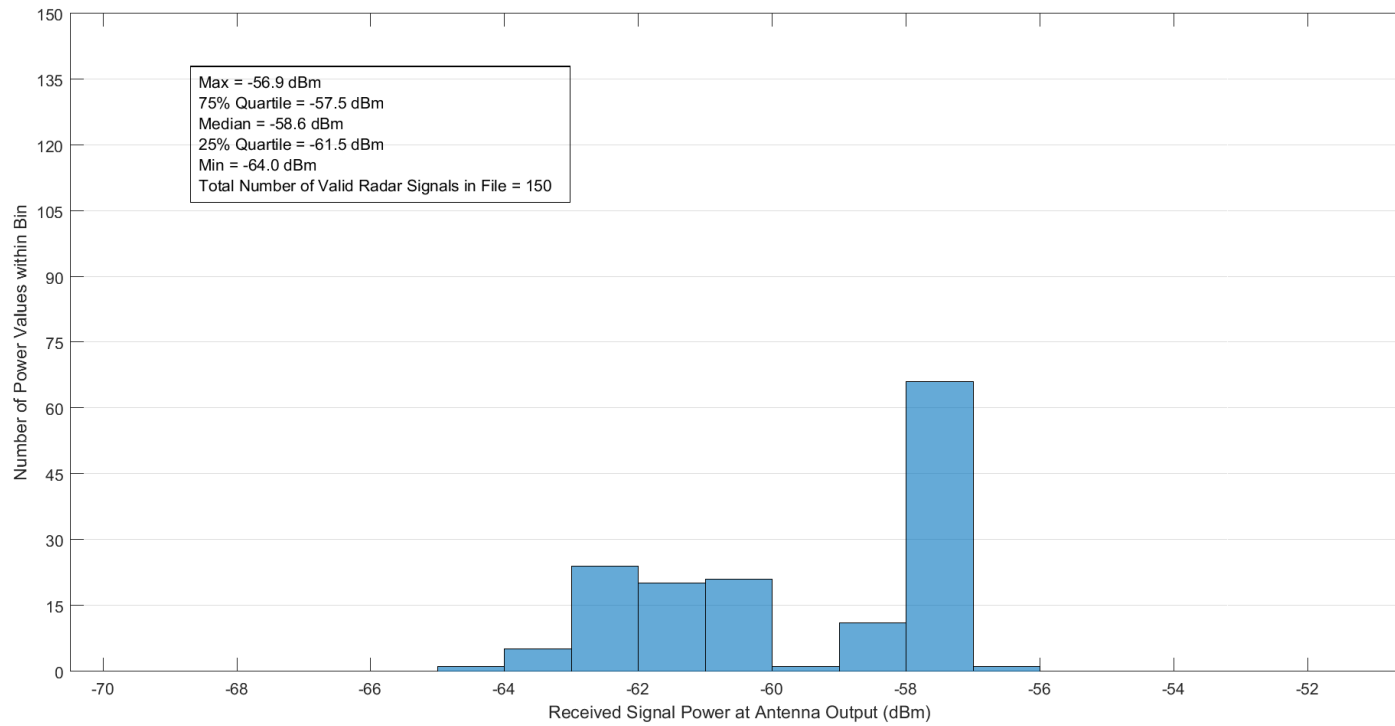


Figure B-53. Received radar signal power statistics at Location 2 in Zone J2 for the CARSR.

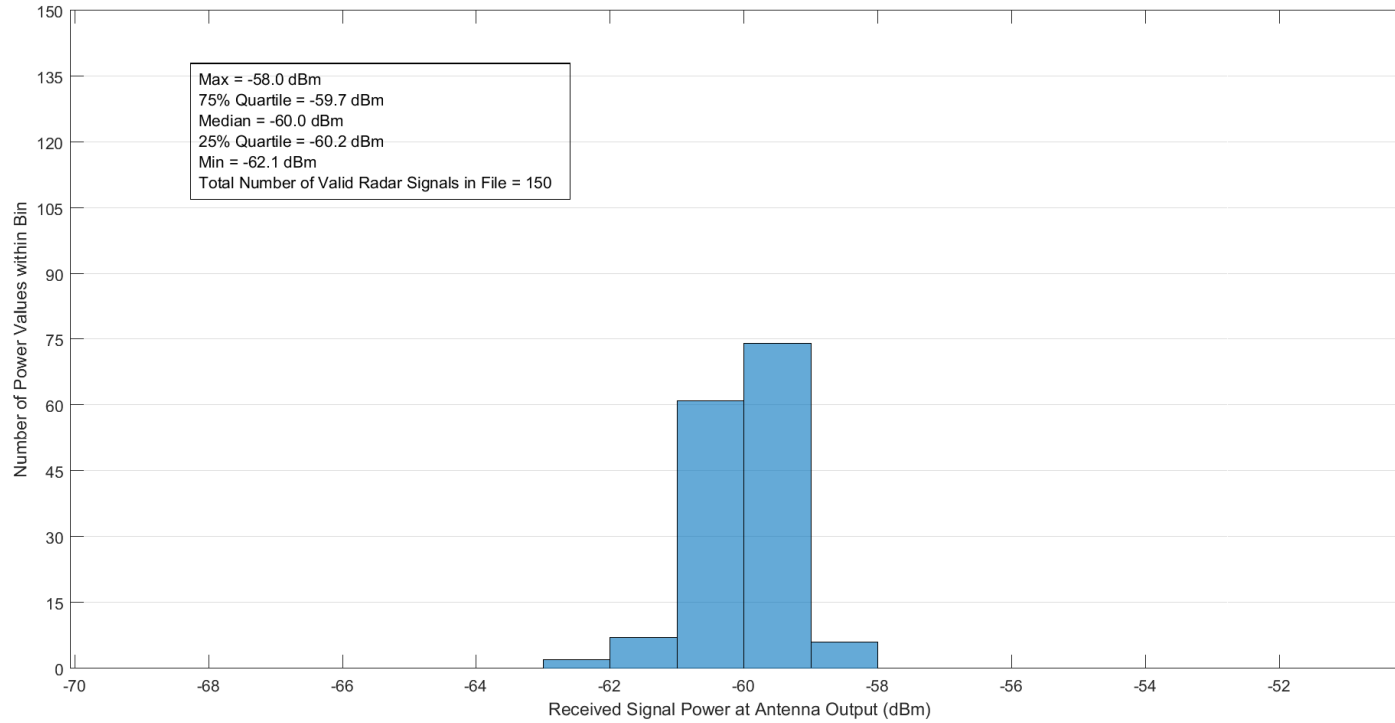


Figure B-54. Received radar signal power statistics at Location 3 in Zone J2 for the CARSR.

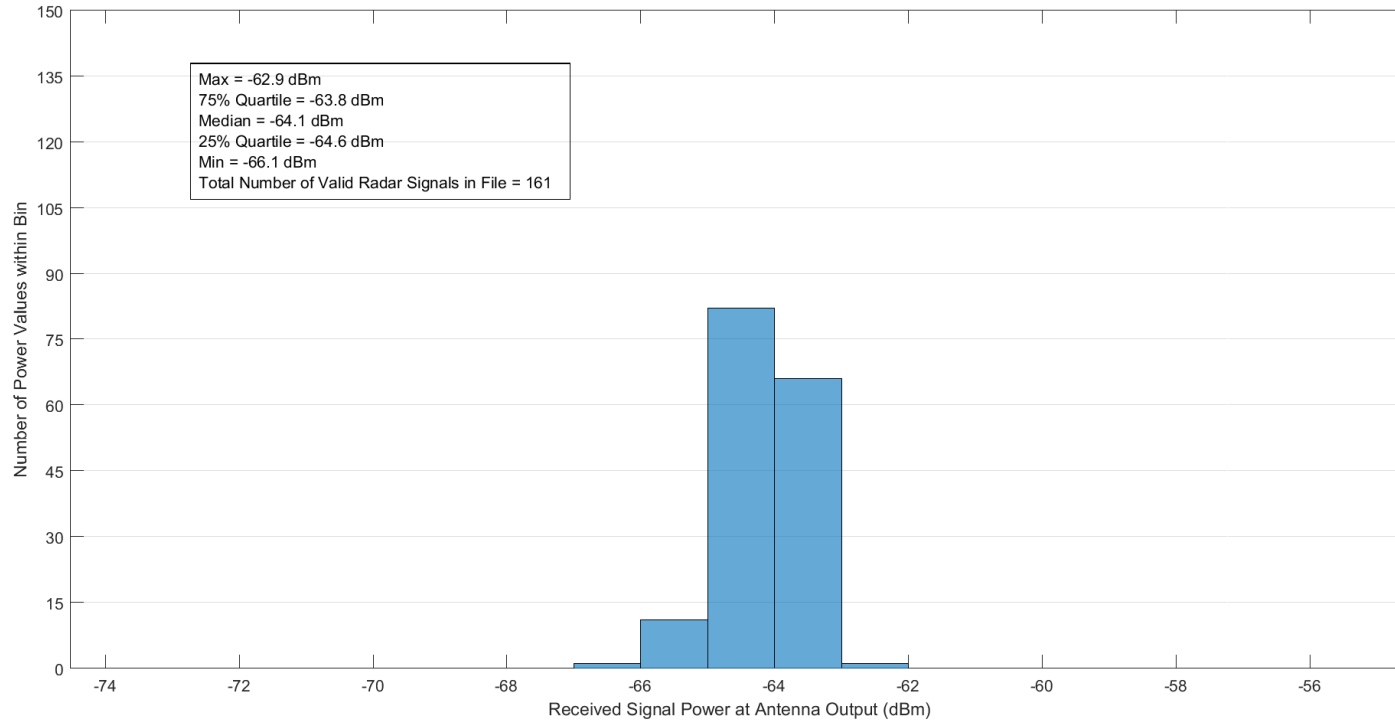


Figure B-55. Received radar signal power statistics at Location 4 in Zone J2 for the CARSR.

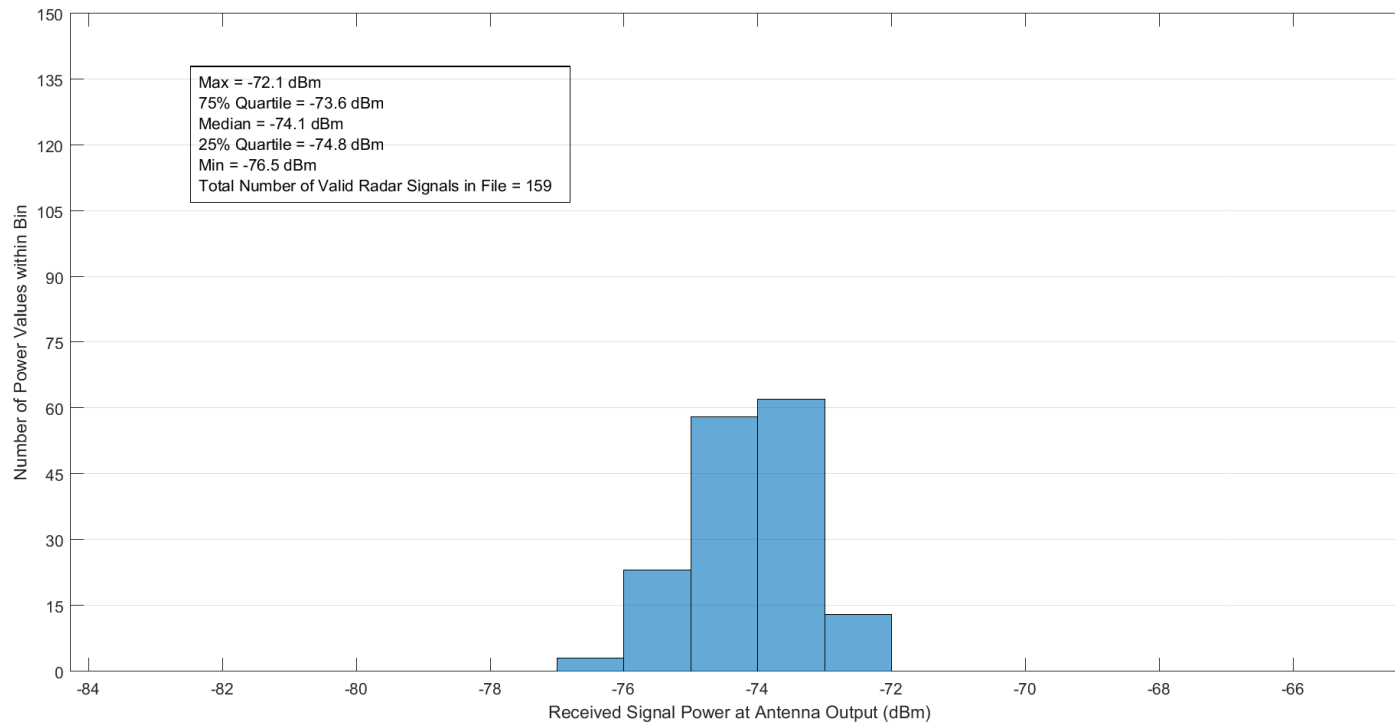


Figure B-56. Received radar signal power statistics at Location 5 in Zone J2 for the CARSR.

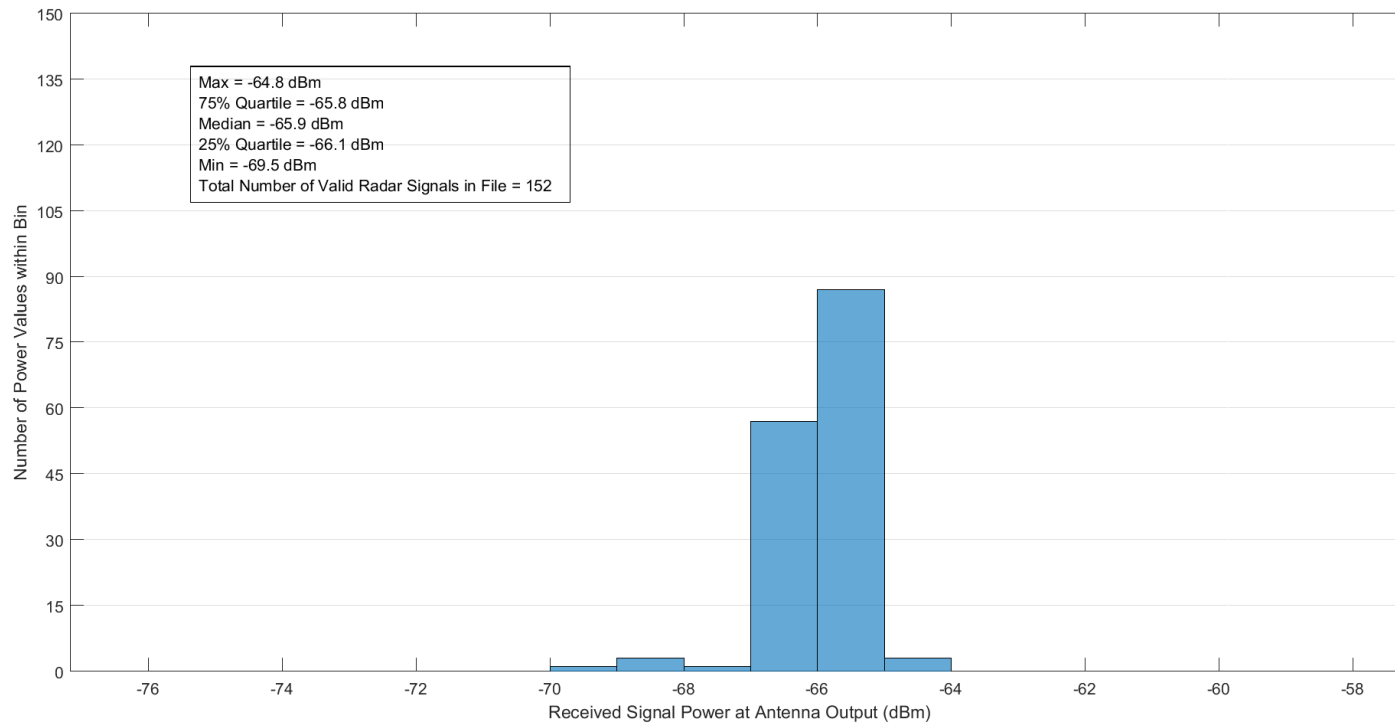


Figure B-57. Received radar signal power statistics at Location 1 in Zone J3 for the CARSR.

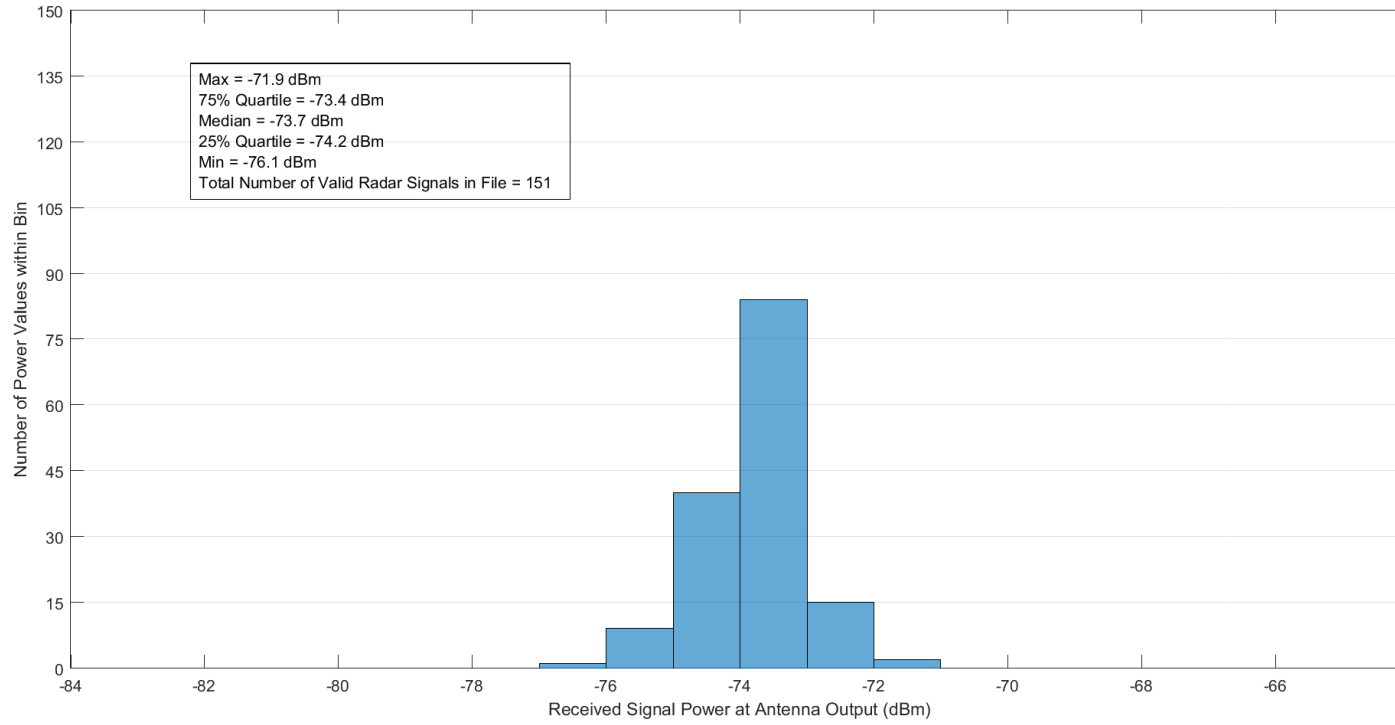


Figure B-58. Received radar signal power statistics at Location 2 in Zone J3 for the CARSR.

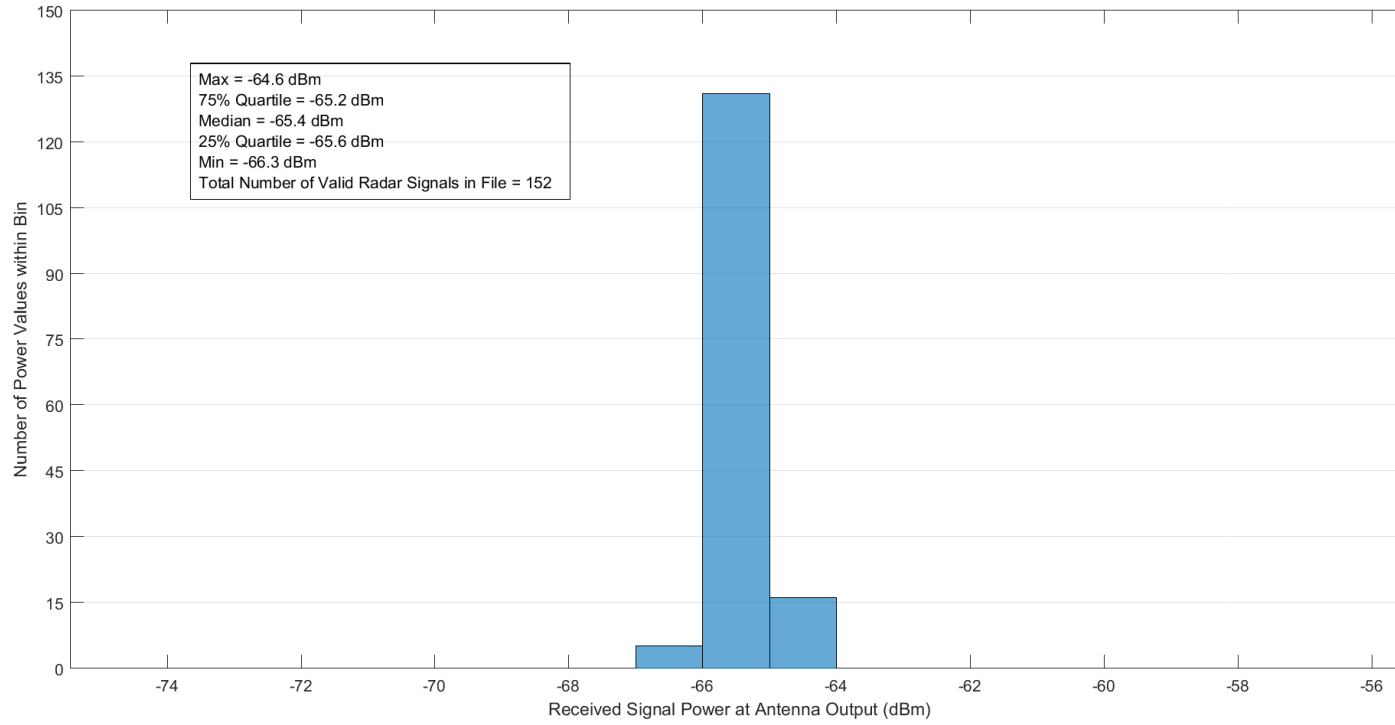


Figure B-59. Received radar signal power statistics at Location 3 in Zone J3 for the CARSR.

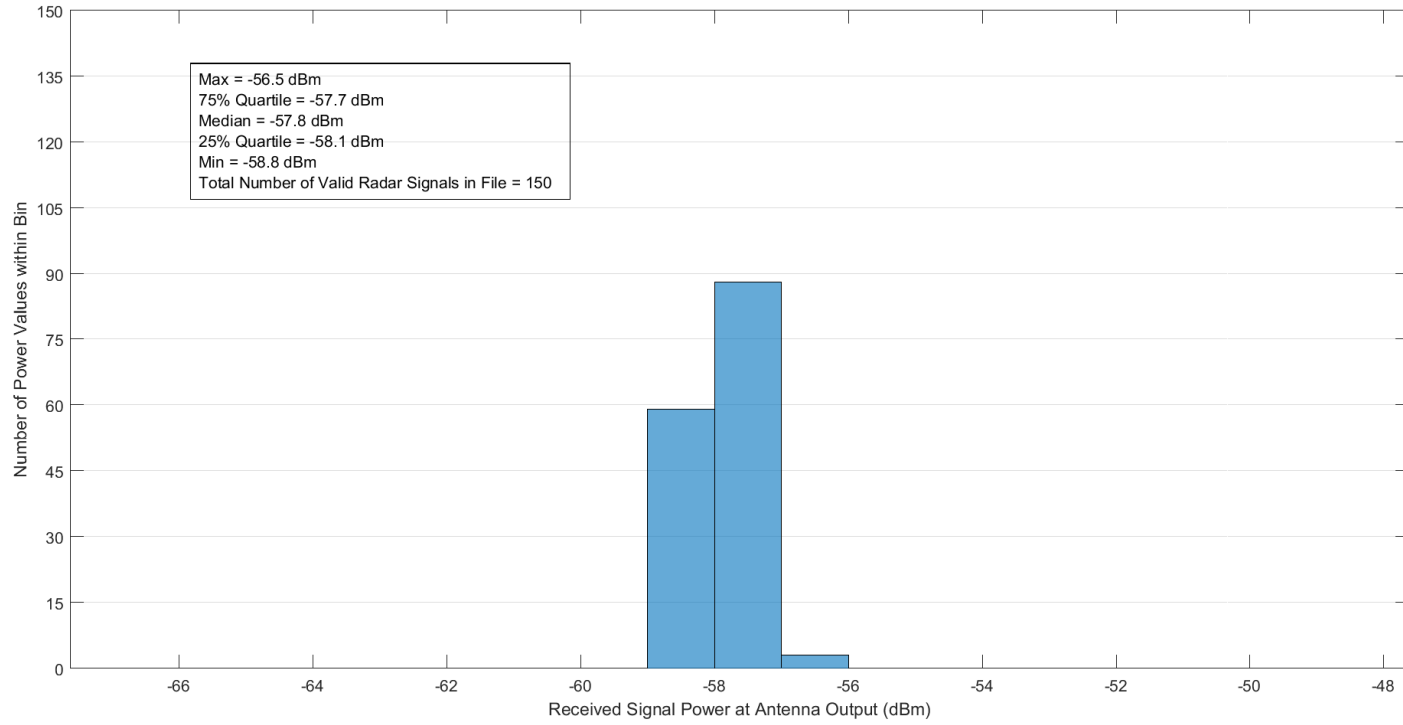


Figure B-60. Received radar signal power statistics at Location 4 in Zone J3 for the CARSR.

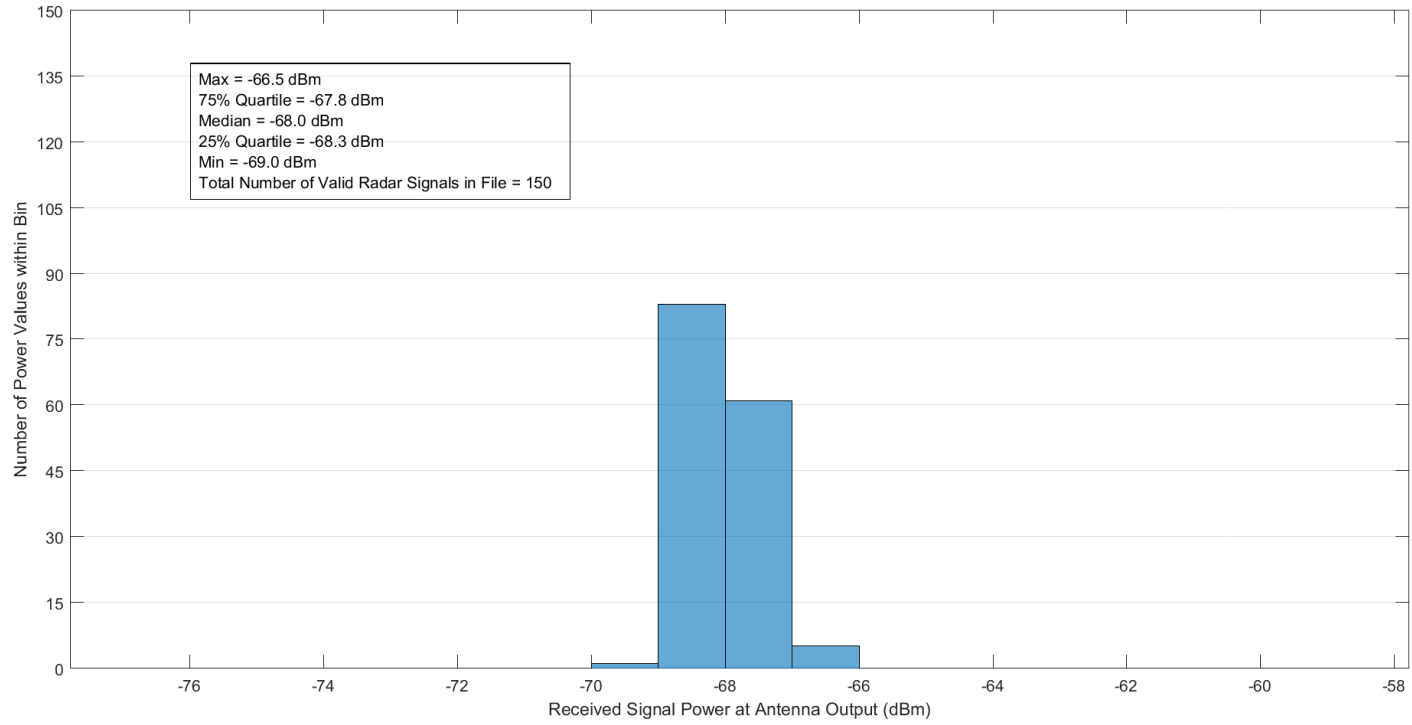


Figure B-61. Received radar signal power statistics at Location 5 in Zone J3 for the CARSR.

CC CARSR

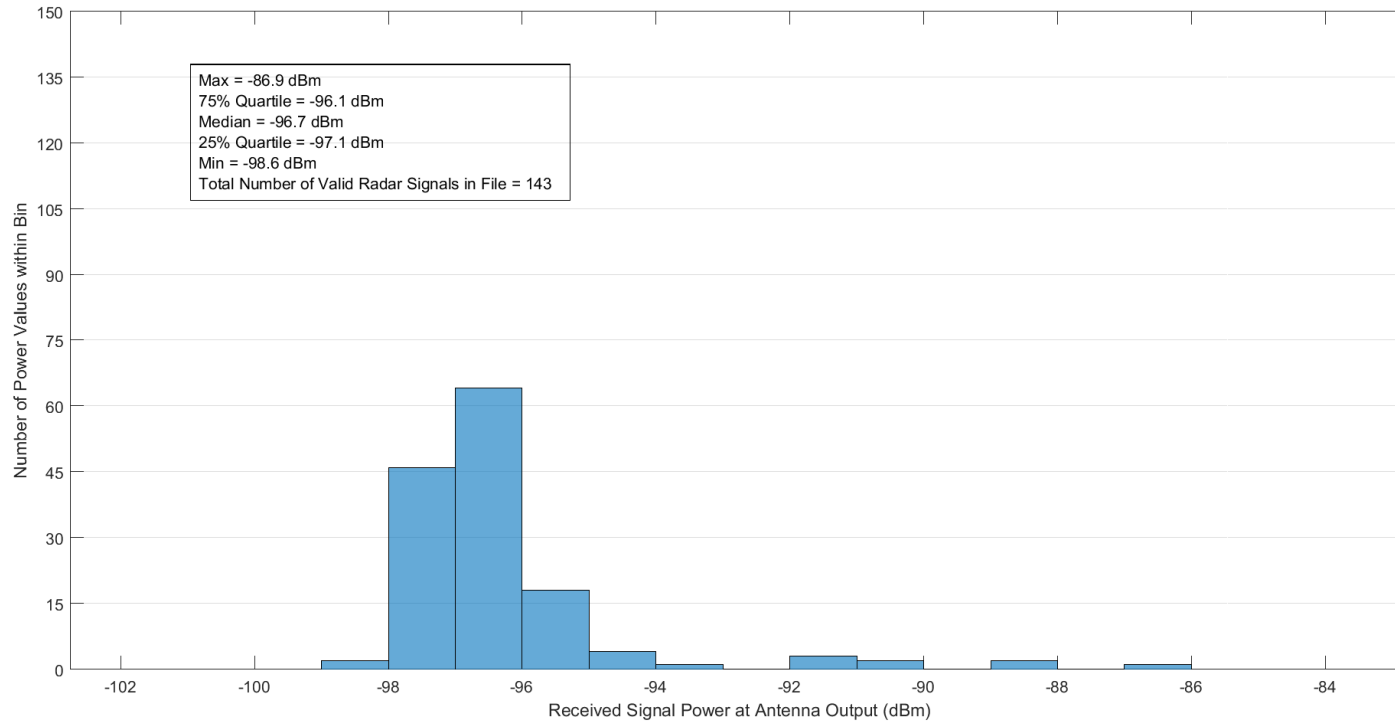


Figure B-62 Received radar signal power statistics at Location 1 in Zone D4 for the CARSR.

CC CARSR

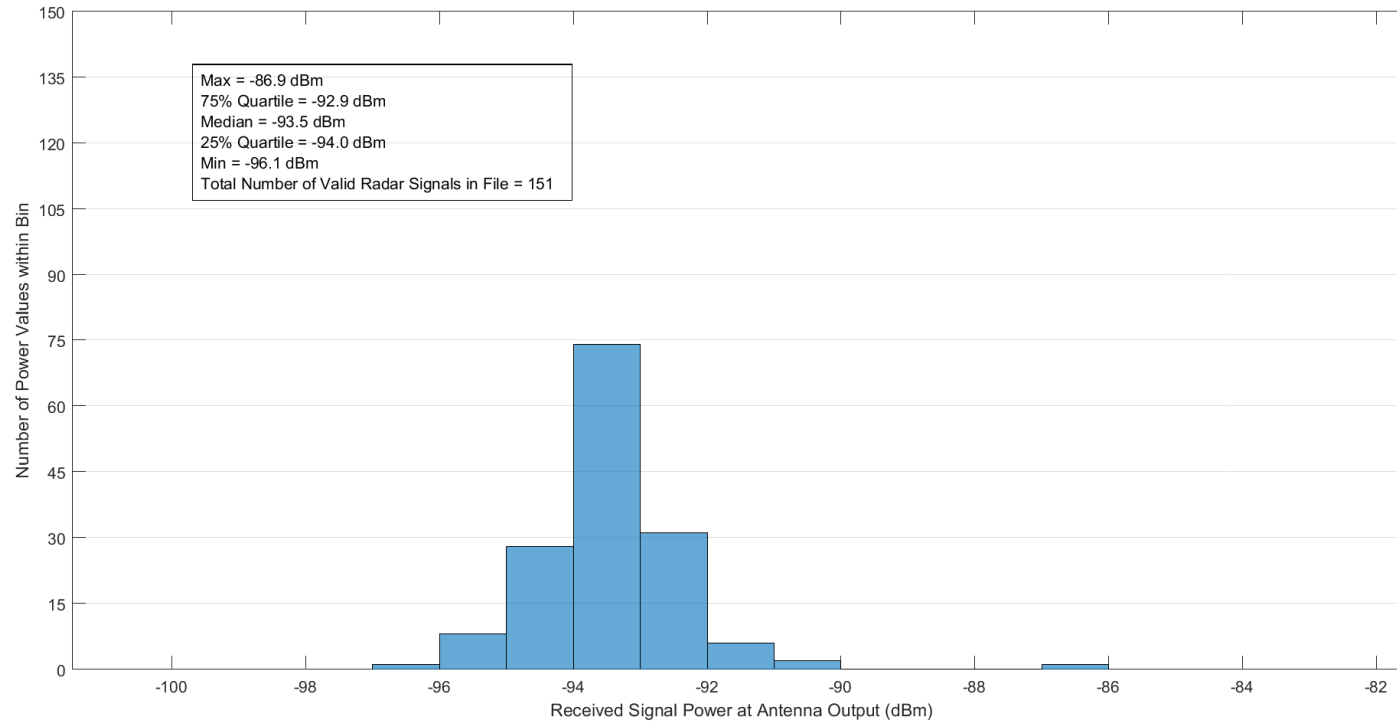


Figure B-63 Received radar signal power statistics at Location 1 in Zone D5 for the CARSR.

BIBLIOGRAPHIC DATA SHEET

1. PUBLICATION NO. TR-20-543	2. Government Accession No.	3. Recipient's Accession No.
4. TITLE AND SUBTITLE Received Signal Power Measurements On Select Air Traffic Control Radars In Utah		5. Publication Date October 2019
		6. Performing Organization Code NTIA/ITS.T
7. AUTHOR(S) Jeffery A. Wepman, Edward F. Drocella, April Lundy, Mike Chang, Linh P. Vu, Kenneth J. Brewster, and Paul M. McKenna		9. Project/Task/Work Unit No. 6504000-208
		10. Contract/Grant Number.
8. PERFORMING ORGANIZATION NAME AND ADDRESS Institute for Telecommunication Sciences National Telecommunications & Information Administration U.S. Department of Commerce 325 Broadway Boulder, CO 80305		12. Type of Report and Period Covered
11. Sponsoring Organization Name and Address National Telecommunications & Information Administration Herbert C. Hoover Building 14 th & Constitution Ave., NW Washington, DC 20230		
14. SUPPLEMENTARY NOTES		
15. ABSTRACT (A 200-word or less factual summary of most significant information. If document includes a significant bibliography or literature survey, mention it here.) Received signal power measurements were performed on the Common Air Route Surveillance Radar (CARSR) operating in the 1300–1370 MHz band in Cedar City, Utah, and on the Airport Surveillance Radar (ASR-9) operating in the 2700–2900 MHz band in Trout Creek, Utah. The measurements were taken at sites relatively far from each radar transmitter. The measurement locations represent different predicted propagation modes (such as line-of-sight, diffracted, tropospheric scatter, etc.) and varying predicted received signal powers (from strong to weak). Distances from the transmitter to the measurement locations varied from roughly 56 km to 141 km for the ASR-9 and 17 km to 194 km for the CARSR. Multiple peak received signal power measurements were made at each location to provide statistically significant results. In another effort, these measurements will be used to validate spectrum usage contours and the methodology used to generate them as developed by the Office of Spectrum Management (OSM) of the National Telecommunications and Information Administration (NTIA).		
16. Key Words (Alphabetical order, separated by semicolons) Received signal power measurements, peak received signal power, ASR-9, CARSR, radar measurements, spectrum usage contours		
17. AVAILABILITY STATEMENT <input checked="" type="checkbox"/> UNLIMITED. <input type="checkbox"/> FOR OFFICIAL DISTRIBUTION.	18. Security Class. (This report) Unclassified	20. Number of pages 174
	19. Security Class. (This page) Unclassified	21. Price:

NTIA FORMAL PUBLICATION SERIES

NTIA MONOGRAPH (MG)

A scholarly, professionally oriented publication dealing with state-of-the-art research or an authoritative treatment of a broad area. Expected to have long-lasting value.

NTIA SPECIAL PUBLICATION (SP)

Conference proceedings, bibliographies, selected speeches, course and instructional materials, directories, and major studies mandated by Congress.

NTIA REPORT (TR)

Important contributions to existing knowledge of less breadth than a monograph, such as results of completed projects and major activities.

JOINT NTIA/OTHER-AGENCY REPORT (JR)

This report receives both local NTIA and other agency review. Both agencies' logos and report series numbering appear on the cover.

NTIA SOFTWARE & DATA PRODUCTS (SD)

Software such as programs, test data, and sound/video files. This series can be used to transfer technology to U.S. industry.

NTIA HANDBOOK (HB)

Information pertaining to technical procedures, reference and data guides, and formal user's manuals that are expected to be pertinent for a long time.

NTIA TECHNICAL MEMORANDUM (TM)

Technical information typically of less breadth than an NTIA Report. The series includes data, preliminary project results, and information for a specific, limited audience.

For information about NTIA publications, contact the NTIA/ITS Technical Publications Office at 325 Broadway, Boulder, CO, 80305 Tel. (303) 497-3572 or e-mail ITSinfo@ntia.gov.